

SOFT AND HARD MESONS IN CHIRAL PERTURBATION THEORY

Ilaria Jemos

Department of Astronomy and Theoretical Physics
Lund University

Thesis for the degree of Doctor of Philosophy

Thesis Advisor: *Johan Bijnens*
Faculty Opponent: *Christopher Sachrajda*

To be presented, with the permission of the Faculty of Science of Lund University, for public criticism in lecture hall F of the Department of Astronomy and Theoretical Physics on Friday, the 20th of May 2011, at 10.15.

Organization LUND UNIVERSITY Department of Astronomy and Theoretical Physics Sölvegatan 14A SE-223 62 LUND Sweden		Document name DOCTORAL DISSERTATION	
		Date of issue April 2011	
Author(s) Ilaria Jemos		Sponsoring organization	
Title and subtitle Soft and hard mesons in Chiral Perturbation Theory			
Abstract This thesis deals with Chiral Perturbation Theory (ChPT), an effective field theory for the strong force used to describe meson interactions. The work done can be split in two parts. The first one is on ChPT in its standard formulation. This theory has been very successful so far in describing low energetic processes. However, it is still not entirely clear how much it can be trusted for precision determinations of hadronic observables. Paper I and II explore this aspect. Paper I shows the results of a search for relations between several observables calculated with ChPT at order p^6 . The relations are built up such that the couplings of the theory cancel out. These combinations can then be used to test the convergence of the perturbative expansion in a way that is almost independent from the unknown couplings. Paper II presents the results for a new global fit at order p^6 of the couplings of the p^4 ChPT Lagrangian. The fit includes the most recent phenomenological information. Furthermore, a new way to deal with the p^6 couplings, based on a random walk algorithm, is considered. This method allows to study correlations between the couplings. The second part, paper III and IV, focuses on an extension of ChPT out of its usual energy range. This approach is called hard pion ChPT and it is expected to be useful for the analysis of lattice data. Paper III provides arguments that further support the use of hard pion ChPT to calculate chiral logarithms when hard external pions arise. The hard pion ChPT approach is applied in this paper to semileptonic decays of B and D mesons to pions. In Paper IV hard pion ChPT is extended to the three-flavour case, thereby describing the B and D meson transitions to all the light pseudoscalar mesons (π , K and η). A comparison with data is also presented and it shows that the corrections are sizable. Moreover, the procedure is applied to scalar and vector formfactors of the pions and kaons and to $B \rightarrow D$ decay.			
Key words: Chiral Perturbation Theory, Mesons, Phenomenological Models, QCD Phenomenology			
Classification system and/or index terms (if any):			
Supplementary bibliographical information:		Language English	
ISSN and key title:		ISBN 978-91-7473-100-2	
Recipient's notes		Number of pages 169	Price
		Security classification	

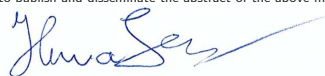
Distributor

Ilaria Jemos

Department of Astronomy and Theoretical Physics, Sölvegatan 14A, SE-223 62 Lund, Sweden

I, the undersigned, being the copyright owner of the abstract of the above-mentioned dissertation, hereby grant to all reference sources the permission to publish and disseminate the abstract of the above-mentioned dissertation.

Signature



Date 2011-04-04

Sammanfattning

Många av er har kanske redan hört uttrycket *partikelfysik*, men kanske inte alla vet vad det handlar om. Detta är en gren av fysiken som studerar system av mycket små objekt, allmänt kallade partiklar. Med små menar vi en miljondels miljarddels meter (vilket är exempelvis protonens radie) eller ännu mindre.

För att undersöka partiklarnas egenskaper, behöver vi både ett teoretiskt och ett experimentellt angreppssätt. Det teoretiska angreppssättet producerar modeller för att studera partiklars beteende. Det experimentella angreppssättet mäter olika partikelegenskaper (massor, sönderfallstid och så vidare). Kopplingen mellan dessa två är *fenomenologi* som beräknar och jämför teoretiska förutsägelser med experimentell data. Arbetet samlat i denna avhandling faller inom detta sista område av partikelfysiken.

I vanlig materia finns protoner, neutroner och elektroner, men det finns också många fler sorters partiklar. Några av dessa återfinns till exempel i jordens atmosfär. De är subatomära partiklar som rör sig genom universum och växelverkar med atmosfärens partiklar. Dessa partiklar är också lätta att producera i partikelkolliderare. Metoden som används är att accelerera partiklar till mycket hög energi och låta dem kollidera. De partiklar som produceras vid kollisionen studeras sedan och kan användas för att dra slutsatser om strukturen hos de partiklar som skapats vid kollisionen.

I denna avhandling fokuserar vi på en speciell sorts partiklar kallade *mesoner*. De är inte elementära, utan består av två elementarpartiklar kallade *kvarkar*.

Det finns en teori för att beskriva samspelet mellan kvarkar som kallas *Kvantkromodynamik*. Denna teori beskriver framgångsrikt kvarkar och kraften mellan dem vid väldigt höga energier. Men i en sådan framställning är det mycket svårt att utföra beräkningar för mesoner vid låg energi. Det kan endast göras med mycket stor datorkraft. Därför har en annan metod utvecklats och detta är *Kiral Störningsteori*. Den beskriver de fysikaliska systemen i termer av mesoner istället för kvarkar. En sådan teori förenklar avsevärt beräkningarna eftersom den bortser från mesonernas interna dynamik. Kiral Störningsteori gör det möjligt att med framgång modellera många processer, exempelvis sönderfall av tunga mesoner till lättare eller spridningsprocesser. Bland de mesonerna fokuserar vi på de lättaste, som är pioner, kaoner och η -mesoner.

Kiral Störningsteoris största fördel är att den tillåter studier av processer genom successiva approximationer. Åtminstone i princip kan vi få precisa förutsägelser om vi adderar tillräckligt många steg. Men vi måste också klargöra vilka av dessa som ger stora bidrag och vilka som med säkerhet kan försummas. Detta är en fråga vi undersöker i denna avhandling.

Det finns också flera okända parametrar i Kiral Störningsteori som måste bestämmas från experimentella data. Eftersom alla beräkningar vi gör är beroende av dessa okända konstanter, är det viktigt att fastställa dem. Detta är

ett annat problem som vi undersöker i denna avhandling.

Kiral Störningsteoris standardformulering är bara giltig om mesonerna är mjuka, det vill säga de måste ha låg energi. Å andra sidan produceras det också mesoner med hög energi, även kallat hårda. Vad kan vi göra i dessa fall? Är det fortfarande möjligt att använda Kiral Störningsteori till en viss del? Svaret är ja. Det finns fortfarande några viktiga korrekationer som vi kan beräkna. Vi undersöker också dessa möjligheter genom att utvidga den Kiral Störningsteorin till ett större energiintervall. Denna utvidgning kallas *Kiral Störningsteori för hårda pioner*.

To Giuliana

This thesis is based on the following publications:

- I Johan Bijnens and Ilaria Jemos,
Relations at order p^6 in Chiral Perturbation Theory,
European Physical Journal C **64** (2009) 273 [arXiv:0906.3118 [hep-ph]].
- II Johan Bijnens and Ilaria Jemos,
A new global fit of the L_i^r at next-to-next-to-leading order in Chiral Perturbation Theory,
submitted to *Nuclear Physics B* [arXiv:1103.5945 [hep-ph]].
- III Johan Bijnens and Ilaria Jemos,
Hard pion Chiral Perturbation Theory for $B \rightarrow \pi$ and $D \rightarrow \pi$ formfactors¹,
Nuclear Physics **B840** (2010) 54, [Erratum-ibid. **B844** (2011) 182],
[arXiv:1006.1197 [hep-ph]].
- IV Johan Bijnens and Ilaria Jemos,
Vector formfactors in hard pion Chiral Perturbation Theory,
Nuclear Physics **B846** (2011) 145 [arXiv:1011.6531 [hep-ph]].

During my time as a PhD student, I have also co-authored the following proceedings:

- I Johan Bijnens and Ilaria Jemos,
Determination of Low Energy Constants and testing Chiral Perturbation Theory at next-to-next-to-leading order,
PoS EFT09 (2009) 032 [arXiv:0904.3705 [hep-ph]].
- II Johan Bijnens and Ilaria Jemos,
Determination of Low Energy Constants and testing Chiral Perturbation Theory at order p^6 (NNLO),
PoS CD09 (2009) 087 [arXiv:0909.4477 [hep-ph]].

¹In this thesis the corrected arXiv version is included.

Contents

<i>i</i>	Introduction	1
<i>i.1</i>	Introduction	1
<i>i.2</i>	Units and typical scales in particle physics	2
<i>i.3</i>	Constituents and particles	3
<i>i.4</i>	Quantum field theory (QFT)	5
	<i>i.4.1</i> Fields, Lagrangians and free fermions	6
	<i>i.4.2</i> Symmetries and interactions	7
	<i>i.4.3</i> Probability amplitudes, perturbation theory and Feynman diagrams	9
<i>i.5</i>	Effective field theories	11
<i>i.6</i>	Chiral Perturbation Theory	12
	<i>i.6.1</i> QCD and chiral symmetry	13
	<i>i.6.2</i> Local chiral symmetry	15
	<i>i.6.3</i> Chiral Perturbation Theory formalism	16
	<i>i.6.4</i> Decay constants and meson masses at lowest order ($\mathcal{O}(p^2)$)	19
	<i>i.6.5</i> Power counting	22
	<i>i.6.6</i> The main prediction of ChPT at $\mathcal{O}(p^4)$: chiral loga- rithms	24
<i>i.7</i>	Hard pion Chiral Perturbation Theory	26
<i>i.8</i>	Heavy Quark Effective Theory	28
	<i>i.8.1</i> Heavy Meson Chiral Perturbation Theory	30
<i>i.9</i>	Interplay between ChPT and Lattice QCD	32
<i>i.10</i>	Introduction to papers	33
	<i>i.10.1</i> Paper I	34
	<i>i.10.2</i> Paper II	34
	<i>i.10.3</i> Paper III	35
	<i>i.10.4</i> Paper IV	35
<i>i.11</i>	List of contributions	36
	Acknowledgments	38
	References	39

I	Relations at order p^6 in Chiral Perturbation Theory	41
I.1	Introduction	42
I.2	Notation	42
I.3	$\pi\pi$ scattering	43
I.4	πK scattering	46
I.5	$\pi\pi$ and πK scattering	51
I.6	$K_{\ell 4}$	52
I.7	$\eta \rightarrow 3\pi$	53
I.8	Scalar formfactors	54
I.9	Scalar formfactors, masses and decay constants	55
I.10	Vector formfactors	56
I.11	Scalar formfactors, $\pi\pi$ and πK scattering	56
I.12	A final relation: $K_{\ell 4}$, πK scattering and scalar formfactors	57
I.13	Conclusions	58
I.A	Relation between threshold and subthreshold parameters	59
	References	61
II	A new global fit of the L_i^r at next-to-next-to-leading order in Chiral Perturbation Theory	65
II.1	Introduction	66
II.2	Chiral Perturbation Theory	67
II.3	Fitting procedure and input observables	69
II.3.1	χ^2	69
II.3.2	Masses and decay constants	69
II.3.3	F_K/F_π	70
II.3.4	The quark-mass ratio m_s/\hat{m}	71
II.3.5	$K_{\ell 4}$ formfactors	71
II.3.6	$\pi\pi$ scattering	73
II.3.7	πK scattering	74
II.3.8	Scalar formfactor	75
II.3.9	L_9^r and L_{10}^r	76
II.4	Resonance estimates for the C_i^r	76
II.5	Existing fits	78
II.6	New Fits	80
II.6.1	Linear fit for $K_{\ell 4}$ decays	83
II.6.2	Some small variations on fit All	84
II.6.3	Adding input: $\bar{\ell}_i$ constants in two-flavour ChPT	85
II.6.4	A chiral quark model estimate for the C_i^r	87
II.7	Releasing the C_i^r	89
II.7.1	Convergence constraints	92
II.7.2	Results	93
II.8	Conclusions	98

II.A	C_i^r values	102
	References	105
III	Hard pion Chiral Perturbation Theory for $B \rightarrow \pi$ and $D \rightarrow \pi$ formfactors	109
III.1	Introduction	110
III.2	Heavy Meson Chiral Perturbation Theory	111
III.3	Relativistic Theory	113
III.4	$B \rightarrow \pi$ formfactors: formalism	114
III.5	Hard pion Chiral Perturbation Theory	116
III.6	The Coefficients of the Chiral Logarithms	118
III.7	Conclusions	122
III.A	Loop integrals expansions	123
	References	126
IV	Vector formfactors in hard pion Chiral Perturbation Theory	129
IV.1	Introduction	130
IV.2	Chiral Perturbation Theory	131
IV.2.1	Standard Chiral Perturbation Theory	131
IV.2.2	Heavy meson Chiral Perturbation Theory	132
IV.2.3	Relativistic theory	133
IV.2.4	Hard pion Chiral Perturbation Theory	134
IV.3	Pion and kaon formfactors	135
IV.3.1	Electromagnetic formfactors in three-flavour HPChPT	135
IV.3.2	Vector and scalar pion formfactors in two-flavour HPChPT	136
IV.4	$B \rightarrow M$ and $D \rightarrow M$ transitions	137
IV.4.1	Definition of formfactors	137
IV.4.2	The chiral logarithms away from the endpoint	139
IV.4.3	Comparison with experiment	144
IV.4.4	Chiral logarithms at the endpoint	145
IV.5	$B \rightarrow D$ transition	147
IV.5.1	Definition of formfactors	147
IV.5.2	Chiral logarithms	149
IV.6	Conclusions	150
IV.A	Expansion of the needed loop integrals	151
	References	157

Introduction

i.1 Introduction

Particle physics is a branch of physics studying systems composed of extremely small objects, called generically particles. With small we mean sizes of order 10^{-15} meters (which is e.g., the radius of a proton) or even smaller.

To investigate the properties of the particles there are basically two approaches needed. A theoretical one, whose task is mostly to produce models for studying particle behaviours, and an experimental one, so that their properties (masses, decay times and so on) are measured. The link between the two is *phenomenology* that mostly calculates and compares the theoretical predictions with experimental data. The work collected in this thesis finds its location in this last field of particle physics.

More specific, we study a particular type of particles called *mesons*, and among them we will focus on the lightest ones. The mesons are composite systems. So they are not elementary objects, but are rather constituted by point-like particles. The mesons are not easy to find in ordinary matter. They have first been observed as products of cosmic rays interacting in the atmosphere of the earth, but are mostly produced and studied doing particle experiments.

There exists a theory, the so-called *quantum chromodynamics*, describing the interactions of the mesons' constituents. Unfortunately doing calculations in such a framework is prohibitive when we deal with low energetic mesons. They can be performed only by heavily using computer power. Therefore a different approach has been developed to deal with this problem. This is the effective field theory one. The underlying idea is to find a way to predict measurable quantities by successive approximation. For some theories even that is not at all straightforward and can be done only by simplifying the system under study. This is achieved, for example, by not trying to describe the internal dynamics of the mesons and promoting the mesons as the relevant degrees of freedom. In the case of quantum chromodynamics such an effective field theory exists and it is called Chiral Perturbation Theory.

In this introduction we try to give an idea of how Chiral Perturbation Theory is built up and how we can calculate physical observables starting from the basis. In these first sections no preliminary knowledge is needed, but further down the subject matter will become more and more complicated.

Hereafter we list the contents of the different sections. Section *i.2* deals with the basic units of measure we use throughout this thesis, which are also widely adopted in several branches of particle physics. We also try there to give an idea of which kind of objects we are studying, namely of the scales they live at. In Section *i.3* we introduce the constituents of matter and name the main forces among them. In Section *i.4* we shortly describe the mathematical background needed for our purposes: Quantum Field Theory. This is commonly used when we want to deal with systems that are both microscopic (small distances) and relativistic (high velocities) as the particles are. Section *i.5* explains the basics of effective field theories. The largest part of this introduction is Section *i.6*. It focuses on Chiral Perturbation Theory in its standard formulation. The work done during my PhD is mainly in this framework. Section *i.7* presents an extension of Chiral Perturbation Theory over a wider energy range. This is called hard pion Chiral Perturbation Theory. Section *i.8* shortly introduces another effective theory called Heavy Quark Effective Theory used to include more mesons in the description. Section *i.9* is devoted to a method used to attack involved calculations in particle physics: lattice quantum chromodynamics. We try to show there how Chiral Perturbation Theory and lattice quantum chromodynamics need each other to reach further progress. Finally a summary of the four publications included in this thesis closes the introduction.

***i.2* Units and typical scales in particle physics**

Before entering into the technical aspects, it is important to know which are the typical scales and units used in particle physics and throughout this thesis [1]. We will therefore devote this section to an overview of the orders of magnitude involved. The calculations are much simplified by the use of units such that $\hbar = c = 1$, called *natural units*. The speed of light has the value $c \approx 3 \times 10^8 \text{m/s}$. Instead of using the meter, we can also decide to use a new unit of length (or a new unit of time) defined by the statement that in these units $c = 1$. Then, the velocity v of a particle is measured in units of the speed of light, what is very natural since we typically deal with relativistic objects. The Planck constant \hbar has instead dimensions $[\text{energy}] \times [\text{time}]$. We can choose units of time such that $\hbar = 1$. Then all multiplicative factors of \hbar

Leptons			Quarks		
Flavour	Mass	Charge	Flavour	Mass	Charge
e	0.511 MeV	-1	u	1.7 – 3.3 MeV	2/3
ν_e	< 0.5 MeV	0	d	4.1 – 5.8 MeV	-1/3
μ	105.7 MeV	-1	c	1.18 – 1.34 GeV	2/3
ν_μ	< 0.19 MeV	0	s	80 – 130 MeV	-1/3
τ	1.777 GeV	-1	t	170 – 174 GeV	2/3
ν_τ	< 18.2 MeV	0	b	4.13 – 4.37 GeV	-1/3

Table i.1: The elementary constituents of matter. The electric charge is given in units of e , charge of an electron. The values for the masses are taken from [2]

and c disappear from our equations and

$$\begin{aligned}
 [v] &= \text{dimensionless}, & [\text{energy}] &= [\text{momentum}] = [\text{mass}], \\
 [\text{length}] &= [\text{mass}]^{-1}. & & (i.1)
 \end{aligned}$$

The first two equations follow immediately from $c = 1$ while the third follows from $\hbar = 1$. Thus all physical quantities have dimensions that can be expressed as powers of mass or, equivalently, as powers of length or of momentum.

Once we settle our favourite units we can look at which are the typical energies, masses, lengths involved. For convenience we express all of them using eV (and its positive or negative powers). This is defined as the amount of kinetic energy gained by a single unbound electron when it accelerates through an electric potential difference of 1 Volt. Here we typically deal with distances of order of $10^{-15}\text{m} \approx (0.2 \text{ GeV})^{-1}$ and with masses of order of $10^{-27} \text{ kg} \approx 0.5 \text{ GeV}$. So for example the proton has an approximate radius of 1 GeV^{-1} and a mass around 1 GeV.

i.3 Constituents and particles

Ordinary matter can be understood in terms of neutron n , proton p , (which are *hadrons*, from the Greek stout particles) and of electron e and electronic neutrino ν_e (which are *leptons*, i.e. light particles). However there exist many more particles than these. Let us show briefly how they are organized and their main features.



The leptons are, as far as we know, fundamental point-like spin $1/2$ particles. Two main classes of leptons exist: charged leptons (also known as the electron-like leptons), and neutral leptons (the *neutrinos*). The best known of all leptons is the electron e which is found in atoms and is directly tied to all chemical properties. The leptons are divided into *families* as shown in the left side of Table *i.1*. The first family is the electronic one, comprising the electron e and electron neutrinos ν_e . The second is the muonic, with muon μ and muonic neutrino ν_μ ; and the third is the tauonic, composed by the tau τ and tau neutrinos ν_τ .

For each of the leptons listed in Table *i.1* there exists also a corresponding antiparticle. These are particles with the same kinematical properties (such as mass and spin) as the corresponding particle, but with opposite internal quantum numbers (as the electric charge). For example the “antielectron” is called positron e^+ and has the same mass and spin as the electron but positive charge.

Besides the leptons there are the hadrons which are subdivided into *baryons*, with half-odd integral spin, and *mesons*, with integral spin. Hundreds of baryons and mesons have been found and they are all listed in [2]. They can be organized according to regular patterns. For example there exist eight mesons which have mass lower than all the other hadrons and they all have spin equal to 0 and the same parity. These mesons are commonly represented as in Figure *i.1*. The reason why such regular patterns exist is that the hadrons are not fundamental particles, but composite states of more fundamental entities called *quarks*. So far we have proof of the existence of six kinds of quarks (and the corresponding antiquarks), all listed in Tab. *i.1*.

Baryons turn out to be bound states of three quarks while mesons are quark-antiquark states. This thesis deals only with the mesons, and mainly focuses on the lightest eight of Figure *i.1*. These are composed of the lightest quarks, namely u , d and s .

Now that we have settled the scene as far as regards the objects under study, we can look at their interactions. These, in the framework of Quantum Field Theory, happen thanks to the exchanges of special particles called *gauge bosons*. In particle physics the relevant interactions and their gauge bosons are:

- Electromagnetic interaction: It is mediated by the *photon*, which is a massless gauge boson. Particles with a non-zero electric charge feel this interaction. It is the force responsible for the binding of the electrons to the nuclei in atoms and molecules.
- Weak interaction: It is mediated by the massive W^\pm and Z bosons (whose masses are of order 100 GeV). This interaction can occur e.g. be-

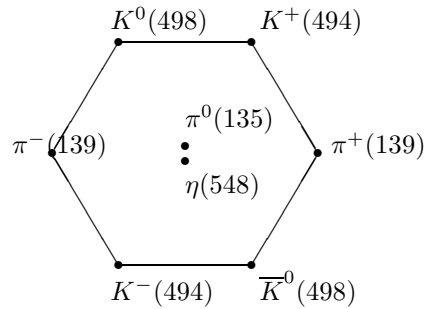


Figure i.1: The lightest “octet” of the mesons. The single components are called pions (π^+ , π^0 , π^-), kaons (K^+ , K^0 , K^- , \bar{K}^0) and eta (η). The number between parenthesis are the masses of each particle expressed in MeV. The least massive hadron after these ones is the ρ meson with a mass of 770 MeV [2].

tween leptons alone, leptons and quarks, quarks alone. It is responsible for the β -decay, where a decaying nucleus emits an electron and a neutrino.

- Strong interaction: The *gluon* is the massless gauge boson mediating this interaction. It takes place between quarks or also between gluons. It is the force that keeps the quarks bound together into hadrons. This thesis is devoted to the study of this interaction. The quantum field theory that describes it is called quantum chromodynamics (QCD). In this theory the particles that are assumed to interact strongly, i.e. the quarks, have a charge (analogous to the electric one) called *colour*. This is the reason for the word *chromo* in QCD.

Now that we have summarized which are the objects we are dealing with, we can turn to a short introduction of the mathematical description of such objects. This will be the subject of the next section.

i.4 Quantum field theory (QFT)

Considering the difficulty of the subject, giving a short summary of quantum field theory is a highly non-trivial task. We point out that this is not the aim of this section. Here we only mean to list very briefly the principles that will turn out useful for the next sections. Some textbooks for further reading are [3–5].

i.4.1 Fields, Lagrangians and free fermions

In field theories the particles are represented by *fields* which are special functions of time and of the spatial coordinates, collected all in the four vector x .

In QFT there are different kinds of fields. The *scalar*, usually denoted with ϕ , represents spin-0 bosons, while the *spinor* ψ identifies fermions. This distinction is based on the fact that the fields follow different quantization rules according e.g. to the spin of the particle. In QFT ϕ and ψ are not only simple functions, but they are a superposition of *annihilation* and *creation* operators. As the names suggest the creation operators act on the vacuum state to produce field states of given momenta and spins, while the annihilation operators transform back these states to the vacuum [4].

As remarked in Section i.3, there are also special spin-1 bosons called *gauge bosons*. They are the responsible for mediating the interactions and are often represented with the symbols A^μ for the photon and the gluon, W^μ and Z^μ for the weak gauge bosons.

The fundamental quantity that is built up starting from these objects is the so-called *Lagrangian density* \mathcal{L} . In natural units it has dimension $[\text{mass}]^4$ [6]. The reason why such a quantity is so important is that it rules the way the system under study evolves from one configuration to another [4]. In classical field theory it does so along the “path” for which its integral over space and time (called *action*) $S = \int d^4x \mathcal{L}$ is minimum. In quantum mechanics, the system does not follow a single path whose action is stationary, but its behaviour depends on all permitted paths and the value of their action. The action corresponding to the various paths is used to calculate the path integral, that gives the probability amplitudes of the various outcomes. Richard Feynman’s path integral formulation of quantum mechanics is inspired by the stationary-action principle, but it replaces the classical notion of a single, unique trajectory for a system with a sum, or functional integral, over the infinite number of possible trajectories to compute a quantum amplitude. In QFT, that is a combination of classical field theory and quantum mechanics, the Lagrangian and the action play again a leading role in ruling the evolution of a system. QFT can be formulated using functional methods along the lines of quantum mechanics. We remark however that while there the dynamical variable is the position of a particle, in QFT the dynamical variable is the whole field at each point in space-time.

Typically a Lagrangian density contains (as in classical field theory) a kinetic term, a mass term if the particle under study is massive and the interaction terms, that as the name suggests describe the interactions between particles. As an example we can take a look at the Lagrangian density for a free

fermion of mass m , the so-called Dirac Lagrangian¹

$$\mathcal{L}_{\text{Dirac}} = \bar{\psi}(i\gamma^\mu\partial_\mu - m)\psi. \quad (i.2)$$

where ∂_μ is a shorter notation to indicate the partial derivative $\partial/\partial x^\mu$. In (i.2) γ^μ are the so-called Dirac matrices entering into our equations every time we have to make manifest the intrinsic spin properties of the particles. In (i.2), $\bar{\psi} = \psi^\dagger\gamma^0$ is the adjoint field, describing an antiparticle of the fermion corresponding to ψ . One example of a particle/antiparticle pair are the electron e^- and its antiparticle the positron e^+ . The first term in (i.2) is the kinetic term. It contains the partial derivative of the field ψ . The second term is instead the mass term. Starting from (i.2) it is possible to write down the equations of motion, analogous to the Euler-Lagrange equations of classical mechanics. Those would describe then how a massive free fermion evolves.



i.4.2 Symmetries and interactions

In (i.2) we have shown the Lagrangian of a non interacting fermion. These fermions can be identified with the leptons and the quarks of Section i.3. As was said above, from the Lagrangian (i.2) we can derive the equations of motion and thus the dynamics of a free fermion. However we would also like to discover how the particles interact. Therefore we need to add in (i.2) terms describing such interactions. To this goal we introduce the concept of symmetry that will be the topic of this section.

Suppose that we want to describe the interactions of a particle ϕ with a certain Lagrangian $\mathcal{L}(\phi, \partial_\mu\phi)$. When we apply a transformation to the field $\phi \rightarrow \phi'$, the Lagrangian containing those fields will become in general $\mathcal{L}(\phi, \partial_\mu\phi) \rightarrow \mathcal{L}(\phi', \partial_\mu\phi')$. We say that the Lagrangian is *invariant* under a transformation if its form remains unaffected i.e. if $\mathcal{L}(\phi', \partial_\mu\phi') = \mathcal{L}(\phi, \partial_\mu\phi)$. In this case one can also say that the Lagrangian is symmetric under that particular transformation.

Symmetries are relevant because they provide us with a powerful tool to describe our systems [7]. This is true both in QFT and in classical field theory. Indeed the Noether theorem states that each symmetry for the Lagrangian leads to a conservation law for a current/charge. This is extremely important because such a conservation can be used to infer information about the evolution of our particles. (Think for example of the conservation of energy)

Symmetries play a leading role also in deciding how to include the interactions between particles in the Lagrangians. The reason is that symmetries

¹It is customary to use the word Lagrangian referring to the Lagrangian density, although strictly speaking the two quantities are not the same thing. The Lagrangian is indeed the integral over the spatial-coordinates of the Lagrangian density. In the following we will also drop this distinction for brevity.

can be manifest. Imagine to have particles interacting with each other. In general it is hard to imagine how the interactions among them occur, and therefore how to build up the Lagrangian. However looking at the outcomes of such interactions it is often possible to recover some patterns (as in the spectra of the hadrons in Section *i.3*). Those are usually consequences of the symmetries of the Lagrangians. Once these are identified it is possible to build up operators containing the chosen particle field content and respecting such symmetries, i.e. invariant under the appropriate field transformations.

One example of Lagrangians with interactions is given by *quantum electrodynamics* (QED) [5]. We can start from the free fermion Lagrangian in (*i.2*). Our aim is to add an interaction term such that for the new Lagrangian the charge density vector current is conserved. Such a current can be represented by the term² $-Qe\bar{\psi}\gamma^\mu\psi$ where Qe is the charge of the particle described by ψ . Noether's theorem guarantees that such a current is conserved because the Lagrangian (*i.2*) is symmetric under the *global* transformation for the fields

$$\psi \rightarrow \psi' = e^{-iQ\vartheta}\psi. \quad (i.3)$$

Invariance under (*i.3*) allows us to change the phase of the field by the same amount at each space-time point. This appears unnecessarily restrictive in a *local* field theory. We shall therefore demand invariance with respect to the more general *local* transformation

$$\psi \rightarrow \psi' = e^{-iQ\vartheta(x)}\psi. \quad (i.4)$$

where now $\vartheta(x)$ is a real valued function of x . The invariance under (*i.4*) can be achieved by adding a new field, the gauge boson A^μ representing the photon, and two new terms in the free Lagrangian (*i.2*):

$$\mathcal{L}_{\text{QED}} = \bar{\psi}(i\gamma^\mu\partial_\mu - eQ\gamma^\mu A_\mu - m)\psi - \frac{1}{4}F_{\mu\nu}F^{\mu\nu}. \quad (i.5)$$

One can verify that the field A_μ must transform as $A_\mu \rightarrow A'_\mu = A_\mu + \frac{1}{e}\partial_\mu\vartheta(x)$ so that (*i.5*) is invariant for $\psi \rightarrow \psi'$ as in (*i.4*). The term $-\frac{1}{4}F_{\mu\nu}F^{\mu\nu}$ has been included to provide a kinetic term for the new field A_μ . $F_{\mu\nu}$ is defined as

$$F_{\mu\nu} = \partial_\mu A_\nu - \partial_\nu A_\mu. \quad (i.6)$$

This term is also symmetric and contains only the A_μ field.

The interaction term $-eQ\bar{\psi}\gamma^\mu A_\mu\psi$ of (*i.5*) is composed by two different elements. One is the coefficient Qe called *coupling*. The other is the part containing the fields and is called *operator*. This new term $-eQ\bar{\psi}\gamma^\mu A_\mu\psi$ will affect

²It can be shown that $\bar{\psi}\gamma^\mu\psi$ correctly behaves as a vector under Lorentz transformations. see e.g. [4].

the equation of motions of the particle ψ . The operator part describes how this modification occurs, while the coupling determines how strong the change is, namely how strong is the electromagnetic interaction.

i.4.3 Probability amplitudes, perturbation theory and Feynman diagrams



We have seen that the Lagrangians provide us with a set of field operators and couplings, but we must still work out their experimental consequences. First of all we must point out which are the quantities we aim at calculating. In a quantum-mechanical system the probability amplitude for a specific process to occur is the one important prediction we need. Once this is found, we can derive our physical observables as e.g. scattering cross sections³, decay rates and so on. We are thus trying to calculate expectation values of specific operators given by our Lagrangians over particle states.

We must now address the question of how to compute such probability amplitudes from the fundamental theory. Unfortunately it is usually not possible to solve explicitly the equations of motion for interacting theories like (i.5). Therefore we need to find approximate solutions. If the coupling is small enough, for example smaller than 1, it can be treated as a perturbative parameter. The approximate solutions can then be obtained treating the interacting terms as perturbations added to the free particle solution.

We will not attempt to describe in detail how to calculate the probability amplitudes. For our purposes it is enough to know that there exists a relation, developed by Feynman, between contributions to the expansions and diagrams representing the particle processes [4]. Such a correspondence is very useful not only to perform the calculations, but also to identify and visualize quite easily the different contributions.

Let us show a few examples of Feynman diagrams for QED described by the Lagrangian in (i.5). We remark that a field is represented in our diagrams by a line: a straight line for a lepton or a quark ψ , while we use a wiggly line for the photon A^μ . An interaction is a vertex point where ψ and A^μ lines meet. (i.5) tells us that whenever such an interaction occurs a coupling must arise and therefore we know that a diagram like the one in Figure i.2 (1) will be of order eQ .

The ψ lines in Figure i.2 contain arrows as well. They help in reading how the process happens. E.g. reading the diagram from left to right we can say

³The scattering cross section is a quantity reflecting the probability that a given scattering reaction will occur. It can be interpreted as the effective area that a target particle shows to the incoming one.



Figure i.2: Two Feynman diagrams for QED. The wiggly lines represent photons, while the straight lines are fermions (leptons or quarks). The diagram on the left contains only one vertex therefore it is of order Qe . The one on the right instead contains two vertices, thus it is of higher order $(Qe)^2$. The second diagram contains also an internal line: the propagator of a photon.

that a particle ψ is incoming, meets the photon and continues its course. But it is also possible to read the diagram from right to left. In this case we would have an antiparticle $\bar{\psi}$ incoming, interacting and going out. Or also it might as well represent a photon creating a particle antiparticle state.

Notice that where there is a vertex we must make sure that the conservation rules are satisfied. E.g. the vectorial sum of the momenta of all the outgoing and incoming particles must be zero.

We can also encounter diagrams with internal lines as the one in Figure i.2(2). Such internal lines are called *propagators* and they represent the propagation of free particles between two points in space-time. Their mathematical expressions can be obtained from the Lagrangian without interactions. For instance for the fermions this would be the Green function of the Dirac operator in (i.2)

$$i(\partial_\mu \gamma^\mu - m)S_F(x - y) = i\delta^4(x - y), \quad (i.7)$$

where $S_F(x - y)$ is the Fourier transform of the propagator. (i.7) can be solved by Fourier transforming both sides of the equation [4]. The solution reads

$$S_F(x - y) = \int \frac{d^4p}{(2\pi)^4} \tilde{S}_F(p) e^{-ip(x-y)} = \int \frac{d^4p}{(2\pi)^4} \frac{i(p_\mu \gamma^\mu + m)}{p^2 - m^2} e^{-ip(x-y)} \quad (i.8)$$

where $\tilde{S}_F(p)$ is the propagator.

A similar procedure can be applied to the photons, but then the operators to be used are in the last term of (i.5).

We can draw many different diagrams, each containing more and more lines and vertices. Perturbation theory lets us order them and determine which are the largest contributions.

In QED the perturbative parameter is the coupling, therefore it is enough to count how many vertices appear in each diagram to organize the expansions. For other theories the expansion might be organized in terms of different parameters. This is indeed the case of many *effective field theories*.

i.5 Effective field theories

The basic premise of all the effective theories is that dynamics at low-energies (or large distances) do not depend on the details of the dynamics at high-energies (or short distances) [6, 8, 9]. For example, if we want to study the motion of a macroscopic object, a ball, we will not care at all about the internal dynamics of the molecules, atoms, nuclei or quarks. These will not macroscopically produce any significant modification. The reason is that the macroscopic object lives at scales (meters) widely separated from e.g. the quarks' ones ($\approx 10^{-15}$ meters).

When we say *low energy physics* we mean those processes that happen at an energy smaller than a certain scale Λ . The value of such a scale depends on the particular system we study. Low-energy physics can be described using an effective Lagrangian that contains only a few degrees of freedom, ignoring additional degrees of freedom present at higher energies. This is clearly an approximation to the problem, which can always be improved adding corrections induced by the neglected energy scales. Eventually we will need to check that a more complete description including all the degrees of freedom (both heavy or light) gives the same outcomes as the effective theory, at least approximately.

So let us show how an effective field theory is built up. First remember that since we are talking about relativistic microscopic particles we are bound to use QFT. We must find a good set of variables to describe the dynamics of the system under study, which means we must select the relevant degrees of freedom. Thus we select the fields we want to include in our description and we build up the Lagrangian starting from them. As explained in Section i.4.2 to do this we find out the symmetries of the system and write down all the operators invariant under those symmetries. The resulting Lagrangian is a sum of operators O_i [8]

$$\mathcal{L} = \sum_i c_i O_i. \quad (i.9)$$

As remarked at the end of Section i.4.2 the operators O_i are built up of the fields and their derivatives. In (i.9) the constants c_i are couplings. They determine how important the operator they multiply is.

We are already facing a problem in (i.9). In principle there is no limit to the number of operators satisfying the symmetries we have required. But we cannot calculate the probability amplitudes with an infinite number of operators. However dimensional analysis offers us a way out. As was said in Section i.2, the Lagrangian density has dimension 4 in power of masses thus each term $c_i O_i$ in the sum (i.9) must have dimension 4. As was explained in Section i.4.3 this means that if the dimension of the operator O_i is d_i then the coupling c_i

must have dimension $-d_i + 4$.

There is another striking feature in (i.9) that we have not observed yet. The operators O_i contain only the light degrees of freedom, the light fields. On the other hand, as was mentioned at the beginning of this section, this Lagrangian must be equivalent to a complete one where also the heavy degrees of freedom are included. The information from these heavy degrees of freedom can only be encoded then in the c_i which therefore must somehow depend on the high energy scales, so on Λ .

This last consideration, together with the dimensional analysis done before, leads us to assume that the c_i -couplings scale as

$$c_i \approx \frac{1}{\Lambda^{d_i-4}}. \quad (i.10)$$

This assumption imposes an ordering in the operators of (i.9). If O_i has a large dimension d_i ($d_i > 4$) the corresponding coupling c_i is small. This means that the dynamics predicted by that term of the Lagrangian are suppressed and therefore can be neglected at a first approximation. The operators of (i.9) are thus ordered according to their dimensions. The larger the dimension of O_i the less important the corresponding term of \mathcal{L} is. As a consequence also the observables calculated in the effective field theory framework will be ordered in an expansion of terms of increasing importance. In Section i.6.3 we will explain how this expansion for the observables works and what are the quantities that determine the sizes of the various orders in the theory.

Beware that (i.10) is an assumption and it is anyway not enough to guarantee that the resulting expansions are convergent and ordered in terms of increasing importance. It is our task to check whether it is the case. This is indeed an important test for any effective field theory. Paper I will deal precisely with such a check in a very successful effective field theory: Chiral Perturbation Theory (ChPT) [10, 11]. This theory will be the subject of the rest of the thesis.

We stress also that while the form of the operators O_i in (i.9) can be inferred by the symmetries and the field content, we do not have any information on the couplings c_i . We need phenomenology to infer their values. This is also another limit of the effective field theories. Paper II will explore this problem in the case of ChPT.

i.6 Chiral Perturbation Theory

Chiral Perturbation Theory (ChPT) [10, 11] is the effective field theory of the strong interactions at low energy. In this section we first focus on QCD and on the need of an effective field theory approach [7, 8, 12, 13]. We show then the properties used to build up ChPT.

i.6.1 QCD and chiral symmetry

In Section i.4.2 it was remarked how important the Lagrangian is in our studies. In some cases it can be extremely difficult to extract useful predictions even when the Lagrangian is well-known. The usual way to calculate physical observables from the Lagrangian is through the use of perturbation theory. This means that if the coupling that governs the interaction is smaller than 1 it is possible to order the different contributions to physical observables in terms of increasing powers in the couplings and thus in decreasing order of importance. To obtain a prediction it is therefore sufficient to add enough contributions to this perturbative expansion.

In the case of QCD at low energy (i.e. $E < 1 \text{ GeV} \equiv \Lambda$), it is unfortunately not possible to achieve such a perturbative expansion. The coupling for the strong interaction α_s is small only for very energetic interactions, but for low-energy processes α_s can be very large. Indeed the value of α_s turns out to be dependent on the energies (technically it is called *running coupling*). α_s is very large around $300 \text{ MeV} \approx \Lambda_{\text{QCD}}$. One way to avoid this problem is to develop an effective theory and recover an expansion as the one explained in Section i.5. To build up such a theory let us first show the QCD Lagrangian⁴

$$\mathcal{L} = \sum_{i=u,d,s,c,b,t} \bar{\psi}_i (i\gamma^\mu \partial_\mu + g_s A^\mu \gamma_\mu - m_i) \psi_i - \frac{1}{4} G_{\mu\nu} G^{\mu\nu} \quad (i.11)$$

where A^μ is the gluon field and $G_{\mu\nu}$ is the gluon field strength tensor. It is defined as

$$G_{\mu\nu} = \partial_\mu A_\nu - \partial_\nu A_\mu - g_s f A_\mu A_\nu, \quad (i.12)$$

where the f -coefficient collects the structure constants of the group $SU(3)_{\text{colour}}$. Keep in mind that we have dropped colour indices in (i.11) and in (i.12). As you can see from (i.12) $G_{\mu\nu}$ contains only gluon fields and it is the operator for the gluon kinetic energy and its self-interactions. In (i.11) $g_s^2 / (4\pi) = \alpha_s$. The field ψ_i refers to a quark of type (flavour) i and of mass m_i . For completeness we should also add a term as $\theta G_{\mu\nu} G_{\alpha\beta} \epsilon^{\mu\nu\alpha\beta}$ to (i.11), which is the so called θ -term. The numerical value of the coupling θ is very small ($\theta < 10^{-10}$). A lot of interesting physics arises from such a term. However we will not consider its effects in here, since it is beyond the scope of this thesis. For more detailed explanations we recommend [7, 11].

The QCD Lagrangian in (i.11) has a very special feature. To make it evident

⁴(i.11) is achieved similarly to the QED Lagrangian in (i.5). This time \mathcal{L} is required to be invariant under local transformations in $SU(3)_{\text{colour}}$. The reader can find the definition of the group $SU(n)$ in the text after (i.15).

we must first define left-handed and right-handed fields starting from the ψ_i :

$$\psi_R = \frac{1}{2}(1 + \gamma_5)\psi \quad \psi_L = \frac{1}{2}(1 - \gamma_5)\psi \quad (i.13)$$

and thus $\psi = \psi_L + \psi_R$. The QCD Lagrangian rewritten in terms of these left- and right-handed fields and after using some γ -matrix algebra reads

$$\begin{aligned} \mathcal{L} = & \sum_{i=u,d,s,c,b,t} \bar{\psi}_{iL}(i\gamma^\mu\partial_\mu + g_s A^\mu \gamma_\mu)\psi_{iL} + \bar{\psi}_{iR}(i\gamma^\mu\partial_\mu + g_s A^\mu \gamma_\mu)\psi_{iR} \\ & - m_i \bar{\psi}_{iL}\psi_{iR} - m_i \bar{\psi}_{iR}\psi_{iL} - \frac{1}{4}G_{\mu\nu}G^{\mu\nu}. \end{aligned} \quad (i.14)$$

The Lagrangian in (i.14) has most terms diagonal in the indices L, R , while the mass terms are off diagonal. If we drop these mass terms the Lagrangian is invariant under the following rotations in the flavour indices of the left- and right-handed fields⁵:

$$\begin{aligned} \psi_{iR} &\rightarrow \psi'_{iR} = (g_R)_{ij}\psi_{jR} & g_R &\in SU(n_f)_R \\ \psi_{iL} &\rightarrow \psi'_{iL} = (g_L)_{ij}\psi_{jL} & g_L &\in SU(n_f)_L \end{aligned} \quad (i.15)$$

where $SU(n)$ is the *special unitary group* defined as the group of $n \times n$ unitary matrices with determinant 1. It has dimension $n^2 - 1$. In (i.15) $g_{R(L)}$ are *global* transformations, i.e. they do not depend on the space-time coordinates.

Of course the masses are not really zero, but for the less massive quarks (u,d,s)⁶ this might be a good approximation. $SU(n_f)_{L(R)}$ becomes then $SU(3)_{L(R)}$ and the QCD Lagrangian acquires an approximate $SU(3)_L \times SU(3)_R = G$ global symmetry which is the so-called *chiral symmetry*. From now on we restrict ourselves to these light quarks. We will see how to include the heavy quarks in this description later on when we will deal with another effective field theory: Heavy Quark Effective Theory.

Chiral symmetry should however be visible in the spectrum of the (light) hadrons. If this symmetry were exactly realized hadrons with the same mass and spin but opposite in parity should appear (see for an explanation e.g. [12]). But this turns out not to be the case. One could point out that the symmetry is not really realized because the masses of u, d , and s quarks are small but not zero. On the other hand if this were the only source of the symmetry breaking there would still be pair of hadrons with the same spin and with similar

⁵In fact the Lagrangian is also invariant under transformations of $U(1)_V$ ($\psi \rightarrow \psi' = e^{i\theta}\psi$) and of $U(1)_A$ ($\psi \rightarrow \psi' = e^{i\theta\gamma_5}\psi$). The first leads to the conservation of the baryon number. The second is only a symmetry of the classical Lagrangian but it is broken at the quantum level. Their effects are beyond the scope of this thesis and therefore hereafter we drop them.

⁶It is actually an even better approximation for only u and d quarks. The chiral symmetry group is then $SU(2)_L \times SU(2)_R$ and in this case we would talk about two-flavour ChPT.

masses but opposite parity. I.e. the spectrum would at least approximately show the existence of parity doublets. If one looks at the spectrum this is clearly not the case: there are no obvious parity partners with a mass close to e.g. the π mesons. The possible candidates are very far away in mass and have in general very different properties.

Another mechanism to break the symmetry exists. This is called *spontaneous symmetry breaking* (SSB). We will not explain here the details of this procedure. We refer the reader to [7, 13] for further explanations. Here it suffices to know that this corresponds to have a symmetry in the Lagrangian that is not satisfied by the vacuum state. This is instead only symmetric under transformations of a subgroup of the original symmetry. In the case of low energy QCD the subgroup is⁷ $H = SU(3)_V$. The notation used to summarize the situation is

$$G = SU(3)_L \times SU(3)_R \longrightarrow H = SU(3)_V$$

The so-called Goldstone theorem dictates that this SSB gives rise to a certain number n of massless particles known as *Goldstone bosons*. n is the number of broken generators. In QCD we have 16 generators for the group $SU(3)_L \times SU(3)_R$ and 8 generators in the final group $SU(3)_V$. The number of broken generators is $16 - 8 = 8$, so 8 Goldstone bosons should arise.

Since chiral symmetry for QCD is also explicitly broken, due to the presence of the small quark mass terms, it is possible to show that the Goldstone bosons arising are not massless and are thus called *pseudo-Goldstone bosons*. Their masses must however be rather small since they arise from the light quark masses. They are then identified with the 8 lightest mesons reported in Figure i.1.

We end this section with a remark. It is an assumption that the SSB mechanism for chiral symmetry takes place. Its correctness is confirmed by several phenomenological observations [12, 13] and a few theoretical indications. One of them was cited above: the non-existence of parity doublets in the hadronic spectrum.

i.6.2 Local chiral symmetry

Before entering into the construction of ChPT we need another ingredient: the *external fields formalism*. This was introduced in [11] to simplify the calculations and to include interactions like the electromagnetic and some of the weak ones. Furthermore it allows to perform calculations maintaining the chiral symmetry throughout. This section is devoted to introduce these fields that will be used in Section i.6.3 to build up the ChPT Lagrangian.

⁷Actually \mathcal{L}_{QCD} is only approximately symmetric under $SU(3)_V$ transformation. It would be an exact symmetry if $m_u = m_d = m_s$.

We consider again the Lagrangian for three-flavour QCD dropping the mass terms and the gluon tensor field $G^{\mu\nu}$. But we incorporate now also a few new fields called *external fields* (or *sources*)

$$\begin{aligned} \mathcal{L}_{m_i=0} = & \sum_{i,j=u,d,s} \bar{\psi}_{iL}(i\gamma^\mu\partial_\mu + g_s A^\mu\gamma_\mu)\psi_{iL} + \bar{\psi}_{iR}(i\gamma^\mu\partial_\mu + g_s A^\mu\gamma_\mu)\psi_{iR} \\ & - \bar{\psi}_{iL}(s - ip)_{ij}\psi_{jR} - \bar{\psi}_{iR}(s + ip)_{ij}\psi_{jL} + \bar{\psi}_{iL}(v_\mu - a_\mu)_{ij}\psi_{jL} + \bar{\psi}_{iR}(v_\mu + a_\mu)_{ij}\psi_{jR}. \end{aligned} \quad (i.16)$$

In (i.16) there are four new fields s, p, v_μ, a_μ . These depend on the space-time coordinates and are Hermitian 3×3 matrices. As was stressed in Section i.6.1, chiral symmetry for the massless QCD Lagrangian is a global symmetry, but thanks to these new sources it is possible to promote⁸ it to a *local symmetry* for the Lagrangian in (i.16). We assume the operator $(g_L, g_R) \in SU(3)_L \times SU(3)_R$, depending now on the space-time coordinates, to act on the fields as

$$\begin{aligned} \psi_L &\rightarrow g_L \psi_L & \psi_R &\rightarrow g_R \psi_R & (s + ip) &\rightarrow g_R(s + ip)g_L^\dagger \\ l_\mu \equiv (v_\mu - a_\mu) &\rightarrow g_L l_\mu g_L^\dagger - i\partial_\mu g_L g_L^\dagger & r_\mu \equiv (v_\mu + a_\mu) &\rightarrow g_R r_\mu g_R^\dagger - i\partial_\mu g_R g_R^\dagger. \end{aligned} \quad (i.17)$$

By plugging the transformation rules (i.17) in (i.16) it is possible to show that the Lagrangian (i.16) is invariant under local chiral transformations. This is due to the particular transformations of the fields l_μ and r_μ .

Normally the external fields we have introduced are identified with specific quantities to include new interactions. For example if we identify the field v_μ with a photon field eQA_μ where

$$Q = \frac{1}{3} \begin{pmatrix} 2 & 0 & 0 \\ 0 & -1 & 0 \\ 0 & 0 & -1 \end{pmatrix} \quad (i.18)$$

we can recover the electromagnetic interactions. Furthermore the field s provides us with a very elegant way to include also the quark masses. We can indeed identify

$$s = \mathcal{M} = \begin{pmatrix} m_u & 0 & 0 \\ 0 & m_d & 0 \\ 0 & 0 & m_s \end{pmatrix}. \quad (i.19)$$

i.6.3 Chiral Perturbation Theory formalism

We are now ready to build up the effective field theory for QCD at low energy. We do it step by step.

⁸Note that there are no kinetic terms for the external fields, hence they are not gauge fields.

First we must select the degrees of freedom. As was mentioned at the beginning of Section *i.6.1*, in the low-energy domain a thorough analysis of the QCD dynamics in terms of quarks and gluons is a highly non perturbative problem. A description in terms of the hadronic states seems more adequate. We have seen that there are 8 pseudo-Goldstone bosons arising from the SSB of chiral symmetry identified with the mesons in the octet of Figure *i.1*. Notice that there is a mass gap separating these pseudoscalars from the rest of the hadronic spectrum, the next particle in mass, the ρ meson, being away from the octet. This allows us to build an effective field theory containing only the Goldstone bosons as degrees of freedom and basically forgetting about the quarks and gluons. The fields representing the mesons of the octet must be organized in a convenient way. Group theory helps us in this respect. Keep in mind that the SSB pattern is

$$G = SU(3)_L \times SU(3)_R \longrightarrow H = SU(3)_V.$$

It is possible to show that there is a one to one correspondence between the Goldstone bosons and the elements of the quotient G/H [12]. This is defined as the set of all the left cosets $\{gH|g \in G\}$. The correspondence is due to the fact that the space G/H is of dimension $n_G - n_H = 8$. One then needs as many coordinates to label the elements of G/H as there are Goldstone bosons. Thus we can identify the fields $\phi_i(x)$ representing the Goldstone bosons with the coordinates of G/H . The fields are seen as a mapping between the x space-time and G/H .

We make use of this correspondence to find a convenient way to collect our Goldstone fields. To show how we need a bit of group algebra. If we pick an element $g = (g_L, g_R) \in G$ we can uniquely characterize the corresponding left coset gH through the matrix $U = g_R g_L^\dagger \in SU(3)$. This corresponds to pick the representative of each coset such that the identity transforms the left sector. Indeed for any element $(g_L h, g_R h)$ in the coset gH we have

$$(g_L h, g_R h) = (g_L h, g_R g_L^\dagger g_L h) = (1, U)(g_L, g_L)h. \quad (i.20)$$

Since $(g_L, g_L)h$ also belongs to H it follows that $gH = (1, U)H$.

Thanks to the correspondence between Goldstone bosons and the left cosets, U is a suitable candidate to collect the Goldstone fields. How does the matrix U transform under $g' = (g'_L, g'_R) \in G$? We need to show what happens to the coset represented by U

$$g'gH = (g'_L, g'_R)(1, U)H = (g'_L, g'_R U)H = (1, g'_R U g'_L{}^\dagger)(g'_L{}^\dagger, g'_L{}^\dagger)H. \quad (i.21)$$

So when we move from the coset gH to $g'gH$, U must transform as

$$U \rightarrow g'_R U g'_L{}^\dagger. \quad (i.22)$$

Remember that we are considering local transformations, which means that g_L, g_R and U depend all on x .

Summarizing, we have discovered that the $SU(3)$ matrix U is suitable to collect the Goldstone bosons and we also know its transformation properties (i.22) under chirality. Now we can decide in which way the Goldstone fields are organized inside U . A customary choice is

$$U = \exp\left(\frac{i\sqrt{2}}{F_0}\phi\right), \quad (i.23)$$

where ϕ is a hermitian 3×3 matrix:

$$\phi = \begin{pmatrix} \frac{1}{\sqrt{2}}\pi^0 + \frac{1}{\sqrt{6}}\eta & \pi^+ & K^+ \\ \pi^- & -\frac{1}{\sqrt{2}}\pi^0 + \frac{1}{\sqrt{6}}\eta & K^0 \\ K^- & \bar{K}^0 & -\frac{2}{\sqrt{6}}\eta \end{pmatrix}. \quad (i.24)$$

Once we have selected the object we want to work with, i.e. the fields ϕ organized in the matrix U in (i.23), we can focus on the symmetries of the Lagrangian. If we want an effective field theory for the strong interactions we need the Lagrangian to satisfy the same symmetries as QCD. Therefore we will need Lorentz, parity, time-reversal invariance and also local chiral symmetry (which now is also a symmetry for \mathcal{L}_{QCD} thanks to the external fields). To write down all the possible operators we introduce the notation

$$\langle A \rangle = \text{Tr}A \quad (i.25)$$

where A is an operator and the trace is over the flavour indices. Now we are ready to find the most general operators starting from our building block, the U matrix of (i.23) [13]. As was mentioned in Section i.5, we order the possible operators in the Lagrangian according to their dimensions. At order p^0 we cannot form operators with derivatives because they would introduce a dimension (a derivative is equivalent to a momentum). Therefore we are left with:

$$\mathcal{L}_0 = \alpha_0 \langle U^\dagger U \rangle + \alpha_1 \det U + \alpha_1^* \det U^\dagger. \quad (i.26)$$

(i.26) is just a constant since $U \in SU(3)$ thus $U^\dagger U = 1$ and $\det U = 1$. A constant clearly does not provide us with any information for the dynamics of the system and thus it can be dropped. Now we can try to go to order p . At this order though we cannot write down any invariant operator. If we include a partial derivative ∂_μ we would need two of them to preserve Lorentz invariance, so the corresponding operator would be of order p^2 . As a

consequence we cannot have operators at order p (or at any odd power of p). We arrive then at order p^2 and the Lagrangian reads

$$\mathcal{L}_2 = \frac{F_0^2}{4} \langle D_\mu U^\dagger D^\mu U + \chi U^\dagger + U \chi^\dagger \rangle \quad (i.27)$$

where the external fields introduced in Section *i.6.2* are hidden in D_μ and in χ

$$D_\mu U \equiv \partial_\mu U - i r_\mu U + i U l_\mu \quad \chi \equiv 2B_0(s + ip) = 2B_0 \mathcal{M}. \quad (i.28)$$

As you see in the Lagrangian of (*i.27*) we have also introduced two constants in front of the operators: F_0 and B_0 . These are two couplings and they have the role in ChPT of the c_i in (*i.9*). As was said earlier we need to infer their values from experiments. In order to identify from which physical observables we can find out their values, we must look at the operators they multiply and check which are the processes they are responsible for. This will partially be the subject of the next section.

In the next sections we will often talk about the expansion that ChPT leads to. This is organized in powers of momenta p and mass. Let us try to explain a bit better this point. When we want to calculate an observable we need to take matrix elements of the operators in the Lagrangian. At sufficiently low energies, such matrix elements are small since each derivative becomes a factor of the momentum p . From the discussion in Section *i.5* the coefficient of an operator with d derivatives behaves as $1/\Lambda^{d-4}$. Therefore the effect of a d derivatives vertex is of order p^d/Λ^{d-4} and at an energy small compared to Λ , the more derivatives are involved the smaller is the contribution to the matrix element. In the following we will talk only about the momentum expansion, but we should keep in mind that it is also in fact a mass expansion. This is both a consequence of what was said in Section *i.2*, but also because we are restricting ourselves to low-energies so the masses and the momenta of the particles are of the same order of magnitude, less than 1 GeV. Notice that in the Lagrangian (*i.27*) the external fields appear as well. The fields l_μ and r_μ count as a derivative so as p , while s and p contribute as p^2 .

***i.6.4* Decay constants and meson masses at lowest order ($\mathcal{O}(p^2)$)**

In this section we aim at showing shortly the meaning of the coupling constants arising in the leading order Lagrangian (*i.27*) of ChPT. In this way we also show briefly how we calculate physical observables with this theory [8].

First of all we need to expand the exponential U (*i.23*) in the meson fields. For our purposes it is enough to arrive at the second order

$$U = 1 + i \frac{\sqrt{2}}{F_0} \phi - \frac{1}{F_0^2} \phi^2 + \dots, \quad (i.29)$$

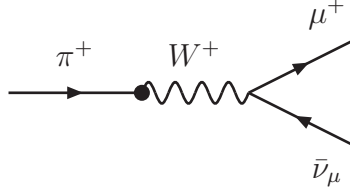


Figure *i.3*: The Feynman diagram corresponding to the leptonic decay for the π^+ meson. The field a^μ in (i.30) can be identified with the W^+ gauge boson responsible for the weak decays. Notice that now we use a straight line to represent the whole meson π^+ . This is due to the fact that our relevant degrees of freedom are not the quarks any longer, but the mesons, as explained in Section *i.5*. The black dot is the interaction vertex $\langle a_\mu \partial \phi^\mu \rangle$ of ChPT, whose coupling is F_0 .

and a similar expansion holds for U^\dagger . We can substitute these expansions in the Lagrangian (i.27). From the term $D_\mu U^\dagger D^\mu U$ we obtain, among the other terms,

$$\frac{1}{2} \langle \partial_\mu \phi \partial^\mu \phi \rangle - i\sqrt{2}F_0 \langle a_\mu \partial \phi^\mu \rangle + \dots \quad (i.30)$$

In (i.30) there are two terms. In the first one the kinetic terms for the pseudoscalar mesons in the octet are collected. In the second one instead we have an interaction term of the mesons in ϕ with the external axial field a_μ . This interaction is the one responsible for the leptonic decays of the mesons. The corresponding Feynman diagram for a decay of a π^+ is depicted in Figure *i.3*. The coupling of such an interaction is F_0 . If we want to calculate the probability amplitude of the π^+ meson to decay we need to evaluate the matrix element between the state $|\pi^+\rangle$ and the vacuum $\langle 0|$ of the hadronic part of the operator describing the weak interaction

$$\langle 0 | i\sqrt{2}F_0 \partial^\mu \pi^+ | \pi^+ \rangle \equiv i\sqrt{2}F_\pi p^\mu. \quad (i.31)$$

From (i.31) we infer that the coupling F_0 is nothing else than the physical decay constant of the pion F_π at the lowest order in the chiral expansion. Therefore if we content us with lowest order predictions we have a way to measure F_0 .

We can also discover something about the masses of our mesons. We focus on the term $\chi U^\dagger + U \chi^\dagger$ in (i.27) and substitute the expansion in (i.29). We obtain the term

$$\langle -2B_0 \mathcal{M} \phi^2 \rangle \dots \quad (i.32)$$

Evaluating explicitly the traces in (i.32) it is possible to recognize the mass terms for the mesons. We define $\hat{m} = (m_u + m_d)/2$ and set $m_u = m_d = \hat{m}$ ⁹. At leading order the several masses read

$$M_\pi^2 = 2B_0\hat{m}, \quad M_K^2 = B_0(\hat{m} + m_s), \quad M_\eta^2 = \frac{2}{3}B_0(\hat{m} + 2m_s). \quad (i.33)$$

From (i.33) we conclude that the meson masses depend linearly on the quark masses. (i.33) leads to a relation between the squared meson masses known as the Gell-Mann Okubo relation

$$3M_\eta^2 = 4M_K^2 - M_\pi^2. \quad (i.34)$$

If we substitute in (i.34) the experimental masses quoted in Figure i.1 we find less than 10% discrepancy from experiments. Considered that (i.34) is valid at the lowest order in the chiral expansion and up to $\mathcal{O}(m_u - m_d)$ corrections this is a very good result.

Notice that the relations in (i.33) can be used to estimate the values of the quark masses. These are free parameters for QCD and thus unknown.

There is still one coupling in (i.27) whose meaning is not entirely clear. It is B_0 . We have seen it appears as a coefficient of proportionality in (i.33). However it can be also related to another quantity: the vacuum expectation value of the scalar bilinears $\bar{\psi}_i\psi_i$. In (i.16) the operator $\bar{\psi}_i\psi_i$ is coupled with s_{ij} to preserve chiral symmetry. The operator $\bar{\psi}_i\psi_i$ thus corresponds to the term $2B_0(U + U^\dagger)_{ii}$ in \mathcal{L}_2 . Substituting in the expansion of U we obtain $2B_0(U + U^\dagger)_{ii} = 4B_0 + \dots$ where the ellipsis stands for higher order terms in the expansions of U . If we evaluate the expectation value of this operator on the vacuum state we find the result

$$\langle 0|\bar{\psi}_i\psi_i|0\rangle = -F_0^2 B_0. \quad (i.35)$$

Since $\langle 0|\bar{\psi}_i\psi_i|0\rangle$ cannot be invariant under separate right handed and left handed $SU(3)$ transformations, the quantity on the left side of (i.35) characterizes the non invariance of the QCD vacuum state under chiral symmetry. B_0 is then a measure on how the vacuum breaks chiral symmetry. The masses of the mesons have the form

$$M^2 = m_q \times (-\langle 0|\bar{\psi}_i\psi_i|0\rangle) \times \frac{1}{F_0^2} \quad (i.36)$$

i.e. they depend on both the explicit (through the quark mass m_q) and spontaneous (through the vacuum condensate) breaking of chiral symmetry.

⁹Thus we also neglect the mixing term arising between the η and the π^0 .

Notice that (i.36) tells us that in principle to measure B_0 we need to have full experimental control on the masses (both of the mesons and of the quarks). But this is not possible, since we cannot vary the masses in experiments. As will also be pointed out in Section i.9 and in paper II this is the problem behind all the determinations of the couplings related to the masses [14].

i.6.5 Power counting

In Section i.5 we have already indicated that the effective Lagrangian can be written in terms of a sum of Lagrangians ordered by the dimensions of their operators as in (i.9). In ChPT after the $\mathcal{O}(p^2)$ Lagrangian we can decide to go to higher order and build up the $\mathcal{O}(p^4)$ one containing operators of dimension 4

$$\begin{aligned}
\mathcal{L}_4 = & L_1 \langle D_\mu U^\dagger D^\mu U \rangle^2 + L_2 \langle D_\mu U^\dagger D_\nu U \rangle \langle D^\mu U^\dagger D^\nu U \rangle \\
& + L_3 \langle D^\mu U^\dagger D_\mu U D^\nu U^\dagger D_\nu U \rangle + L_4 \langle D^\mu U^\dagger D_\mu U \rangle \langle \chi^\dagger U + \chi U^\dagger \rangle \\
& + L_5 \langle D^\mu U^\dagger D_\mu U (\chi^\dagger U + U^\dagger \chi) \rangle + L_6 \langle \chi^\dagger U + \chi U^\dagger \rangle^2 \\
& + L_7 \langle \chi^\dagger U - \chi U^\dagger \rangle^2 + L_8 \langle \chi^\dagger U \chi^\dagger U + \chi U^\dagger \chi U^\dagger \rangle \\
& - i L_9 \langle F_{\mu\nu}^R D^\mu U D^\nu U^\dagger + F_{\mu\nu}^L D^\mu U^\dagger D^\nu U \rangle \\
& + L_{10} \langle U^\dagger F_{\mu\nu}^R U F^{L\mu\nu} \rangle, \tag{i.37}
\end{aligned}$$

where the operator $F_{\mu\nu}^{L(R)}$ contains only the external fields l_μ (r_μ).

Each of the operators in (i.27) and (i.37) can contain in principle as many mesons as wanted. These arise from the expansions of the U matrix, as was shown in Section i.6.4. As a consequence we can draw infinitely many Feynman diagrams. We clearly cannot calculate contributions from an infinite set of diagrams¹⁰. One might wonder whether with ChPT we can predict any quantity at all.

Luckily also the Feynman diagrams, as the Lagrangians, can be ordered in a systematic way according to the expected size of their contributions. This is once again done through a power counting of the momenta in the different parts of the diagram. Thus if we want to calculate an observable we first must decide at which order in the momentum expansion we want to stop to get the desired precision. Then we calculate as many diagrams as needed.

The procedure is illustrated in Figure i.4.

A *tree level* diagram (see Figure i.4(1)) with a vertex from \mathcal{L}_2 in (i.27) counts as two powers of momenta since it always contains two derivatives or M^2 .

¹⁰Unless we manage to find some recursive formulas to resum the infinite series, but this is a very difficult task and not yet accomplished.

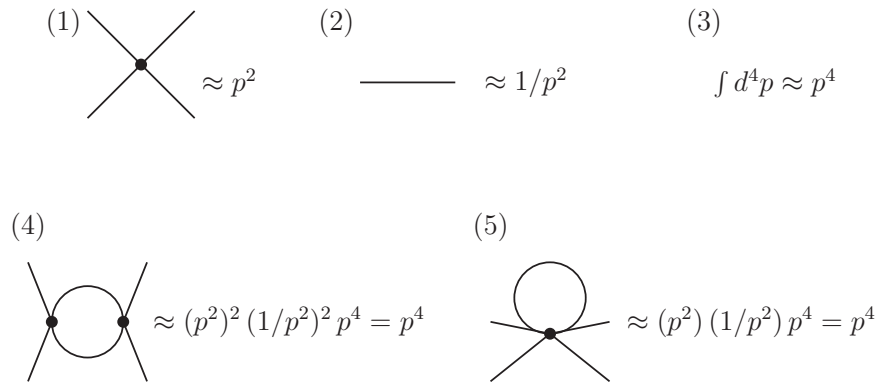


Figure i.4: In the upper part of the figure we list the power counting rules. While the two diagrams below are loop diagrams [13]. More details about the rules and the loops diagrams can be found in the text.

An internal line (Figure i.4 (2)) counts as $1/p^2$. This is because from (i.27) the mathematical expression of the propagator is $1/(p^2 - m^2)$.

Finally there are the *loop diagrams* as (4) and (5) in Figure i.4. In those diagrams appear internal lines in closed loops whose momenta are not constrained by the conservation of momentum for each vertex. Therefore when we encounter such kind of diagrams we must integrate over all the possible internal momenta running in the loop. This integration counts as p^4 and is shown by the counting rule in Figure i.4 (3). The two loop diagrams (4) and (5) in Figure i.4 turn out to both count as p^4 . As long as p is small, the momentum is a good perturbative parameter of our expansion and thus p^2 diagrams give larger contributions than the p^4 ones.

There is an issue that we have not addressed yet. We said before that when we encounter a loop diagram we need to integrate all the momenta over all the spacetime. This often leads to diagrams that give infinitely large contributions. On the other hand the resulting physical observables must not be infinite.

In ChPT and in general in QFT such divergencies are canceled with a *renormalization procedure*. It basically consists of including in the theory other sources of infinities such that they cancel the loop ones. Similar approaches have been powerful and successful also in other quantum field theories as e.g. QED where a similar problem arises. In ChPT the “counter” infinities are introduced by redefining the couplings of the higher order Lagrangian \mathcal{L}_4 in the

following way

$$L_i = L_i^r(\mu) - \frac{\Gamma_i}{32\pi^2} \lambda_0 + \dots \quad (i.38)$$

In (i.38) λ_0 contains the divergent part. Γ_i are constants chosen such that the λ_0 divergencies correctly cancel with the loop ones. $L_i^r(\mu)$ is the finite part of the coupling L_i and it will in general depend on a scale μ called *renormalization scale*. This scale is introduced to make sure that the results are dimensionally consistent, but it is an arbitrary scale. Eventually it is important to check that the predictions for the physical observables are independent of μ .

Therefore to renormalize a loop diagram of order p^4 we use a tree level diagram with a vertex from \mathcal{L}_4 (i.37) which is also of order p^4 . It is important that the two diagrams are of the same order, otherwise it is not possible to sum them up and correctly cancel the divergencies.

All what was said so far is not only valid at the p^4 order. In general to calculate a physical observable at order p^{2n} we must include the loop diagrams with vertices from the Lagrangians $\mathcal{L}_{2n'}$ with $n' < n$, and also tree level diagrams from \mathcal{L}_{2n} .

i.6.6 The main prediction of ChPT at $\mathcal{O}(p^4)$: chiral logarithms

One might wonder how the results based on one loop calculations look like. We notice first that the quantities predicted by ChPT are always dependent on the squared momenta of the external mesons and the meson masses. Usually the results are split in different contributions, each of them attributed to a set of diagrams. The tree level Feynman diagrams usually have a polynomial dependence on the momenta and masses.

From the loop diagrams arise also more complicated functions of the masses and of the momenta that typically have a logarithmic form. Thus they are usually called *chiral logarithms*. Let us show how they come out. As an example we take the easiest loop function that one might encounter in doing loop calculations

$$\frac{1}{i} \int \frac{d^4k}{(2\pi)^4} \frac{1}{k^2 - M^2} \quad (i.39)$$

where M is the mass of the particle in the loop. (i.39) is a loop integral where the propagator $1/(k^2 - M^2)$ gets integrated over all the possible momenta k . (i.39) enters in the evaluation of diagrams such as (5) in Figure i.4 or the one in Figure i.5. We do not go into the details on how this integral is solved. The procedure to arrive to the solution in (i.42) below is called *regularization* and can be found in [15]. We just say that to compute (i.39), the integral is performed in $d = 4 - 2\epsilon$ dimensions. In order to maintain correct dimensionality

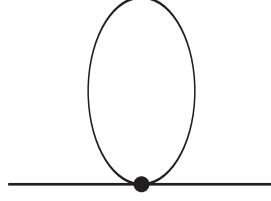


Figure i.5: An example of one-loop diagram contributing to the meson masses. The vertex comes from \mathcal{L}_2 in (i.27).

i

while regularizing the integral we shall also modify the measure

$$\int \frac{d^4k}{(2\pi)^4} \rightarrow \mu^{2\epsilon} \int \frac{d^d k}{(2\pi)^d}, \quad (i.40)$$

while μ is a arbitrary parameter used to recover the correct dimensions and has dimension of a momentum. It is the same scale appearing in (i.38). So the integral reads in d dimensions

$$A(M^2) = \frac{\mu^{2\epsilon}}{i} \int \frac{d^d k}{(2\pi)^d} \frac{1}{k^2 - M^2}. \quad (i.41)$$

The result turns out to be written in terms of an expansion in ϵ

$$A(M^2) = \frac{M^2}{16\pi^2} \left[\lambda_0 - \ln \left(\frac{M^2}{\mu^2} \right) \right] + \mathcal{O}(\epsilon), \quad (i.42)$$

where $\lambda_0 = 1/\epsilon + \text{constants}$. λ_0 of (i.42) is again the same appearing in (i.38).

We need the result when $d = 4$ i.e. when $\epsilon \rightarrow 0$. Thus the λ_0 term in (i.42) is divergent. The divergency is canceled thanks to the redefinition of the couplings as shown in (i.38) of Section i.6.5. The logarithms instead remain present in the final results of the physical observables. They also turn out to be the largest contributions in each order (after the leading one).

To understand this we can consider, as an example, the diagram in Figure i.5 [9]. It contributes to the meson masses at one loop. The vertex is from \mathcal{L}_2 and it contributes with a coefficient F_0^{-2} . The contribution from the loop integral is instead $A(M^2)$ in (i.42). The $\mathcal{O}(p^2)$ term is listed in (i.33) for the different mesons. After the divergencies are canceled, the mass gets contributions of the size

$$\mathcal{O}(p^2) \approx m_0^2, \quad \mathcal{O}(p^4)_{\text{loop}} \approx \frac{m_0^4}{(4\pi)^2 F_0^2} \ln \frac{m_0^2}{\mu^2}. \quad (i.43)$$

The tree-level diagram with vertices from \mathcal{L}_4 contributes to the mass as $L_i^r(\mu)m_0^4/F_0^2$. As discussed in Section (i.5), the couplings scale in powers of Λ so to be suppressed order by order. At $\mathcal{O}(p^2)$ the coupling is F_0^2 , therefore we can assume $L_i^r(\mu) \approx F_0^2/\Lambda^2$. So the size of the corresponding contribution to the masses is

$$\mathcal{O}(p^4)_{\text{tree diagram}} \approx \frac{m_0^4}{\Lambda^2}. \quad (i.44)$$

We can compare the $\mathcal{O}(p^4)_{\text{loop}}$ with the $\mathcal{O}(p^4)_{\text{tree diagram}}$. Since $\Lambda \approx 1$ GeV in ChPT and since $F_0 \approx 90$ MeV, we have $4\pi F_0 \approx \Lambda$. At a first sight $\mathcal{O}(p^4)_{\text{tree diagram}} \approx \mathcal{O}(p^4)_{\text{loop}}$. However $2 \lesssim \ln \mu^2/m_0^2 \lesssim 4$ choosing¹¹ $\mu = \Lambda = 1$ GeV and $m_0 \lesssim 0.4$ GeV. Thus a term with a logarithm is somewhat enhanced relative to the corresponding tree-level contributions. This means that the terms containing chiral logarithms give us an indication of the size of the higher order corrections and often correspond to the most important part of the predictions in ChPT at higher orders. This is also the reason why, in evaluating observables in ChPT, one first focuses on calculating the loop diagrams.

Anyway keep in mind that if we want to predict an observable precisely at the selected order the chiral logarithms alone are usually not enough. We also need to know the contributions of the polynomials and the couplings they contain. Moreover if one is willing to go to even higher orders e.g. $\mathcal{O}(p^6)$ the couplings of the \mathcal{L}_4 Lagrangian will also be multiplied by chiral logarithms. Their determination is therefore an important task, but unfortunately a non straightforward one.

In ChPT it is especially made difficult by their number. We have already seen that in the leading order Lagrangian of (i.27) two unknown couplings appear (F_0 and B_0). At $\mathcal{O}(p^4)$ there are 10 more, the L_i of (i.37). When we go to even higher order $\mathcal{O}(p^6)$, 90 extra couplings, denoted C_i , have been found [16]. Inevitably, whenever a precise prediction is wanted, also a precise determination of such couplings is needed.

i.7 Hard pion Chiral Perturbation Theory

We have studied so far a theory suitable to describe interactions between mesons at low energies, namely *soft* mesons. What happens if a *hard* meson arises? As explained in Section i.6.5, the power counting of ChPT breaks down in this limit. The momentum of the mesons would not be any longer a good perturbative parameter and not even the ordering of the Lagrangians would work properly. For example in this case operators containing 4 derivatives, as the ones of \mathcal{L}_4 would not necessarily lead to smaller contributions than the

¹¹This is the usual choice for μ in ChPT, but remember that μ is an arbitrary scale.

ones with 2 derivatives of \mathcal{L}_2 . The typical process affected by such an issue is, for example, the decay of a heavy particle into one (or more) light hadrons. In this case the outgoing mesons produced can acquire a large energy that prevents the use of ChPT.

Nevertheless for some processes it is important to know the mass dependence of the amplitudes, and thus the contributions of the chiral logarithms, in the whole energy range. The reason will be shortly explained in Section *i.9*. Keep in mind that a chiral logarithm has the form $m^2 \log m^2/\mu^2$ with m the mass of the light mesons in the loop, as seen in (*i.42*).

In such a framework performing loop calculations for hard mesons seems to be unreasonable, but it turns out not to be the case. To understand this, we first notice that the chiral logarithms are obtained from the loop integrals. The part of the integral responsible for such logarithms is the infrared [10,17]. Namely where the integration variable k of (*i.41*) is small. At least one of the particles inside of the loop is soft in that regime. This indicates that the chiral logarithms are still calculable, even though the momenta of the external mesons are large [18–20].

The problem then becomes whether the hard external mesons do affect the results for the chiral logarithms through operators containing many derivatives. Let us try to explain this point a bit better with an example. We consider the loop diagram in Figure *i.5*. In standard ChPT the vertex of the diagram contains an operator from the Lagrangian \mathcal{L}_2 so with two derivatives (or a m^2). For soft mesons the insertion of an operator with more derivatives would lead to a diagram of higher order. For example if it were an operator of \mathcal{L}_4 the loop diagram in Figure *i.5* would be of order p^6 . If the external mesons are soft (p is small) the higher order diagram is suppressed compared to the leading one. But if the external mesons are hard the higher order diagram is not suppressed and it must be included in the calculation. These new diagrams might spoil the dependence on the masses and lead to large terms with different dependencies on the light meson masses. We are talking about e.g. terms proportional to m which are larger than $m^2 \log(m^2/\mu^2)$.

In the work done so far it has not been the case [18–21]. Process by process it has been proven that such diagrams are in fact proportional to the ones containing only leading order operators up to small terms of order m^2 without logarithms. The coefficient of proportionality depends on the hard quantities (heavy masses or large momenta squared). For this reason ChPT is still enough to predict the light mass dependence: we can perform loop calculations including only the leading order diagrams. However we lose predictivity on the part containing the hard quantities. To achieve it we would need all the diagrams, also those with operators containing more derivatives.

This extension of ChPT is called hard pion ChPT and it is at a preliminary stage. There is yet no concrete proof that it is applicable in all the processes, but there are arguments that suggest so. So far it has only been applied up to order $\mathcal{O}(m^2 \log(m^2/\mu^2))$. Paper III and IV develop this extension for a few processes. Some of them also involve heavy mesons which are not in the octet of Figure *i.1*. Therefore a modification of ChPT is needed to include them in the study. The next two sections will focus exactly on such modification called Heavy Meson ChPT.

i.8 Heavy Quark Effective Theory

Chiral Perturbation theory is not the only effective field theory treated in the papers that form this thesis. Paper III and IV deal indirectly also with another effective field theory called Heavy Quark Effective theory (HQET). It can be used, as its name suggests, to describe the role of heavy quarks (namely the c and b quarks in Table *i.1*) in QCD [22]. The theory is relevant for our aims when it is combined with ChPT to study the dynamics of the heavy mesons and their interactions with the light pseudoscalar mesons in the octet. This combination is called Heavy Meson ChPT (HMChPT) [23] and it will be the subject of the next section. Here we describe very briefly and schematically the symmetries leading to HQET, that are also at the basis of HMChPT [23–25].

We have seen that the light u , d and s quarks have masses small compared to the non perturbative strong dynamics scale Λ . Consequently it is a good approximation to take the limit where these masses disappear and use the arising chiral symmetry to predict their dynamics. Analogously the QCD Lagrangian shows other symmetries when the masses of the c and b quarks (which are larger than Λ) are instead sent to infinity. In this limit QCD acquires a *spin-flavour symmetry* which has important applications for mesons containing a single heavy quark.

We consider a $Q\bar{q}$ meson where Q denotes the heavy quark, and \bar{q} the light antiquark. This is a bound system whose binding arises exactly from the non-perturbative strong dynamics. The typical size of a momentum transfer between Q and \bar{q} is then of order Λ . Indicating with v the four-velocity of the heavy quark Q , the variation Δv due to such momentum transfer will be of order Λ/m_Q . Being $m_Q \gg \Lambda$, Δv is small, so the velocity of Q does not change with time. We can think that Q behaves like a static source of “strong force” and the relevant meson dynamics reduces to that of the light degrees of freedom affected by such a source. This means that as long as m_Q is large, it does not matter which is exactly its value and thus which particular Q we are describing: the dynamics are unchanged under the exchange of heavy flavour. This is in practice *heavy flavour symmetry*.

There is also another symmetry that can be made manifest in the heavy

Meson	Mass	Quark Content	J^P
D^+	1.869 GeV	$c\bar{d}$	0^-
D^{*+}	2.010 GeV	$c\bar{d}$	1^-
D^0	1.864 GeV	$c\bar{u}$	0^-
D^{*0}	2.006 GeV	$c\bar{u}$	1^-
D_s^+	1.968 GeV	$c\bar{s}$	0^-
D_s^{*+}	2.112 GeV	$c\bar{s}$	1^-

Table i.2: The lowest-mass D mesons. The masses are all quite similar and close to 2 GeV. The differences in the spin doublets can be explained adding $1/m_Q$ corrections. Notice also the presence of the $SU(3)_V$ symmetry pattern discussed in Section i.6.1: exchanging the light antiquark does not produce large differences in masses. A similar pattern is found also for B mesons (composed by a \bar{b} quark and a light quark), showing the correctness of heavy flavour symmetry. They have however a larger mass, around 5 GeV.

quark limit. The QCD Lagrangian in (i.11) shows that the strong interactions occur due to the interactions with gluons, indicated by the fields A^μ . The operators responsible for that have the form $\bar{\psi}_i \gamma_0 A^0 \psi_i + \bar{\psi}_i \vec{\gamma} \cdot \vec{A} \psi_i$. Such term is similar to the QED one appearing in (i.5). As in QED the second term is related to the (chromo-)magnetic moment [4], whose dependence on the mass is $1/m_Q$. Therefore it can be neglected for heavy quarks [7]. The first term is instead spin independent. To see it, one can use the Dirac-representation of the γ matrices and notice that γ_0 does not mix the different spin-components of the ψ_i -spinor. So it corresponds to a spin conserved interaction leading to *heavy spin symmetry*.

These symmetries are approximately valid and there is no evidence for a spontaneous breaking as for chiral symmetry. Indeed such symmetries can be found in the spectra of the hadrons. For example the D mesons, composed by a c quark and a light antiquark, are organized in doublets of spin 0 and 1 with approximately the same mass as shown in Table i.2

Notice that identifying the symmetries we also discover the good quantum numbers to describe a heavy-light system such as the D or the B mesons. These are the four velocity v and the spin of the heavy quark (or of the light degrees of freedom) $S_Q (s_\ell)$.

Also in HQET we can introduce a perturbative approach. The expansion parameter in this case is $1/m_Q$. Such corrections can be systematically included as it was done for ChPT. Notice that we expect such an expansion to work better for hadrons containing a b quark than for those containing a c

quark, since $1/m_b < 1/m_c$.

We do not give further details about HQET since it is of little relevance for the results presented in the papers. In the next section we focus on the combination of HQET with ChPT.

***i.8.1* Heavy Meson Chiral Perturbation Theory**

Here we very shortly sketch the theory used to study heavy-light mesons and their interactions with the pseudoscalar mesons. This has been extensively used in paper III and IV. However since the main topic of those papers was hard pion ChPT we try to give in this section only a few ideas on how HM-ChPT is built up. This description is far from being complete. We recommend the interested reader to check for details the book [22].

As was done with ChPT, here we need to identify the degrees of freedom organized in a convenient way, the symmetries used to build up the Lagrangians and look for a well defined power counting.

We need to deal with two different kinds of mesons: the light pseudoscalar mesons, that can be nicely organized in the matrix U of (i.23), and the heavy mesons D and B . As illustrated in Table i.2 they appear in the spectrum in spin doublets and flavour triplets. It is therefore convenient to collect them in a unique object H_a , where a is a flavour index. H_a must contain the two mesons in the doublets: the spin-1 meson field $P_a^{*\mu}$, which is a vector under Lorentz transformations, and the spin-0 P_a , which is instead a pseudoscalar. Keep in mind that H_a , $P_a^{*\mu}$ and P_a travel with constant four-velocity v^μ . It turns out that a convenient way to build H_a is

$$H_a = \frac{1 + v^\mu \gamma_\mu}{2} \left[P_a^{*\mu} \gamma_\mu - P_a \gamma_5 \right]. \quad (i.45)$$

For brevity we do not explain why this particular form is chosen. The interested reader can look for further explanation [22]. Notice that H_a is a 4×4 matrix in spin indices, the gamma matrix indices. It is also possible to show that H_a transforms linearly under the heavy quark symmetries.

Since our aim is to combine together HQET and ChPT we need a Lagrangian that satisfies all the symmetries for both theories. To this aim we need to pick a convenient transformation for H under chiral symmetry. This is simplified by choosing a different way to organize the pseudoscalar mesons as well, i.e. from now on we use the matrix $u \equiv \sqrt{U} = e^{i/(\sqrt{2}F_0)\phi}$. Notice that u has a more complicated transformation rule under chiral symmetry than (i.22), because the square root is a non linear operation. Despite that it turns out that it is more convenient to use this field rather than U to collect the Goldstone bosons.

Starting from u_{ab} and H_a we must identify all the operators invariant under heavy quark symmetries and chiral symmetry and then write down the Lagrangian. This reads

$$\mathcal{L}_{\text{heavy}} = -i \text{Tr} \bar{H}_a v \cdot D_{ab} H_b + g \text{Tr} \bar{H}_a u_{ab}^\mu H_b \gamma_\mu \gamma_5, \quad (i.46)$$

where g is the coupling of the heavy meson doublet to the mesons in the octet and the traces, Tr , are over spin indices, the γ -matrix indices. The indices a, b run over the light quark flavours. In (i.46) we defined the derivatives

$$\begin{aligned} D_{ab}^\mu H_b &= \delta_{ab} \partial^\mu H_b + \Gamma_{ab}^\mu H_b, \\ \Gamma_{ab}^\mu &= \frac{1}{2} \left[u^\dagger (\partial^\mu - ir^\mu) u + u (\partial^\mu - il^\mu) u^\dagger \right]_{ab}, \\ u_{ab}^\mu &= i \left[u^\dagger (\partial^\mu - ir^\mu) u - u (\partial^\mu - il^\mu) u^\dagger \right]_{ab}, \end{aligned} \quad (i.47)$$

The Lagrangian (i.46) satisfies chiral symmetry and heavy quark spin flavour symmetry.

Let us take a look now at the interactions included in (i.46). They can be obtained by substituting in Γ^μ and in u^μ the expansions of u and u^\dagger in terms of ϕ

$$u = 1 + \frac{i}{\sqrt{2}F_0} \phi - \frac{1}{2F_0^2} \phi^2 \dots \quad (i.48)$$

Substituting the expression for H_a in (i.45) and doing some γ -matrix algebra one can study the field content of the interaction terms. So one achieves that the term in $\mathcal{L}_{\text{heavy}}$ (i.46) of the form $\text{Tr} \bar{H}_a v \cdot \Gamma_{ab} H_b$ contains interactions of the type $PPMM$ or P^*P^*MM where M indicates the light mesons and P the heavy ones. Instead the term $\text{Tr} \bar{H}_a u_{ab}^\mu H_b \gamma_\mu \gamma_5$ contains interactions like PP^*M or P^*P^*M . This second term has a coupling g which is the same, at leading order in $1/m_Q$, for the B and the D mesons. This is due to heavy flavour symmetry.

What about the power counting? There are two scales in the game. One is the scale of ChPT Λ , and the other is dictated by HQET m_Q . They both must be considered. Therefore there are two types of higher order corrections that can be included: the ones dictated by ChPT and the $1/m_Q$ of HQET.

In paper III and IV HMChPT has been used to calculate the amplitudes for *semileptonic decays* of B and D mesons. A semileptonic decay is a decay of a hadron into other hadrons and leptons (see Figure i.6). The weak interaction is responsible for these processes. For example the decay $B^+ \rightarrow \pi^0 \mu^+ \bar{\nu}_\mu$ is a semileptonic decay. The problem related to these decays is that the initial meson is much heavier than the outgoing light meson, allowing this last particle to acquire a large energy. As we have also discussed in Sections i.6.5, i.6.6 and i.7 the use of the perturbative expansion of ChPT is valid as long as the momenta of the mesons in the octet are small compared to the scale

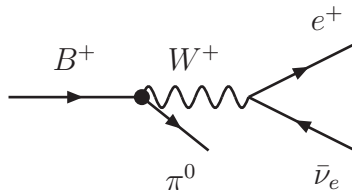


Figure *i.6*: The Feynman diagram corresponding to the semileptonic decay for the B^+ meson into a π^0 and leptons. Similar diagrams can be drawn with different outgoing hadrons (e.g. Kaons, η meson or D meson) and with different initial hadron (e.g. D mesons).

$\Lambda \approx 1$ GeV. In the processes involving interactions between light pseudoscalar mesons and heavy-light systems there are often regions of energy where hard pseudoscalar mesons appear. In such regions we fail at predicting the energy behaviour of the physical observables. But the light-mass dependence is still achievable with the use of hard pion ChPT as it is shown in paper III and IV.

i.9 Interplay between ChPT and Lattice QCD

At the beginning of Section *i.6.1* we remarked that although the Lagrangian of QCD is well known, calculating its predictions is not easy at low energies because of the non applicability of perturbation theory. To overcome this problem one can proceed in two ways. One of them is the effective field theory approach, described in the previous sections. The other one is through Lattice QCD. This basically consists in calculating observables from first principles. With the use of the path integral formulation of QCD it is possible to evaluate numerically functional integrals on a discretized spacetime lattice [26].

Even though this approach is promising, the properties of low-mass particles (as the pions) have so far been difficult to calculate. The reason is that light particles can propagate over large distances, but using large lattice volumes in simulations is computer demanding. Therefore the lattice sizes, with the available computer resources, limit the precision for calculations with light mesons.

As a consequence most simulations have been performed with heavier mesons than the physical ones. Presently one typically requires that $m_\pi \gtrsim 200$ MeV (but there are also lattice collaborations that reach smaller values e.g. $m_\pi \approx 150$ MeV). The results then need to be extrapolated down to the physical masses, namely at $m_\pi \approx 139$ MeV.

ChPT provides exactly the formulae needed to perform such extrapolations. Indeed, as was also noted in Section *i.6.5*, the main results are the chiral

logarithms $m_\pi^2 \log(m_\pi^2/\mu^2)$, which rule the dependence on the meson masses of the physical observables.

ChPT, being a low energy effective theory, can be applied only in the region of energy where the light mesons have a low momentum. This also means that the lattice results for those processes where the external hadrons have a large energy cannot be extrapolated at the physical masses. This is the case of the semileptonic decays of B and D mesons. However as was explained in Section *i.7* the calculation of the chiral logarithms is still possible with the use of hard pion ChPT. In paper III and IV we calculated such quantities in the energy range where the momenta of the outgoing light mesons are large. Our results can be used on the lattice to extrapolate to lower masses even in the limit of hard external mesons, where standard ChPT is not applicable.

On one side ChPT helps in solving problems of Lattice QCD, but also the viceversa turns out to be true. Lattice QCD can indeed play a leading role in the determination of the couplings of ChPT [27].

This can be understood if you think of the quantities on which ChPT depends: external momenta and meson masses. The couplings can either appear multiplied by the momenta (Type A) or show up multiplied by the masses (Type B) [14, 28]. This distinction can be inferred by the operators the couplings multiply in the Lagrangian. As far as regards Type A couplings, experiments can help us since it is possible to study the dependence on energy of the physical observables. But for the Type B couplings this is not true: it is not possible to vary the masses in experiment, since they are fixed physical parameters. Lattice calculations instead let us study the mass dependencies directly from QCD. By fitting their results to the ChPT formulae we can determine the values of the couplings. Paper II, where a phenomenological global fit of the couplings is presented, lacks of such kind of information.

***i.10* Introduction to papers**

Before entering into the short description of the work presented in paper I and II we summarize the notation we use. The observables are written in ChPT as sums of different contributions organized in the chiral expansion:

$$O = O_{p^2} + O_{p^4} + O_{p^6} + \dots \quad (i.49)$$

The calculations so far have been done up to order $\mathcal{O}(p^6)$ in ChPT [13]. \mathcal{L}_2 is the Lagrangian at $\mathcal{O}(p^2)$ in (i.27). Its couplings appear in the expansions (i.49) at order $\mathcal{O}(p^2)$ through tree-level diagrams, at order $\mathcal{O}(p^4)$ in one-loop diagrams and at order $\mathcal{O}(p^6)$ in two-loop diagrams. \mathcal{L}_4 is the Lagrangian at $\mathcal{O}(p^4)$ in (i.37). The unknown couplings appearing there are the L_i . They contribute at order $\mathcal{O}(p^4)$ in tree level diagrams and at order $\mathcal{O}(p^6)$ in one-loop diagrams. Finally there is \mathcal{L}_6 , the Lagrangian at $\mathcal{O}(p^6)$. The unknown

couplings appearing there are the C_i . They contribute at order $\mathcal{O}(p^6)$ through tree level diagrams.

***i.10.1* Paper I**

As was also explained in Section *i.5*, deciding whether the effective field theory expansions of the physical observables converge or not is an important task. In this paper we study such convergence in the case of ChPT. At order p^6 the study is very difficult due to the large number of unknown couplings appearing both in \mathcal{L}_4 and, even worse, in \mathcal{L}_6 . Therefore we develop a strategy to get rid of them.

As was noted in Section *i.6.6* the physical observables in ChPT can be split in different parts. The polynomial one, coming from the tree level diagrams, is the only one where the C_i appear. Therefore the dependence of the physical observables on the \mathcal{L}_6 couplings is not too complicated. It is then possible to look for special combinations of observables such that the C_i cancel out. Studying these combinations we isolate the known p^2 , p^4 and p^6 contributions in a consistent way and test the convergence of the chiral expansion.

The results show that three flavour ChPT works reasonably well, namely the $\mathcal{O}(p^4)$ contribution is around 30% of the experimental result and the $\mathcal{O}(p^6)$ is around 10%. However we also find a few trouble cases that show violations from the expected convergence. Notice that, although two flavour ChPT is expected to converge better, it does not show a net improvement compared to the three flavour case for the special combinations.

***i.10.2* Paper II**

Also this paper attacks another problematic feature of ChPT: the unknown couplings. Here we perform a fit of the L_i couplings of \mathcal{L}_4 in (*i.37*) using $\mathcal{O}(p^6)$ predictions. As input we include all the available phenomenological information on several processes.

In the $\mathcal{O}(p^6)$ calculations a large number of \mathcal{L}_6 couplings contribute. Since they are so many, we do not have enough constraints to fit those as well. We are instead forced to rely on estimates of different nature. Basically we consider three different treatments. The first one is resonance saturation, which is also the most used estimate. In this model the C_i are believed to receive major contributions from resonances at higher energies. Therefore a matching between the Lagrangian \mathcal{L}_6 of ChPT and a Lagrangian describing the resonances is performed. Through this matching we can estimate the values of the $\mathcal{O}(p^6)$ couplings. The second one relies on an estimate from a QCD model. In the third one we allow the \mathcal{L}_6 couplings to take random values. This last study shows that many different sets of $\mathcal{O}(p^6)$ couplings can be chosen and

those lead to quite different good fits of the L_i .

The fits found show significant changes compared to the old ones of [29]. Such changes are mostly due to the different results obtained from new measurements of several observables. Furthermore it is very hard to constrain the Type B couplings with the available phenomenological information.

Among all the fits of the L_i that can be produced, we choose one whose predictions, unfortunately, still show a few trouble cases. On the other hand it fits well most of the phenomenological data available. It is clear that further studies are still needed to cope with these problems.



i.10.3 Paper III

Here we deal with hard pion ChPT applied to semileptonic decays of the B and D mesons into pions. We use two flavour hard pion ChPT to calculate the chiral logarithms when the hadronic products of the decays, (i.e. the pions) have an energy $E > 1$ GeV.

We show why such an approach can be used in this case, proving that matrix elements of operators with many derivatives are proportional up to higher orders, to the leading ones. We also clarify the arguments at the basis of the extension of ChPT.

Finally, we perform the calculation in the framework of a relativistic theory as well. The motivation is that the approximation of constant velocity for the heavy mesons, underlying HMChPT, might lead to incorrect chiral logarithms when hard pions appear. In fact in this last case we should not use non-relativistic propagators as those implied by HMChPT, but relativistic ones. This modification affects the loop integrals and in principle it can change the chiral logarithms. To check that this is not the case, as our arguments predict, we calculate also in a relativistic formalism. As expected, this second calculation gives the same results as the HMChPT one.

As explained in Section *i.9*, hard pion ChPT can be very useful to perform chiral extrapolations of the lattice QCD data points in those energy ranges where standard ChPT does not hold.

i.10.4 Paper IV

This paper extends the use of hard pion ChPT in the three flavour case. So we can calculate the chiral logarithms for processes involving different hadronic final states as $D \rightarrow K$ or $D \rightarrow \eta$. This lets us compare our predictions with experiments, showing that the contributions from the chiral logarithms are sizeable and also go in the correct direction.

In this paper we also apply hard pion ChPT at one loop for both the vector and the scalar formfactor of the pion. We show that the correct chiral loga-

rithms are predicted even when including two loop diagrams. This is a nice test of the correctness of our assumptions in a more standard calculation.

We dedicate a section to $B \rightarrow D$ semileptonic decays, which have been previously studied in the limit where the velocity of the final D hadron is the same of the incoming B meson (*zero-recoil limit*). With the use of hard pion ChPT we could justify the use of these formulae even away from this limit. All these calculations are done both in the relativistic formalism of paper III and in HMChPT. Again we find agreement between the results in the two frameworks.

i.11 List of contributions

My supervisor Johan Bijnens proposed the basic ideas for all the four projects included in this thesis. The actual calculations/programming have been done by the two of us mostly independently and sometimes using different strategies. Most of the times I first produced the results and then my supervisor compared with his own, but there are also cases where the ordering was inverted. Hereafter I list the contributions I gave for the four papers:

Paper I I worked on finding the relations first and independently from my supervisor. The paper was written by my supervisor. However a few results were partially reported earlier in the proceedings [30,31], written by me.

Paper II In a preliminary phase of this project a large amount of time was spent in converting the programs used to calculate the ChPT amplitudes from FORTRAN to C++. The actual translation into C++ code was done mainly by my supervisor but I helped in comparing the results of all these C++ programs with the old results in FORTRAN.

Besides that, the actual project consisted primarily in writing down a new C++ program to perform the fits. This was done independently by the two of us. This project took a long time before being completed, so first results came pretty much from both sides. I wrote the bulk of the paper that was afterwards revised by my supervisor. Also for this project, some preliminary results were reported earlier in the proceedings [31], written by me.

Paper III I calculated the final results using HMChPT. The calculation in the relativistic framework was first done by my supervisor and then redone by me. I wrote the bulk of the paper that has been later polished by my supervisor.

Paper IV I calculated the results for the decays of heavy mesons with HM-ChPT and in the relativistic theory. I also made the plots for comparing the outcomes with experimental data. Afterwards my supervisor did the relativistic formalism calculations independently and checked the comparison with experiment. He made first the two loop check for the scalar and vector formfactors of the pions. I wrote the bulk of the paper that has been then rearranged and revised by my supervisor.

i

Acknowledgments

First of all, I thank my supervisor Hans Bijmens for all his help and support. He is an excellent researcher and it was a privilege to work with him.

Many people patiently read the introduction of this thesis. Karol Kampf, Johan Rathsman, Hans Bijmens and Martijn Gosselink thanks a lot for having done it.

I also thank the department of Theoretical Physics and the division of High Energy Physics at Lund University for the friendly atmosphere. I realize I have been sitting in front of a computer for a significant part of my time, but it is always nice to get out of the office and have a break, possibly talking about anything but physics.

I really enjoyed my time in Lund and this is also thanks to all the people I met here. So a super-big “thank you” goes to Lisa, Francesca, Angela, Erica, Simona e Florido, Weina, Lu Jie, Nele, Richard, Philippe, Alejandro, Stefan, Alex, José, Mariana, Sofia, Mafalda, Joanne, Chrissss, Iskra, Nils, Karol and many many others. I will have a good memory of the time we spent together.

Especially Nils, Richard, Lisa and Karol, thanks for the computing help and the fun discussions.

Support and encouragement came also from the “external” world, left somewhere in the rest of Europe. Thanks to my family, to my dear friend Morena and to mijn schatje Martijn.

i References

- [1] G. L. Kane, "Modern elementary particle physics," *Addison Wesley, Advanced Book Program* (1987) .
- [2] **Particle Data Group** Collaboration, K. Nakamura *et al.*, "Review of particle physics," *J.Phys.G* **G37** (2010) 075021.
- [3] L. Ryder, "Quantum Field Theory," *Cambridge University Press* (1985) .
- [4] M. E. Peskin and D. V. Schroeder, "An Introduction to quantum field theory," *Westview Press* (1995) .
- [5] F. Mandl and G. Shaw, "Quantum field theory," *Wiley* (1985) .
- [6] D. B. Kaplan, "Effective field theories," arXiv:nucl-th/9506035 [nucl-th].
- [7] J. Donoghue, E. Golowich, and B. R. Holstein, "Dynamics of the standard model," *Camb.Monogr.Part.Phys.Nucl.Phys.Cosmol.* **2** (1992) 1–540.
- [8] A. Pich, "Effective field theory: Course," arXiv:hep-ph/9806303 [hep-ph].
- [9] D. B. Kaplan, "Five lectures on effective field theory," arXiv:nucl-th/0510023 [nucl-th].
- [10] S. Weinberg, "Phenomenological Lagrangians," *Physica* **A96** (1979) 327.
- [11] J. Gasser and H. Leutwyler, "Chiral Perturbation Theory: Expansions in the Mass of the Strange Quark," *Nucl. Phys.* **B250** (1985) 465.
- [12] S. Scherer, "Introduction to chiral perturbation theory," *Adv.Nucl.Phys.* **27** (2003) 277, arXiv:hep-ph/0210398 [hep-ph].
- [13] J. Bijnens, "Chiral Perturbation Theory Beyond One Loop," *Prog. Part. Nucl. Phys.* **58** (2007) 521–586, arXiv:hep-ph/0604043.
- [14] J. Gasser, "Light quark dynamics," *Lect.Notes Phys.* **629** (2004) 1–35, arXiv:hep-ph/0312367 [hep-ph].
- [15] J. C. Collins, "Renormalization," *Cambridge University Press* (1984) .
- [16] J. Bijnens, G. Colangelo, and G. Ecker, "The mesonic chiral Lagrangian of order p^6 ," *JHEP* **02** (1999) 020, arXiv:hep-ph/9902437.
- [17] H. Lehmann, "Chiral invariance and effective range expansion for pion pion scattering," *Phys.Lett.* **B41** (1972) 529.

- [18] **RBC Collaboration**, J. M. Flynn and C. T. Sachrajda, “ $SU(2)$ chiral perturbation theory for $K_{\ell 3}$ decay amplitudes,” *Nucl. Phys.* **B812** (2009) 64–80, arXiv:0809.1229 [hep-ph].
- [19] J. Bijnens and A. Celis, “ $K \rightarrow \pi\pi$ Decays in $SU(2)$ Chiral Perturbation Theory,” *Phys. Lett.* **B680** (2009) 466–470, arXiv:0906.0302 [hep-ph].
- [20] J. Bijnens and I. Jemos, “Hard Pion Chiral Perturbation Theory for $B \rightarrow \pi$ and $D \rightarrow \pi$ Formfactors,” *Nucl. Phys.* **B840** (2010) 54–66, [Erratum–ibid. **B844** (2011) 182], arXiv:1006.1197 [hep-ph].
- [21] J. Bijnens and I. Jemos, “Vector Formfactors in Hard Pion Chiral Perturbation Theory,” *Nucl. Phys.* **B846** (2011) 145–166, arXiv:1011.6531 [hep-ph].
- [22] A. V. Manohar and M. B. Wise, “Heavy quark physics,” *Camb. Monogr. Part. Phys. Nucl. Phys. Cosmol.* **10** (2000) 1–191.
- [23] M. B. Wise, “Combining chiral and heavy quark symmetry,” arXiv:hep-ph/9306277.
- [24] M. B. Wise, “Chiral perturbation theory for hadrons containing a heavy quark,” *Phys. Rev.* **D45** (1992) 2188–2191.
- [25] G. Burdman and J. F. Donoghue, “Union of chiral and heavy quark symmetries,” *Phys. Lett.* **B280** (1992) 287–291.
- [26] R. Gupta, “Introduction to lattice QCD: Course,” arXiv:hep-lat/9807028 [hep-lat].
- [27] G. Colangelo, S. Durr, A. Juttner, L. Lellouch, H. Leutwyler, *et al.*, “Review of lattice results concerning low energy particle physics,” arXiv:1011.4408 [hep-lat].
- [28] G. Colangelo, J. Gasser, and H. Leutwyler, “ $\pi\pi$ scattering,” *Nucl. Phys.* **B603** (2001) 125–179, arXiv:hep-ph/0103088.
- [29] G. Amoros, J. Bijnens, and P. Talavera, “QCD isospin breaking in meson masses, decay constants and quark mass ratios,” *Nucl. Phys.* **B602** (2001) 87–108, arXiv:hep-ph/0101127.
- [30] J. Bijnens and I. Jemos, “Determination of Low Energy Constants and testing Chiral Perturbation Theory at Next to Next to Leading Order,” *PoS EFT09* (2009) 032, arXiv:0904.3705 [hep-ph].
- [31] J. Bijnens and I. Jemos, “Determination of Low Energy Constants and testing Chiral Perturbation Theory at order p^6 (NNLO),” *PoS CD09* (2009) 087, arXiv:0909.4477 [hep-ph].

I

Relations at order p^6 in Chiral Perturbation Theory

Johan Bijnens and Ilaria Jemos

Department of Theoretical Physics, Lund University,
Sölvegatan 14A, SE-223 62 Lund, Sweden

I

European Physical Journal C **64** (2009) 273 [arXiv:0906.3118 [hep-ph]]

We report on a search of relations valid at order p^6 in Chiral Perturbation Theory. We have found relations between $\pi\pi$, πK scattering, $K_{\ell 4}$ decays, masses and decay constants and scalar and vector form factors. In this paper we give the relations and a first numerical check of them.

PACS: 12.39.Fe Chiral Lagrangians, 11.30.Rd Chiral symmetries, 14.40.Aq π , K , and η mesons, 12.38.Lg Other nonperturbative calculations,

With kind permission from Springer+Business Media: European Physical Journal C, Relations at Order p^6 in Chiral Perturbation Theory, 64(2009) 273, Johan Bijnens and Ilaria Jemos

I.1 Introduction

Chiral Perturbation Theory (ChPT) [1–3] is the effective field theory for the strong interaction at low energies. Some recent reviews are [4–6]. In the mesonic sector many calculations have now been performed to two-loop or next-to-next-to-leading order (NNLO), see the review [5]. Since in an effective field theory like ChPT there appear new Lagrangians at every order, tests of ChPT at NNLO are difficult to perform since for most processes new combinations of these parameters, called low-energy constants (LECs), appear.

One way to test ChPT at NNLO order is to find observables where the same combinations of LECs appear. Many of these pairs of observables were found in the explicit calculations but no systematic study had been done. That is the purpose of this work. We take systematically all observables that can contain a dependence on the NNLO LECs in $\pi\pi$ and πK scattering, the masses and decay constants, $\eta \rightarrow 3\pi$, $K_{\ell 4}$ and the scalar and vector formfactors and determine how many of these contain the same combinations of NNLO LECs. Of the 76 observables we include, we find 35 such combinations. These are discussed in Sects. I.3 to I.12. These allow in principle to test the validity of three flavour ChPT at NNLO. However, many relations involve poorly known quantities from the scalar formfactors so we have restricted the numerical discussion to the $\pi\pi$, πK and $K_{\ell 4}$ sector. The tests in the vector formfactors were already discussed extensively in the earlier work, so we do not present numerical results for those either. We find a mixed picture. Three flavour ChPT mostly works but there are problems. Some preliminary results were presented in [7].

We first discuss the $\pi\pi$ threshold parameters relations in both two and three flavour ChPT in Sect. I.3. After that we restrict ourselves to three flavour ChPT, first πK threshold parameters relations in Sect. I.4 and the relations between both sectors in Sect. I.5. Sect. I.6 discusses the relation between $K_{\ell 4}$ and πK scattering. For $\eta \rightarrow 3\pi$ we find relations involving the cubic dependence of the Dalitz plot in Sect. I.7. For the scalar formfactors we find the known relations and one new one, Sect. I.8, but when relating the scalar sector to other sectors we find several new relations as discussed in Sects. I.9, I.10, I.11 and I.12. We shortly recapitulate our conclusions in Sect. I.13. For completeness, we have added in an appendix the correspondence between the subthreshold and threshold parameters for $\pi\pi$ and πK scattering.

I.2 Notation

The Lagrangian at NNLO contains 90 LECs, called the C_i in [8,9]. Since in this work we check whether the same combinations of LECs appear we use the

notation

$$[A]_{C_i} = C_i^r \text{-dependent part of } A. \quad (\text{I.1})$$

We also use the notation B_0 and F_0 , the chiral limit of F_π , the two constants that appear in the lowest order Lagrangian [3]. For the physical observables we use for each case the established notation.

We always express dimensionful quantities in the appropriate units of m_{π^+} , which is in any case standard practice for many of the quantities we consider. We use the symbol $\rho = m_K/m_\pi$ to indicate the kaon mass. This way the relations are easier to write down.

I.3 $\pi\pi$ scattering

The $\pi\pi$ scattering amplitude can be written as a function $A(s, t, u)$ which is symmetric in the last two arguments:

$$A(\pi^a \pi^b \rightarrow \pi^c \pi^d) = \delta^{a,b} \delta^{c,d} A(s, t, u) + \delta^{a,c} \delta^{b,d} A(t, u, s) + \delta^{a,d} \delta^{b,c} A(u, t, s), \quad (\text{I.2})$$

where s, t, u are the usual Mandelstam variables. The isospin amplitudes $T^I(s, t)$ ($I = 0, 1, 2$) are

$$\begin{aligned} T^0(s, t) &= 3A(s, t, u) + A(t, u, s) + A(u, s, t), \\ T^1(s, t) &= A(s, t, u) - A(u, s, t), \\ T^2(s, t) &= A(t, u, s) + A(u, s, t), \end{aligned} \quad (\text{I.3})$$

and can be expanded in partial waves

$$T^I(s, t) = 32\pi \sum_{\ell=0}^{+\infty} (2\ell + 1) P_\ell(\cos \theta) t_\ell^I(s), \quad (\text{I.4})$$

where t and u have been written as $t = -\frac{1}{2}(s - 4m_\pi^2)(1 - \cos \theta)$, $u = -\frac{1}{2}(s - 4m_\pi^2)(1 + \cos \theta)$. Near threshold the t_ℓ^I are further expanded in terms of the threshold parameters

$$t_\ell^I(s) = q^{2\ell} \left(a_\ell^I + b_\ell^I q^2 + c_\ell^I q^4 + d_\ell^I q^6 + \mathcal{O}(q^8) \right) \quad q^2 = \frac{1}{4}(s - 4m_\pi^2), \quad (\text{I.5})$$

where $a_\ell^I, b_\ell^I \dots$ are the scattering lengths, slopes, ... and q is the magnitude of the pion three momenta in the center of mass frame. We studied only those observables where a dependence on the C_i s shows up. Using $s + t + u = 4m_\pi^2$ we can write the amplitude to order p^6 as

$$\begin{aligned} A(s, t, u) &= b_1 + b_2 s + b_3 s^2 + b_4 (t - u)^2 + b_5 s^3 + b_6 s (t - u)^2 \\ &\quad + \text{non polynomial part} \end{aligned} \quad (\text{I.6})$$

The tree level Feynman diagrams give polynomial contributions to $A(s, t, u)$ which must be expressible in terms of b_1, \dots, b_6 .

The threshold parameters $a_0^0, b_0^0, c_0^0, d_0^0, a_0^2, b_0^2, c_0^2, d_0^2, a_1^1, b_1^1, c_1^1, a_2^0, b_2^0, a_2^2, b_2^2, a_3^1$ are all those that can receive contributions from tree level LECs up to order p^6 , but results [10] have only been presented for $a_0^0, b_0^0, a_0^2, b_0^2, a_1^1, b_1^1, a_2^0, b_2^0, a_2^2, b_2^2$ and a_3^1 . At present we thus can only use those 11 to test ChPT. We do not consider b_3^1 for which numerical results are also given in [10] since it does not depend at tree level on any LECs to order p^6 . For those 11 we obtain the following five relations:

$$\left[5b_0^2 - 2b_0^0 - 27a_1^1 - 15a_0^2 + 6a_0^0\right]_{C_i} = -18 \left[b_1^1\right]_{C_i}, \quad (\text{I.7})$$

$$\left[3a_1^1 + b_0^2\right]_{C_i} = 20 \left[b_2^2 - b_2^0 - a_2^2 + a_2^0\right]_{C_i}, \quad (\text{I.8})$$

$$\left[b_0^0 + 5b_0^2 + 9a_1^1\right]_{C_i} = 90 \left[a_2^0 - b_2^0\right]_{C_i}, \quad (\text{I.9})$$

$$\left[3b_1^1 + 25a_2^2\right]_{C_i} = 10 \left[a_2^0\right]_{C_i}, \quad (\text{I.10})$$

$$\left[-5b_2^2 + 2b_2^0\right]_{C_i} = 21 \left[a_3^1\right]_{C_i}, \quad (\text{I.11})$$

All quantities are expressed in units of $m_{\pi^+}^2$. In fact, since these relations hold for every contribution to the polynomial part, they are valid for the NLO tree level contribution as well and for two- and three-flavour ChPT. Therefore they do not get contributions from the L_i s at NLO, but only at NNLO via the non polynomial part of Eq. (I.6).

The first three involve quantities that already have tree level contributions at lowest order, the fourth starts with tree level at NLO and the last only has tree level contributions starting at NNLO. The terms in the first three are arranged such that the quantities starting at lowest order are all on the left-hand-side.

Let us now look at the numerical results. As experimental input we use the Roy equation analysis together with input from ChPT and the pion scalar form-factor done in [10]. In Tab. 1.1 we quote the left-hand-side (LHS) and right-hand-side (RHS) of each of the relations with the threshold parameters as quoted in [10]. We have added the errors for the several quantities quadratically which probably results in an underestimate of the error. The results are quoted in the second column of Tab. 1.1. The next columns give the contribution from pure one-loop at NLO, the tree level NLO contribution at one-loop using the fitted values of fit 10 in [11], the pure two-loop contribution, and the L_i dependent part at NNLO (called NNLO 1-loop) using again fit 10 of [11]. Of these the tree level NLO contribution must satisfy the relations, the others need not. The numerical results have been calculated using the formulas

of [12]. The column labeled remainder is the result of [10] minus the three-flavour ChPT prediction. This is thus the contribution of the NNLO LECs and from higher orders.

The theoretical errors are more difficult to estimate. The error shown in the sixth column in brackets in Tab. I.1 is obtained by varying all the L_i^r around the central values of fit 10 of [11] exploring the region with $\chi^2/dof \approx 1$ using the full covariance matrix as obtained for that fit by the authors of [11]. The error is then estimated as the maximum deviation observed. The error for the L_i^r contribution at NLO is not shown since it drops out of the relations.

As we see, the first three relations are very well satisfied. The last two work at a level around two sigma. Uncertainties on the theoretical results are mostly on the last quoted digit, no uncertainty due to fit 10 is included. Note that the $\pi\pi$ threshold parameters were not used as input in fit 10.

We can also check how the two-flavour predictions hold up. Here the expansion parameter is different. The corrections are in powers of m_π^2 rather than in powers of m_K^2 . The expansion should thus converge better and the conclusion was drawn in [10] that two-flavour ChPT works for $\pi\pi$ -scattering at threshold (and even better where they performed their subtractions). We do not use the numbers quoted in [13–15] since the LECs used there have been superseded by those of [10] and [11] respectively. Testing our relations for two-flavour ChPT thus gives a good indication of the best results we can expect for the three-flavour case. We use the threshold parameters as quoted in [10] for their best fit of the NLO LECs and using the formulas of [16]. The result is shown in Tab. I.2. We see the same pattern as for the three flavour case. The first three relations are very well satisfied while the last two are somewhat worse but here below two sigma.

An alternative way to look at the results is to directly test the relations. In the previous tables we have presented results separately for the LHS and RHS in order to show how well the combinations of the NNLO LECs would be the same if determined in the two different ways. We can also instead show LHS minus RHS for our relations which directly tests the loop content of ChPT. For the $\pi\pi$ and πK case this is equivalent to comparing the exact results for the dispersive part with the ChPT result for the dispersive part since the subtraction constants used in [10] drop out in the relations we consider¹. This is shown in Tab. I.3. We see here also good agreement for the first three and about two sigma for the last two relations. The results given in Tab. I.3 are depicted graphically in Fig. I.1. Keep in mind here that the errors for the dispersive result might be underestimated since we combined them quadratically.

¹We thank the referee for pointing this out.

	[10]	NLO 1-loop	NLO LECs	NNLO 2-loop	NNLO 1-loop	remainder
LHS (I.7)	0.009 ± 0.039	0.054	-0.044	-0.041	-0.002(3)	0.041 ± 0.039
RHS (I.7)	-0.102 ± 0.002	-0.009	-0.044	-0.060	-0.008(6)	0.018 ± 0.002
10 LHS (I.8)	0.334 ± 0.019	0.209	0.097	0.103	0.029(11)	-0.105 ± 0.019
10 RHS (I.8)	0.322 ± 0.008	0.177	0.097	0.120	0.034(13)	-0.107 ± 0.008
LHS (I.9)	0.216 ± 0.010	0.166	0.029	0.053	0.016(6)	-0.047 ± 0.010
RHS (I.9)	0.189 ± 0.003	0.145	0.029	0.049	0.020(7)	-0.054 ± 0.003
10 LHS (I.10)	0.213 ± 0.005	0.137	0.032	0.053	0.035(12)	-0.043 ± 0.005
10 RHS (I.10)	0.175 ± 0.003	0.121	0.032	0.050	0.029(10)	-0.057 ± 0.003
10^3 LHS (I.11)	0.92 ± 0.07	0.36	0.00	0.56	-0.01(13)	0.00 ± 0.07
10^3 RHS (I.11)	1.18 ± 0.04	0.42	0.00	0.57	0.03(13)	0.15 ± 0.04

Table I.1: The relations found in the $\pi\pi$ -scattering. The lowest order contribution is always zero by construction. The NLO LEC part satisfies the relation. Notice the extra factors of ten for some of them. All quantities are in the units of powers of m_{π^+} . See text for a longer discussion.

I.4 πK scattering

The πK scattering amplitude has amplitudes $T^I(s, t, u)$ in the isospin channels $I = 1/2, 3/2$. As for $\pi\pi$ scattering, it is possible to define scattering lengths

	[10]	two-flavour [10]	remainder
LHS (i.7)	0.009 ± 0.039	-0.003	0.007 ± 0.039
RHS (i.7)	-0.102 ± 0.002	-0.097	-0.005 ± 0.002
10 LHS (i.8)	0.334 ± 0.019	0.332	0.002 ± 0.019
10 RHS (i.8)	0.322 ± 0.008	0.318	0.004 ± 0.075
LHS (i.9)	0.216 ± 0.010	0.206	0.010 ± 0.010
RHS (i.9)	0.189 ± 0.003	0.189	0.000 ± 0.003
10 LHS (i.10)	0.213 ± 0.005	0.204	0.009 ± 0.005
10 RHS (i.10)	0.175 ± 0.003	0.176	-0.001 ± 0.003
10^3 LHS (i.11)	0.92 ± 0.07	1.00	-0.08 ± 0.07
10^3 RHS (i.11)	1.18 ± 0.04	1.15	0.04 ± 0.04

Table I.2: The relations found in the $\pi\pi$ -scattering evaluated in two-flavour ChPT. In the second column we have used the NNLO results quoted in [10]. Notice the extra factors of ten for some of them. See text for a longer discussion.

	disp/exp	NLO	NLO+NNLO	NLO+NNLO(2)
LR (i.7)	0.111 ± 0.039	0.062	0.087(3)	0.094
10 LR (i.8)	0.012 ± 0.021	0.031	0.010(2)	0.014
LR (i.9)	0.026 ± 0.011	0.021	0.020(3)	0.017
10 LR (i.10)	0.038 ± 0.006	0.016	0.024(2)	0.028
10^3 LR (i.11)	-0.26 ± 0.08	-0.06	-0.11(2)	-0.14
LR (i.23)	-1.5 ± 0.7	-0.26	-0.34(7)	-
10 LR (i.21)	-0.05 ± 0.02	0.02	0.03(5)	-
100 LR (i.24)	0.36 ± 0.60	0.06	-0.13(13)	-
100 LR (i.22)	0.12 ± 0.01	0.03	0.06(1)	-
10^3 LR (i.26)	-0.03 ± 0.08	0.07	0.03(2)	-
10^3 LR (i.28)	-0.04 ± 0.03	0.00	0.08(5)	-
10 LR (i.29)	-0.04 ± 0.02	-0.06	-0.07(2)	-
LR (i.33)	-1.24 ± 0.11	-0.41	-0.74(10)	-

Table I.3: Tests of the relations as seen as a test of the loop contributions. disp/exp are the dispersive and experimental inputs used as described in the text. LR stands for LHS-RHS. All quantities are in units of m_{π^+} . Results are shown for the relations for $\pi\pi$, πK , $\pi\pi$ vs πK and $K_{\ell 4}$ vs πK .

a_ℓ^I, b_ℓ^I . So we introduce the partial wave expansion of the isospin amplitudes

$$T^I(s, t, u) = 16\pi \sum_{\ell=0}^{+\infty} (2\ell + 1) P_\ell(\cos \theta) t_\ell^I(s), \quad (\text{I.12})$$

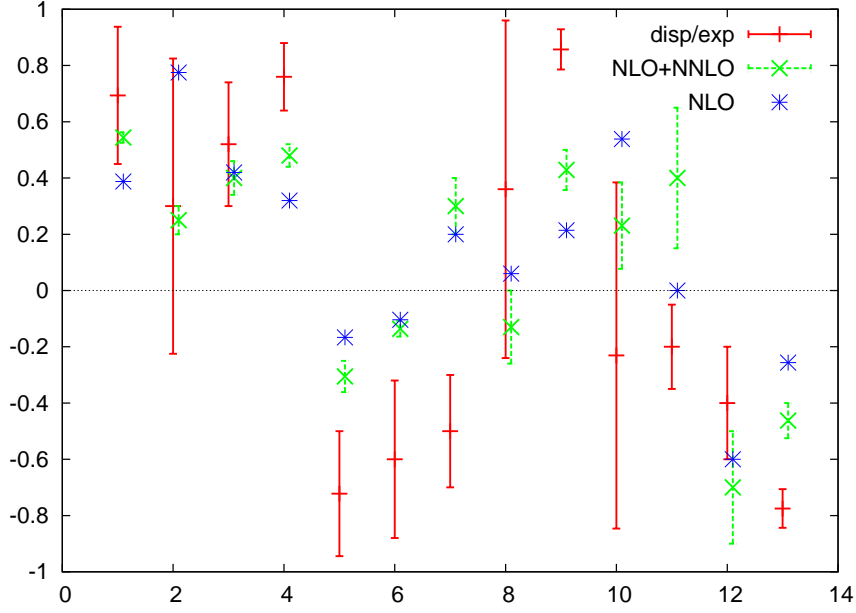


Figure 1.1: The relations with the dispersive/experimental results shown as full lines with errors, the NLO result as stars and the sum of NLO+NNLO as crosses with the errors indicated as dashed lines. The scale is arbitrary. The relations appear in the order given in Tab. I.3. 1-5 $\pi\pi$, 6-10 πK , 11-12 $\pi\pi$ vs πK and 13 $K_{\ell 4}$ vs πK .

and we expand the $t_\ell^I(s)$ near threshold:

$$t_\ell^I(s) = \frac{1}{2} \sqrt{s} q_{\pi K}^{2\ell} \left(a_\ell^I + b_\ell^I q_{\pi K}^2 + c_\ell^I q_{\pi K}^4 + \mathcal{O}(q_{\pi K}^6) \right), \quad (I.13)$$

where

$$q_{\pi K}^2 = \frac{s}{4} \left(1 - \frac{(m_K + m_\pi)^2}{s} \right) \left(1 - \frac{(m_K - m_\pi)^2}{s} \right), \quad (I.14)$$

is the magnitude of the three-momentum in the center of mass system. The Mandelstam variables are in terms of the scattering angle given by

$$t = -2q_{\pi K}^2(1 - \cos\theta), \quad u = -s - t + 2m_K^2 + 2m_\pi^2. \quad (I.15)$$

Again we studied only those observables where a dependence on the C_i s shows up.

It is also customary to introduce the crossing symmetric and antisymmetric amplitudes $T^\pm(s, t, u)$ which can be expanded around $t = 0$, $s = u$ using $v = (s - u)/(4m_K)$, called the subthreshold expansion:

$$T^+(s, t, u) = \sum_{i,j=0}^{\infty} c_{ij}^+ t^i v^{2j}, \quad T^-(s, t, u) = \sum_{i,j=0}^{\infty} c_{ij}^- t^i v^{2j+1}. \quad (I.16)$$

There are ten subthreshold parameters that have tree level contributions from the NNLO LECs. In c_{01}^- and c_{20}^- the same combination $-C_1 + 2C_3 + 2C_4$ appears [12], thus

$$16\rho^2 [c_{20}^-]_{C_i} = 3 [c_{01}^-]_{C_i}. \quad (I.17)$$

Eq. (I.17) leads to one relation between the subthreshold parameters.

If we look at the a_ℓ^I and b_ℓ^I that get contributions from the NNLO LECs there are 14 such. 7 for each isospin channel. The isospin odd channel only involves T^- :

$$T^{1/2}(s, t, u) - T^{3/2}(s, t, u) = 3T^-(s, t, u). \quad (I.18)$$

This combination has only three subthreshold parameters that get independent contributions from the NNLO LECs. So for 7 differences of a_ℓ^I and b_ℓ^I and three parameters we expect four relations. The threshold parameters are expressed in units of m_{π^+} and we use the symbol $\rho = m_K/m_\pi$. We use the notation $a_\ell^- = a_\ell^{1/2} - a_\ell^{3/2}$ and $b_\ell^- = b_\ell^{1/2} - b_\ell^{3/2}$

$$70\rho^3 (\rho + 1)^2 [a_3^-]_{C_i} = -(\rho^2 + \rho + 1) [a_0^-]_{C_i} + 2\rho^2 [b_0^-]_{C_i} + 6\rho^2 [a_1^-]_{C_i}, \quad (I.19)$$

$$140\rho^3 (\rho^2 + 1) [a_3^-]_{C_i} = (\rho^2 + 1) [a_0^-]_{C_i} + 6(-\rho^2 + \rho - 1)\rho [a_1^-]_{C_i} + 12\rho^3 [b_1^-]_{C_i}, \quad (I.20)$$

$$5(\rho^2 + 1) [a_2^-]_{C_i} = [a_1^-]_{C_i} + 2\rho [b_1^-]_{C_i}, \quad (I.21)$$

$$7(\rho^2 + 1) [a_3^-]_{C_i} = [a_2^-]_{C_i} + 2\rho [b_2^-]_{C_i}. \quad (I.22)$$

We can eliminate $[a_3^-]_{C_i}$ from (I.19) and (I.20) to obtain a relation involving only $\ell = 0, 1$ threshold parameters:

$$\begin{aligned} (\rho^4 + 3\rho^3 + 3\rho + 1) [a_1^-]_{C_i} &= 2\rho^2 (\rho + 1)^2 [b_1^-]_{C_i} - \frac{2}{3}\rho (\rho^2 + 1) [b_0^-]_{C_i} \\ &\quad + \frac{1}{2\rho} \left(\rho^2 + \frac{4}{3}\rho + 1 \right) (\rho^2 + 1) [a_0^-]_{C_i} \end{aligned} \quad (I.23)$$

We prefer to express the other relation in one involving b_2^-

$$5(\rho+1)^2 [b_2^-]_{C_i} = \frac{(\rho-1)^2}{\rho^2} [a_1^-]_{C_i} - \frac{\rho^4 + \frac{2}{3}\rho^2 + 1}{4\rho^4} [a_0^-]_{C_i} + \frac{\rho^2 - \frac{2}{3}\rho + 1}{2\rho^2} [b_0^-]_{C_i}. \quad (\text{I.24})$$

The combination that involves only T^+ is

$$T^{1/2}(s, t, u) + 2T^{3/2}(s, t, u) = 3T^+(s, t, u). \quad (\text{I.25})$$

This brings in 7 more threshold parameters, but there are 6 fully independent subthreshold parameters so we expect only one more relation. Using the notation $a_\ell^+ = a_\ell^{1/2} + 2a_\ell^{3/2}$ and $b_\ell^+ = b_\ell^{1/2} + 2b_\ell^{3/2}$, we find:

$$7[a_3^+]_{C_i} = \frac{1}{2\rho} [a_2^+]_{C_i} - [b_2^+]_{C_i} + \frac{1}{5\rho} [b_1^+]_{C_i} - \frac{1}{60\rho^3} [a_0^+]_{C_i} - \frac{1}{30\rho^2} [b_0^+]_{C_i}. \quad (\text{I.26})$$

These relations hold for all tree-level contributions up to NNLO². In particular, the lowest order contributions satisfy them.

Note that because of the nonlinearity in s present in (I.14) the higher order threshold parameters are already nonzero at lowest order. This makes fitting the threshold-expansion numerically more unstable since we need to use a fitting polynomial to higher order in $q_{\pi K}^2$ compared to what was needed for the $\pi\pi$ case.

The column labeled [17] uses the results of the Roy-Steiner analysis of [17] of πK scattering. We have combined errors quadratically which due to the presence of correlations can lead to a serious underestimate of the errors on the combinations.

The numerical results for the theory are calculated with the formulas of [18] where the NLO LECs we use are those of fit 10 of [11]. The columns in Tab. I.4 have the same meaning as in Tab. I.1 and the errors on the ChPT part have been evaluated as discussed for the $\pi\pi$ case. The first relation is reasonably well satisfied, somewhat below two sigma. The second relation has a large discrepancy in view of the experimental error but if we assume a theory error of about half the NNLO contribution it seems reasonable given The third relation is well satisfied but the RHS has a rather large experimental error. The fourth relation does not work well, mainly due to the fact that we seem to underestimate the value for a_3^- . The last relation again works reasonably well. The same relations but now LHS-RHS are shown in Tab. I.3 and depicted graphically in Fig. I.1. The conclusions are the same.

²This was written wrong in the preliminary report [7].

	[17]	NLO 1-loop	NLO LECs	NNLO 2-loop	NNLO 1-loop	remainder
LHS (i.23)	5.4 ± 0.3	0.16	0.97	0.77	$-0.11(11)$	0.6 ± 0.3
RHS (i.23)	6.9 ± 0.6	0.42	0.97	0.77	$-0.03(7)$	1.8 ± 0.6
10 LHS (i.21)	0.32 ± 0.01	0.03	0.12	0.11	0.00(2)	0.07 ± 0.01
10 RHS (i.21)	0.37 ± 0.01	0.02	0.12	0.10	$-0.01(2)$	0.14 ± 0.01
100 LHS (i.24)	-0.49 ± 0.02	0.08	-0.25	-0.17	0.05(3)	-0.21 ± 0.02
100 RHS (i.24)	-0.85 ± 0.60	0.03	-0.25	0.11	$-0.03(13)$	-0.71 ± 0.60
100 LHS (i.22)	0.13 ± 0.01	0.04	0.00	0.01	0.03(1)	0.05 ± 0.01
100 RHS (i.22)	0.01 ± 0.01	0.01	0.00	0.00	0.00(1)	-0.01 ± 0.01
10^3 LHS (i.26)	0.29 ± 0.03	0.09	0.00	0.06	0.01(2)	0.13 ± 0.03
10^3 RHS (i.26)	0.31 ± 0.07	0.03	0.00	0.06	0.05(3)	0.17 ± 0.07

Table I.4: The relations found in the πK -scattering. The tree level contribution to the LHS and RHS of relation 1 is 3.01 and vanishes for the others. The NLO LECs part satisfies the relation. Notice the extra factors of ten for some of them. See text for a longer discussion. All quantities are in the units of powers of m_{π^+} .

I.5 $\pi\pi$ and πK scattering

I

If we consider the $\pi\pi$ and πK system together we get two more relations due to the identities

$$[b_5]_{C_i} = [c_{30}^+]_{C_i} + \frac{3}{\rho} [c_{20}^-]_{C_i}, \quad [b_6]_{C_i} = \frac{1}{4\rho} [c_{20}^-]_{C_i} + \frac{1}{16\rho^2} [c_{11}^+]_{C_i}, \quad (I.27)$$

where c_{ij}^- (c_{ij}^+) are expressed in units of $m_\pi^{2i+2j+1}$ (m_π^{2i+2j}). We can express these relations in terms of the threshold parameters:

$$6 [a_3^1]_{C_i} = (1 + \rho) [a_3^+ + 3a_3^-]_{C_i}, \quad (I.28)$$

$$3 \left[(1 + \rho)^2 [b_2^2]_{C_i} + 7(1 - \rho)^2 [a_3^1]_{C_i} \right] = (1 + \rho) \left[7(1 - 4\rho + \rho^2) [a_3^-]_{C_i} + [a_2^+ + 2\rho b_2^+]_{C_i} \right]. \quad (I.29)$$

Here all the quantities are expressed in powers of m_{π^+} .

The numerical results are quoted in Tab. I.5. The first relation does not work but the second is well satisfied. If we look in the numerical results we see that a_3^- plays a minor role in the RHS of the second relation but is important in the first, so this could be the same problem that appeared for relation (I.22). The same relations but now LHS-RHS are shown in Tab. I.3 and depicted graphically in Fig. I.1. The conclusions are the same. A related analysis can be found in [19].

	[10], [17] [20], [21]	NLO 1-loop	NLO LECs	NNLO 2-loop	NNLO 1-loop	remainder
10^3 LHS (i.28)	0.34 ± 0.01	0.12	0.00	0.16	0.00(4)	0.05 ± 0.01
10^3 RHS (i.28)	0.38 ± 0.03	0.12	0.00	0.05	0.04(2)	0.16 ± 0.03
10 LHS (i.29)	-0.13 ± 0.01	-0.12	0.00	-0.05	0.02(2)	0.01 ± 0.01
10 RHS (i.29)	-0.09 ± 0.02	-0.05	0.00	-0.02	-0.01(1)	-0.01 ± 0.02
LHS (i.33)	-0.73 ± 0.10	-0.23	0.00	-0.15	-0.05(6)	-0.29 ± 0.10
RHS (i.33)	0.50 ± 0.07	0.19	0.00	0.10	0.03(4)	0.18 ± 0.07

Table I.5: The relations found between $\pi\pi$ and πK -scattering lengths and between the curvature in F in $K_{\ell 4}$ and πK scattering. See text for a longer discussion. All quantities are in units of powers of m_{π^+} .

I.6 $K_{\ell 4}$

The decay $K^+(p) \rightarrow \pi^+(p_1)\pi^-(p_2)e^+(p_\ell)\nu(p_\nu)$ is given by the amplitude [22]

$$T = \frac{G_F}{\sqrt{2}} V_{us}^* \bar{u}(p_\nu) \gamma_\mu (1 - \gamma_5) v(p_\ell) (V^\mu - A^\mu) \quad (I.30)$$

where V^μ and A^μ are parametrized in terms of four form factors: F , G , H and R (but the R -form factor is negligible in decays with an electron in the final state). Using partial wave expansion and neglecting d wave terms one obtains [23]:

$$\begin{aligned} F &= f_s + f'_s q^2 + f''_s q^4 + f'_e s_e / 4m_\pi^2 + f_t \sigma_\pi X \cos \theta + \dots, \\ G_p &= g_p + g'_p q^2 + g''_p q^4 + g'_e s_e / 4m_\pi^2 + g_t \sigma_\pi X \cos \theta + \dots \end{aligned} \quad (I.31)$$

Here $s_\pi(s_e)$ is the invariant mass of dipion (dilepton) system, and $q^2 = s_\pi / (4m_\pi^2) - 1$. θ is the angle of the pion in their restframe w.r.t. the kaon momentum and $t - u = -2\sigma_\pi X \cos \theta$. We found one relation between the quantities defined in (I.31) and πK scattering:

$$\sqrt{2} [f''_s]_{C_i} = 64\rho F_\pi [c_{30}^+]_{C_i}. \quad (I.32)$$

This translates into a relation between πK threshold parameters and f''_s which, with all quantities expressed in units of m_{π^+} , reads:

$$\sqrt{2} [f''_s]_{C_i} = 32\pi \frac{\rho}{1+\rho} F_\pi \left[\frac{35}{6} (2 + \rho + 2\rho^2) [a_3^+]_{C_i} - \frac{5}{4} [a_2^+ + 2\rho b_2^+]_{C_i} \right]. \quad (I.33)$$

There is no more relation involving the quantities discussed so far, $\pi\pi$ and πK scattering, and $K_{\ell 4}$.

Numerical results for (I.33) are shown in Tab. I.5. The experimental results is taken from [21] for f''_s / f_s and from [20] for f_s . This should be an acceptable

combination since the central value for f'_s/f_s and f''_s/f_s from [20] are within 10% of those of [21]. The theoretical results are using the formulas of [14, 15] and fit 10 of [11]. This relation has problems. The sign is even different on both sides. In both cases we also see that the ChPT series has a large NNLO contribution. For completeness, LHS-RHS is given in Tab. I.3 and Fig. I.1.

There have been indications from dispersive methods that ChPT might underestimate the curvature f''_s . Dispersion relations were used in [24] for $K_{\ell 4}$. If one looks at Fig. 7 in [11], one can see that the dispersive result of [24] has a larger curvature than the two-loop result. For this reason, we do not consider this discrepancy a major problem for ChPT.

I.7 $\eta \rightarrow 3\pi$

The amplitude for the decay $\eta(p_\eta) \rightarrow \pi^+(p_+)\pi^-(p_-)\pi^0(p_0)$ can be written as

$$A(\eta \rightarrow \pi^+\pi^-\pi^0) = \sin \epsilon M(s, t, u). \quad (I.134)$$

Here we used the Mandelstam variables

$$\begin{aligned} s &= (p_+ + p_-)^2 = (p_\eta - p_0)^2, \\ t &= (p_+ + p_0)^2 = (p_\eta - p_-)^2, \\ u &= (p_- + p_0)^2 = (p_\eta - p_+)^2, \end{aligned} \quad (I.135)$$

which are linearly dependent $s + t + u = m_{\pi^0}^2 + m_{\pi^-}^2 + m_{\pi^+}^2 + m_\eta^2 \equiv 3s_0$. G-parity requires the amplitude to vanish at the limit $m_u = m_d$ and therefore it must inevitably be accompanied by an overall factor of $m_u - m_d$ which we have chosen to be in the form of $\sin(\epsilon) \approx (\sqrt{3}/4)(m_d - m_u)/(m_s - \hat{m})$. Since the amplitude is invariant under charge conjugation we have $M(s, t, u) = M(s, u, t)$. Similar to the $\pi\pi$ scattering, we can write the amplitude as

$$\begin{aligned} M(s, t, u) &= \eta_1 + \eta_2 s + \eta_3 s^2 + \eta_4 (t - u)^2 + \eta_5 s^3 + \eta_6 s (t - u)^2 \\ &\quad + \text{non polynomial part} \end{aligned} \quad (I.136)$$

to NNLO in ChPT. Using the results of [25] we then obtain two relations

$$[\eta_5]_{C_i} = 3 [\eta_6]_{C_i}, \quad (I.137)$$

$$[\eta_5]_{C_i} = -768\rho^3 [c_{01}^-]_{C_i} = -\pi(1 + \rho) \frac{35}{2} [a_3^-]_{C_i}. \quad (I.138)$$

Since η_5 is not unambiguously determined from the measured Dalitz-plot parameters and η_6 is not measured at all we do not present numerical results for this. The overall factor $\sin \epsilon$ itself is part of the uncertainty involved. Unfortunately, no relations are present for η_1, \dots, η_4 which would have helped in the numerical prediction for $\eta \rightarrow 3\pi$ using the results of [25].

I.8 Scalar formfactors

The scalar form factors for the pions and the kaons are defined as

$$F_{ij}^{M_1 M_2}(t) = \langle M_2(p) | \bar{q}_i q_j | M_1(q) \rangle, \quad (I.39)$$

where $t = p - q$, $i, j = u, d, s$ are flavour indices and M_i denotes a meson state with the indicated momentum. Due to isospin symmetry not all of them are independent, therefore we consider only

$$\begin{aligned} F_S^\pi &= 2F_{uu}^{\pi^0\pi^0} & F_{Ss}^\pi &= F_{ss}^{\pi^0\pi^0}, & F_{Ss}^K &= F_{ss}^{K^0K^0}, \\ F_S^K &= F_{Su}^K + F_{Sd}^K = F_{uu}^{K^0K^0} + F_{dd}^{K^0K^0}, & F_S^{\pi K} &= F_{su}^{K^+\pi^0}. \end{aligned} \quad (I.40)$$

Near $t = 0$ these are expanded via

$$F_S(t) = F_S(0) + F_S' t + F_S'' t^2 + \dots \quad (I.41)$$

The NNLO ChPT calculation for these quantities was performed in [26] where it was found that the curvatures F_S'' only depend on two of the NNLO LECs. As a consequence there are four relations

$$\begin{aligned} [F_S^{\pi''}]_{C_i} &= 2 [F_{Su}^{K''}]_{C_i} = 2 [F_{Ss}^{K''}]_{C_i}, \\ [F_{Ss}^{\pi''}]_{C_i} &= [F_{Sd}^{K''}]_{C_i}, \\ 2 [F_S^{K\pi''}]_{C_i} &= [F_S^{\pi''}]_{C_i} - 2 [F_{Ss}^{\pi''}]_{C_i}. \end{aligned} \quad (I.42)$$

There is also a relation involving the slopes

$$[F_S^{\pi'}]_{C_i} - 2 [F_{Ss}^{\pi'}]_{C_i} - 2 [F_{Sd}^{K'}]_{C_i} + 2 [F_{Ss}^{K'}]_{C_i} - 4 [F_S^{K\pi'}]_{C_i} = 0. \quad (I.43)$$

This is a consequence of the ‘‘scalar Sirlin’’ relation derived in general in [26].

In addition to those already known we found a relation between the values at $t = 0$ which with $\rho = m_K/m_\pi$ reads

$$\begin{aligned} 2\rho^6 [F_S^\pi(0)]_{C_i} &= \rho^4 (2\rho^4 - \rho^2 - 3) [F_{Ss}^\pi(0)]_{C_i} + (3\rho^2 - 1) [F_{Su}^K(0)]_{C_i} \\ &+ (6\rho^4 - 3\rho^2 - 1) [F_{Sd}^K(0)]_{C_i} + (\rho^2 + 1) [F_{Ss}^K(0)]_{C_i} \end{aligned} \quad (I.44)$$

The scalar formfactors had a significant dependence on what was used as input for L_4^r and L_6^r [26]. The curvature relations were studied there and found to sometimes work and sometimes not, see Tab. 2 and Sect. 5.5 in [26]. We intend to come back to these relations when constraints on L_4^r and L_6^r have been included in a general fit.

I.9 Scalar formfactors, masses and decay constants

The three masses M_π^2 , M_K^2 , M_η^2 and decay constants F_π , F_K , F_η are not related, they all have a different dependence on the NNLO LECs. We do find some relations however when we combine them with the scalar formfactors. The two-loop calculations for masses and decay constants can be found in [27,28] for π and η and in [27] for the kaon.

There are two relations between the $F_S(0)$ and the ChPT expansion of the masses M_π^2 , M_K^2 :

$$\begin{aligned} 2B_0 \left[M_\pi^2 \right]_{C_i} &= \frac{1}{3} \left\{ (2\rho^2 - 1) \left[F_{Ss}^\pi(0) \right]_{C_i} + \left[F_S^\pi(0) \right]_{C_i} \right\} \\ 2B_0 \left[M_K^2 \right]_{C_i} &= \frac{1}{3} \left\{ (2\rho^2 - 1) \left[F_{Ss}^K(0) \right]_{C_i} + \left[F_S^K(0) \right]_{C_i} \right\}. \end{aligned} \quad (1.45)$$

Remember we express everything in units powers of m_π . One could arrive to the same conclusion using the Feynman-Hellmann Theorem (see e.g. [29] or [26]) which implies for $q = u, d, s$ and $M = \pi, K$

$$F_{Sq}^M(t=0) = \langle M | \bar{u}u | M \rangle = \frac{\partial m_M^2}{\partial m_q}. \quad (1.46)$$

On the other hand the ChPT expansion leads to

$$\left[M_\pi^2 \right]_{C_i} = \sum_i C_i (m_q)^3 = f(m_u, m_d, m_s), \quad (1.47)$$

that is an homogeneous function of order three. Thanks to the Euler Theorem, $\left[M_\pi^2 \right]_{C_i}$ can be written in terms of its derivatives ($f(\mathbf{x}) = \frac{1}{3} \sum_{i=1}^n \frac{\partial f}{\partial x_i} x_i$ $\mathbf{x} \in \mathbb{R}^n$). These are exactly the relations in Eq. (1.45). Something similar holds for the p^4 expression but with a factor 1/2 instead of 1/3.

There are two more relations if we also include the decay constants. The first one is

$$\begin{aligned} (\rho^2 - 1)^2 \frac{B_0}{F_0} [F_K - F_\pi]_{C_i} + (\rho^2 + 1) B_0 [M_K^2 - M_\pi^2]_{C_i} = \\ (\rho^4 - 1) \left[F_S^{K\pi}(0) \right]_{C_i} + (\rho^2 - 1)^3 \left[F_S^{K\pi'} \right]_{C_i} + (\rho^2 - 1)^3 (\rho^2 + 1) \left[F_S^{K\pi''} \right]_{C_i}. \end{aligned} \quad (1.48)$$

This relation is the same as the one found in [30] for the $K_{\ell 3}$ scalar formfactor when one uses

$$\partial^\mu \bar{s} \gamma_\mu u = (m_s - m_u) i \bar{s} u, \quad (1.49)$$

and rewrites the quark masses into the pion and kaon mass. The second relation, in the simplest form we found, reads

$$\begin{aligned} \left(4\rho^2 [F_\pi]_{C_i} - 4 [F_K]_{C_i}\right) \frac{B_0}{F_0} &= 2\rho^4 [F_S^{\pi'}]_{C_i} + \left(2\rho^6 - \rho^4 + \rho^2\right) [F_{Ss}^{\pi'}]_{C_i} \\ &+ \left(-2\rho^4 + \rho^2 - 1\right) [F_{Sd}^{K'}]_{C_i} - \left(\rho^2 + 1\right) [F_{Su}^{K'}]_{C_i} + \left(-3\rho^2 + 1\right) [F_{Ss}^{K'}]_{C_i}. \end{aligned} \quad (1.50)$$

We have not presented numerical results for the relations in this section since the assumptions underlying fit 10 of [11] were such that all the left hand sides evaluate to zero. In addition the right hand sides tend to contain poorly known quantities.

I.10 Vector formfactors

The vector formfactors have been discussed extensively in [31] and [30]. There three relations between the curvatures and the the Sirlin relation between the slopes [32,33] were found. We also find the expected relationship between the scalar formfactors and the scalar formfactor in $K_{\ell 3}$ which followed from (1.49). The numerical results for the relation between the slopes and curvatures were discussed extensively in [30,31] and found to work well. So this sector had the expected total of 7 relations added to those discussed above.

I.11 Scalar formfactors, $\pi\pi$ and πK scattering

There are two more relations when we combine the scalar formfactors and the scattering amplitudes for $\pi\pi$ and πK scattering. All three quantities are needed. These relations are rather complicated. The first relation is:

$$\begin{aligned} &\rho^4 \left[105a_3^1 + 15b_2^2 - 3a_1^1 + 3b_0^2 - 8a_0^2\right]_{C_i} + (1 + \rho) \left(35\rho^4 [a_3^-]_{C_i} - \frac{1}{3}\rho [a_0^-]_{C_i}\right) \\ &+ \frac{2}{\rho+1}\rho^3 [a_1^+]_{C_i} + \frac{2}{3}(\rho+1)(\rho^2+1)[a_0^+]_{C_i} + \frac{10}{\rho+1}\rho^4(2+\rho+2\rho^2)[b_2^+ + 7a_3^+]_{C_i} \\ &- \frac{10}{\rho+1}\rho^3(2+3\rho+2\rho^2) [a_2^+]_{C_i} - \frac{4}{\rho+1}\rho^3(1+\rho+\rho^2) [b_1^+]_{C_i} = \\ &\frac{\rho^2}{8\pi B_0 F_0^2 (1-3\rho^2)} \left[- (1-\rho^2) [F_{Ss}^K(0)]_{C_i} + 2(1-3\rho^2+3\rho^4) [F_{Sd}^K(0)]_{C_i} \right] \end{aligned}$$

$$+ (1 - 3\rho^2 + 3\rho^4 - 5\rho^6 + 2\rho^8) [F_{Ss}^\pi(0)]_{C_i} + \frac{1}{2}(1 - 5\rho^2 + 8\rho^4 - 4\rho^6) [F_S^\pi(0)]_{C_i} \Big]. \quad (1.51)$$

The second relation involves even more quantities:

$$\begin{aligned} & - (1 - \rho^4)8\pi B_0 F_0^2 \left[\rho^2 [b_0^0 - 12a_0^2 + 2b_0^2 + 45b_2^2 - 315a_3^1]_{C_i} + 210\rho^2(1 + \rho) [a_3^-]_{C_i} \right. \\ & \left. - 2\frac{1+\rho}{\rho} [a_0^-]_{C_i} \right] + 8\pi B_0 F_0^2(\rho - 1) \left[120\rho^4 [b_2^+ + 7a_3^+]_{C_i} - 6\rho^2 [a_1^+ + 2\rho b_1^+]_{C_i} \right. \\ & \left. + 2(1 + \rho)^2 [2a_0^+ - 15\rho^2 a_2^+]_{C_i} \right] \\ & = (1 - \rho^2) \left[12(1 - \rho^4)(F_{Ss}^{K''} - F_{Sd}^{K''}) + 12(1 - \rho^2 - 2\rho^4)F_S^{K\pi'} + 6\rho^2(1 + 2\rho^2)F_{Ss}^{K'} \right. \\ & \quad \left. - 12\rho^4 F_{Sd}^{K'} + 6\rho^2 F_{Su}^{K'} - 12\rho^4 F_{Ss}^{\pi'} \right] \\ & \quad + (1 + \rho^2)12F_S^{K\pi}(0) + 12\rho^2 F_{Su}^K(0) + 3(-1 + 3\rho^2 + 6\rho^4)F_{Sd}^K(0) \\ & \quad + (1 - \rho^2)(2 - \rho^2 - 8\rho^4 - 8\rho^6)F_{Ss}^\pi(0) - 2(1 + 2\rho^2 + 2\rho^4 + 4\rho^6)F_S^\pi(0). \quad (1.52) \end{aligned}$$

I

I.12 A final relation: $K_{\ell 4}$, πK scattering and scalar formfactors

The final relation we found is between $K_{\ell 4}$, πK scattering and the scalar formfactors. The version below is the simplest we found.

$$\begin{aligned} & (1 - \rho^2)^2(1 + \rho^2)B_0 \left[12\sqrt{2}\frac{F_0}{\rho} \left(g_p - g'_p + \left(1 - \frac{1}{4}\rho^2\right) g''_p + \frac{1}{2}\rho^2 f_t \right) \right. \\ & \quad \left. - 16\pi\frac{1+\rho}{\rho} a_0^- + 70\pi(1 + \rho)(20\rho^2 + \rho^4)a_3^- \right] \\ & = 12(1 + \rho^2)\rho^4 F_S^{K\pi}(0) + 12\rho^6 F_{Su}^K(0) + 24\rho^8 F_{Sd}^K(0) \\ & \quad + 2\rho^4(1 - \rho^4)(1 - 4\rho^4)F_{Ss}^\pi(0) - 2\rho^4(1 + 2\rho^2 + 2\rho^4 + 4\rho^6)F_S^\pi(0). \quad (1.53) \end{aligned}$$

I.13 Conclusions

We have performed a systematic search for combinations that allow a test of ChPT at NNLO order. We have therefore looked at the three masses and three decay constants, 11 $\pi\pi$ threshold parameters, 14 πK threshold parameters, 6 $\eta \rightarrow 3\pi$ parameters, 10 observables in $K_{\ell 4}$, 18 in the scalar formfactors and 11 in the vectorformfactors. This means a total of 76 quantities. We found a total of 35 relations between these. Most of these had been noticed earlier but we did find several new ones. We have presented the relations in a form as simple as we found but given the total number they can be rewritten in many equivalent forms.

These are relations that should allow independent determinations of combinations of the NNLO LECs in ChPT. For the vector formfactors this was already done in [30,31] and partly for the $\pi\pi$, πK system [12,18,19] and scalar formfactors [26]. Here we studied in detail the relations for the $\pi\pi$, πK scattering and $K_{\ell 4}$ since for these cases enough experimental and/or dispersion theory results exist. Fig. I.1 is a summary of the numerical relations.

The resulting picture is that ChPT at NNLO works in most cases but there are some problems. The $\pi\pi$ system alone is working well, the πK system alone works satisfactorily but with some problems. The same can be said for the combinations of both systems. A common part in these two cases is the presence of a_3^- . Comparing πK scattering and $K_{\ell 4}$ there is a clear contradiction. In fact, both sides of the relation seem to be difficult to explain within ChPT. It was already noticed in [14, 15] that getting such a large negative curvature in $K_{\ell 4}$ was difficult. It should be noted that none of the quantities involved in the tested relations was used as input for the fit of the NLO LECs in [11].

Acknowledgements

IJ gratefully acknowledges an Early Stage Researcher position supported by the EU-RTN Programme, Contract No. MRTN-CT-2006-035482, (Flavianet) This work is supported in part by the European Commission RTN network, Contract MRTN-CT-2006-035482 (FLAVIANet), European Community-Research Infrastructure Integrating Activity "Study of Strongly Interacting Matter" (HadronPhysics2, Grant Agreement n. 227431) and the Swedish Research Council.

I.A Relation between threshold and subthreshold parameters

For completeness we quote here the relations between the threshold and subthreshold parameters for the tree level part, i.e. that analytic dependence on s , t and u . The $\pi\pi$ ones can also be found in [13] and [14, 15]. For the πK case we have already used the relation (I.17)

$$\begin{aligned}
\pi a_0^0 &= 6b_5 + b_4 + (3/2)b_3 + (3/8)b_2 + (5/32)b_1, \\
\pi b_0^0 &= -2b_6 + 18b_5 + 3b_4 + 3b_3 + (1/4)b_2, \\
\pi a_0^2 &= b_4 + (1/16)b_1, \\
\pi b_0^2 &= -2b_6 + 3b_4 - (1/8)b_2, \\
\pi a_1^1 &= (2/3)b_6 + (1/3)b_4 + (1/24)b_2, \\
\pi b_1^1 &= (4/3)b_6 + (1/2)b_4 - (1/6)b_3, \\
\pi a_2^0 &= (16/15)b_6 + (7/30)b_4 + (1/30)b_3, \\
\pi b_2^0 &= (17/15)b_6 - (1/5)b_5, \\
\pi a_2^2 &= (4/15)b_6 + (1/30)b_4 + (1/30)b_3, \\
\pi b_2^2 &= (1/3)b_6 - (1/5)b_5, \\
\pi a_3^1 &= (1/35)b_6 + (1/35)b_5.
\end{aligned} \tag{I.54}$$

I

$$\begin{aligned}
\pi(\rho+1)a_0^- &= 24\rho^3 c_{01}^- + (3/2)\rho c_{00}^-, \\
\pi(\rho+1)b_0^- &= (36\rho + 24\rho^2 + 36\rho^3)c_{01}^- - 3\rho c_{10}^- + ((3/4)\rho^{-1} + (3/4)\rho)c_{00}^-, \\
\pi(\rho+1)a_1^- &= 12\rho^2 c_{01}^- + \rho c_{10}^- + (1/4)c_{00}^-, \\
\pi(\rho+1)b_1^- &= (12 - 6\rho + 12\rho^2)c_{01}^- + (-1/2 + (1/2)\rho^{-1} + (1/2)\rho)c_{10}^- \\
&\quad - (1/8)\rho^{-1}c_{00}^-, \\
\pi(\rho+1)a_2^- &= (24/5)\rho c_{01}^- + (1/5)c_{10}^-, \\
\pi(\rho+1)b_2^- &= (-(12/5) + (12/5)\rho^{-1} + (12/5)\rho)c_{01}^- - (1/10)\rho^{-1}c_{10}^-, \\
\pi(\rho+1)a_3^- &= (24/35)c_{01}^-, \\
\pi(\rho+1)a_0^+ &= 6\rho^2 c_{01}^+ + (3/8)c_{00}^+, \\
\pi(\rho+1)b_0^+ &= -12\rho^2 c_{11}^+ + (6 + 3\rho + 6\rho^2)c_{01}^+ - (3/4)c_{10}^+ - (3/16)\rho^{-1}c_{00}^+, \\
\pi(\rho+1)a_1^+ &= 4\rho^2 c_{11}^+ + 2\rho c_{01}^+ + (1/4)c_{10}^+, \\
\pi(\rho+1)b_1^+ &= (4 - 2\rho + 4\rho^2)c_{11}^+ + (\rho^{-1} + \rho)c_{01}^+ - c_{20}^+ - (1/8)\rho^{-1}c_{10}^+, \\
\pi(\rho+1)a_2^+ &= (8/5)\rho c_{11}^+ + (1/5)c_{01}^+ + (1/5)c_{20}^+,
\end{aligned}$$

$$\begin{aligned}
\pi(\rho+1)b_2^+ &= (-2/5) + (4/5)\rho^{-1} + (4/5)\rho)c_{11}^+ - (1/10)\rho^{-1}c_{01}^+ \\
&\quad - (6/5)c_{30}^+ - (1/10)\rho^{-1}c_{20}^+, \\
\pi(\rho+1)a_3^+ &= (6/35)c_{11}^+ + (6/35)c_{30}^+ \tag{1.55}
\end{aligned}$$

It can be checked that these satisfy the relations given in Sects. I.3, I.4 and I.5.

I References

- [1] S. Weinberg, "Phenomenological Lagrangians," *Physica* **A96** (1979) 327.
- [2] J. Gasser and H. Leutwyler, "Chiral Perturbation Theory to One Loop," *Ann. Phys.* **158** (1984) 142.
- [3] J. Gasser and H. Leutwyler, "Chiral Perturbation Theory: Expansions in the Mass of the Strange Quark," *Nucl. Phys.* **B250** (1985) 465.
- [4] V. Bernard and U.-G. Meissner, "Chiral perturbation theory," *Ann. Rev. Nucl. Part. Sci.* **57** (2007) 33–60, arXiv:hep-ph/0611231.
- [5] J. Bijnens, "Chiral Perturbation Theory Beyond One Loop," *Prog. Part. Nucl. Phys.* **58** (2007) 521–586, arXiv:hep-ph/0604043.
- [6] J. Bijnens, "Status of Strong ChPT," *PoS EFT09* (2009) 022, arXiv:0904.3713 [hep-ph].
- [7] J. Bijnens and I. Jemos, "Determination of Low Energy Constants and testing Chiral Perturbation Theory at Next to Next to Leading Order," *PoS EFT09* (2009) 032, arXiv:0904.3705 [hep-ph].
- [8] J. Bijnens, G. Colangelo, and G. Ecker, "The mesonic chiral Lagrangian of order p^6 ," *JHEP* **02** (1999) 020, arXiv:hep-ph/9902437.
- [9] J. Bijnens, G. Colangelo, and G. Ecker, "Renormalization of chiral perturbation theory to order p^6 ," *Annals Phys.* **280** (2000) 100–139, arXiv:hep-ph/9907333.
- [10] G. Colangelo, J. Gasser, and H. Leutwyler, " $\pi\pi$ scattering," *Nucl. Phys.* **B603** (2001) 125–179, arXiv:hep-ph/0103088.
- [11] G. Amoros, J. Bijnens, and P. Talavera, "QCD isospin breaking in meson masses, decay constants and quark mass ratios," *Nucl. Phys.* **B602** (2001) 87–108, arXiv:hep-ph/0101127.
- [12] J. Bijnens, P. Dhonte, and P. Talavera, " $\pi\pi$ scattering in three flavour ChPT," *JHEP* **01** (2004) 050, arXiv:hep-ph/0401039.
- [13] J. Bijnens, G. Colangelo, G. Ecker, J. Gasser, and M. E. Sainio, "Elastic $\pi\pi$ scattering to two loops," *Phys. Lett.* **B374** (1996) 210–216, arXiv:hep-ph/9511397.
- [14] G. Amoros, J. Bijnens, and P. Talavera, "Low energy constants from $K_{\ell 4}$ form-factors," *Phys. Lett.* **B480** (2000) 71–76, arXiv:hep-ph/9912398.

- [15] G. Amoros, J. Bijnens, and P. Talavera, “ $K_{\ell 4}$ form-factors and $\pi\pi$ scattering,” *Nucl. Phys.* **B585** (2000) 293–352, [Erratum–ibid. **B598** (2001) 665], arXiv:hep-ph/0003258.
- [16] J. Bijnens, G. Colangelo, G. Ecker, J. Gasser, and M. E. Sainio, “Pion pion scattering at low energy,” *Nucl. Phys.* **B508** (1997) 263–310, arXiv:hep-ph/9707291.
- [17] P. Buettiker, S. Descotes-Genon, and B. Moussallam, “A re-analysis of πK scattering a la Roy and Steiner,” *Eur. Phys. J.* **C33** (2004) 409–432, arXiv:hep-ph/0310283.
- [18] J. Bijnens, P. Dhonte, and P. Talavera, “ πK scattering in three flavor ChPT,” *JHEP* **05** (2004) 036, arXiv:hep-ph/0404150.
- [19] K. Kampf and B. Moussallam, “Tests of the naturalness of the coupling constants in ChPT at order p^6 ,” *Eur. Phys. J.* **C47** (2006) 723–736, arXiv:hep-ph/0604125.
- [20] S. Pislak *et al.*, “High statistics measurement of K_{e4} decay properties,” *Phys. Rev.* **D67** (2003) 072004, arXiv:hep-ex/0301040.
- [21] NA48/2 Collaboration, J. R. Batley *et al.*, “New high statistics measurement of K_{e4} decay form factors and $\pi\pi$ scattering phase shifts,” *Eur. Phys. J.* **C54** (2008) 411–423.
- [22] J. Bijnens, G. Colangelo, G. Ecker, and J. Gasser, “Semileptonic kaon decays,” arXiv:hep-ph/9411311.
- [23] G. Amoros and J. Bijnens, “A parametrization for $K^+ \rightarrow \pi^+ \pi^- e^+ \nu$,” *J. Phys.* **G25** (1999) 1607–1622, arXiv:hep-ph/9902463.
- [24] J. Bijnens, G. Colangelo, and J. Gasser, “ $K_{\ell 4}$ decays beyond one loop,” *Nucl. Phys.* **B427** (1994) 427–454, arXiv:hep-ph/9403390.
- [25] J. Bijnens and K. Ghorbani, “ $\eta \rightarrow 3\pi$ at Two Loops In Chiral Perturbation Theory,” *JHEP* **11** (2007) 030, arXiv:0709.0230 [hep-ph].
- [26] J. Bijnens and P. Dhonte, “Scalar form factors in $SU(3)$ chiral perturbation theory,” *JHEP* **10** (2003) 061, arXiv:hep-ph/0307044.
- [27] G. Amoros, J. Bijnens, and P. Talavera, “Two-point functions at two loops in three flavour chiral perturbation theory,” *Nucl. Phys.* **B568** (2000) 319–363, arXiv:hep-ph/9907264.
- [28] E. Golowich and J. Kambor, “Two-loop analysis of axialvector current propagators in chiral perturbation theory,” *Phys. Rev.* **D58** (1998) 036004, arXiv:hep-ph/9710214.

- [29] J. Gasser and H. Leutwyler, "Low-Energy Expansion of Meson Form-Factors," *Nucl. Phys.* **B250** (1985) 517–538.
- [30] J. Bijnens and P. Talavera, " $K_{\ell 3}$ decays in chiral perturbation theory," *Nucl. Phys.* **B669** (2003) 341–362, arXiv:hep-ph/0303103.
- [31] J. Bijnens and P. Talavera, "Pion and kaon electromagnetic form factors," *JHEP* **03** (2002) 046, arXiv:hep-ph/0203049.
- [32] P. Post and K. Schilcher, "Higher-order corrections to Sirlin's theorem in $\mathcal{O}(p^6)$ chiral perturbation theory," *Phys. Rev. Lett.* **79** (1997) 4088–4091, arXiv:hep-ph/9701422.
- [33] P. Post and K. Schilcher, " K_0 form factor at order p^6 of chiral perturbation theory," *Nucl. Phys.* **B599** (2001) 30–54, arXiv:hep-ph/0007095.

II

A new global fit of the L_i^r at next-to-next-to-leading order in Chiral Perturbation Theory

Johan Bijnens and Ilaria Jemos

Department of Astronomy and Theoretical Physics, Lund University,
Sölvegatan 14A, SE 223-62 Lund, Sweden

II

submitted to *Nuclear Physics B*, [arXiv:1103.5945 [hep-ph]]

A new fit is done to obtain numerical values for the order p^4 low-energy-constants L_i^r in Chiral Perturbation Theory. This includes both new data and new calculated observables. We take into account masses, decay constants, $K_{\ell 4}$, $\pi\pi$ and πK scattering lengths and slopes and the slope of the pion scalar formfactor. We compare in detail where the changes w.r.t. to the 10 year old “fit 10” come from. We discuss several scenarios for estimating the order p^6 constants C_i^r and search for possible values of them that provide a good convergence for the ChPT series. We present two such sets. One big change is that the fits do not have the expected behaviour in the limit of large N_c as well as before.

II.1 Introduction

Since its very beginning Chiral Perturbation Theory (ChPT) [1–3], the effective field theory of QCD at low energies, has been successful in the description of several hadronic observables. Unfortunately when one tries to perform loop calculations to improve the precision of the predictions, one faces a problem. The couplings appearing in the \mathcal{L}_4 Lagrangian are many, i.e. 10, and they must be determined from phenomenology. One of the first determinations of such couplings was done already in [3]. There most of the next-to-leading order (NLO) couplings were inferred both from phenomenology and from considerations lead by large N_c estimates (where N_c is the number of colours).

Considering such good results it is important to decide whether ChPT is a suitable theory to achieve precise determinations of the hadronic observables. It urged then to carry on a program and perform next-to-next-to-leading order (NNLO) calculations [4]. In the last 10 years many two-loop calculations in three-flavour ChPT have been done, see [5] for a review.

Notice however that going to higher orders raises a serious issue: the number of the unknown couplings increases rapidly. If on the one side adding loop diagrams should allow us to include better corrections and improve our descriptions, on the other side, many unknown parameters contribute and this seriously threatens the predictivity of the theory. Furthermore without knowing the values of such constants the convergence of the chiral expansions are difficult to test, although feasible with the method described in [6].

The two-loop expressions now available can be used to perform a new global fit at NNLO of some of the next-to-leading-order (NLO) low-energy-constants (LECs) into the game, the L_i^r . A first attempt was done [7] when some experimental information was available for the $K_{\ell 4}$ decay and by estimating the NNLO contributions using dispersive analysis. The fit was refined later on, when the full NNLO calculation for this process was performed [8,9]. After that many other observables have been calculated at NNLO and many of them are also better known experimentally. Therefore the time has come to perform a new fit of the L_i^r couplings at a NNLO precision. In this paper we present results for such a fit. Some studies using the extra observables but without performing a full new fit were reported in [10–12]. Notice that in a preliminary phase we converted all the FORTRAN programs used to evaluate the amplitudes up to NNLO into C++ code. Our fits are all performed using such programs.

The paper is organized as follows. In Section II.2 we sketch out the ChPT formalism and its main underlying ideas. In Section II.3 we review the phenomenological input we used in our results. We also show which are the L_i^r that give the largest contributions for each observable we included. Notice that now much more input is present compared to the past fits [8,9]. In

Section II.4 we present the main model we used to estimate the C_i^r , i.e. the coupling constants appearing in the NNLO Lagrangian. Such an estimate is usually called the resonance estimate. In Section II.5 we summarize the status of the main existing NNLO fit so far: fit 10 of [9]. In Section II.6 we show our main findings using the C_i^r estimates of Section II.4. We quote different fits so to show how each observable we include affects our findings. The best fit we get we call fit All and should be considered the main output of this work. This fit exhibits several differences with fit 10. One especially striking feature is that it does not respect any longer the large N_c relation $2L_1^r \approx L_2^r$. We also show for fit All the convergence of the expansions for masses and decay constants, which is much improved compared to the one of fit 10. In Section II.6.1 we perform a fit of the L_i^r using as input different experimental results for the $K_{\ell 4}$ amplitude. We show that with this input the large N_c relation $2L_1^r \approx L_2^r$ is better satisfied, although the resulting fit is not as good as fit All in convergence for the masses. In Section II.6.2 we try to justify and test our estimate of the C_i^r . In Section II.6.3 we compare further the fits obtained using their predictions for the two-flavour LECs ℓ_i . Fit All again results as the most convincing one. In Section II.6.4 we show results for fits based on a different estimate of the C_i^r couplings that can be found in [13], this is essentially a chiral quark model estimate (CQM). The fits are not as good as fit All, nor for the χ^2 nor for the convergence of the expansions. Also in this case the large N_c relation is not satisfied. In Section II.7 we show results for an another treatment of the C_i^r . We let the C_i^r couplings to take random values, although they are forced to keep the size $1/(16\pi^2)^2$. These fits have been done requiring extra constraints of convergence for mass and decay constant expansions, as explained in Section II.7.1. In this way it is easier to select only credible fits. The results of such a study are finally shown in Section II.7.2. We found very many good fits that correctly predict all the observables used as input and with low χ^2 . These fits are unfortunately different looking from each other. Therefore we can only show which are the ranges where we found the L_i^r to vary. For some of the NLO constants such ranges are very wide. This method shows however that it is possible to fit the NNLO expressions to the observables with C_i^r of the expected size and it also allows to study well the strong correlations between the couplings. Finally in the appendix we present a table where we quote our estimates for the NNLO couplings.

II.2 Chiral Perturbation Theory

We devote this section to a brief description of the formalism of three-flavour ChPT [1–3]. Introductory references are [14, 15]. The notation in the following is the same as in [4]. ChPT relies on the assumption that the

flavour symmetry of QCD is spontaneously broken to the diagonal subgroup, $SU(3)_L \times SU(3)_R \rightarrow SU(3)_V$. According to the Goldstone theorem, 8 pseudo Goldstone bosons then arise. These are identified with the low lying pseudoscalar mesons and are organized in a unitary 3×3 matrix

$$u = \exp\left(\frac{i}{\sqrt{2}F}\phi\right), \quad (\text{II.1})$$

where ϕ is a hermitian 3×3 matrix:

$$\phi = \begin{pmatrix} \frac{1}{\sqrt{2}}\pi^0 + \frac{1}{\sqrt{6}}\eta & \pi^+ & K^+ \\ \pi^- & -\frac{1}{\sqrt{2}}\pi^0 + \frac{1}{\sqrt{6}}\eta & K^0 \\ K^- & \bar{K}^0 & -\frac{2}{\sqrt{6}}\eta \end{pmatrix}. \quad (\text{II.2})$$

The Lagrangian describing the low-momentum strong interactions of the light mesons must be invariant under $SU(3)_L \times SU(3)_R$ local transformations. The most general lowest order Lagrangian is

$$\mathcal{L}_2 = \frac{F_0^2}{4} (\langle u_\mu u^\mu \rangle + \langle \chi_\pm \rangle), \quad (\text{II.3})$$

with

$$\begin{aligned} u_\mu &= i\{u^\dagger(\partial_\mu - ir_\mu)u - u(\partial_\mu - il_\mu)u^\dagger\}, \\ \chi_\pm &= u^\dagger\chi u^\dagger \pm u\chi^\dagger u, \\ \chi &= 2B_0(s + ip). \end{aligned}$$

The fields s , p , $l_\mu = v_\mu - a_\mu$ and $r_\mu = v_\mu + a_\mu$ are the standard external scalar, pseudoscalar, left- and right-handed vector fields introduced by Gasser and Leutwyler [2, 3]. The constant F_0 and B_0 are instead the leading-order (LO) LECs. The notation $\langle X \rangle$ stands for trace over up, down and strange quark flavour.

Starting from this Lagrangian we can then build up an effective field theory by including loop diagrams and higher order Lagrangians, where operators of higher dimensions are included. Their coupling constants are then counter-terms, i.e. their infinities absorb the UV divergences coming from the loop diagrams. In this way one obtains a theory renormalized order by order. Unfortunately going to higher orders the number of operators allowed by the symmetries increase and therefore also the number of unknown coupling constants. At NLO there are 12 LECs, called L_i^r , while at NNLO there are as many as 94, called C_i^r . We will always quote the renormalized versions where the C_i^r are made dimensionless by using the physical value of F_π . The renormalization scale is chosen to be $\mu = 770$ MeV. While there is in principle enough phenomenological information to fit the first ones, we still need

to rely on theoretical models or on some other method for the latter ones, as those described in Sections II.4, II.6.4 and II.7.

II.3 Fitting procedure and input observables

In this section we first show how we perform the fits and then we review shortly the observables we use as input and their values.

II.3.1 χ^2

The fit is performed using MINUIT in its C++ version [16, 17]. MINUIT is a routine to find the minimum value of a multi-parameter function. The procedure to perform the fits is very similar to the one explained in [9]. The function to be minimized is the χ^2 of the fit. It is obtained summing up the partial contributions $\chi_{i(\text{part})}^2$ for each input observables

$$\begin{aligned}\chi_{i(\text{part})}^2 &= \left(\frac{x_{i(\text{meas})} - x_{i(\text{calc})}}{\Delta x_i} \right)^2 \\ \chi^2 &= \sum_i \chi_{i(\text{part})}^2\end{aligned}\quad (\text{II.4})$$

where $x_{i(\text{meas})}$ are the physical values for each input observables and Δx_i their associated errors. $x_{i(\text{calc})}$ are the results as calculated by ChPT up to NNLO. The rest of this section is devoted to list the values and the uncertainties used for each x_i .

II.3.2 Masses and decay constants

The masses and decay constants of the light pseudoscalar mesons have been calculated at NNLO in [18]. We use them as physical parameters, namely as input to calculate the several observables, similarly to what was done in [9]. Their values are given in [19] and are

$$\begin{aligned}m_{\pi^+} &= 139.57018 \text{ MeV}, & m_{\pi^0} &= 134.9766 \text{ MeV}, & m_{\eta} &= 547.853 \text{ MeV}, \\ m_{K^+} &= 493.677 \text{ MeV}, & m_{K^0} &= 497.614 \text{ MeV},\end{aligned}\quad (\text{II.5})$$

$$F_{\pi} = 0.0922 \pm 0.0002 \text{ GeV}.\quad (\text{II.6})$$

The measurements in (II.5) and (II.6) differ slightly from the ones used in the latest full fit [9].

$$\begin{aligned}m_{\pi^+} &= 139.56995 \text{ MeV}, & m_{\pi^0} &= 134.9764 \text{ MeV}, & m_{\eta} &= 547.30 \text{ MeV}, \\ m_{K^+} &= 493.677 \text{ MeV}, & m_{K^0} &= 497.672 \text{ MeV},\end{aligned}\quad (\text{II.7})$$

$$F_{\pi} = 0.0924 \text{ GeV}.\quad (\text{II.8})$$

Notice that preliminary results of our work have been reported in the proceedings [20, 21] and several unpublished talks. Those results were based on the masses of [22], that differ slightly from both (II.5), (II.6) and (II.7), (II.8).

All the new fits shown in this paper have been produced using the values in (II.5) and (II.6). However we have not observed any substantial modification of the outputs when using the old masses (II.7) and pion decay constant (II.8). As discussed below other changes in experimental input are behind the changes of central values.

The masses depend at LO on $B_0\hat{m}$ (with $\hat{m} = (m_u + m_d)/2$) and on B_0m_s . L_4^r , L_6^r , L_5^r and L_8^r appear in the expression at NLO. In m_η^2 there is also a NLO contribution from L_7^r . The decay constant F_π depends instead on F_0 , as an overall factor, and on L_4^r and L_5^r .

II.3.3 F_K/F_π

As input observable for our fits we will use the ratio F_K/F_π to eliminate the dependence on the unknown constant F_0 , since it contributes as an overall factor for F_K as well. In the end the value of F_π then determines the value for F_0 .

The ratio takes the value [19]

$$\frac{F_K}{F_\pi} = 1.197 \pm 0.007, \quad (\text{II.9})$$

that is also in full agreement with several lattice estimates as reported in [23]. Using F_K/F_π at NLO we are sensitive both to L_4^r and L_5^r . To perform the fit we expand the ratio as

$$\frac{F_K}{F_\pi} = 1 + \underbrace{\frac{F_K}{F_0}\Big|_{p^4} - \frac{F_\pi}{F_0}\Big|_{p^4}}_{\text{NLO}} + \underbrace{\frac{F_K}{F_0}\Big|_{p^6} - \frac{F_\pi}{F_0}\Big|_{p^6} - \frac{F_K}{F_0}\Big|_{p^4} \frac{F_\pi}{F_0}\Big|_{p^4} + \frac{F_\pi}{F_0}\Big|_{p^4}^2}_{\text{NNLO}}, \quad (\text{II.10})$$

so that we can keep track of the exact contributions from the different orders. However we also check that the same quantity estimated as

$$\frac{F_K}{F_\pi} = \frac{F_0 + F_K|_{p^4} + F_K|_{p^6}}{F_0 + F_\pi|_{p^4} + F_\pi|_{p^6}} \quad (\text{II.11})$$

gives approximately the same value¹.

Notice the experimental result for the ratio F_K/F_π (II.9) differs substantially from the one used in [9]. Ref. [9] used $F_K/F_\pi = 1.22 \pm 0.01$. The change in F_K/F_π is one of the major sources of difference with [9] as will be shown later in Section II.6.

¹We thank Veronique Bernard and Emilie Passemar for pointing out that these were significantly different for some of our preliminary fits.

II.3.4 The quark-mass ratio m_s/\hat{m}

For the masses we have a similar problem, they depend on the quark masses and on B_0 . We thus use as was done in [8, 9] the ratio of the strange quark mass over the isospin doublet quark mass \hat{m} as input observable. The two following relations involving the light pseudoscalar meson masses hold at LO in ChPT

$$\left. \frac{m_s}{\hat{m}} \right|_1 = \frac{2m_{0K}^2 - m_{0\pi}^2}{m_{0\pi}^2} \quad \left. \frac{m_s}{\hat{m}} \right|_2 = \frac{3m_{0\eta}^2 - m_{0\pi}^2}{2m_{0\pi}^2} \quad (\text{II.12})$$

where with m_0 we indicate the meson masses at LO. They are calculated subtracting from the physical values the NLO and NNLO expressions. We include both relations in (II.12) in the fits. For the pion mass we use the neutral pion mass m_{π^0} . In the kaon case we need to correct the physical value for the mass since its electromagnetic contribution is sizeable. We take the average between m_{K^+} and m_{K^0} and then we subtract the electromagnetic contribution as stated by the Dashen's theorem and an estimate of its violation:

$$m_{\text{Kav}}^2 = \frac{1}{2}(m_{K^+}^2 + m_{K^0}^2 - 1.8(m_{\pi^+}^2 - m_{\pi^0}^2)) = (494.50 \text{ MeV})^2. \quad (\text{II.13})$$

The factor 1.8 in (II.13) is due to the corrections to Dashen's theorem where we use the value of [24].

The value of the quark mass ratio has been calculated by several lattice collaborations. The authors of [9] used as standard input $m_s/\hat{m} = 24$ with a 10% uncertainty, but they also checked that $m_s/\hat{m} = 26$ was compatible. Here instead we use $m_s/\hat{m} = 27.8$ as obtained by the Flavianet Lattice Averaging Group in [23], and we again adopt a 10% uncertainty for the error to be used in the fits when comparing with the theoretical values (II.12).

In the end the calculated NLO and NNLO masses are used to determine the lowest order mass or alternatively $B_0\hat{m}$.

II.3.5 $K_{\ell 4}$ formfactors

The decay $K^+(p) \rightarrow \pi^+(p_1)\pi^-(p_2)e^+(p_\ell)\nu(p_\nu)$ is given by the amplitude [7]

$$T = \frac{G_F}{\sqrt{2}} V_{us}^* \bar{u}(p_\nu) \gamma_\mu (1 - \gamma_5) v(p_\ell) (V^\mu - A^\mu). \quad (\text{II.14})$$

In (II.14) V^μ and A^μ can be parametrized in terms of four formfactors: F , G , H and R . However the R -formfactor is negligible in decays with an electron in the final state. Using partial wave expansion and neglecting d wave terms

one obtains for the F , G and the H formfactors [25]:

$$\begin{aligned} F(s_\pi, s_\ell, \cos \theta) &= f_s(s_\pi, s_\ell) e^{i\delta_s} + f_p e^{i\delta_p} \cos \theta + \dots, \\ G(s_\pi, s_\ell, \cos \theta) &= g_p(s_\pi, s_\ell) e^{i\delta_p} + \dots, \\ H(s_\pi, s_\ell, \cos \theta) &= h_p(s_\pi, s_\ell) e^{i\delta_p} + \dots, \end{aligned} \quad (\text{II.15})$$

where we also assumed that the p phase is the same for the three formfactors. In (II.15) $s_\pi(s_\ell)$ is the invariant mass of dipion (dilepton) system, θ is the angle of the pion in their rest frame w.r.t. the kaon momentum. The F and G formfactors were calculated at NNLO in [8]. The quantities are especially sensitive to L_1^r , L_2^r and L_3^r . Also the H formfactor is known at order p^6 [26] but we do not use it as input observable since it depends on a different set of LECs, those from the anomalous intrinsic parity sector.

The measured observables are obtained by further parametrizing $f_s(s_\pi, s_\ell)$ and $g_p(s_\pi, s_\ell)$ as

$$\begin{aligned} f_s(s_\pi, s_\ell) &= f_s + f_s' q^2 + f_s'' q^4 + f_e' s_\ell / 4m_\pi^2, \\ g_p(s_\pi, s_\ell) &= g_p + g_p' q^2, \end{aligned} \quad (\text{II.16})$$

where $q^2 = s_\pi / (4m_\pi^2) - 1$. (II.16) can be used to fit the measured data points. In [9] the preliminary linear fit from the E865 measurement [27] was used as input. It has the values

$$\begin{aligned} f_s &= 5.77 \pm 0.097, & f_s' &= 0.47 \pm 0.15, \\ g_p &= 4.684 \pm 0.092, & g_p' &= 0.54 \pm 0.20. \end{aligned} \quad (\text{II.17})$$

Now more precise results from the NA48/2 experiment are available [28] and their second order fit of the formfactors read

$$\begin{aligned} \frac{f_s'}{f_s} &= 0.152 \pm 0.009, & \frac{f_s''}{f_s} &= -0.073 \pm 0.009, \\ \frac{g_p'}{f_s} &= 0.868 \pm 0.01, & \frac{g_p''}{f_s} &= 0.089 \pm 0.02, \end{aligned} \quad (\text{II.18})$$

Notice that in [28] no measure of f_s is reported, therefore we always use the $f_s = 5.75 \pm 0.097$ from the E865 collaboration [29] in our fits. Multiplying by f_s and combining the errors in quadrature we obtain as measures

$$\begin{aligned} f_s &= 5.750 \pm 0.097, & f_s' &= 0.874 \pm 0.054, & f_s'' &= -0.420 \pm 0.052, \\ g_p &= 4.99 \pm 0.12, & g_p' &= 0.512 \pm 0.121. \end{aligned} \quad (\text{II.19})$$

In [28] there is also a linear fit which gives $\frac{f_s'}{f_s} = 0.073 \pm 0.004$ and thus $f_s' = 0.420 \pm 0.024$. Deciding which of the two fits for the F_s formfactor should

be used is a relevant issue. The problem is how much we can rely on the curvature of the formfactor F_s . As a matter of fact it is difficult for NNLO ChPT to reproduce the large negative curvature f_s'' , as was also noted in [6,9]. A dispersive analysis approach combined to two loops ChPT, similar to the one done for $\pi\pi$ scattering [30], might clarify the situation. An indication of this is given by Figure 7 of [9]. It is visible there that the dispersive result for $K_{\ell 4}$ decay [7] has a larger curvature than the two-loop result [9].

II.3.6 $\pi\pi$ scattering

The $\pi\pi$ scattering amplitude can be written as a function $A(s, t, u)$ which is symmetric in t, u :

$$A(\pi^a \pi^b \rightarrow \pi^c \pi^d) = \delta^{a,b} \delta^{c,d} A(s, t, u) + \delta^{a,c} \delta^{b,d} A(t, u, s) + \delta^{a,d} \delta^{b,c} A(u, t, s), \quad (\text{II.20})$$

where s, t, u are the usual Mandelstam variables. The three flavour ChPT calculation of $A(s, t, u)$ was done in [11]. The isospin amplitudes $T^I(s, t)$ ($I = 0, 1, 2$) are

$$\begin{aligned} T^0(s, t) &= 3A(s, t, u) + A(t, u, s) + A(u, s, t), \\ T^1(s, t) &= A(s, t, u) - A(u, s, t), \\ T^2(s, t) &= A(t, u, s) + A(u, s, t), \end{aligned} \quad (\text{II.21})$$

and are expanded in partial waves

$$T^I(s, t) = 32\pi \sum_{\ell=0}^{+\infty} (2\ell + 1) P_{\ell}(\cos \theta) t_{\ell}^I(s), \quad (\text{II.22})$$

where t and u have been written as $t = -\frac{1}{2}(s - 4m_{\pi}^2)(1 - \cos \theta)$, $u = -\frac{1}{2}(s - 4m_{\pi}^2)(1 + \cos \theta)$. In (II.22) we indicate with $P_{\ell}(\cos \theta)$ the Legendre polynomials. Near threshold the t_{ℓ}^I are further expanded in terms of the threshold parameters

$$t_{\ell}^I(s) = q^{2\ell} (a_{\ell}^I + b_{\ell}^I q^2 + \mathcal{O}(q^4)), \quad q^2 = \frac{1}{4}(s - 4m_{\pi}^2), \quad (\text{II.23})$$

where $a_{\ell}^I, b_{\ell}^I \dots$ are the scattering lengths, slopes, \dots . These thresholds parameters constitute our observables. Currently a very precise determination of these parameters exists. It is based on a dispersive analysis approach and on two-flavour ChPT and can be found in [30]. In Table II.1 we quote the values of the threshold parameters we use in our fits and their corresponding uncertainties, which we took to be double the ones in [30]. For most fits we used only a_0^0 and a_0^2 but we have checked that the others listed in Table II.1 are also

a_0^0	0.220 ± 0.010	m_π^0
b_0^0	0.276 ± 0.012	m_π^{-2}
a_0^2	-0.444 ± 0.020	$10^{-1}m_\pi^0$
b_0^2	-0.803 ± 0.024	$10^{-1}m_\pi^{-2}$
a_1^1	0.379 ± 0.010	$10^{-1}m_\pi^{-2}$
b_1^1	0.567 ± 0.026	$10^{-2}m_\pi^{-4}$

Table II.1: The values of the scattering lengths and slopes as found in [30] and our fitting uncertainties. In the third column the normalization factors are given. We quote here only those scattering parameters added as input in our fits.

well within the uncertainties quoted. Notice also that the NA48/2 experiment in [28] obtained compatible values for a_0^0 and a_0^2 from the measurement of the $\delta = \delta_p - \delta_s$ phase shift in $K_{\ell 4}$ decays.

II.3.7 πK scattering

The πK scattering process has amplitudes $T^I(s, t, u)$ in the isospin channels $I = 1/2, 3/2$. They have been calculated at NNLO in ChPT in [12]. As for $\pi\pi$ scattering, it is possible to define scattering lengths and slopes a_ℓ^I, b_ℓ^I . So we introduce the partial wave expansion of the isospin amplitudes

$$T^I(s, t, u) = 16\pi \sum_{\ell=0}^{+\infty} (2\ell + 1) P_\ell(\cos \theta) t_\ell^I(s), \quad (\text{II.24})$$

where $P_\ell(\cos \theta)$ are the Legendre polynomials. Then we expand the $t_\ell^I(s)$ near threshold

$$t_\ell^I(s) = \frac{1}{2} \sqrt{s} q_{\pi K}^{2\ell} \left(a_\ell^I + b_\ell^I q_{\pi K}^2 + \mathcal{O}(q_{\pi K}^4) \right), \quad (\text{II.25})$$

where

$$q_{\pi K}^2 = \frac{s}{4} \left(1 - \frac{(m_K + m_\pi)^2}{s} \right) \left(1 - \frac{(m_K - m_\pi)^2}{s} \right), \quad (\text{II.26})$$

is the magnitude of the three-momentum in the center of mass system. The Mandelstam variables are given in terms of the scattering angle θ by

$$t = -2q_{\pi K}^2(1 - \cos \theta), \quad u = -s - t + 2m_K^2 + 2m_\pi^2. \quad (\text{II.27})$$

$a_0^{1/2}$	0.224 ± 0.044	m_π^{-1}
$b_0^{1/2}$	0.85 ± 0.08	$10^{-1} m_\pi^{-3}$
$a_0^{3/2}$	-0.448 ± 0.154	$10^{-1} m_\pi^{-1}$
$b_0^{3/2}$	-0.37 ± 0.06	$10^{-1} m_\pi^{-3}$
$a_1^{1/2}$	0.19 ± 0.02	$10^{-1} m_\pi^{-3}$
$b_1^{1/2}$	0.18 ± 0.04	$10^{-2} m_\pi^{-5}$
$a_1^{3/2}$	0.65 ± 0.88	$10^{-3} m_\pi^{-3}$
$b_1^{3/2}$	-0.92 ± 0.34	$10^{-3} m_\pi^{-5}$

Table II.2: The values of the scattering lengths and slopes as found in [31]. The uncertainties quoted here are those used in our fits and are double the ones of [31]. In the third column the normalization factors are given. We quote only those scattering parameters added as input in our fits.

(II.25) defines the πK scattering parameters a_ℓ^I and b_ℓ^I that are our input observables. These have been computed from Roy and Steiner type equations in [31]. The results for the s and p waves scattering parameters we use are reported in Table II.2. For most numerical results we used only $a_0^{1/2}$ and $a_0^{3/2}$ but we have checked that all the others agree within uncertainties.

II

II.3.8 Scalar formfactor

The scalar formfactor for the pion is defined as

$$F_S^\pi(t) = \langle \pi^0(p) | \bar{u}u + \bar{d}d | \pi^0(q) \rangle, \quad (\text{II.28})$$

where $t = p - q$. Near $t = 0$ it is expanded via

$$F_S^\pi(t) = F_S^\pi(0) \left(1 + \frac{1}{6} \langle r^2 \rangle_S^\pi t + c_S^\pi t^2 + \dots \right). \quad (\text{II.29})$$

The observables $\langle r^2 \rangle_S^\pi$ and c_S^π are used as input in our fits. The NNLO ChPT calculation for these quantities was performed in [10]. The scalar formfactor cannot be measured experimentally. Measuring the $\pi\pi$ phase shifts and using a dispersive representation it is possible to infer its energy behaviour and therefore the values of $\langle r^2 \rangle_S^\pi$ and c_S^π [32–34]

$$\langle r^2 \rangle_S^\pi = 0.61 \pm 0.04 \text{ fm}^2, \quad c_S^\pi = 11 \pm 2 \text{ GeV}^{-4}. \quad (\text{II.30})$$

Notice that the result for $\langle r^2 \rangle_S^\pi$ is also compatible with the lattice result of [35].

This is all the information we can extract from the scalar formfactors. Currently, there are basically no results available for $F_S^\pi(0)$ and for the energy behaviour of the kaon scalar formfactors or of the strange contribution to the pion formfactor.

II.3.9 L_9^r and L_{10}^r

We do not attempt to fit the remaining NLO LECs, L_9^r and L_{10}^r . Those LECs we fit are independent of L_9^r and L_{10}^r , or alternatively, none of the observables² we discuss depend on them. One needs to include additional information to constrain their values.

L_9^r appears alone at NLO in the electromagnetic radius of the pion vector formfactor. The NNLO contribution dependent on the other L_i^r is rather small [36]. It was therefore possible to fit that constant almost independently from the other couplings [36]. Furthermore it never appears at NLO in any of the observables used here as input thus it does not affect much our fits. We always set $L_9^r = (0.593 \pm 0.43) \times 10^{-2}$ for $\mu = 0.77$ GeV.

L_{10}^r can be estimated using τ decays data on the $V - A$ spectral function [37]. Its value was found to be $L_{10}^r = (-4.06 \pm 0.39) \times 10^{-3}$ at $\mu = 0.77$ GeV. However this constant never appears in the observables under study not even at NNLO. Therefore it does not have any influence on our fits. For this reason we always set such constant to zero in our fits.

II.4 Resonance estimates for the C_i^r

The many unknown coupling constants that appear in the p^6 Lagrangian, the C_i^r , represent the major problem for performing the fit with a $\mathcal{O}(p^6)$ precision. A lot of effort went into trying to estimate them using different models and treatments. The one we present here, also used in [8], is the resonance saturation model [38, 39]. It is based on the idea that the LECs encode the information from physics above $\Lambda_{\text{ChPT}} \approx 1$ GeV, and that they are dominated by the physics just above this scale, i.e. the physics of low-lying resonances. Therefore we need a Lagrangian that describes these new particles and their interactions with the pseudoscalar mesons of the octet. We include only vector, scalar and the η' fields. We use the same estimate described in [8], thus we refer the reader to that paper for further details, including the Lagrangians used at the resonance level.

The model is used then to estimate the p^6 contributions depending on the C_i^r . In [8], the heavier mesons were integrated out producing p^6 Lagrangians

²with the exception of $K_{\ell 4}$ where a very small dependence is present for $s_\ell \neq 0$.

for the pseudo-Goldstone boson. The heavy resonance fields for the vector mesons produce

$$\begin{aligned} \mathcal{L}_V = & -\frac{if_\chi g_V}{\sqrt{2M_V^2}} \langle \nabla_\lambda ([u^\lambda, u^\nu]) [u^\nu, \chi_-] \rangle + \frac{g_V \alpha_V}{\sqrt{2M_V^2}} \langle [u_\lambda, f_-^{\nu\lambda}] (\nabla^\mu [u_\mu, u_\nu]) \rangle \\ & - \frac{ig_V f_V}{2M_V^2} \langle (\nabla_\lambda f_+^{\lambda\nu}) (\nabla^\mu [u_\mu, u_\nu]) \rangle - \frac{i\alpha_V f_\chi}{M_V^2} \langle [u_\nu, \chi_-] [u_\lambda, f_-^{\nu\lambda}] \rangle \\ & - \frac{f_\chi f_V}{\sqrt{2M_V^2}} \langle (\nabla_\lambda f_+^{\lambda\mu}) [u_\mu, \chi_-] \rangle, \end{aligned} \quad (\text{II.31})$$

and the scalar mesons

$$\begin{aligned} \mathcal{L}_S = & \frac{c_d^2}{2M_S^4} \langle \nabla_\nu (u_\mu u^\mu) \nabla^\nu (u_\lambda u^\lambda) \rangle + \frac{c_m^2}{2M_S^4} \langle (\nabla_\nu \chi_+) (\nabla^\nu \chi_+) \rangle \\ & + \frac{c_d c_m}{M_S^4} \langle \nabla_\nu (u_\mu u^\mu) (\nabla^\nu \chi_+) \rangle. \end{aligned} \quad (\text{II.32})$$

While for the η' they obtained

$$\mathcal{L}_{\eta'} = -\frac{\tilde{d}_m^2}{2M_{\eta'}^4} \partial_\mu \langle \chi_- \rangle \partial^\mu \langle \chi_- \rangle \quad (\text{II.33})$$

In (II.31) and (II.32) $f_\pm^{\mu\nu}$ are defined as

$$f_\pm^{\mu\nu} = u(v^{\mu\nu} - a^{\mu\nu})u^\dagger \pm u^\dagger(v^{\mu\nu} + a^{\mu\nu})u.$$

In [8] the above Lagrangians were not rewritten in the standard form of the Lagrangian at p^6 . That work has since been done using more general resonance lagrangians in [40,41]. We have checked that the results using the Lagrangians (II.31,II.32) directly agrees with the same inputs using the C_i^r directly in terms of resonance parameters as derived in [40,41]. The η' contribution was rewritten in the C_i^r in [42].

The values we choose for the different couplings are the same as in [8]

$$\begin{aligned} f_V = 0.20, \quad f_\chi = -0.025, \quad g_V = 0.09, \\ \alpha_V = -0.014, \quad c_m = 42 \text{ MeV}, \quad c_d = 32 \text{ MeV}, \\ \tilde{d}_m = 20 \text{ MeV}. \end{aligned} \quad (\text{II.34})$$

and the masses are the experimental ones [19].

$$m_V = m_\rho = 0.77 \text{ GeV}, \quad m_S = 0.98 \text{ GeV}, \quad m_{\eta'} = 0.958 \text{ GeV}, \quad (\text{II.35})$$

In Table II.15 in the appendix we quote the C_i^r as estimated through the resonance model. We did not include more sophisticated resonance models

	fit 10	fit 10 iso
$10^3 L_1^r$	0.43	0.39 ± 0.12
$10^3 L_2^r$	0.73	0.73 ± 0.12
$10^3 L_3^r$	-2.35	-2.34 ± 0.37
$10^3 L_4^r$	$\equiv 0$	$\equiv 0$
$10^3 L_5^r$	0.97	0.97 ± 0.11
$10^3 L_6^r$	$\equiv 0$	$\equiv 0$
$10^3 L_7^r$	-0.31	-0.30 ± 0.15
$10^3 L_8^r$	0.60	0.60 ± 0.20
χ^2 (dof)	--	0.26 (1)

Table II.3: The results for fit10 of [8] and for a similar fit done without including isospin breaking corrections for the masses (fit10 iso) and also using the masses in (II.5) and decay constant F_π as in (II.6). The uncertainties are those calculated by MINUIT. The two fits reported are in agreement within uncertainties.

because this would have again increased strongly the number of free parameters to be fitted. As discussed below we also have indications that terms suppressed by $1/N_c$, N_c the number of colours, might be important. These cannot at present be estimated using this type of approach.

II.5 Existing fits

In this section we describe a bit more in detail the earlier fits. The main full fit done is fit 10 in [9]³. Earlier determination of the L_i^r did not fully include NNLO effects and we thus do not discuss them here. The values for the L_i^r obtained in fit 10 are reproduced in Table II.3 in the column labelled fit 10. This is a full NNLO fit of the L_i^r and it was done including the quantities and the L_i^r whose value they influence most:

1. masses and pion decay constant with the old values as in (II.7) and (II.8)
2. the $K_{\ell 4}$ formfactor parameters: $f_{s\ell}, f'_{s\ell}, g_{s\ell}, g'_{s\ell}$. They constrained mostly L_1^r, L_2^r, L_3^r .
3. $F_K/F_\pi = 1.22 \pm 0.01$, sensitive to L_5^r .
4. $m_s/\hat{m} = 24$ constrains L_7^r, L_8^r via the masses in (II.12).
5. $L_4^r \equiv L_6^r \equiv 0$ since they are $1/N_c$ suppressed couplings.

The C_i^r contributions were estimated using resonance saturation as described in Section II.4. They also included there the axial-vector resonances,

³The E865 data were still preliminary then, the main fit in [9] was with older $K_{\ell 4}$ data.

	p^2	p^4	p^6
m_π^2	0.753	0.006	0.241
m_K^2	0.702	0.007	0.291
m_η^2	0.747	-0.047	0.300
F_π/F_0	1	0.136	-0.075
F_K/F_0	1	0.307	-0.003
F_K/F_π	1	0.171	0.049

Table II.4: The convergence of the expansion for the meson masses and the decay constants for fit 10 iso. A similar behaviour holds for fit10. The masses quoted are normalized to the physical masses, while the decay constants to F_0 ($F_0 = 0.0869$ GeV).

although their contribution was rather small. The scale of saturation was set to $\mu \equiv 0.77$ GeV, but $\mu = 0.5, 1$ GeV were within errors. In fit 10 isospin breaking corrections in the masses and decay constants were also included, though the authors of [9] noticed that the neglect of isospin violation was a good approximation. Indeed the fits performed including or not these effects are in agreement within errors as can be seen from Table II.3 comparing the columns fit 10 and fit 10 iso.

Fit 10 has been so far a quite successful fit. Not only because it already included many quantities at order p^6 , but also because the resulting L_i^r nicely confirmed the estimates from resonance models. These are lead by the large N_c expansion which predicts e.g. $2L_1^r \approx L_2^r$ and $L_4^r \approx L_6^r \approx 0$. While the second relation was imposed, the first one was found to be well satisfied. This added credibility to the fit itself even though it relied on the resonance estimate for the tree-level p^6 contributions.

However the convergence of the perturbative expansion for this fit is not as expected. The different orders for the masses and decay constants are reported in Table II.4 for fit 10 iso⁴. The $\mathcal{O}(p^4)$ order of the masses turns out to be tiny, far less than the expected 30%. On the other hand the NNLO contribution is definitely too large. The sources of this bad convergence are basically two. First the constraint $L_4^r \equiv L_6^r \equiv 0$ that clearly sends to zero many contributions coming from the NLO tree-level diagrams. Secondly most of the C_i^r appearing in the masses expressions are estimated to be zero as well. Therefore they cannot help in canceling large two-loop contributions. On the other hand the convergence for the decay constants is quite satisfying.

After fit 10 was performed many other observables have been calculated at $\mathcal{O}(p^6)$ in $SU(3)$ ChPT such as the $\pi\pi$ and πK scattering threshold parameters. Of course it is very important to compare the pure ChPT predictions obtained

⁴The numbers for fit 10 itself can be found in Table 2 of [10].

using fit 10 with the values of Tables II.1 and II.2. These comparisons have been done and can be found in Table 1 of [11] and in Table 4 of [12]. Fit 10 is mostly in agreement within errors, although there are small discrepancies in some of the threshold parameters. Some comparison with scalar formfactors was done in [10]. The last three papers used the same inputs as fit 10 and tried to vary L_4^r and L_6^r to see if some preferred regions could be found. Here we redo the fit from the beginning with all inputs.

II.6 New Fits

The aim of this section is to show how the new measurements and observables included in our global fits, change the results compared to fit 10. We have rewritten as mentioned above all programs into C++ and are using the isospin symmetric versions of the calculations. We therefore first redid the fit using the same inputs as fit 10. The outputs are given in Table II.3 in the column labelled fit 10 iso. This also shows that the minor changes in masses and F_π as well the isospin breaking corrections do not affect the fit values appreciably. We will now add the effects of the changed experimental inputs and of the additional inputs to see how they change the fitted values of the L_i^r .

In Table II.5 we present several fits. These have all been performed using the resonance estimate of the C_i^r of Section II.4 and Table II.15 in the appendix, setting the scale of saturation $\mu = 0.77$ GeV. Furthermore, we used the new values of the masses and decay constant of (II.5) and (II.6). We remind the reader that the use of these new parameter-values affects the output only within the uncertainties. Hereafter we summarize the steps in which we have included the new information.

NA48/2 The input observables and their values are the same as for fit 10 iso, but we use the new measurements in (II.19) for the $K_{\ell 4}$ decay from the NA48/2 collaboration [28]. The new measurements lead immediately to a striking feature: the large N_c relation $2L_1^r \approx L_2^r$ does not hold any longer. It even turns out that $L_2^r \lesssim L_1^r$. Notice that, as explained in Section II.3.5, the slope f_s' comes from a second order fit of the f_s formfactor and therefore it differs from the one used in fit 10. In Section II.6.1 we will present also results for the linear fit of the f_s formfactor.

F_K/F_π Same as fit NA48/2 but with the new value in (II.9) for F_K/F_π . L_5^r is mainly affected and becomes smaller than in fit 10. As a consequence also the convergence of the decay constants expansion is worsened, e.g. $F_\pi/F_0|_{p^4} \approx 0.134$ while $F_\pi/F_0|_{p^6} \approx -0.126$.

All★ In this fit we include a few more observables, i.e. the $\pi\pi$ scattering parameters a_0^0 and a_2^0 , the πK scattering parameters $a_0^{\frac{1}{2}}$ and $a_0^{\frac{3}{2}}$ and the pion

	fit 10 iso	NA48/2	F_K/F_π	All \star	All	$C_i^r \equiv 0$	All p^4
$10^3 L_1^r$	0.39 ± 0.12	0.88	0.87	0.89	0.88 ± 0.09	0.65	1.12
$10^3 L_2^r$	0.73 ± 0.12	0.79	0.80	0.63	0.61 ± 0.20	0.11	1.23
$10^3 L_3^r$	-2.34 ± 0.37	-3.11	-3.09	-3.06	-3.04 ± 0.43	-1.47	-3.98
$10^3 L_4^r$	$\equiv 0$	$\equiv 0$	$\equiv 0$	0.60	0.75 ± 0.75	0.80	1.50
$10^3 L_5^r$	0.97 ± 0.11	0.91	0.73	0.58	0.58 ± 0.13	0.68	1.21
$10^3 L_6^r$	$\equiv 0$	$\equiv 0$	$\equiv 0$	0.08	0.29 ± 0.85	0.29	1.17
$10^3 L_7^r$	-0.30 ± 0.15	-0.30	-0.26	-0.22	-0.11 ± 0.15	-0.14	-0.36
$10^3 L_8^r$	0.60 ± 0.20	0.59	0.49	0.40	0.18 ± 0.18	0.19	0.62
χ^2	0.26	0.01	0.01	1.20	1.28	1.67	2.60
dof	1	1	1	4	4	4	4

Table II.5: Several global fits compared to fit10 iso. For all the fit $\mu = 0.77$ GeV. The errors quoted are the ones as calculated by MINUIT. The numbers in the row labelled dof are the degrees of freedom for the fit. See the description in the text for further details on how the fits have been performed. The column labelled All is our main new result.



scalar radius $\langle r \rangle_S^2$. We also release the constraint $L_4^r = L_6^r = 0$ because now we have many more observables included. Unfortunately since none of the new observables involve information on the masses (and therefore on those two couplings), we still cannot achieve the precise values of L_4^r and L_6^r . They are highly correlated and MINUIT gives a very large uncertainty for those. Furthermore since now the $\mathcal{O}(p^4)$ con-

tributions to the masses due to L_4^r and L_6^r are not zero, L_5^r and L_8^r diminish.

All This fit is very similar to fit All*. Here we adopt the new value for the quark mass ratio $m_s/\hat{m} = 27.8$. However we find that using values for the quark mass ratio between 27 and 29 does not change the results considerably. The constants L_7^r , that appears in the η mass, and L_8^r are strongly affected by this change. This is also relatively true for L_4^r and L_6^r . We also tried to perform the same fit but setting $L_4^r \equiv L_6^r \equiv 0$. The resulting fit is very similar to fit NA48/2 but it has a huge χ^2 ($\chi^2 = 45$).

$C_i^r \equiv 0$ In the last column of the table we quote the fit obtained including the same input as for fit All, but setting all the $C_i^r \equiv 0$. This fit has been done to show how the different C_i^r can affect the L_i^r fit. Notice that the constants L_1^r , L_2^r and L_3^r change a lot, while the others stay in the same area as in fit All. This is not surprising: the last few constants are indeed primarily fitted from quantities where many contributing C_i^r are large- N_c suppressed and those which are not are set to zero also in the simple resonance estimate used.

All p^4 Same fit as All but all expressions are now at NLO. Use this fit for one-loop ChPT results. Note that this produces very high values for L_4^r and L_6^r . The underlying reason is that the lower value of F_K/F_π requires a smaller L_5^r than before and the pion scalar radius then requires at this order a larger L_4^r . This effect is also visible in fit All but is reduced when including the NNLO corrections.

Fit All is what we consider as the present best fit for NNLO ChPT calculations, it thus supersedes fit 10 of [9].

Let us discuss how the ChPT expansion is affected by the new values for the L_i^r . The various terms of the mass expansions read for fit All

$$\begin{aligned} m_\pi^2|_{p^2} &= 1.035 & m_\pi^2|_{p^4} &= -0.084 & m_\pi^2|_{p^6} &= +0.049, \\ m_K^2|_{p^2} &= 1.106 & m_K^2|_{p^4} &= -0.181 & m_K^2|_{p^6} &= +0.075, \\ m_\eta^2|_{p^2} &= 1.186 & m_\eta^2|_{p^4} &= -0.224 & m_\eta^2|_{p^6} &= +0.038, \end{aligned} \quad (\text{II.36})$$

while those for the decay constants are

$$\begin{aligned} \frac{F_\pi}{F_0} \Big|_{p^4} &= 0.311 & \frac{F_\pi}{F_0} \Big|_{p^6} &= 0.108 \\ \frac{F_K}{F_0} \Big|_{p^4} &= 0.441 & \frac{F_K}{F_0} \Big|_{p^6} &= 0.216, \\ \frac{F_K}{F_\pi} \Big|_{p^4} &= 0.129 & \frac{F_K}{F_\pi} \Big|_{p^6} &= 0.068. \end{aligned} \quad (\text{II.37})$$

In (II.36) and (II.37) we used the same normalizations as in Table II.4, although now $F_0 = 0.065$ GeV, this is due to the larger value of L_4^r which comes however with a large error. Notice that the convergence of the mass expansions in (II.36) is improved compared to the one of fit 10 in Table II.4. However (II.36) looks strange: the LO masses are larger than the physical ones and there are significant cancellations between NLO and NNLO. Furthermore, even if the convergence is improved, it is still quite different from the one expected. E.g. the $m_\pi^2|_{p^4}$ contribution is much smaller than the expected 30% and it is of the same size as the p^6 order. The convergence for the decay constants is a bit worsened compared to the one of fit 10, due to the low value of L_5^r , but it is still acceptable. Notice also that when the ratio F_K/F_π is calculated with (II.11) the resulting value is 1.168, which is 3% smaller than the expected 1.197. This can be due to higher order corrections that are included in the ratio of (II.11), but not in (II.10).

We performed more fits than those quoted in Table II.5. We included more $\pi\pi$ scattering parameters and πK scattering parameters. We found that these fits are compatible with fit All of Table II.5 within uncertainties. The same is true when we add the quantity c_s^π .

II.6.1 Linear fit for $K_{\ell 4}$ decays

One of the most striking features of the results presented in Table II.5 is that as soon as the new results from the quadratic fit of the NA48/2 collaboration [28] are included, the constant L_1^r and L_2^r take unexpected values. Indeed, as was noted above, they do not respect any longer the large- N_c relation $2L_1^r \approx L_2^r$, but already in fit NA48/2 they are $L_1^r \approx L_2^r$ while when also the $\pi\pi$ and the πK scattering lengths are included (fit All) we even obtain $L_1^r > L_2^r$. On the other hand when we calculate the curvature f_s'' using the L_i^r as obtained in fit All we obtain $f_s'' = -0.124$ to be contrasted with the experimental value $f_s'' = -0.437$. Furthermore, whenever we include as input also f_s'' we again obtain fits compatible to the ones in Table II.5, but with much larger χ^2 (e.g. $\chi^2 \sim 35$ for fit All) and the largest contribution comes exactly from f_s'' . These results confirm what was already stated at the end of Section II.3.5, i.e. the state-of-art ChPT does not reproduce such a large negative bend. Since f_s' and f_s'' are highly correlated, the linear and the quadratic fit of the F_s formfactor present rather different slopes.

For such reasons we perform fits using the slope of the linear fit $f_s'/f_s = 0.073$ [28] as well. The resulting fit, analogous to fit All, is reported in Table II.6. By inspection one can see that the large N_c relation $2L_1^r = L_2^r$ still does not precisely hold, but at least $1.4L_1^r \approx L_2^r$. On the other hand L_4^r and L_6^r are again not suppressed, while L_7^r and L_8^r are unexpectedly small. Also all the constants have large uncertainties.

	All linear
$10^3 L_1^r$	0.58 ± 0.10
$10^3 L_2^r$	0.80 ± 0.12
$10^3 L_3^r$	-3.33 ± 1.42
$10^3 L_4^r$	0.93 ± 0.31
$10^3 L_5^r$	0.71 ± 0.24
$10^3 L_6^r$	0.86 ± 0.87
$10^3 L_7^r$	-0.04 ± 0.40
$10^3 L_8^r$	0.02 ± 0.79
$\chi^2(\text{dof})$	1.16(4)

Table II.6: The analogous of fit All, but the linear fit of the $K_{\ell 4}$ formfactors have been used. The values of the L_i^r are at $\mu = 0.77$ GeV.

The convergence of the chiral expansions is worse than the one for fit All. The various terms of the mass expansions read

$$\begin{aligned}
m_\pi^2|_{p^2} = 0.655 & & m_\pi^2|_{p^4} = 0.370 & & m_\pi^2|_{p^6} = -0.025, \\
m_K^2|_{p^2} = 0.699 & & m_K^2|_{p^4} = 0.181 & & m_K^2|_{p^6} = 0.120, \\
m_\eta^2|_{p^2} = 0.751 & & m_\eta^2|_{p^4} = 0.151 & & m_\eta^2|_{p^6} = 0.098,
\end{aligned} \tag{II.38}$$

while those for the decay constants are

$$\begin{aligned}
\left. \frac{F_\pi}{F_0} \right|_{p^4} = 0.355 & & \left. \frac{F_\pi}{F_0} \right|_{p^6} = 0.157 \\
\left. \frac{F_K}{F_0} \right|_{p^4} = 0.498 & & \left. \frac{F_K}{F_0} \right|_{p^6} = 0.262, \\
\left. \frac{F_K}{F_\pi} \right|_{p^4} = 0.143 & & \left. \frac{F_K}{F_\pi} \right|_{p^6} = 0.054.
\end{aligned} \tag{II.39}$$

In the light of these results it is rather difficult to draw a conclusion. The very different predictions for L_1^r and L_2^r obtained in fit All and this fit confirm that the picture of ChPT for $K_{\ell 4}$ decays is still incomplete. As mentioned earlier, we expect a dispersive analysis to produce a larger curvature.

II.6.2 Some small variations on fit All

In the resonance estimate described in Section II.4 there is at least an assumption not entirely justified. We assume the scale at which the saturation happens to be 0.77 GeV, i.e. the mass of the lowest lying resonance. Nothing

prevents us to choose a larger or smaller scale, although this is still expected to be in the same range of energy. To check whether this assumption is safe we try to fit from data the saturation scale parameter as well. The results are rather reassuring. Fit All of Table II.5 is completely unaffected by this procedure. The fitted saturation scale is 0.77 ± 0.45 GeV.

The fit in Table II.6 shows a little difference. The fitted saturation scale is now 0.71 ± 0.31 GeV. However the L_i^r do not change that much and the look of the fit is pretty much the same as before.

We also attempt to find better estimates of the C_i^r constants releasing the values of the couplings g_V , c_d and c_m . Again we try to fit them using both the input of fit All and of the fit in Table II.6 (linear fit of NA48/2 instead of quadratic). In the first case we find in fact g_V and c_m close to the ones in (II.34). They read $g_V = 0.097 \pm 0.123$ and $c_m = 0.045 \pm 0.049$ GeV. For c_d we find instead a value larger than expected, i.e. $c_d = 0.093 \pm 0.100$ GeV. Anyway they are all affected by large uncertainties. The L_i^r fit is somewhat compatible with the one of Table II.5, fit All, within uncertainties because of the large ranges allowed for g_V, c_m, c_d . The fits are in a very broad minimum here with only one degree of freedom.

If we apply the same procedure but with the same $K_{\ell 4}$ input as for Table II.6 (NA48/2 linear fit) we arrive to similar conclusions: the values of g_V and c_d are similar to the ones in (II.34), while c_d is larger. Again all the resonance couplings present large uncertainties. The L_i^r are here rather well compatible with those in Table II.6.

We also try to multiply the C_i^r by an overall constant α and include it as a fitting parameter. It is encouraging to see that the result is $\alpha \approx 1.03$, namely the best fit is reached with basically the same values of the C_i^r from resonance estimate. Obviously the fit obtained is very similar to fit All. When we apply the same procedure to the fit in Table II.6 the constant α takes the value 0.90. This affects the fit of Table II.6, but still within uncertainties.

From this we conclude that fit All is stable against small changes in the resonance estimate of the C_i^r .

II.6.3 Adding input: $\bar{\ell}_i$ constants in two-flavour ChPT

The authors of [43, 44] study three flavour ChPT in the limit where the m_s is assumed to be much larger than \hat{m} and the external momenta. In this case they can integrate out the strange quarks and $SU(3) \times SU(3)$ ChPT reduces to $SU(2) \times SU(2)$ ChPT. Matching the results from the two frameworks they calculate explicitly the dependence of the two-flavour LECs (the scale-independent $\bar{\ell}_i$ and the c_i^r) on the strange quark mass and on the three-flavour LECs. These relations have been worked out using two different methods at order p^6 in [43, 44].

	fit 10 iso	All	All linear	[23,30]
$\bar{\ell}_1$	-0.6	-0.1	-1.9	-0.4 ± 0.6
$\bar{\ell}_2$	5.7	5.3	5.7	4.3 ± 0.1
$\bar{\ell}_3$	1.3	4.2	4.1	3.3 ± 0.7
$\bar{\ell}_4$	4.0	4.8	4.5	4.4 ± 0.4

Table II.7: The values of the scale-independent $SU(2)$ LECs $\bar{\ell}_i$. In the first three columns we show the values as predicted by fit 10, fit All and fit All linear. In the last column we quote the known values from [23,30]. Notice that the uncertainty over $\bar{\ell}_4$ is double the one quoted in [30] due to the still unclear situation for the lattice results [23].

There exist different evaluations of the $\bar{\ell}_i$. $\bar{\ell}_3$ has been estimated rather well using lattice results [23]. $\bar{\ell}_1, \bar{\ell}_2, \bar{\ell}_4$ and $\bar{\ell}_6$ have been obtained by matching two-flavour ChPT with dispersive results [30], but (contradictory) lattice results exist for those too [23]. We have increased the error on $\bar{\ell}_4$ because of this.

In Table II.7 we summarize all the values of these constants and the results obtained by plugging the L_i^r and C_i^r of fit 10 iso, fit All and fit All linear in the relations of [43,44]. By comparison of the first three columns with the last one of Table II.7 it is easy to see that none of the fits correctly reproduces all the $\bar{\ell}_i$ values. A similar conclusion holds also for the fit in the next-to-last column of Table II.5, where all the C_i^r are zero. The disagreement with the $\bar{\ell}_i$ in this case is actually even stronger. These fits encounter particular trouble in fitting $\bar{\ell}_2$.

We tried to fit the $\bar{\ell}_i$ whose values appear on the last column of Table II.7 in addition to the inputs used for fit All. Not surprisingly it is not possible to accommodate all those inputs at the same time. The resulting χ^2 is approximately 22 and its largest contributions come exactly from the $\bar{\ell}_i$. Excluding from the fit $\bar{\ell}_2$ but including the others improves the situation. The resulting L_i^r values are very close to the ones of fit All, the most important deviation being $10^3 L_3^r = -3.18$. The χ^2 takes the value 3.15 with 7 degrees of freedom. Also in this case the value for $\bar{\ell}_2$ is still far from the expected one.

This is not surprising. In [43] it was found that the constant $\bar{\ell}_2$ depends on the couplings L_2^r, L_3^r and on the combination $2C_{13}^r - C_{11}^r$. The authors of [43] observed there that to find agreement with the determined value of $\bar{\ell}_2$ the combination of C_i^r must not be zero. Unfortunately those are two large- N_c suppressed couplings and therefore they are set to zero in our resonance estimate (see Table II.15). We also try to fit those two C_i^r using also $\bar{\ell}_2$ as input observable, but this has been unsuccessful as well. In this way we manage to accommodate the value for $\bar{\ell}_2$, but then $\bar{\ell}_1$ is off, since it contains also a different combination of C_{11}^r, C_{13}^r and of C_6^r . This last coupling is also N_c -suppressed and thus estimated to be zero. In the end there is no way out: when we try to

fit C_6^r too, there are other quantities taking very different values. The C_i^r are too correlated to be able to fit only a few of them.

As far as regards the fit in Table II.6 the results for the $\bar{\ell}_i$ are even less clear. Its predictions are reported in the third column of Table II.7. It is straightforward to see that now even the predicted $\bar{\ell}_1$ is off. Of course when we try to fit all the $\bar{\ell}_i$ the χ^2 is very large ($\chi^2 \approx 37.7$). Contrary to what happened for fit All, the situation does not improve that much when we exclude $\bar{\ell}_2$. For this fit seems to be very hard to reach the correct value for $\bar{\ell}_1$ too. The resulting χ^2 in this second case is 5.82 with $\bar{\ell}_1 = -1.4$.

Finally an extra cautionary remark. Requiring that the $SU(3)$ ChPT constants predict the values for the $SU(2)$ ones might not be a very safe assumption. What it assumes is that both $SU(2)$ and $SU(3)$ ChPT work well for the same quantities. For the $\pi\pi$ scattering quantities, which are very much determined by loop parts, relatively small differences can become amplified in the resulting values of the LECs.

II.6.4 A chiral quark model estimate for the C_i^r

We discussed above a simple resonance saturation estimate for the NNLO LECs C_i^r . There are other attempts at predicting these values as well from chiral quark models. As a representative of this we choose [13]. It also is a large N_c approximation but with a somewhat different pattern than our resonance saturation. Their method is based on a study of the relation between the chiral Lagrangian up to order p^6 and QCD, they find as expected that the LECs can be given in terms of some Green functions of QCD. In the evaluation of these Green functions, several assumptions and approximations are made such that it is not a full derivation but something like a chiral quark model. Their results are presented in Table IV of [13].

We also use their estimate to perform the fits. The results can be found in Table II.8. There are results for two different fits. They have been obtained including all the observables as for fit All of Table II.5. In the first column we use the C_i^r as quoted in Table IV of [13], whereas in the second column we multiply them by an overall constant α that is also fitted. This second fit was done because we observed that the values for the C_i^r of [13] are somewhat larger than the ones of the resonance estimates of Table II.15. The fit confirms this observation and finds as best value for $\alpha = 0.27$, i.e. C_i^r considerably smaller than the ones in [13]. The value of the χ^2 for the two fits of Table II.8 is somewhat worse than for fit All. Indeed it seems that it is now very difficult to fit the slope g_p' of the G formfactor for $K_{\ell 4}$ decay. From the second fit of Table II.8 one can notice that when the C_i^r are allowed to take smaller values the L_2^r constant compensates for that. This allows the fit to reach a better value for the g_p' .

	C_i^r [13]	$\alpha \times C_i^r$ [13]
$10^3 L_1^r$	0.66 ± 0.11	0.66 ± 0.10
$10^3 L_2^r$	0.59 ± 0.13	0.24 ± 0.32
$10^3 L_3^r$	-2.74 ± 0.48	-1.80 ± 0.75
$10^3 L_4^r$	0.75 ± 0.16	0.77 ± 0.84
$10^3 L_5^r$	1.64 ± 0.83	0.83 ± 0.39
$10^3 L_6^r$	0.64 ± 0.41	0.32 ± 0.99
$10^3 L_7^r$	-0.25 ± 0.30	-0.15 ± 0.14
$10^3 L_8^r$	0.76 ± 0.75	0.27 ± 0.23
α	–	0.27 ± 0.47
χ^2 (dof)	3.71 (4)	1.35 (3)

Table II.8: The results as obtained using the C_i^r estimates of [13]. Both the fits include the same observables as fit All of Table II.5. In the second column the coefficient α multiplied by the C_i^r has been included as fitting parameter. The L_i^r are given at $\mu = 0.77$ GeV.

	p^2	p^4	p^6
m_π^2	0.988	-0.066	0.078
m_K^2	1.056	-0.177	0.121
m_η^2	1.131	-0.225	0.094
F_π/F_0	1	0.318	0.108
F_K/F_0	1	0.475	0.198
F_K/F_π	1	0.156	-0.050

Table II.9: The results as obtained using the C_i^r estimates of [13] showing the convergence for the fit where α is left free. The normalizations are the same as explained in Table II.4. Now $F_0 = 0.065$ GeV.

As can be seen in Table II.9, even the convergence for the masses and decay constants is worse than the one for fit All reported in (II.36) and (II.37) respectively. Notice that we have not quoted the convergence for the fit obtained without multiplying the C_i^r by the coefficient α . In fact this is found to be even worse than the one of Table II.8, the p^4 terms being constantly larger than, although comparable in size to, the p^6 ones.

In Table II.10 and II.11 we quote the results obtained with the C_i^r of [13], but fitting the slope of the linear fit for the F_s formfactor as in the fit of Table II.6. Conclusions similar to the ones drawn for Table II.8 hold here too.

	C_i^r [13]	$\alpha \times C_i^r$ [13]
$10^3 L_1^r$	0.38 ± 0.10	0.35 ± 0.11
$10^3 L_2^r$	0.88 ± 0.12	0.43 ± 0.30
$10^3 L_3^r$	-3.20 ± 0.47	-2.04 ± 0.79
$10^3 L_4^r$	0.42 ± 0.17	0.91 ± 0.35
$10^3 L_5^r$	1.62 ± 0.77	1.03 ± 0.57
$10^3 L_6^r$	0.43 ± 0.21	0.87 ± 0.77
$10^3 L_7^r$	-0.32 ± 0.45	-0.11 ± 0.34
$10^3 L_8^r$	0.92 ± 1.07	0.17 ± 0.71
α	–	0.22 ± 0.47
χ^2 (dof)	4.13 (4)	1.20 (3)

Table II.10: The results as obtained using the C_i^r estimates of [13]. Both the fits include the same observables as the fit in Table II.6, i.e. as fit All but with the linear fit from NA48/2. In the second column the coefficient α multiplied by the C_i^r has been included as fitting parameter. The L_i^r are given at $\mu = 0.77$ GeV.

	p^2	p^4	p^6
m_π^2	0.624	0.384	-0.008
m_K^2	0.667	0.189	0.144
m_η^2	0.716	0.149	0.135
F_π/F_0	1	0.354	0.142
F_K/F_0	1	0.531	0.225
F_K/F_π	1	0.177	-0.020

Table II.11: The convergence for the fit where α is left free is shown. The normalizations are the same as explained in Table II.4. Now $F_0 = 0.062$ GeV. Fit as in rightmost column of Table II.10.

II.7 Releasing the C_i^r

All the fits presented in the previous section have unusual NNLO corrections to the masses and many also to the decay constants. In addition, if we included the requirement that the $\bar{\ell}_i$ were also fitted well we could not find a simple good fit.

An additional reason to go beyond what we have is that all the estimates used above with the exception of the singlet η contribution only contribute to the NNLO LECs⁵ that are leading in N_c . In the masses and decay constants

⁵This is true with the exception of terms involving $\langle \chi_- \rangle$ which can get produced by the equations of motion.

in addition the estimates from the resonance exchange give no contribution at leading order in N_c at all. This is an unsatisfying situation, we do expect that the masses and decay constants should get some contribution from the NNLO constants. Inspection of the relations between the $\bar{\ell}_i$ and the $SU(3)$ LECs [43] shows that only combinations of the C_i^r appear that are suppressed by N_c . Thus especially the problem with $\bar{\ell}_2$ above requires some nonzero values for the N_c suppressed constants.

We could in principle allow all the C_i^r to be free and include them in the fit as well. However, from our earlier work in [6] it is clear that with the inputs used at present there are enough free combinations of the C_i^r to fit all physical inputs directly. For this reason we also have explored another technique of C_i^r estimate, based on a random walk⁶ method. Hereafter we describe the main features of the algorithm used. See also the flowchart in Figure II.1. The algorithm is a version of simulated annealing.

We first start with an initial set $C_i^{r(\text{in})} = C_i^{r(\text{old})}$. These are chosen to be

1. random (with a size given by $1/3/(16\pi^2)^2$ for those leading in $1/N_c$ and $1/3$ of that for the subleading ones),
2. all zero
3. as obtained by resonance estimate (see Table II.15)
4. as obtained by multiplying the constants of [13] by 0.27 (see Table II.15).

Then we perform the fit on the L_i^r using those $C_i^{r(\text{old})}$. After this we take a random step according to the formula

$$C_i^{r(\text{new})} = C_i^{r(\text{old})} + C_i^{r(\text{step})} \equiv C_i^{r(\text{old})} + \frac{1}{(16\pi^2)^2} \epsilon r_i, \quad (\text{II.40})$$

where r_i in (II.40) is a random number generated through a uniform distribution in the interval $(-1, 1)$ and we have used $\epsilon = 0.01$ and 0.001 . For those C_i^r that are N_c suppressed we further multiply $C_i^{r(\text{step})}$ by $1/3$. In this way the random generated C_i^r set still respects the large- N_c suppressions to a certain extent. We perform the fit of the L_i^r using the new set $C_i^{r(\text{new})}$ and we check the χ^2 obtained. If the χ^2 decreases then we substitute the $C_i^{r(\text{old})}$ with $C_i^{r(\text{new})}$. Sometimes we also allow $C_i^{r(\text{new})}$ to be selected even though the corresponding χ^2 is not smaller than the previous one (see last step in the flow diagram of Figure II.1). This is done so to let the C_i^r to take quite different values and thus to test as many different sets as possible. It is also needed for our algorithm to be able to move out of local minima. We find that, when we let our algorithm run long enough, we cover quite many different sets of C_i^r . We chose different initial C_i^r to widen their range of variability. In addition we have started

⁶The idea was born thanks to a discussion with Juerg Gasser and Gerhard Ecker.

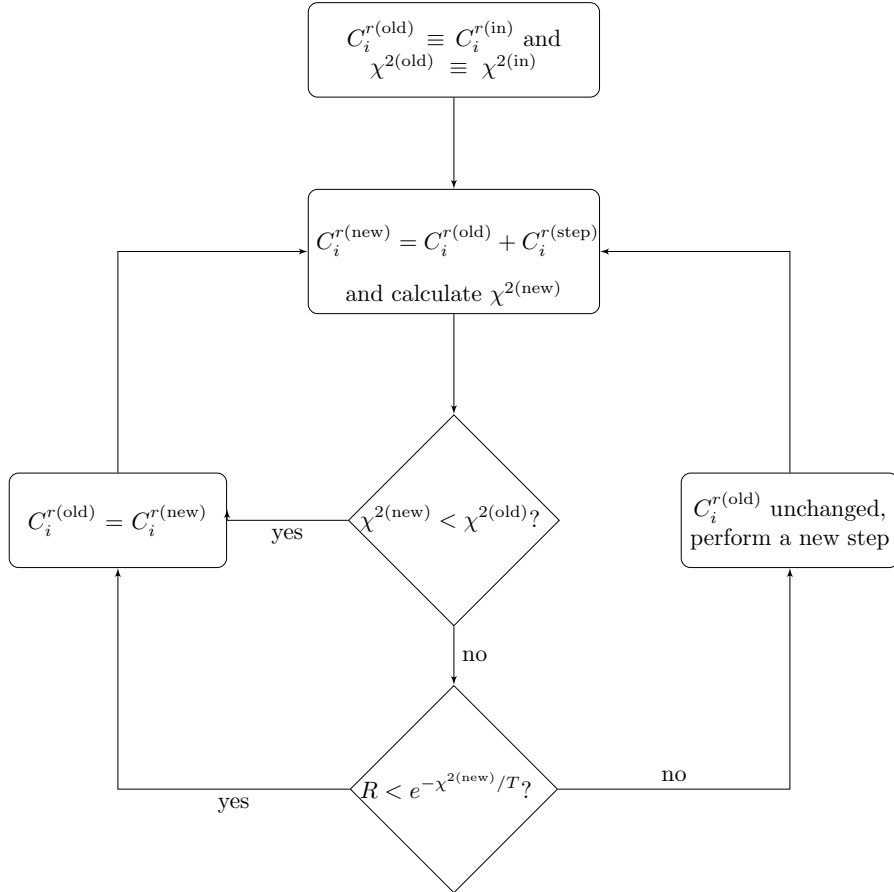


Figure II.1: Algorithm used to select the random C_i^r . It has been started with different values of the initial $C_i^{r(\text{in})}$, as explained in the text. In the bottom decision square R is a random number selected with a uniform distribution in the interval $(0,1)$, while T is a parameter set such that it is of the same order of magnitude of the χ^2 . More details can be found in the text.

the random walk from the same starting point several times including different random starting points. We chose as random starting points $1/3/(16\pi^2)^2$ with the extra factor of $1/3$ since without the extra $1/3$ we never reached a χ^2 smaller than one.

The fits are performed including the same input as for fit All but with a few extra requirements. We add as input the curvature of the scalar formfactor c_S^π

in (II.30) and all the \bar{l}_i of the last column of Table II.7. We do not instead demand to fit all the $\pi\pi$ and πK scattering parameters, since it costs in terms of computing time. So, as done for fit All, we include only a_0^0 , a_2^0 , $a_0^{1/2}$ and $a_0^{3/2}$. Notice that we do not find any large discrepancies when we add more scattering parameters in fit All, as was remarked at the end of Section II.6.

We also require a good convergence of the masses and decay constants expansions. The reason is that in this way we have the possibility to “select” those C_i^r granting us convergence for those quantities. This also allows to keep under control the quality of the fits. Otherwise too much freedom would be left to the C_i^r constants, and many different fits with a low χ^2 but with very bad convergences, can be reached. Clearly such convergence constraints have a strong effect on the L_i^r constants as described in the next Section II.7.1.

II.7.1 Convergence constraints

We devote this section to a discussion of the convergence constraints imposed on the masses and decay constants in the fits with random C_i^r . Let us first show the case of the decay constants.

We performed the fits constraining the NNLO contributions to F_π , F_K and F_K/F_π constants to be small, i.e. less than the 10% of the LO ones. Remember that the expansions for the F_π and F_K decay constants are

$$\begin{aligned} F_K &= F_0 + F_K|_{p^4} + F_K|_{p^6}, \\ F_\pi &= F_0 + F_\pi|_{p^4} + F_\pi|_{p^6}, \end{aligned} \quad (\text{II.41})$$

and that in our fits, as explained in Section II.3.2, we include their ratio as

$$\frac{F_K}{F_\pi} \approx 1 + \underbrace{\frac{F_K}{F_0}\Big|_{p^4} - \frac{F_\pi}{F_0}\Big|_{p^4}}_{\text{NLO}} + \underbrace{\frac{F_K}{F_0}\Big|_{p^6} - \frac{F_\pi}{F_0}\Big|_{p^6} - \frac{F_K}{F_0}\Big|_{p^4} \frac{F_\pi}{F_0}\Big|_{p^4} + \frac{F_\pi}{F_0}\Big|_{p^4}^2}_{\text{NNLO}}. \quad (\text{II.42})$$

Specifically the convergence constraints are included through the following partial $\chi_{i(\text{part})}^2$:

$$\begin{aligned} \chi_{i(\text{part})}^2 &= \left(\frac{F_\pi}{F_0}\Big|_{p^6} / 0.05 \right)^2, & \chi_{i(\text{part})}^2 &= \left(\frac{F_K}{F_0}\Big|_{p^6} / 0.05 \right)^2, \\ \chi_{i(\text{part})}^2 &= \left(\frac{F_K}{F_\pi}\Big|_{\text{NNLO}} / 0.07 \right)^2, \end{aligned} \quad (\text{II.43})$$

With (II.43) we have been able to find many fits with a good convergence. On the other hand the NLO contribution for F_π turns out to be smaller than the

expected 30%. The reason resides in the third of the relations in (II.43). Requiring all the NNLO pieces for all the decay constants to be small implies that the single contributions $F_\pi|_{p^6}$ and $F_K|_{p^6}$ are small. But also the term $(F_\pi/F_0)|_{p^4}^2$ must be small, otherwise the NNLO contribution of F_K/F_π is allowed to be large. This leads to small NLO corrections for F_π and thus a $F_0 \approx F_\pi$.

We apply similar restrictions also to the masses

$$\chi_{i(\text{part})}^2 = \left(\left. \frac{m_M^2}{m_{M0}^2} \right|_{p^6} / 0.1 \right)^2 \quad (\text{II.44})$$

where M stands for π , K and η mesons and m_{M0} are the leading order contributions to the masses. We have kept the value of m_s/\hat{m} fixed at 27.8 as for fit All.

We conclude this section with a final remark. One might wonder why we have not imposed similar constraints also for fit All, since these could improve the convergence of the expansions. The reason is that when we require them, we obtain a reasonably good fit ($\chi^2 \approx 8$ with 10 degrees of freedom) and with better constrained L_4^r and L_6^r . But it also causes much worse predictions for the $\bar{\ell}_i$, e.g. $\bar{\ell}_3 \approx 6.5$.

II.7.2 Results

Now we are ready to show the outcomes of our studies when the C_i^r are set to random values using the procedure of Figure II.1 and with the constraints listed in Section II.7.1 above. First of all we must point out that due to the freedom we allow to the C_i^r many different fits of the L_i^r have a low χ^2 . We set initial C_i^r equal to zero, resonance exchange or chiral quark model estimates as well more random starts. We easily reach $\chi^2 < 1$, and we found many fits with $\chi^2 \approx 0.5$. Reducing the steps of the random walk we can even find smaller values. However once the χ^2 reaches a reasonably low value, e.g. 1, there is no apparent reason why one should prefer one specific fit to another. Due to the several different sets of C_i^r under study, we can only quote the ranges where the L_i^r vary and where we obtain a $\chi^2 < 1$. Such ranges are quoted in Table II.12 and are obtained, starting from different initial sets $C_i^{r(\text{in})}$. Keep in mind that these ranges depend on the C_i^r chosen. Plugging in a L_i^r fit without the corresponding C_i^r will not produce any sensible results. The way we determined those numbers is shown in Figure II.2 on the example for L_1^r where we have plotted a number of fits that gave $\chi^2 < 1$ for the different starting points. We have typically stopped the fits when a χ^2 of about 0.4 or below was found and the tails at low χ^2 are an artefact, they were done with runs with a very low ϵ and a very low T .

$C_i^{r(\text{in})}$	resonance	zero	CQM	random
$10^3 L_1^r$	(0.6, 1.2)	(0.5, 1.1)	(0.2, 0.6)	(0.3, 1.2)
$10^3 L_2^r$	(0.4, 1.2)	(0.2, 0.8)	(-0.2, 0.5)	(0, 1.6)
$10^3 L_3^r$	(-5.5, -3.0)	(-4.5, -3.0)	(-3.3, -1.2)	(-6.2, -2.0)
$10^3 L_4^r$	(0.15, 0.35)	(-0.1, 0.25)	(-0.1, 0.2)	(0.05, 0.35)
$10^3 L_5^r$	(1.2, 1.6)	(1.35, 1.5)	(1.25, 1.55)	(1.2, 1.6)
$10^3 L_6^r$	(-0.05, 0.25)	(-0.2, 0.2)	(-0.15, 0.15)	(-0.05, 0.3)
$10^3 L_7^r$	(-0.45, -0.1)	(-0.43, -0.18)	(-0.43, -0.24)	(-0.45 - 0.2)
$10^3 L_8^r$	(0.4, 0.8)	(0.45, 0.72)	(0.5, 0.731)	(0.45, 75)

Table II.12: The ranges for L_i^r values as obtained changing the C_i^r according to a random walk algorithm. The different ranges correspond to different initial values for the C_i^r . With CQM we indicate the C_i^r of the chiral quark model. All the fits have a $\chi^2 < 1$. For all the fits $\mu = 0.77$ GeV. See the description in the text for further details on how the fits have been performed.

The results are rather cumbersome. L_1^r , L_2^r and L_3^r look quite free to vary in large ranges. Notice also that the large N_c relation $2L_1^r \approx L_2^r$ is still not recovered. On the other hand, due to the converge constraints of Section II.7.1 we narrow the intervals for the other constants. Especially L_5^r takes a large value and L_4^r a small one. As explained in Section II.7.1, we essentially require that F_K/F_π , F_K and F_π have small NNLO corrections which give that F_K/F_π is given by the NLO and thus determines L_5^r at a fairly large value. That F_π has small corrections at all then in turn requires a fairly small L_4^r . The choice to constrain the convergence of those quantities is dictated by the lack of information to constrain more the C_i^r . When we release such constraints indeed we find different looking fits, but affected by a bad convergence. Somewhat more surprising is that the L_6^r typically takes on values that are smaller than L_8^r .

As you can see no clear final conclusion can be drawn with such results. When we performed this study we were hoping not to find as many good fits and smaller ranges for the L_i^r . The study shows instead that it is very difficult, if not impossible, to narrow the ranges for the L_i^r with such a poor knowledge of the C_i^r . On the other hand it also shows that fits of the L_i^r with good convergence do exist, if the C_i^r are changed. In Table II.13 we show the L_i^r obtained for the smallest χ^2 found starting from the resonance estimate and from fully random C_i^r as described above and we show the convergence for some quantities in those two fits in Table II.14. The fits with very low χ^2 we have obtained, such as the two shown here, tend to have similar expansions for the masses and the decay constants. In order to see how the various C_i^r look like we have added the values for these two fits in the appendix.

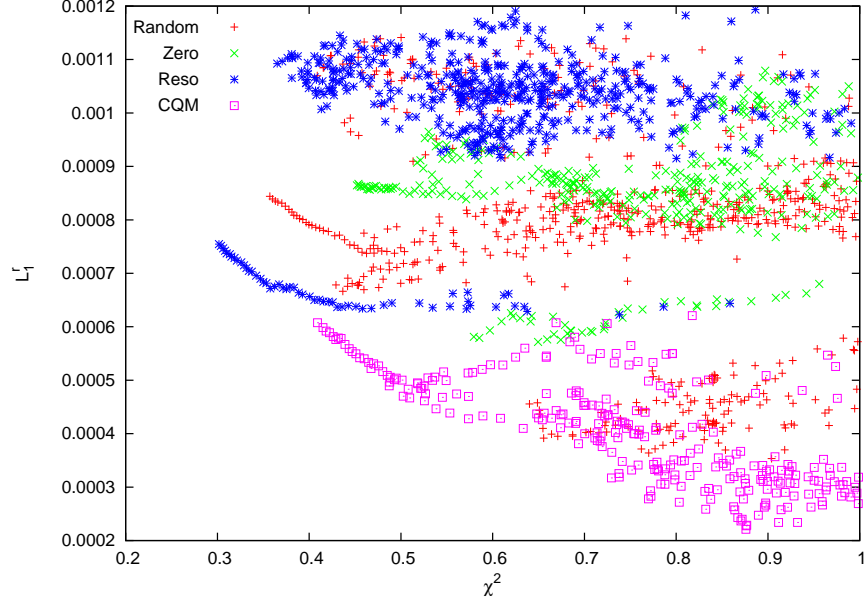


Figure II.2: The values of L_1^r for the random walk fits of Table II.12. In the plot all the fits are collected. The ranges of variability for L_1^r is quite large. In the picture it is also evident how the two values of the couplings depend somewhat on the different initial values of the C_i^r constants. The L_i^r are at the scale $\mu = 0.77$ GeV.

II

We can draw some conclusions by studying correlations. The effect of $\bar{\ell}_2$ is very visible if we plot for the various fits with $\chi^2 < 1$ L_2^r , which is the NLO dependence of $\bar{\ell}_2$ on the LECs, versus $2C_{13}^r - C_{11}^r$, which is the dependence on the NNLO LECs. The tight correlation shows that the NNLO contribution depends very little on the other L_i^r . More precisely, this shows the NLO LEC combination at NLO versus the NNLO LEC combination at NNLO and that the NNLO contribution depends fairly little on the value of the L_i^r . We get more of those constraints directly. A very similar is from the value of $\bar{\ell}_1$ shown in Figure II.4. The correlations for other observables tend to be weaker indicating that the NNLO contributions are more dependent on the value of the L_i^r for these cases. We show examples with a weaker but still existing correlation in Figure II.5 where the correlations resulting from F_K/F_π are shown and in Figure II.6 for $\langle r^2 \rangle_S^\pi$. In both cases we have plotted on the horizontal axis the combination of L_i^r the quantity depends on at NLO and on the vertical axis the combination of C_i^r the quantity depends on at NNLO.

C_i^r	best reso	best random
$10^3 L_1^r$	0.75 ± 0.09	0.85 ± 0.09
$10^3 L_2^r$	0.81 ± 0.45	0.54 ± 0.05
$10^3 L_3^r$	-3.91 ± 0.28	-3.51 ± 0.28
$10^3 L_4^r$	0.16 ± 0.10	0.20 ± 0.10
$10^3 L_5^r$	1.40 ± 0.09	1.40 ± 0.09
$10^3 L_6^r$	0.10 ± 0.14	0.12 ± 0.14
$10^3 L_7^r$	-0.32 ± 0.13	-0.32 ± 0.13
$10^3 L_8^r$	0.64 ± 0.16	0.63 ± 0.16
χ^2	0.30 (4)	0.36 (3)

Table II.13: The results as obtained using the C_i^r from the best χ^2 found starting from the resonance or from a completely random one as described in the text. The L_i^r are given at $\mu = 0.77$ GeV. The corresponding C_i^r sets can be found in Table II.15 in appendix.

C_i^r	best reso			best random		
	p^2	p^4	p^6	p^2	p^4	p^6
m_π^2	0.987	0.021	-0.008	0.993	0.021	-0.012
m_K^2	1.057	-0.054	-0.003	1.060	-0.058	-0.002
m_η^2	1.132	-0.133	0.001	1.136	-0.135	-0.001
F_π/F_0	1	0.178	-0.010	1	0.187	-0.010
F_K/F_0	1	0.395	0.009	1	0.404	0.011
F_K/F_π	1	0.217	-0.020	1	0.217	-0.020

Table II.14: The convergence for the best χ^2 found starting from the resonance estimate, here $F_0 = 0.079$ GeV. Fit as in left column of Table II.13. The convergence for the best χ^2 found starting from the fully random estimate, here $F_0 = 0.078$ GeV. Fit as in left column of Table II.13.

There are also correlation between the fitted values of the L_i^r . L_1^r , L_2^r and L_3^r show a reasonable correlation among themselves but are essentially not correlated with the others. There are weaker correlations between L_4^r and L_6^r and between L_7^r and L_8^r . These correlations are shown in Figures II.7, II.8, II.9, II.10, and II.11. We have shown a curve in all plots guiding the eye as well and given it in the caption of the figure.

Note that throughout this section we have considered all fits with a $\chi^2 < 1$ to be essentially possible.

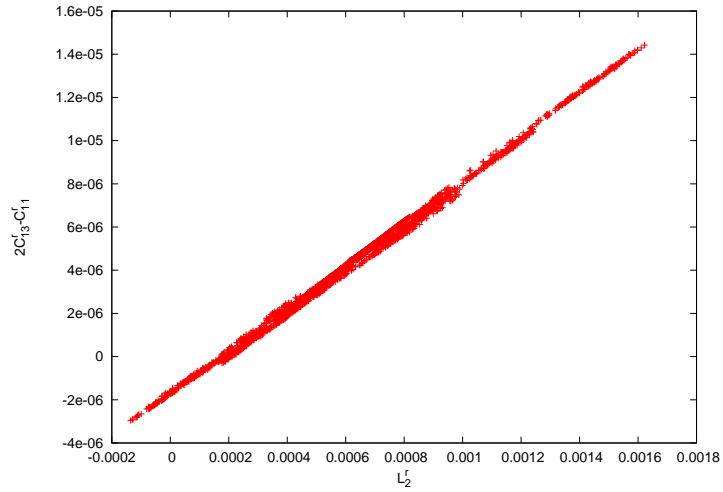


Figure II.3: The correlations between L_2^r and $2C_{13}^r - C_{11}^r$. This results from including the value of $\bar{\ell}_2$ in the fit.

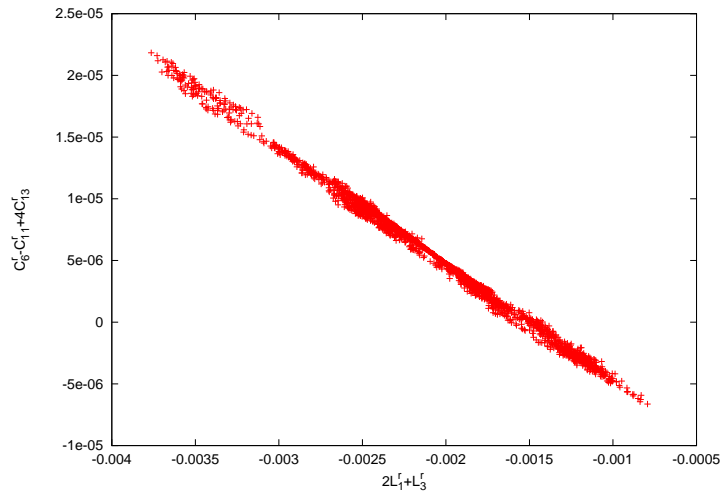
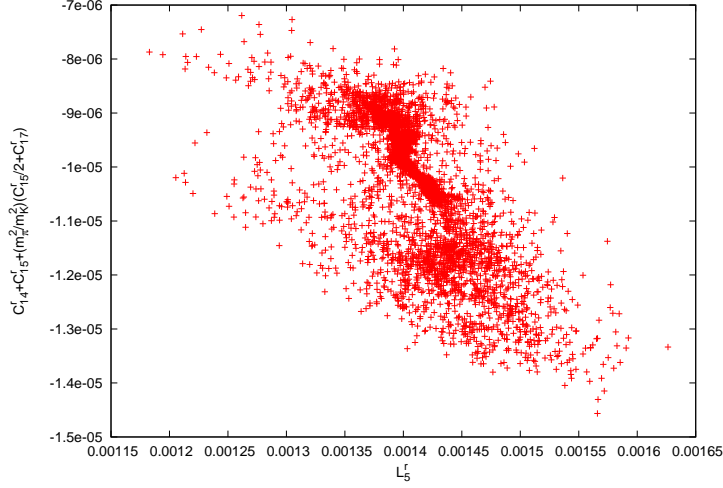
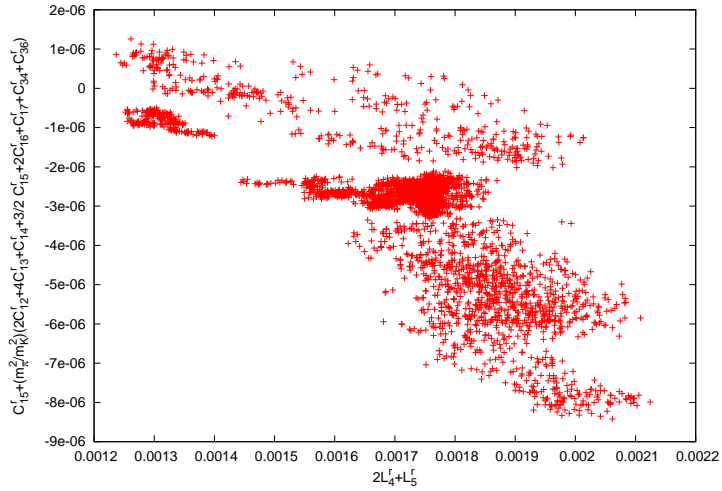


Figure II.4: The correlations between $2L_1^r + L_3^r$ and $C_6^r - C_{11}^r + 4C_{13}^r$. This results from including the value of $\bar{\ell}_1$ in the fit.



Figure II.5: The correlations resulting from F_K/F_π .Figure II.6: The correlations resulting from the pion scalar radius $\langle r^2 \rangle_S^\pi$.

II.8 Conclusions

In this paper we have shown the results for a new global fit of the L_i^r at NNLO, with techniques similar to the ones in [8, 9]. Different treatments of the p^6

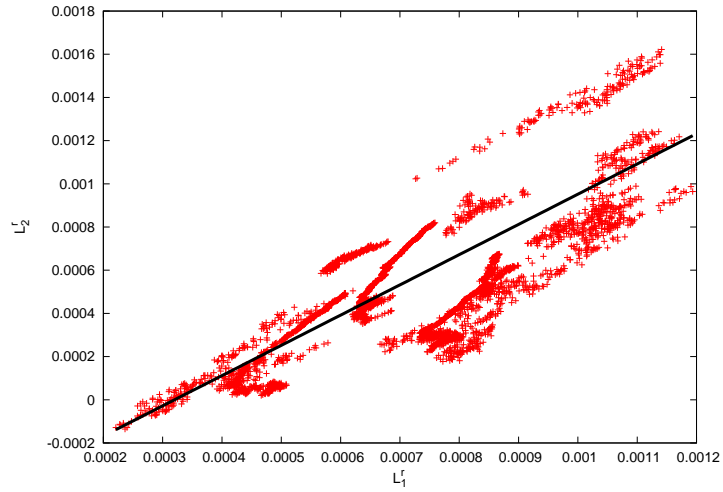


Figure II.7: The correlations between L_1^r and L_2^r , the curve shown is $L_2^r = 1.4(L_1^r - 0.00032)$.

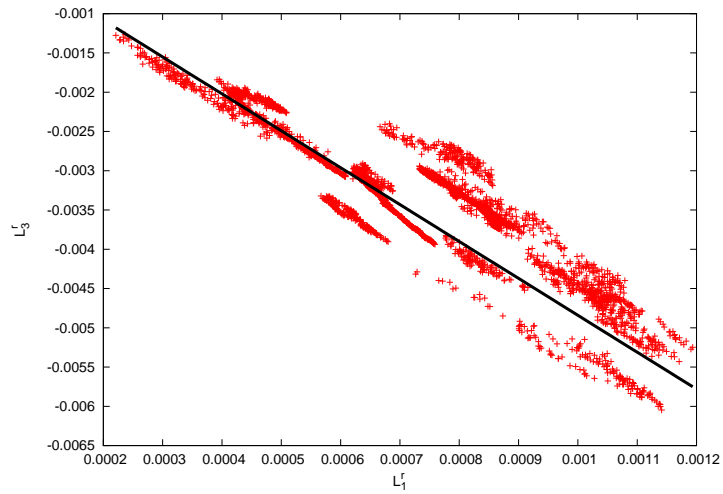


Figure II.8: The correlations between L_1^r and L_3^r , the curve shown is $L_3^r = -4.7(L_1^r + 0.00003)$.



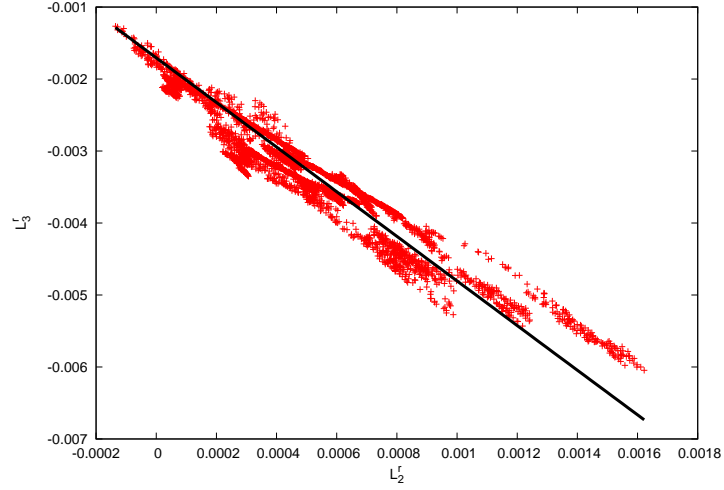


Figure II.9: The correlations between L_2^r and L_3^r , the curve shown is $L_3^r = -3.1(L_2^r + 0.00055)$.

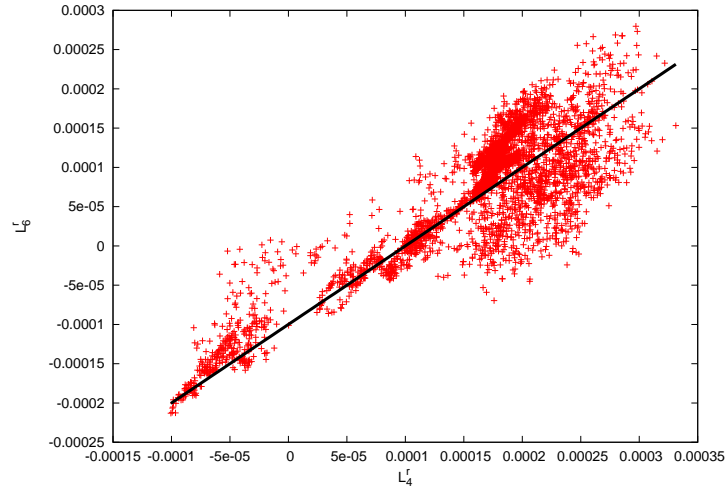


Figure II.10: The correlations between L_4^r and L_6^r , the curve shown is $L_6^r = L_4^r - 0.0001$.

coupling constants have been considered: the resonance estimate of [8], the results of [13] and the use of randomly selected C_i^r . The results are difficult

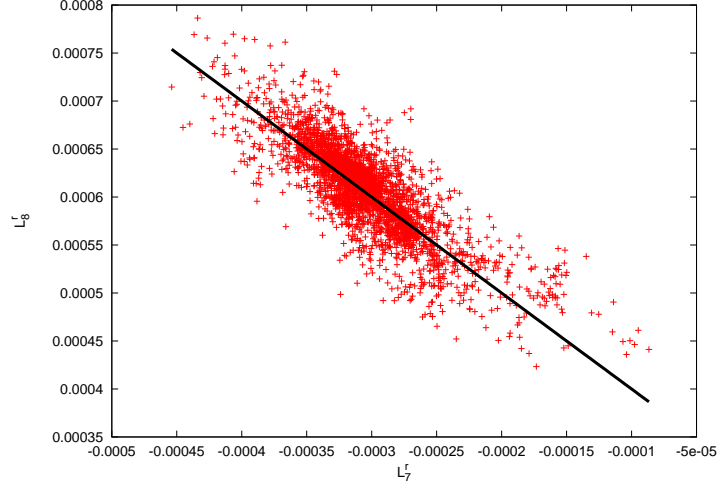


Figure II.11: The correlations between L_7^r and L_8^r , the curve shown is $L_8^r = -(L_7^r - 0.0003)$.

II

to interpret and unexpected. All the fits that have been performed using the NNLO couplings from [8] or [13] show both strong and weak points. The fits obtained from the randomly selected C_i^r are too different from each other to draw a final conclusion, although they give a rough indication on where we can expect to find the values of L_i^r . They also provide a proof of principle that with reasonable values of the C_i^r a reasonably convergent series for $SU(3)$ ChPT can be obtained for many quantities.

The fit that presents the least discrepancies and best convergence of the chiral expansion is fit All in Table II.5, which has been obtained with the resonance estimate of the C_i^r . It succeeds in fitting many observables like the $\pi\pi$ and πK scattering parameters and the slope of the scalar formfactor of the pion. It also reproduces quite well the experimental results for the f_s and $g_p \bar{K}\ell_4$ formfactors although it does not predict the curvature of f_s . The perturbative expansions for masses and decay constants reported in (II.36) and (II.37) look suspicious but are acceptable. On the other hand it does not satisfy the large N_c relation $2L_1^r \approx L_2^r$ and it fails in well constraining the L_4^r and L_6^r values. Finally its prediction for $\bar{\ell}_2$ is far from the current estimate of that constant. We have at present not included many results from lattice QCD. We expect that this should improve in a few years allowing for another step forward in confronting ChPT with data.

Acknowledgments

We thank Juerg Gasser, Gerhard Ecker, Veronique Bernard, Emilie Passemar, Antonio Pich and Gilberto Colangelo for discussions. This work is supported in part by the European Community-Research Infrastructure Integrating Activity “Study of Strongly Interacting Matter” (HadronPhysics2, Grant Agreement n. 227431) and the Swedish Research Council grants 621-2008-4074 and 621-2010-3326.

II.A C_i^r values

The aim of this section is to present the values used for the C_i^r . We only present results for the C_i^r that actually contribute to the observables we have included in the fits and we indicate with the superscript * the ones that are subleading in N_c . They can all be found in Table II.15. The column labelled *reso* is the resonance exchange estimate of Section II.4. The column labelled *CQM* is the estimate of [13] as discussed in Section II.6.4. The values directly from their model can be found in Table IV of [13]. The values in the column labelled *CQM* have been multiplied with normalization factor $\alpha = 0.27$ from the fit in the right column of Table II.8. The normalization from the fit to the linear NA48/2 input, Table II.10 is a little smaller but essentially the same. The last two columns are from the random walk/simulated annealing estimates for the C_i^r reported in Section II.7 from the best χ^2 found starting from the resonance estimate and a fully random starting point. These are the C_i^r for the fits reported in Table II.13.

The main purpose is to show the typical sizes of the C_i^r we obtained for the fits and that the pattern for the good fits can be quite different.

Table II.15: The C_i^r constants as obtained by several methods. In the table we quote $10^5 \times C_i^r$ where the i is given in the first column. The i^* indicates a N_c suppressed C_i^r . The second column corresponds to the resonance model of Section II.4. In the third one we quote the C_i^r of [13] multiplied by $\alpha = 0.27$. The particular value of α is chosen fitting it to the input observables together with the L_i^r , as explained in Section II.6.4. In the last two columns we quote two sets of C_i^r corresponding to the best fits of the L_i^r when the C_i^r are released, as explained in Section II.7. The column labeled best reso comes from initial values of the C_i^r equal to the ones of the resonance estimate, while in the column labeled best rand even the initial values of the C_i^r are chosen randomly. The scale of renormalization for all the sets is $\mu = 0.77$ GeV.

i	res	CQM	best reso	best rand
1	1.216	0.866	1.683	-0.733
2*	0.000	0.000	0.113	0.280
3	0.000	-0.011	0.324	0.084
4	1.452	0.708	2.225	1.266
5	0.619	-0.231	0.779	1.147
6*	0.000	0.000	-0.307	-0.050
7*	0.000	0.000	0.350	-0.003
8	0.619	0.528	1.434	0.615
9*	0.000	0.000	0.148	-0.194
10	-1.239	-0.240	-0.164	0.307
11*	0.000	0.000	-0.112	-0.344
12	-0.619	-0.078	-1.358	-0.512
13*	0.000	0.000	0.265	-0.002
14	0.000	-0.190	-0.759	-0.828
15*	0.000	0.000	-0.228	-0.233
16*	0.000	0.000	0.007	0.063
17	0.000	0.002	0.125	1.121
18*	-0.202	-0.128	-0.284	-0.063
19	0.001	-0.110	-0.411	-1.147
20*	-0.002	0.041	-0.335	-0.043
21*	0.001	-0.014	0.018	-0.088
22	-0.297	0.062	0.545	1.117
23*	0.000	0.000	0.048	0.269
24*	0.811	0.370	0.694	0.013
25	-1.838	-1.366	-1.452	1.282
26	-0.284	0.765	-0.597	-0.485
27*	-0.261	-0.352	-0.228	-0.155
28*	0.135	0.069	0.177	0.147
29	-1.363	-0.704	-1.907	-0.785
30*	0.270	0.137	0.165	0.545

Continued on next page

Table II.15 – continued from previous page

i	res	CQM	best reso	best rand
31	-0.616	-0.144	-0.389	1.310
32*	-0.002	0.041	0.291	0.356
33*	0.208	0.021	0.291	-0.102
34	1.432	0.363	2.321	1.077
35*	-0.009	0.039	0.236	0.146
36*	0.000	0.000	-0.169	-0.087
63	0.619	0.683	0.665	0.776
64*	0.000	0.000	0.389	-0.095
65	1.239	-0.555	0.611	0.432
66	1.049	0.391	1.703	0.416
67*	0.000	0.000	-0.304	0.017
68*	0.000	0.000	0.002	0.536
69	-0.577	-0.196	-0.664	-0.784
83	0.163	0.016	-0.294	-0.553
84*	0.000	0.000	0.357	-0.264
88	-1.383	-1.249	-0.912	-0.331
90	5.069	0.557	5.238	-0.204

II References

- [1] S. Weinberg, "Phenomenological Lagrangians," *Physica* **A96** (1979) 327.
- [2] J. Gasser and H. Leutwyler, "Chiral Perturbation Theory to One Loop," *Ann. Phys.* **158** (1984) 142.
- [3] J. Gasser and H. Leutwyler, "Chiral Perturbation Theory: Expansions in the Mass of the Strange Quark," *Nucl. Phys.* **B250** (1985) 465.
- [4] J. Bijnens, G. Colangelo, and G. Ecker, "The mesonic chiral Lagrangian of order p^6 ," *JHEP* **02** (1999) 020, arXiv:hep-ph/9902437.
- [5] J. Bijnens, "Chiral Perturbation Theory Beyond One Loop," *Prog. Part. Nucl. Phys.* **58** (2007) 521–586, arXiv:hep-ph/0604043.
- [6] J. Bijnens and I. Jemos, "Relations at Order p^6 in Chiral Perturbation Theory," *Eur.Phys.J.* **C64** (2009) 273–282, arXiv:0906.3118 [hep-ph].
- [7] J. Bijnens, G. Colangelo, and J. Gasser, " $K_{\ell 4}$ decays beyond one loop," *Nucl. Phys.* **B427** (1994) 427–454, arXiv:hep-ph/9403390.
- [8] G. Amoros, J. Bijnens, and P. Talavera, " $K_{\ell 4}$ form-factors and $\pi\pi$ scattering," *Nucl. Phys.* **B585** (2000) 293–352, [Erratum–ibid. **B598** (2001) 665], arXiv:hep-ph/0003258.
- [9] G. Amoros, J. Bijnens, and P. Talavera, "QCD isospin breaking in meson masses, decay constants and quark mass ratios," *Nucl. Phys.* **B602** (2001) 87–108, arXiv:hep-ph/0101127.
- [10] J. Bijnens and P. Dhonte, "Scalar form factors in $SU(3)$ chiral perturbation theory," *JHEP* **10** (2003) 061, arXiv:hep-ph/0307044.
- [11] J. Bijnens, P. Dhonte, and P. Talavera, " $\pi\pi$ scattering in three flavour ChPT," *JHEP* **01** (2004) 050, arXiv:hep-ph/0401039.
- [12] J. Bijnens, P. Dhonte, and P. Talavera, " πK scattering in three flavor ChPT," *JHEP* **05** (2004) 036, arXiv:hep-ph/0404150.
- [13] S.-Z. Jiang, Y. Zhang, C. Li, and Q. Wang, "Computation of the p^6 order chiral Lagrangian coefficients," *Phys.Rev.* **D81** (2010) 014001, arXiv:0907.5229 [hep-ph].
- [14] A. Pich, "Effective field theory: Course," arXiv:hep-ph/9806303 [hep-ph].
- [15] S. Scherer, "Introduction to chiral perturbation theory," *Adv.Nucl.Phys.* **27** (2003) 277, arXiv:hep-ph/0210398 [hep-ph].

- [16] F. James and M. Roos, "Minuit: A System for Function Minimization and Analysis of the Parameter Errors and Correlations," *Comput.Phys.Commun.* **10** (1975) 343–367.
- [17] http://lcgapp.cern.ch/project/cls/work_packages/mathlibs/minuit/.
- [18] G. Amoros, J. Bijnens, and P. Talavera, "Two-point functions at two loops in three flavour chiral perturbation theory," *Nucl. Phys.* **B568** (2000) 319–363, arXiv:hep-ph/9907264.
- [19] **Particle Data Group** Collaboration, K. Nakamura *et al.*, "Review of particle physics," *J.Phys.G* **G37** (2010) 075021.
- [20] J. Bijnens and I. Jemos, "Determination of Low Energy Constants and testing Chiral Perturbation Theory at order p^6 (NNLO)," *PoS CD09* (2009) 087, arXiv:0909.4477 [hep-ph].
- [21] J. Bijnens and I. Jemos, "Determination of Low Energy Constants and testing Chiral Perturbation Theory at Next to Next to Leading Order," *PoS EFT09* (2009) 032, arXiv:0904.3705 [hep-ph].
- [22] **Particle Data Group** Collaboration, C. Amsler *et al.*, "Review of Particle Physics," *Phys.Lett.* **B667** (2008) 1–1340.
- [23] G. Colangelo, S. Durr, A. Juttner, L. Lellouch, H. Leutwyler, *et al.*, "Review of lattice results concerning low energy particle physics," arXiv:1011.4408 [hep-lat].
- [24] J. Bijnens and J. Prades, "Electromagnetic corrections for pions and kaons: Masses and polarizabilities," *Nucl.Phys.* **B490** (1997) 239–271, arXiv:hep-ph/9610360 [hep-ph].
- [25] G. Amoros and J. Bijnens, "A parametrization for $K^+ \rightarrow \pi^+ \pi^- e^+ \nu$," *J. Phys.* **G25** (1999) 1607–1622, arXiv:hep-ph/9902463.
- [26] L. Ametller, J. Bijnens, A. Bramon, and F. Cornet, "Semileptonic π and K decays and the chiral anomaly at one loop," *Phys.Lett.* **B303** (1993) 140–146, arXiv:hep-ph/9302219 [hep-ph].
- [27] P. Truovel, "New results on rare and forbidden semileptonic K^+ decays," arXiv:hep-ex/0012012 [hep-ex]. Frascati Physics Series.
- [28] **NA48-2 Collaboration** Collaboration, J. Batley *et al.*, "Precise tests of low energy QCD from K_{e4} decay properties," *Eur.Phys.J.* **C70** (2010) 635–657.
- [29] **BNL-E865 Collaboration** Collaboration, S. Pislak *et al.*, "A New measurement of K_{e4}^+ decay and the s wave $\pi\pi$ scattering length a_0^0 ," *Phys.Rev.Lett.* **87** (2001) 221801, arXiv:hep-ex/0106071 [hep-ex].

- [30] G. Colangelo, J. Gasser, and H. Leutwyler, “ $\pi\pi$ scattering,” *Nucl. Phys.* **B603** (2001) 125–179, arXiv:hep-ph/0103088.
- [31] P. Buettiker, S. Descotes-Genon, and B. Moussallam, “A re-analysis of πK scattering a la Roy and Steiner,” *Eur. Phys. J.* **C33** (2004) 409–432, arXiv:hep-ph/0310283.
- [32] J. F. Donoghue, J. Gasser, and H. Leutwyler, “The decay of a light Higgs boson,” *Nucl.Phys.* **B343** (1990) 341–368.
- [33] B. Moussallam, “ N_f dependence of the quark condensate from a chiral sum rule,” *Eur.Phys.J.* **C14** (2000) 111–122, arXiv:hep-ph/9909292 [hep-ph].
- [34] B. Ananthanarayan, I. Caprini, G. Colangelo, J. Gasser, and H. Leutwyler, “Scalar form-factors of light mesons,” *Phys.Lett.* **B602** (2004) 218–225, arXiv:hep-ph/0409222 [hep-ph].
- [35] **JLQCD Collaboration, TWQCD Collaboration** Collaboration, S. Aoki *et al.*, “Pion form factors from two-flavor lattice QCD with exact chiral symmetry,” *Phys.Rev.* **D80** (2009) 034508, arXiv:0905.2465 [hep-lat].
- [36] J. Bijnens and P. Talavera, “Pion and kaon electromagnetic form factors,” *JHEP* **03** (2002) 046, arXiv:hep-ph/0203049.
- [37] M. Gonzalez-Alonso, A. Pich, and J. Prades, “Determination of the Chiral Couplings L_{10} and C_{87} from Semileptonic Tau Decays,” *Phys.Rev.* **D78** (2008) 116012, arXiv:0810.0760 [hep-ph].
- [38] G. Ecker, J. Gasser, A. Pich, and E. de Rafael, “The Role of Resonances in Chiral Perturbation Theory,” *Nucl.Phys.* **B321** (1989) 311.
- [39] J. F. Donoghue, C. Ramirez, and G. Valencia, “The Spectrum of QCD and Chiral Lagrangians of the Strong and Weak Interactions,” *Phys.Rev.* **D39** (1989) 1947.
- [40] V. Cirigliano, G. Ecker, M. Eidemuller, R. Kaiser, A. Pich, *et al.*, “Towards a consistent estimate of the chiral low-energy constants,” *Nucl.Phys.* **B753** (2006) 139–177, arXiv:hep-ph/0603205 [hep-ph].
- [41] K. Kampf, J. Novotny, and J. Trnka, “On different lagrangian formalisms for vector resonances within chiral perturbation theory,” *Eur.Phys.J.* **C50** (2007) 385–403, arXiv:hep-ph/0608051 [hep-ph].
- [42] J. Bijnens and K. Ghorbani, “ $\eta \rightarrow 3\pi$ at Two Loops In Chiral Perturbation Theory,” *JHEP* **11** (2007) 030, arXiv:0709.0230 [hep-ph].

- [43] J. Gasser, C. Haefeli, M. A. Ivanov, and M. Schmid, "Integrating out strange quarks in ChPT," *Phys.Lett.* **B652** (2007) 21–26, arXiv:0706.0955 [hep-ph].
- [44] J. Gasser, C. Haefeli, M. A. Ivanov, and M. Schmid, "Integrating out strange quarks in ChPT: Terms at order p^6 ," *Phys.Lett.* **B675** (2009) 49–53, arXiv:0903.0801 [hep-ph].

III

Hard pion Chiral Perturbation Theory for $B \rightarrow \pi$ and $D \rightarrow \pi$ formfactors

Johan Bijnens and Ilaria Jemos

Department of Astronomy and Theoretical Physics, Lund University,
Sölvegatan 14A, SE 223-62 Lund, Sweden

Nuclear Physics **B840** (2010) 54, [Erratum-ibid. **B844** (2011) 182],
[arXiv:1006.1197 [hep-ph]]

III

We use one-loop Heavy Meson Chiral Perturbation Theory (HMChPT) as well as a relativistic formulation to calculate the chiral logarithms $m_\pi^2 \log(m_\pi^2/\mu^2)$ contributing to the formfactors of the semileptonic $B \rightarrow \pi$ decays at momentum transfer q^2 away from $q_{\max}^2 = (m_B - m_\pi)^2$. We give arguments why this chiral behavior is reliable even in the energy regime with hard or fast pions. These results can be used to extrapolate the formfactors calculated on the lattice to lower light meson masses.

PACS: 12.39.Fe Chiral Lagrangians, 13.20.He Decays of bottom mesons, 13.20.Fc Decays of charmed mesons, 11.30.Rd Chiral symmetries

Keywords: B and D meson semileptonic decays, Chiral Perturbation Theory

Reprinted from *Nuclear Physics* **B 840**, Johan Bijnens, Ilaria Jemos, Hard pion Chiral Perturbation Theory for $B \rightarrow \pi$ and $D \rightarrow \pi$ formfactors, 54-66, Copyright (2010), with permission from Elsevier.

III.1 Introduction

The study of the formfactors of semileptonic $B \rightarrow \pi$ and $D \rightarrow \pi$ decays has become a task of primary importance for the determination of the KM matrix elements $|V_{ub}|$ and $|V_{cd}|$ respectively. Unfortunately this is a rather difficult mission. The kinematically accessible region is large, the physical pictures emerging at the two extremities of the q^2 range are quite different, requiring different approximation methods and this makes calculations directly from QCD hard.

Nevertheless a lot of effort has been put into studying this decay, both in experiment and in theory. The q^2 spectrum has been measured by different collaborations (CLEO [1, 2], Belle [3], Babar [4]) The QCD based theoretical calculations are either on QCD light-cone sum rules (LCSR), which provide reliable determinations at small q^2 [5], or on lattice simulations [6]. In particular lattice QCD allows to solve the non perturbative QCD effects numerically, but it is at present limited in the light quark masses that can be reached. Thus a final extrapolation in the light quark masses is needed.

At low energies Chiral Perturbation Theory (ChPT) [7, 8] provides a way to do this extrapolation on a theoretically sound basis. For processes with all pions soft this works fine and was extended to include heavy mesons in [9, 10]. The B and B^* mesons were there included using a heavy quark like formalism known as Heavy Meson ChPT (HMChPT). This has been used to extrapolate the behaviour of the form factors near the endpoint, $q_{\max}^2 = (m_B - m_\pi)^2$, where the pions are soft [11, 12]. But a description of the light quark mass dependence of the form factors in the entire range of energy is still missing. Therefore we lack extrapolation formulas in the region away from maximum momentum transfer.

A similar problem exists in the case of $K_{\ell 3}$ decay. Here two-flavour ($SU(2)$) ChPT provides a well defined scheme for the calculation of the formfactors near $q_{\max}^2 = (m_K - m_\pi)^2$. At other values of q^2 including $q^2 \simeq 0$, the (two-flavour) power counting scheme breaks down due to the presence of a large momentum pion in the final state. However, the authors of [13] argued that also in this latter case the coefficient of the chiral logarithm $m_\pi^2 \log m_\pi^2$ is calculable and thus it can be used for the extrapolations on the lattice at q^2 away from q_{\max}^2 . In [14] the argument was clarified and extended to the case of the $K \rightarrow \pi\pi$ decays. It was also argued there that this was a much more general circumstance.

The aim of this paper is to perform the same calculations for heavy meson semileptonic decays. These results can then be used to perform the extrapolation to light quark masses of lattice results also for values of q^2 away from the end-point q_{\max}^2 . The arguments as presented in [14] show that also in this case the coefficient of the logarithm should be calculable as discussed in Sect. III.5.

The discussion implies that both the HMChPT formalism or a relativistic one can be used. We have performed the calculations in both formalisms as a consistency check and have also reproduced the known results for the masses, decay constants and formfactors at q_{\max}^2 in both.

The paper is structured as follow. After a short description of HMChPT in Sect. III.2, we introduce in Sect. III.3 the relativistic Lagrangian that we used as a consistency check, since the off-shell behaviour in both formalisms is rather different. In Sect. III.4 we define the formfactors involved, and how to include the weak current in the Lagrangians of both formalisms. Sect. III.5 gives the arguments why this procedure should produce the correct nonanalytic behaviour in the light quark masses where they are different from [13, 14]. Finally the results for the coefficients are shown in Sect. III.6 where we provide also some checks of the validity of our assumptions. The appendix gives some results for the needed expansions of the loop integrals.

Throughout the paper we focus on $B \rightarrow \pi \ell \nu_\ell$ decay, but the same procedure and calculations go through also in the D semileptonic decays. All formulas are applicable to both cases. We are extending this work to the three flavour case as well as to other vector formfactors like $B \rightarrow D$ [15].

III.2 Heavy Meson Chiral Perturbation Theory

In this section we review the main features of HMChPT [9, 10], see also the lectures by Wise [16] and the book [17]. Chiral Lagrangians can be used to describe the interactions of light mesons, as pions and kaons, with hadrons containing a heavy quark. HMChPT makes use of spontaneously broken $SU(N_f) \times SU(N_f)$ chiral symmetry on the light quarks, and spin-flavour symmetry on the heavy quarks. This formulation lets us study chiral symmetry breaking effects in a chiral-loop expansion by simultaneously performing an expansion in powers of the inverse of the heavy meson mass.

In this paper we deal only with two-flavour ChPT [7] but the theory can be easily extended in the case of three flavours [8], thus including kaons in the description. The notation is the same as in [18]. The lowest order Lagrangian describing the strong interactions of the light mesons is

$$\mathcal{L}_{\pi\pi}^{(2)} = \frac{F^2}{4} (\langle u_\mu u^\mu \rangle + \langle \chi_+ \rangle), \quad (\text{III.1})$$

with

$$\begin{aligned} u_\mu &= i\{u^\dagger(\partial_\mu - ir_\mu)u - u(\partial_\mu - il_\mu)u^\dagger\}, \\ \chi_\pm &= u^\dagger\chi u^\dagger \pm u\chi^\dagger u, \\ u &= \exp\left(\frac{i}{\sqrt{2}F}\phi\right), \end{aligned}$$



$$\begin{aligned}\chi &= 2B(s + ip), \\ \phi &= \begin{pmatrix} \frac{1}{\sqrt{2}}\pi^0 & \pi^+ \\ \pi^- & -\frac{1}{\sqrt{2}}\pi^0 \end{pmatrix}.\end{aligned}\quad (\text{III.2})$$

The fields s , p , $l_\mu = v_\mu - a_\mu$ and $r_\mu = v_\mu + a_\mu$ are the standard external scalar, pseudoscalar, left- and right- handed vector fields introduced by Gasser and Leutwyler [7,8].

The field u and u_μ transform under a chiral transformation $g_L \times g_R \in SU(2)_L \times SU(2)_R$ as

$$u \longrightarrow g_R u h^\dagger = h u g_L^\dagger, \quad u_\mu \longrightarrow h u_\mu h^\dagger. \quad (\text{III.3})$$

In (III.3) h depends on u , g_L and g_R and is the so called compensator field. The notation $\langle X \rangle$ stands for trace over up and down quark indices and all matrices are 2×2 matrices.

We now begin with a brief synopsis of the formalism of HMChPT for the two-flavour case. The three flavour case was the original formulation [9, 10]. In the limit $m_b \rightarrow \infty$, the pseudoscalar B and the vector B^* mesons are degenerate. In the following we neglect the mass splitting $\Delta = m_{B^*} - m_B$. To implement the heavy quark symmetries it is convenient to assemble them into a single field

$$H^a(v) = \frac{1 + \not{v}}{2} [B_\mu^{*a}(v)\gamma^\mu - B^a(v)\gamma_5], \quad (\text{III.4})$$

where v is the fixed four-velocity of the heavy meson, a is a flavour index corresponding to the light quark in the B meson. $B^1 = B^+$, $B^2 = B^0$ and similarly for the vector mesons B_μ^* . In (III.4) the operator $(1 + \not{v})/2$ projects out the particle component of the heavy meson only. The conjugate field is defined as $\bar{H}_a(v) = \gamma_0 H_a^\dagger(v) \gamma_0$. We assume the field $H^a(v)$ to transform under the chiral transformation $g_L \times g_R \in SU(2)_L \times SU(2)_R$ as

$$H_a(v) \longrightarrow h_{ab} H_b(v), \quad (\text{III.5})$$

so we introduce the covariant derivative as

$$D_{ab}^\mu H_b(v) = \delta_{ab} \partial^\mu H_b(v) + \Gamma_{ab}^\mu H_b(v), \quad (\text{III.6})$$

where $\Gamma_{ab}^\mu = \frac{1}{2} [u^\dagger (\partial_\mu - i r_\mu) u + u (\partial_\mu - i l_\mu) u^\dagger]_{ab}$, and the indices a, b run over the light quark flavours. Finally, the Lagrangian for the heavy-light mesons in the static heavy quark limit reads

$$\mathcal{L}_{\text{heavy}} = -i \text{Tr} \bar{H}_a v \cdot D_{ab} H_b + g \text{Tr} \bar{H}_a u_{ab}^\mu H_b \gamma_\mu \gamma_5, \quad (\text{III.7})$$

where g is the coupling of the heavy meson doublet to the Goldstone boson and the traces, Tr , are over spin indices, the γ -matrix indices. The Lagrangian (III.7) satisfies chiral symmetry and heavy quark spin flavour symmetry.

As a final remark of this section we stress that, in general, the use of HMChPT is only valid as long as the interacting pion is soft, i.e. if it has momentum much smaller than the scale of spontaneous chiral symmetry breaking ($\Lambda_{\text{ChSB}} \simeq 1 \text{ GeV}$). In fact, only in this regime the usual ChPT is well defined. For the semileptonic decays of heavy mesons this range of energy covers just a small fraction of the Dalitz plot. In Sect. III.5 we will give an argument why the predictions on the coefficients of the logarithms appearing in the final amplitudes are reliable even outside the range of applicability of HMChPT.

III.3 Relativistic Theory

When $q^2 \neq q_{\text{max}}$ it is possible that in the loops appear very off-shell B and B^* mesons. This in principle changes the non analyticities in the light masses of the loop functions and thus it might affect the coefficients of $m_\pi^2 \log m_\pi^2 / \mu^2$. It could be that different treatments of the off-shell behaviour gave rise to different nonanalyticities. Sect. III.5 argues that this should not be the case. In order to test this, we are not only calculating using HMChPT but also in a relativistic formulation. We also add some redundant higher order terms as an additional check.

For this scope, we construct a relativistic Lagrangian that respects the spin-flavour symmetries of HMChPT. It is built up starting from B^a and B_μ^{*a} fields, but now in the relativistic form, and we treat them as column-vectors in the light-flavour index a .



$$\mathcal{L}_{\text{kin}} = \nabla^\mu B^\dagger \nabla_\mu B - m_B B^\dagger B - \frac{1}{2} B_{\mu\nu}^{*\dagger} B^{*\mu\nu} + m_B B_\mu^{*\dagger} B^{*\mu}, \quad (\text{III.8})$$

$$\begin{aligned} \mathcal{L}_{\text{int}} = & g M_0 \left(B^\dagger u^\mu B_\mu^* + B_\mu^{*\dagger} u^\mu B \right) \\ & + \frac{g}{2} \epsilon^{\mu\nu\alpha\beta} \left(-B_\mu^{*\dagger} u_\alpha \nabla_\mu B_\beta^* + \nabla_\mu B_\nu^{*\dagger} u_\alpha B_\beta^* \right), \end{aligned} \quad (\text{III.9})$$

with $B_{\mu\nu}^* = \nabla_\mu B_\nu^* - \nabla_\nu B_\mu^*$, and $\nabla_\mu = \partial_\mu + \Gamma_\mu$. The constant g of (III.9) is the same in (III.7), M_0 is the mass of the B meson in the chiral limit. In (III.8) and (III.9) we have suppressed flavour indices a, b for simplicity. The fields B and B^* transform under chiral transformations as $B \rightarrow hB$. The two terms of \mathcal{L}_{int} in (III.9) contain the vertices $BB^*\pi$ and $B^*B^*\pi$. No interaction of the kind $BB\pi$ appears because it is forbidden by parity conservation.

From \mathcal{L}_{kin} in (III.8) we find the propagators of the B and B^* meson respec-

tively:

$$\frac{i}{p^2 - m_B^2} \quad \frac{-i \left(g_{\mu\nu} - \frac{p_\mu p_\nu}{m_B^2} \right)}{p^2 - m_B^2}. \quad (\text{III.10})$$

This is to be contrasted with the propagator $1/v \cdot p$ in the HMChPT formalism showing the different off-shell behaviour.

III.4 $B \rightarrow \pi$ formfactors: formalism

In this section we review the semileptonic decay formalism. The hadronic current for pseudoscalar to pseudoscalar semileptonic decays $(P_i(\bar{q}_i, q) \rightarrow P_f(\bar{q}_f, q)\ell^+\nu_\ell)$ has the structure

$$\begin{aligned} \langle P_f(p_f) | \bar{q}_i \gamma_\mu q_f | P_i(p_i) \rangle &= (p_i + p_f)_\mu f_+(q^2) + (p_i - p_f)_\mu f_-(q^2) \\ &= \left[(p_i + p_f)_\mu - q_\mu \frac{(m_i^2 - m_f^2)}{q^2} \right] f_+(q^2) + q_\mu \frac{(m_i^2 - m_f^2)}{q^2} f_0(q^2), \end{aligned} \quad (\text{III.11})$$

where q^μ is the momentum transfer $q^\mu = p_i^\mu - p_f^\mu$. In our case P_f is a pion, P_i is a B meson and $q_i = b$. For example, to find the $B^0 \rightarrow \pi^-$ formfactors we need then to evaluate the hadron matrix elements of the quark bilinear $\bar{b}\gamma_\mu q$, where $q = u$.

Heavy quark and chiral symmetry transformation properties of chiral currents dictate that the matching of QCD bilinears onto operators of HMChPT take the form [11, 16],

$$\begin{aligned} \bar{b}\gamma^\mu (1 - \gamma_5) q_a &\rightarrow i c_L \text{Tr}[\gamma^\mu (1 - \gamma_5) u_{ab}^\dagger H_b(v)], \\ \bar{b}\gamma^\mu (1 + \gamma_5) q_a &\rightarrow i c_R \text{Tr}[\gamma^\mu (1 + \gamma_5) u_{ab} H_b(v)]. \end{aligned} \quad (\text{III.12})$$

The constants c_L and c_R have to be equal because of parity invariance, therefore we can conclude

$$\bar{b}\gamma^\mu q_a \propto \text{Tr}\gamma^\mu (u_{ab}^\dagger + u_{ab}) H_b(v) + \text{Tr}\gamma_5 \gamma^\mu (u_{ab}^\dagger - u_{ab}) H_b(v). \quad (\text{III.13})$$

If no hard pions appear in the final state we can use the definition of decay constant

$$\langle 0 | \bar{b}\gamma_\mu \gamma_5 q | B(p_B) \rangle = i F_B p_B^\mu \quad (\text{III.14})$$

and state $c_L = c_R = \frac{1}{2} F_B \sqrt{m_B}$. Of course this latter result does not hold for momenta away from q_{max}^2 in which case $c_L = c_R$ is just an effective coupling, as explained in Sect. III.5.

In HMChPT it is convenient to use definitions in which the formfactors are independent of the heavy meson mass

$$\left\langle \pi(p_\pi) \left| \bar{b} \gamma_\mu q \right| B(v) \right\rangle_{\text{HMChPT}} = [p_{\pi\mu} - (v \cdot p_\pi) v_\mu] f_p(v \cdot p_\pi) + v_\mu f_v(v \cdot p_\pi). \quad (\text{III.15})$$

In (III.15) $v \cdot p_\pi$ is the energy of the pion in the heavy meson rest frame

$$v \cdot p_\pi = \frac{m_B^2 + m_\pi^2 - q^2}{2m_B}. \quad (\text{III.16})$$

The formfactors defined in (III.11) and in (III.15) are related by matching the relativistic and the HMChPT hadronic current:

$$f_0(q^2) = \frac{1}{\sqrt{m_B}} f_v(v \cdot p_\pi), \quad f_+(q^2) = \frac{\sqrt{m_B}}{2} f_p(v \cdot p_\pi). \quad (\text{III.17})$$

The $\sqrt{m_B}$ factors in (III.17) are due to the different normalizations for states used in the two formalisms. In principle the relations in (III.17) are valid only when $q^2 \approx q_{\text{max}}^2$, i.e. when HMChPT is applicable. On the other hand, for the arguments shown in Sect. III.5 below, the chiral structure of the formfactors in QCD and in HMChPT is the same also for q^2 away from q_{max}^2 . However, this does not imply that (III.17) holds away from q_{max}^2 , at least as far as regard the tree level term and the leading logarithms.

A matching similar to (III.12) has to be done also for the relativistic theory described in Sect. III.3. We identify four possible operators¹

$$J_\mu^L = \frac{1}{2} E_1 t u^\dagger \nabla_\mu B + \frac{i}{2} E_2 t u^\dagger u_\mu B + \frac{i}{2} E_3 t u^\dagger B_\mu^* + \frac{1}{2} E_4 t u^\dagger (\nabla_\nu u_\mu) B^{*\nu}, \quad (\text{III.18})$$

where E_1, \dots, E_4 , are effective couplings. t is a constant spurion vector transforming as $t \rightarrow t g_L^\dagger$, so that J_μ^L is invariant under $SU(2)_L$ transformations. The heavy quark symmetry implies $m_B E_1 = E_3$. Analogously we can introduce a J_μ^R current and thus an axial-vector $J_\mu^5 = J_\mu^R - J_\mu^L$ and a vector $J_\mu^V = J_\mu^R + J_\mu^L$ current. They are used respectively to evaluate the amplitudes of $B \rightarrow \ell \nu_\ell$ and the $B \rightarrow \pi \ell \nu_\ell$ formfactors as defined in (III.11). We leave the discussion for the latter in Sect. III.6, while we quote here the results of the $B \rightarrow$ vacuum matrix element at one loop

$$F_B = E_1 \left[1 + \frac{1}{F^2} \left(\frac{3}{8} + \frac{9}{8} g^2 \right) \bar{A}(m_\pi^2) \right] \quad (\text{III.19})$$

¹The last one is higher order but we included it since it has a different type of contraction of the Lorentz indices and as an explicit check on the arguments of Sect. III.5.



$\bar{A}(m_\pi^2)$ is defined in (III.25) in the appendix. Here we only quoted the nonanalytic dependence on the light quark masses for the one-loop part. We compare (III.19) with the results obtained with HMChPT [19]. We see that E_1 plays the role of F_H in [19] and that the relativistic theory predicts the same coefficient of the chiral logarithm in $\bar{A}(m_\pi^2)$.

III.5 Hard pion Chiral Perturbation Theory

In order to study the chiral behavior of the formfactors at q^2 away from q_{\max}^2 we can not neglect operators with an arbitrary numbers of derivatives on the external pion since now its momentum is large. Therefore we must take into account that the usual power counting of ChPT does not work and we can not be sure a priori that a loop calculation would make sense.

A similar problem arises in the case of $K_{\ell 3}$ decay. The authors of [13] dealt with it using $SU(2)$ ChPT to study the amplitudes whether the outgoing pion was soft or not. They argued they could calculate the corrections of the type $m_\pi^2 \log m_\pi^2$ even in the range of energy where the usual ChPT does not work. Their argument is based on the fact that only the soft internal pions are responsible for the chiral logarithms. These ideas were generalized by the authors of [14] who made clear that those arguments basically corresponds to use an effective Lagrangian to describe the hard part of a general loop calculation in a chiral invariant way. The situation is shown schematically in Fig. III.1. The underlying argument is the same as the analysis for infra-red divergences. Since the soft lines do not see the hard or short-distance structure of the diagram, we can separate them from the rest of the process. We should thus be able to describe the hard part of any diagram by an effective Lagrangian. This effective Lagrangian should include the most general terms allowed consistent with all the symmetries and have coefficients that depend on the hard kinematical quantities and can even be complex. A two-loop example will be given in [15]. We expect that a proof along the lines of SCET [20] should be possible. Once it is accepted that one can do this, a second step is to prove that the effective Lagrangian one uses is sufficient to describe the neighbourhood of the hard process and calculate chiral logarithms.

The latter was done in [13] for the case of $K_{\ell 3}$ decays by showing that the matrix elements of operators with higher derivatives was proportional to the lowest order matrix-element up to terms of order m_π^2 . In particular, the part including the coefficient of the chiral logarithms $m_\pi^2 \log m_\pi^2$ has the same coefficient relative to the tree level matrix-element as the lowest order operator. The same was proven for $K \rightarrow \pi\pi$ in [14].

As a matter of fact, the semileptonic K decay has the same structure *heavy* \rightarrow *light* as the B one when M_K is treated as large compared to m_π as in [13]. The main differences between the two processes are the energies involved and

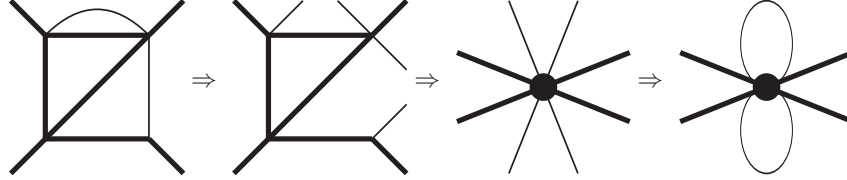


Figure III.1: An example of the argument used. The thick lines contain a large momentum, the thin lines a soft momentum. Left: a general Feynman diagram with hard and soft lines. Middle-left: we cut the soft lines to remove the soft singularity. Middle-right: The contracted version where the hard part is assumed to be correctly described by a “vertex” of an effective Lagrangian. Right: the contracted version as a loop diagram. This is expected to reproduce the chiral logarithm of the left diagram. Figure from [14].

that for the B meson the corresponding vectorial particle B^* is close to its mass-shell. So in order to have a sufficiently complete effective Lagrangian in the neighbourhood we need to include the B^* as was done in the previous sections. However, we expect the kind of arguments presented in [13,14] to work here as well.

We note that the effective Lagrangian needs to be complete enough in the neighbourhood of the underlying process. That also implies that if we have two different formalisms, both sufficiently complete, the logarithms should be the same. In particular, the HMChPT and the relativistic formalism should give the same results.

We are only concerned with terms of order 1, m_π and $m_\pi^2 \log m_\pi^2$, i.e. we are not trying to calculate terms of order $O(m_\pi^2)$ without logarithms. Here we restrict our discussion to the case of $SU(2)$ ChPT, and far from q_{\max}^2 . It is clear that adding (soft) kaon loops does not change the validity of the arguments. First we analyze the case of HMChPT and thus we need to look at the matrix elements $\langle \pi(p_\pi) | O | B(v) \rangle$ where O can be any of the operators in (III.13) with possibly more derivatives. We want to show that matrix elements of operators with higher number of derivatives are all proportional to the lowest order ones up to terms of order m_π^2 (and without logarithms) which are of higher order. We need to look at the cases where extra covariant derivatives D_μ are added in the operators. We can distinguish different possibilities depending on which particle the derivative hits.

- The case where it hits an internal soft pion line, leads to $\int d^d p p_\mu / (p^2 - m_\pi^2)$ which is always suppressed by three powers of m_π .
- If the derivative hits an internal line which is not soft in a loop, it is

part of the loop diagram that is described by our effective Lagrangian and is thus indirectly included via the coefficients. A simple example is when a pair of derivatives hits a B -meson. Then we get terms like $\int d^d p p_B^2 / (v \cdot p_\pi - \Delta) \dots \simeq m_B^2 \int d^d p 1 / (v \cdot p_\pi - \Delta) \dots$, i.e. something that is proportional to the lowest order result and that can be included modifying accordingly the effective coupling. It corresponds to change the hard structure of the loop diagram, what can be described by a proper replacement of the effective coupling, as shown in Fig. III.1.

- All the extra derivatives should thus act on external lines or tree-level internal lines, i.e. those not in a loop. All these can thus be transformed into masses of external particles or other kinematical quantities, as here q^2 . None of these has terms of order m_π or $m_\pi^2 \log m_\pi^2$. The kinematical quantities we keep fixed and masses have corrections at most of order m_π^2 compared to the order 1 terms and the order 1 part can be absorbed into the coefficient of the lowest order term.
- Note that if the extra derivatives are contracted with a v_μ rather than another derivative this can also be put into the value of the coefficients.

Also in the case of the relativistic theory described in Sect. III.3, we need to worry if more chiral logarithms arise including operators like the ones in (III.18) but with extra derivatives. All the above arguments also work except for derivatives that are contracted with B_μ^* . In this case the extra derivatives becomes contracted with the momenta in the B^* propagator or via $g_{\mu\nu}$ to the external current. After that the above arguments again apply. Terms involving a contraction with B^* can always be reduced to the simplest one which we included in (III.18), the E_4 term, and so we have also an explicit test of the last argument.

Near q_{\max}^2 the above arguments fail since kinematical quantities can contain terms of order m_π . However, here all pion lines are soft and we are in the regime of validity of standard HMChPT.

The conclusion from this section is that the coefficient of the chiral logarithm $m_\pi^2 \log m_\pi^2$ is calculable at all values of q^2 .

III.6 The Coefficients of the Chiral Logarithms

In this section we show the results for the semileptonic decay $B \rightarrow \pi \ell \nu_\ell$ amplitudes. Hereafter, we quote only the relevant terms, i.e. the leading ones and the chiral logarithms. The tree-level diagrams contributing to the amplitude are shown in Fig. III.2. The results for the formfactors at tree level for HMChPT are [11, 12]

$$f_v^{\text{Tree}}(v \cdot p_\pi) = \frac{\alpha}{F}, \quad f_p^{\text{Tree}}(v \cdot p_\pi) = \frac{\alpha}{F} \frac{g}{v \cdot p_\pi + \Delta}, \quad (\text{III.20})$$



Figure III.2: The tree-level diagrams contributing to the amplitude. A double line correspond to a B , a zigzag line to a B^* , a single line to a pion. A black circle represents the insertion of a $B \rightarrow \pi$ vector current.

where α is a constant that takes the value $\sqrt{m_B/2}F_B$ at q_{\max}^2 . We also have $c_L = c_R = \alpha/\sqrt{2}$. For the relativistic theory of Sect. III.3 we obtain

$$f_0^{\text{Tree}}(q^2)\Big|_{q_{\max}^2} = \frac{E_1}{F} \frac{1}{4}, \quad f_+^{\text{Tree}}(q^2)\Big|_{q_{\max}^2} = -\frac{1}{4} \frac{E_3}{F} \frac{m_B}{q^2 - m_B^2} g. \quad (\text{III.21})$$

Near $q_{\max}^2 = (m_B - m_\pi)^2$ the results are obviously the same, since the propagators in the second equations of (III.20) and (III.21) become respectively $1/m_\pi$ and $1/(2m_\pi m_B)$. The different factor of 2 is due to the different normalization of states used in HMChPT and in the relativistic formulation. Note that the relation of the coupling constant to F_B is only valid for $q_{\max}^2 = (m_B - m_\pi)^2$. The coupling constant are different at the different values of q^2 and can even be complex. The precise form of (III.21) is only valid near q_{\max}^2 . The full expressions are more complicated.

To proceed with the calculation at one-loop we need the wavefunction renormalization Z_π and Z_B . They are the same for HMChPT and the relativistic theory and read:

$$Z_\pi = 1 - \frac{2}{3F^2} \bar{A}(m_\pi^2), \quad Z_B = 1 + \frac{9}{4F^2} g^2 \bar{A}(m_\pi^2). \quad (\text{III.22})$$

The one-loop diagrams are shown in Fig. III.3. In Tab. III.1 we present the results at q^2 away from q_{\max}^2 . To find the results in HMChPT we expanded the one-loop calculation of [12] at $v \cdot p_\pi \rightarrow m_B$, $m_\pi^2 \rightarrow 0$. In the relativistic theory we first calculated the formfactors and then we expanded the loop integrals for $m_\pi^2 \ll m_B^2, (m_B^2 - q^2)$. These latter expansions are shown in App. III.1. We check that the coefficients of the leading logarithms coincide in the two theories. Summing up all the results in Tab. III.1 and including $(1/2)Z_\pi$ and

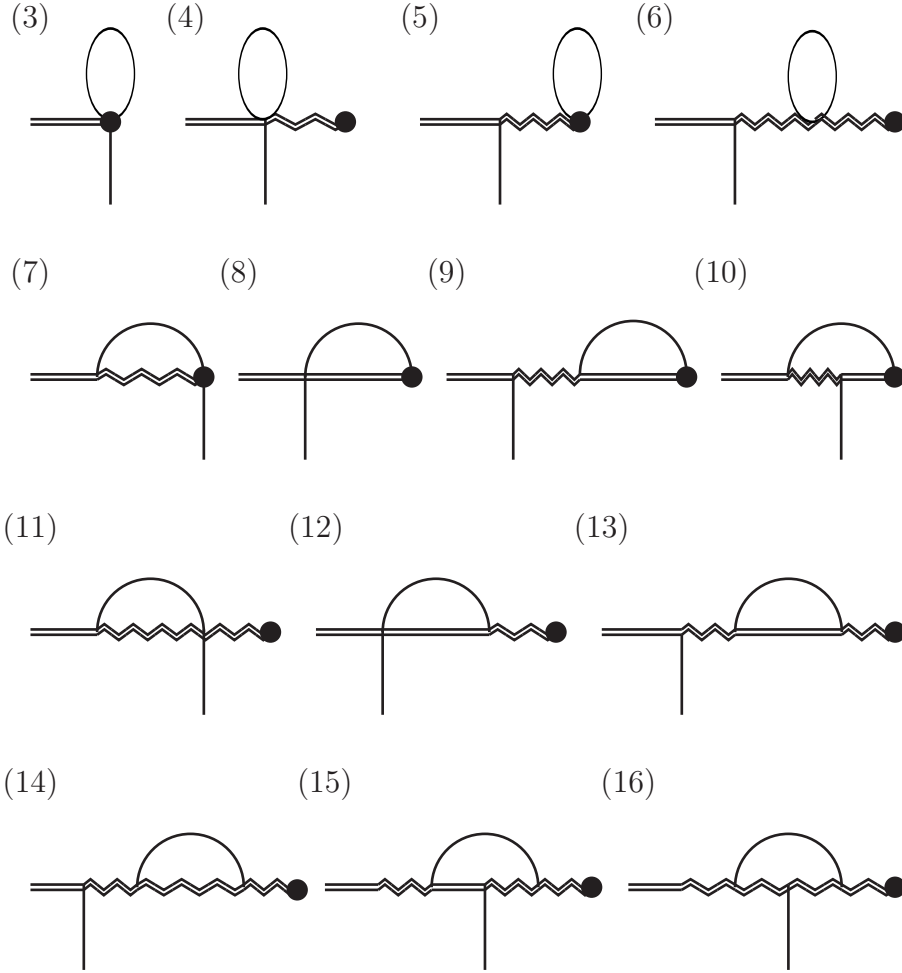


Figure III.3: The one-loop diagrams contributing to the amplitude. Vertices and lines as in Fig. III.2

$(1/2)Z_B$ times tree level, we find

$$\begin{aligned}
 f_{v/p}(v \cdot p_\pi) &= f_{v/p}^{\text{Tree}}(v \cdot p_\pi) \left[1 + \left(\frac{3}{8} + \frac{9}{8}g^2 \right) \frac{1}{F^2} \bar{A}(m_\pi^2) \right], \\
 f_{0/+}(q^2) &= f_{0/+}^{\text{Tree}}(q^2) \left[1 + \left(\frac{3}{8} + \frac{9}{8}g^2 \right) \frac{1}{F^2} \bar{A}(m_\pi^2) \right], \quad (\text{III.23})
 \end{aligned}$$

i.e. as expected the same coefficients in the two theories. The correction is also

Diagram	f_v HMChPT	f_0 Rel. Th.
(3)	$\frac{5}{24} \frac{1}{F^3} \alpha$	$\frac{5}{24F^2} f_0^{\text{Tree}}(q^2)$
(8)	$\frac{1}{2} \frac{1}{F^3} \alpha$	$\frac{1}{2F^2} f_0^{\text{Tree}}(q^2)$
	f_p HMChPT	f_+ Rel. Th.
(4)	$\frac{2}{6} \frac{g}{F^3} \frac{\alpha}{v \cdot p_\pi + \Delta}$	$\frac{1}{3F^2} f_+^{\text{Tree}}(q^2)$
(5)	$\frac{3}{8} \frac{g}{F^3} \frac{\alpha}{v \cdot p_\pi + \Delta}$	$\frac{3}{8F^2} f_+^{\text{Tree}}(q^2)$

Table III.1: The coefficients of the chiral logarithms, $\bar{A}(m_\pi^2)$, at q^2 away from $(m_B - m_\pi)^2$ from the different diagrams in Fig. III.3. The diagrams not listed in the table do not contribute with logarithms. The two Lagrangians give the same coefficients diagram per diagram provided the tree level coefficients are correctly identified.

Diagram	f_v HMChPT	f_0 Rel. Th.
(3)	$\frac{5}{24} \frac{1}{F^3} \alpha$	$\frac{5}{96} \frac{1}{F^3} E_1$
(8)	$\frac{3}{2} \frac{1}{F^3} \alpha$	$\frac{3}{8} \frac{1}{F^3} E_1$
	f_p HMChPT	f_+ Rel. Th.
(4)	$\frac{2}{6} \frac{\alpha}{F^3} \frac{g}{m_\pi}$	$\frac{1}{12} \frac{E_3}{F^3} \frac{g}{2m_\pi}$
(5)	$\frac{3}{8} \frac{\alpha}{F^3} \frac{g}{m_\pi}$	$\frac{3}{32} \frac{E_3}{F^3} \frac{g}{2m_\pi}$
(13)	$-\frac{3}{4} \frac{\alpha}{F^3} \frac{g^3}{m_\pi}$	$\frac{1}{16} \frac{E_3}{F^3} \frac{g^3}{2m_\pi}$
(14)	$\frac{3}{2} \frac{\alpha}{F^3} \frac{g^3}{m_\pi}$	$\frac{1}{8} \frac{E_3}{F^3} \frac{g^3}{2m_\pi}$
(15)	$\frac{1}{12} \frac{\alpha}{F^3} \frac{g^3}{m_\pi}$	$\frac{1}{48} \frac{E_3}{F^3} \frac{g^3}{2m_\pi}$
(16)	$-\frac{1}{6} \frac{\alpha}{F^3} \frac{g^3}{m_\pi}$	$-\frac{1}{24} \frac{E_3}{F^3} \frac{g^3}{2m_\pi}$

Table III.2: The coefficients of the chiral logarithms, $\bar{A}(m_\pi^2)$, at q_{max}^2 from the different diagrams in Fig. III.3. The diagrams not listed in the table do not contribute to the chiral logarithms. The two Lagrangians give the same coefficients provided the tree level coefficients are correctly identified.

the same for the scalar formfactor f_0 and for f_+ . In Tab. III.2 we quote also the results in the limit $q^2 = q_{\text{max}}^2 = (m_B - m_\pi)^2$ where the two theories must give the same outcome, being one the relativistic limit of the other. So this is



another check of the validity of our relativistic theory. Summing up all the results as explained above we find at q_{\max}^2

$$\begin{aligned}
f_v(v \cdot p_\pi) &= f_v^{\text{Tree}}(v \cdot p_\pi) \left[1 + \left(\frac{11}{8} + \frac{9}{8}g^2 \right) \frac{1}{F^2} \bar{A}(m_\pi^2) \right], \\
f_0(q^2) &= f_0^{\text{Tree}}(q^2) \left[1 + \left(\frac{11}{8} + \frac{9}{8}g^2 \right) \frac{1}{F^2} \bar{A}(m_\pi^2) \right], \\
f_p(v \cdot p_\pi) &= f_p^{\text{Tree}}(v \cdot p_\pi) \left[1 + \left(\frac{3}{8} + \frac{43}{24}g^2 \right) \frac{1}{F^2} \bar{A}(m_\pi^2) \right], \\
f_+(q^2) &= f_+^{\text{Tree}}(q^2) \left[1 + \left(\frac{3}{8} + \frac{43}{24}g^2 \right) \frac{1}{F^2} \bar{A}(m_\pi^2) \right], \quad (\text{III.24})
\end{aligned}$$

i.e. agreement between the two theories.

As a final check, we notice that the results obtained including only those diagrams where no B^* appears (i.e. (1),(3) and (8) in Fig. III.2 and III.3) coincide with the ones in [13] for the $K \rightarrow \pi$ amplitudes. The chiral corrections must agree in these two cases since, as we remarked above, the only difference between the two processes is the presence of the vectorial B^* particle.

III.7 Conclusions

In this paper we have calculated the pionic logarithms in the semileptonic $B \rightarrow \pi$ and $D \rightarrow \pi$ transitions. We have reproduced the known results near the endpoint $q^2 = (m_B - m_\pi)^2$, Eq. (III.24) and obtained the chiral logarithm also away from the endpoint in Eq. (III.23) and it was the same for both formfactors.

Acknowledgments

IJ gratefully acknowledges an Early Stage Researcher position supported by the EU-RTN Programme, Contract No. MRTN-CT-2006-035482, (Flavianet) This work is supported in part by the European Commission RTN network, Contract MRTN-CT-2006-035482 (FLAVIANet), European Community-Research Infrastructure Integrating Activity ‘‘Study of Strongly Interacting Matter’’ (HadronPhysics2, Grant Agreement n. 227431) and the Swedish Research Council. This work heavily used FORM [21].

III.A Loop integrals expansions

We collect the relevant expansions of the one-loop integrals needed to evaluate the diagrams in Fig. III.3 in the framework of the relativistic theory of Sect. III.3. In the calculation we need the one-, two- and three-point functions defined as ($d = 4 - 2\epsilon$)

$$A(m_1^2) = \frac{1}{i} \int \frac{d^d k}{(2\pi)^d} \frac{1}{k^2 - m_1^2} \quad (\text{III.25})$$

$$B(m_1^2, m_2^2, p^2) = \frac{1}{i} \int \frac{d^d k}{(2\pi)^d} \frac{1}{(k^2 - m_1^2)((p - k)^2 - m_2^2)} \quad (\text{III.26})$$

$$C(m_1^2, m_2^2, m_3^2, p_1^2, p_2^2, q^2) = \frac{1}{i} \int \frac{d^d k}{(2\pi)^d} \frac{1}{(k^2 - m_1^2)((k - p_1)^2 - m_2^2)((k - p_1 - p_2)^2 - m_3^2)} \quad (\text{III.27})$$

with $q^2 = (p_1 + p_2)^2$. Actually two- and three-point functions with extra powers of momenta in the numerator contribute too, but we do not intend to give their definitions here. They can be found in [22] in precisely the form used here. We only stress that all these functions can be rewritten in terms of (III.25), (III.26) and (III.27) [23]. The finite parts of $A(m_1^2)$ and $B(m_1^2, m_2^2, q^2)$ are [24]

$$\bar{A}(m_1^2) = -\frac{m_1^2}{16\pi^2} \log\left(\frac{m_1^2}{\mu^2}\right), \quad (\text{III.28})$$

$$\bar{B}(m_1^2, m_2^2, q^2) = \frac{1}{16\pi^2} \left[-1 - \int_0^1 dx \log\left(\frac{m_1 x + m_2(1-x) - x(1-x)q^2}{\mu^2}\right) \right]. \quad (\text{III.29})$$

In the calculation of the amplitude the three-point function $C(m_1^2, m_2^2, m_3^2, p_1^2, p_2^2)$ always depends on the masses as $(m^2, M^2, M^2, m^2, q^2)$ with $m = m_\pi$, and $M = m_B$. It can be rewritten using Feynman parameters x, y

$$C(m^2, M^2, M^2, M^2, m^2, q^2) = -\frac{1}{16\pi^2} \int_0^1 dx \int_0^{1-x} dy \left[m^2(1-x-2y+y^2) + M^2(x+y)^2 + (q^2 - M^2 - m^2)(-y+y(x+y)) \right]^{-1}. \quad (\text{III.30})$$

In order to find the appropriate chiral logarithms we expanded (III.29) and (III.30) for small m^2/M^2 . We quote only the terms of the expansions contain-



ing the chiral logarithms $\log(m^2/\mu^2)$

$$\bar{B}(m^2, M^2, q^2) = -\frac{1}{M^2 - q^2} \bar{A}(m^2), \quad q^2 \ll q_{\max}^2 \quad (\text{III.31})$$

$$C(m^2, M^2, M^2, m^2, q^2) = -\frac{1}{(M^2 - q^2)^2} \bar{A}(m^2), \quad q^2 \ll q_{\max}^2 \quad (\text{III.32})$$

$$\bar{B}(m^2, M^2, M^2) = \frac{1}{2M^2} \bar{A}(m^2), \quad (\text{III.33})$$

$$\bar{B}(m^2, M^2, m^2) = 0, \quad (\text{III.34})$$

$$\bar{B}(m^2, M^2, (M - m)^2) = -\frac{1}{mM} \bar{A}(m^2) - \frac{1}{M^2} \bar{A}(m^2). \quad (\text{III.35})$$

The expansions of the three-point functions at q_{\max}^2 are a bit more involved. The reason is that the reduction formulas present a singularity at $q_{\max}^2 = (M - m)^2$ for $m^2 = 0$. Thus we expand each of them directly, from the Feynman parameter integral, without rewriting them in terms of (III.25), (III.26) and (III.27). To do this one rewrites the integral in (III.30) using $z = x + y$ as

$$C(m^2, M^2, M^2, m^2, (M - m)^2) = -\frac{1}{16\pi^2} \int_0^1 dz \int_0^z dy \times \frac{1}{[M^2 z^2 + m^2 + 2mMy + (m^2(-z - y + y^2) - 2mMyz)]}. \quad (\text{III.36})$$

The part in the denominator in brackets is always suppressed by at least m/M compared to the first three terms for all values of z and y and we can thus expand in it. The remaining integrals can be done with elementary means. The result of the expansion is, quoting only up to the order needed for this work,

$$C(m^2, M^2, M^2, M^2, m^2, (M - m)^2) = -\frac{1}{2} \left(\frac{1}{m^2 M^2} \bar{A}(m^2) + \frac{1}{m M^3} \bar{A}(m^2) + \frac{1}{M^4} \bar{A}(m^2) \right), \quad (\text{III.37})$$

$$\bar{C}_{11}(m^2, M^2, M^2, M^2, m^2, (M - m)^2) = \frac{1}{2} \frac{1}{m M^3} \bar{A}(m^2) + \frac{7}{12} \frac{1}{M^4} \bar{A}(m^2), \quad (\text{III.38})$$

$$\bar{C}_{12}(m^2, M^2, M^2, M^2, m^2, (M - m)^2) = \frac{1}{3} \frac{1}{m M^3} \bar{A}(m^2) + \frac{7}{12} \frac{1}{M^4} \bar{A}(m^2), \quad (\text{III.39})$$

$$\bar{C}_{21}(m^2, M^2, M^2, M^2, m^2, (M - m)^2) = -\frac{1}{6} \frac{1}{M^4} \bar{A}(m^2), \quad (\text{III.40})$$

$$\bar{C}_{22}(m^2, M^2, M^2, M^2, m^2, (M - m)^2) = -\frac{7}{30} \frac{1}{M^4} \bar{A}(m^2), \quad (\text{III.41})$$

$$\bar{C}_{23}(m^2, M^2, M^2, M^2, M^2, m^2, (M - m)^2) = -\frac{1}{4} \frac{1}{M^4} \bar{A}(m^2), \quad (\text{III.42})$$

$$\bar{C}_{24}(m^2, M^2, M^2, M^2, m^2, (M - m)^2) = -\frac{1}{12} \frac{1}{M^2} \bar{A}(m^2). \quad (\text{III.43})$$

The other three-point functions do not give any leading logarithm.

III References

- [1] CLEO Collaboration, J. Y. Ge *et al.*, “Study of $D^0 \rightarrow \pi^- e^+ \nu_e$, $D^+ \rightarrow \pi^0 e^+ \nu_e$, $D^0 \rightarrow K^- e^+ \nu_e$, and $D^+ \rightarrow \bar{K}^0 e^+ \nu_e$ in Tagged Decays of the $\psi(3770)$ Resonance,” *Phys. Rev.* **D79** (2009) 052010, arXiv:0810.3878 [hep-ex].
- [2] CLEO Collaboration, N. E. Adam *et al.*, “A Study of Exclusive Charmless Semileptonic B Decay and $|V_{ub}|$,” *Phys. Rev. Lett.* **99** (2007) 041802, arXiv:hep-ex/0703041.
- [3] Belle Collaboration, T. Hokuue *et al.*, “Measurements of branching fractions and q^2 distributions for $B \rightarrow \pi \ell \nu$ and $B \rightarrow \rho \ell \nu$ Decays with $B \rightarrow D^{(*)} \ell \nu$ Decay Tagging,” *Phys. Lett.* **B648** (2007) 139–148, arXiv:hep-ex/0604024.
- [4] BABAR Collaboration, B. Aubert *et al.*, “Measurement of the $B^0 \rightarrow \pi^- \ell^+ \nu$ form-factor shape and branching fraction, and determination of $|V_{ub}|$ with a loose neutrino reconstruction technique,” *Phys. Rev. Lett.* **98** (2007) 091801, arXiv:hep-ex/0612020.
- [5] G. Duplancic, A. Khodjamirian, T. Mannel, B. Melic, and N. Offen, “Light-cone sum rules for $B \rightarrow \pi$ form factors revisited,” *JHEP* **04** (2008) 014, arXiv:0801.1796 [hep-ph].
- [6] E. Gamiz, “Heavy flavour phenomenology from lattice QCD,” *PoS LATTICE2008* (2008) 014, arXiv:0811.4146 [hep-lat].
- [7] J. Gasser and H. Leutwyler, “Chiral Perturbation Theory to One Loop,” *Ann. Phys.* **158** (1984) 142.
- [8] J. Gasser and H. Leutwyler, “Chiral Perturbation Theory: Expansions in the Mass of the Strange Quark,” *Nucl. Phys.* **B250** (1985) 465.
- [9] M. B. Wise, “Chiral perturbation theory for hadrons containing a heavy quark,” *Phys. Rev.* **D45** (1992) 2188–2191.
- [10] G. Burdman and J. F. Donoghue, “Union of chiral and heavy quark symmetries,” *Phys. Lett.* **B280** (1992) 287–291.
- [11] A. F. Falk and B. Grinstein, “ $\bar{B} \rightarrow \bar{K} e^+ e^-$ in chiral perturbation theory,” *Nucl. Phys.* **B416** (1994) 771–785, arXiv:hep-ph/9306310.
- [12] D. Becirevic, S. Prelovsek, and J. Zupan, “ $B \rightarrow \pi$ and $B \rightarrow K$ transitions in partially quenched chiral perturbation theory,” *Phys. Rev.* **D68** (2003) 074003, arXiv:hep-lat/0305001.

- [13] **RBC** Collaboration, J. M. Flynn and C. T. Sachrajda, “ $SU(2)$ chiral perturbation theory for $K_{\ell 3}$ decay amplitudes,” *Nucl. Phys.* **B812** (2009) 64–80, arXiv:0809.1229 [hep-ph].
- [14] J. Bijnens and A. Celis, “ $K \rightarrow \pi\pi$ Decays in $SU(2)$ Chiral Perturbation Theory,” *Phys. Lett.* **B680** (2009) 466–470, arXiv:0906.0302 [hep-ph].
- [15] J. Bijnens and I. Jemos, “Vector Formfactors in Hard Pion Chiral Perturbation Theory,” *Nucl.Phys.* **B846** (2011) 145–166, arXiv:1011.6531 [hep-ph].
- [16] M. B. Wise, “Combining chiral and heavy quark symmetry,” arXiv:hep-ph/9306277.
- [17] A. V. Manohar and M. B. Wise, “Heavy quark physics,” *Camb. Monogr. Part. Phys. Nucl. Phys. Cosmol.* **10** (2000) 1–191.
- [18] J. Bijnens, G. Colangelo, and G. Ecker, “The mesonic chiral Lagrangian of order p^6 ,” *JHEP* **02** (1999) 020, arXiv:hep-ph/9902437.
- [19] J. L. Goity, “Chiral perturbation theory for $SU(3)$ breaking in heavy meson systems,” *Phys. Rev.* **D46** (1992) 3929–3936, arXiv:hep-ph/9206230.
- [20] S. Fleming, “Soft Collinear Effective Theory: An Overview,” *PoS EFT09* (2009) 002, arXiv:0907.3897 [hep-ph].
- [21] J. A. M. Vermaseren, “New features of FORM,” arXiv:math-ph/0010025.
- [22] J. Bijnens and P. Talavera, “Pion and kaon electromagnetic form factors,” *JHEP* **03** (2002) 046, arXiv:hep-ph/0203049.
- [23] G. Passarino and M. J. G. Veltman, “One Loop Corrections for e^+e^- Annihilation Into $\mu^+\mu^-$ in the Weinberg Model,” *Nucl. Phys.* **B160** (1979) 151.
- [24] G. ’t Hooft and M. J. G. Veltman, “Scalar One Loop Integrals,” *Nucl. Phys.* **B153** (1979) 365–401.

IV

Vector formfactors in hard pion Chiral Perturbation Theory

Johan Bijnens and Ilaria Jemos

Department of Astronomy and Theoretical Physics, Lund University,
Sölvegatan 14A, SE 223-62 Lund, Sweden

Nuclear Physics **B846** (2011) 145 [arXiv:1011.6531 [hep-ph]].

We use three-flavour hard pion Chiral Perturbation Theory (HPChPT) in both the heavy meson and a relativistic formulation to calculate the chiral logarithms $m^2 \log(m^2/\mu^2)$ contributing to the formfactors of the $B_{(s)} \rightarrow \pi, K, \eta$ and $D_{(s)} \rightarrow \pi, K, \eta$ transitions at momentum transfer q^2 away from the endpoint $q_{\max}^2 = (m_B - m_M)^2$. We compare our results with CLEO $D \rightarrow \pi$ and $D \rightarrow K$ data. We also calculate the Isgur-Wise function of the $B_{(s)} \rightarrow D_{(s)}$ semileptonic decay away from the endpoint and the chiral logarithms for the pion and kaon electromagnetic formfactor.

In two-flavour HPChPT we calculate the chiral logarithms for the pion vector and the scalar formfactors at $s \gg m_\pi^2$. This allows us to test hard pion ChPT using the existing two-loop calculations for these quantities.

PACS: 12.39.Fe Chiral Lagrangians, 13.20.He Decays of bottom mesons, 13.20.Fc Decays of charmed mesons, 11.30.Rd Chiral symmetries

Keywords: B and D meson semileptonic decays, Chiral Perturbation Theory

Reprinted from *Nuclear Physics* **B 846**, Johan Bijnens, Ilaria Jemos, Vector formfactors in hard pion Chiral Perturbation Theory, 145-166, Copyright (2011), with permission from Elsevier.



IV.1 Introduction

As a result of the rapid progress in computer technology, simulations of full QCD on the lattice are becoming increasingly feasible and thus many results are now available. To improve their precision it is important to acquire control on all the sources of systematic errors involved. One of them is due to the fact that most simulations are done with meson masses larger than the physical ones. It is therefore essential to perform a chiral extrapolation of the lattice data points to achieve smaller meson masses.

In this respect Chiral Perturbation Theory (ChPT) [1–3], the effective field theory of QCD at low energy, plays a key role. This theory can predict the dependence on the light quark masses of the observables under study, via a systematic expansion in the masses and momenta of the light mesons using both the spontaneous and explicit breaking of chiral symmetry. Unfortunately ChPT is often limited by its range of validity. There exist several processes where it is applicable only in a small fraction of the allowed range of energy, while the extrapolations formulas are needed elsewhere. It is the case for example of the $K \rightarrow \pi$, $D \rightarrow \pi, K, \eta$ and $B \rightarrow \pi, K, \eta$ transition formfactors in e.g. semileptonic decays. These processes are very important for the determination of CKM matrix elements, obtained combining knowledge on the amplitudes from experiments [4–7] and the formfactors calculated on the lattice [8]. The matching between lattice and experimental data is done when the momentum transfer squared to the vector boson is small, i.e. when a hard external pion arises and thus the power counting scheme of ChPT breaks down. However it is possible to exploit the chiral symmetry of QCD even there and predict the dependence on the meson masses of the formfactors using the arguments of hard pion Chiral Perturbation Theory (HPChPT).

This was first studied in [9] where it was applied to the semileptonic decay $K \rightarrow \pi$ using two-flavour ChPT. They argued there that it is possible to calculate the corrections of the type $m_\pi^2 \log m_\pi^2/\mu^2$ even when the squared momentum transfer q^2 is very small, i.e. when the outgoing pion is hard. Their arguments are based on the fact that only the soft internal pions are responsible for the chiral logarithms. These ideas have then been generalized and applied to $K \rightarrow \pi\pi$ [10] and to $B \rightarrow \pi\ell\nu_\ell$ [11], always in the framework of two-flavour ChPT. In [10, 11] it was made clear that the underlying arguments correspond basically to separate the hard-structure of a Feynman diagram from the soft one and use this last one to calculate infrared singularities. The arguments are essentially the same as those used for photon infrared singularities.

In this paper we use two-flavour HPChPT for the vector and the scalar formfactors of the pion $F_V^\pi(s)$ and $F_S^\pi(s)$ at $s \gg m_\pi^2$. Our main interest in this calculation is that it allows a test of the arguments of HPChPT using the existing two-loop results in standard two-flavour ChPT [12]. For complete-

ness we also quote the three-flavour HPChPT results for the electromagnetic formfactor for pions and kaons.

The main new result of this work is the three-flavour HPChPT calculation of the transition formfactors in vector transitions of B and D to π , K and η and the Isgur-Wise function in B to D transitions. In the latter case, the calculations did exist and has been used but the validity of the formulas was not discussed. Our results improve the comparison between the measured $D \rightarrow \pi$ and $D \rightarrow K$ formfactors [4]. We also calculate the contributions at the endpoint for all these transitions where the results for the transitions to η are new.

The paper is organized as follows. In Sect. IV.2 we briefly review ChPT and heavy meson ChPT (HMChPT). We present the relativistic theory that has been used to have an extra check of the correctness of our results here as well. At the end of this section we also summarize the arguments why HPChPT works, although we refer the reader for further details to Sect. 5 of [11].

In Sect. IV.3 we present the results for pion and kaon formfactors and test HPChPT using the existing two-flavour two-loop calculations for the pion formfactors. In Sect. IV.4 we define the formfactors of the heavy to light transitions and present our results for them. We also show here the comparison with the experimental data from [4] on the $D \rightarrow \pi(K)$ transitions. The $B \rightarrow D$ transitions are defined and our results for them given in Sect. IV.5. In the appendix we provide some results for the needed expansions of the loop integrals.

IV.2 Chiral Perturbation Theory

IV.2.1 Standard Chiral Perturbation Theory

In this subsection we briefly describe the formalism of ChPT [1–3] for both two- and three-flavour ChPT. The notation in the following is the same as in [13]. The lowest order Lagrangian describing the strong interactions of the light mesons is

$$\mathcal{L}_{\pi\pi}^{(2)} = \frac{F^2}{4} (\langle u_\mu u^\mu \rangle + \langle \chi_+ \rangle), \quad (\text{IV.1})$$

with

$$\begin{aligned} u_\mu &= i\{u^\dagger(\partial_\mu - ir_\mu)u - u(\partial_\mu - il_\mu)u^\dagger\}, \\ \chi_\pm &= u^\dagger\chi u^\dagger \pm u\chi^\dagger u, \\ u &= \exp\left(\frac{i}{\sqrt{2}F}\phi\right), \\ \chi &= 2B(s + ip). \end{aligned}$$

u parametrizes the oscillations around the vacuum in $SU(n)_L \times SU(n)_R/SU(n)_V \sim SU(n)$ for $n = 2, 3$ the number of light flavours. ϕ

is thus a hermitian $n \times n$ matrix:

$$\begin{aligned} \phi &= \begin{pmatrix} \frac{1}{\sqrt{2}}\pi^0 + \frac{1}{\sqrt{6}}\eta & \pi^+ & K^+ \\ \pi^- & -\frac{1}{\sqrt{2}}\pi^0 + \frac{1}{\sqrt{6}}\eta & K^0 \\ K^- & \bar{K}^0 & -\frac{2}{\sqrt{6}}\eta \end{pmatrix}, \\ \phi &= \begin{pmatrix} \frac{1}{\sqrt{2}}\pi^0 & \pi^+ \\ \pi^- & -\frac{1}{\sqrt{2}}\pi^0 \end{pmatrix}. \end{aligned} \quad (\text{IV.2})$$

The fields s , p , $l_\mu = v_\mu - a_\mu$ and $r_\mu = v_\mu + a_\mu$ are the standard external scalar, pseudoscalar, left- and right-handed vector fields introduced by Gasser and Leutwyler [2,3]. We will use the symbol F throughout this paper but it should be kept in mind that F can be either the two-flavour constant called F in [2] or the three-flavour one called F_0 in [3].

The field u and u_μ transform under a chiral transformation $g_L \times g_R \in SU(n)_L \times SU(n)_R$ as

$$u \longrightarrow g_R u h^\dagger = h u g_L^\dagger, \quad u_\mu \longrightarrow h u_\mu h^\dagger. \quad (\text{IV.3})$$

In (IV.3) h depends on u , g_L and g_R and is the so called compensator field. The notation $\langle X \rangle$ stands for trace over up,down quark indices for $n = 2$ and up, down, strange for $n = 3$.

Starting from this Lagrangian we can then build an effective field theory by including loop diagrams and higher order Lagrangians. Introductions to ChPT can be found in [14,15].

IV.2.2 Heavy meson Chiral Perturbation Theory

In this subsection we briefly describe the formalism of HMChPT [16–18]. Longer introductions can be found in the lectures by Wise [19] and the book [20].

The combination of Heavy Quark Effective Theory and of ChPT provides us with a powerful formalism to study hadrons containing a heavy quark. This combination is called HMChPT. It makes use of both spontaneously broken $SU(n)_L \times SU(n)_R$ chiral symmetry on the light quarks, and spin-flavour symmetry on the heavy quarks. Thus HMChPT involves both a heavy and a light scale. The first one is the heavy meson mass and rules an expansion in powers of its inverse. The second is the light meson mass that lets us study chiral symmetry breaking effects in a chiral-loop fashion as in standard ChPT.

The sector of the Lagrangian involving only light-quarks has already been discussed above. We now present the heavy meson part of the HMChPT Lagrangian for the three-flavour case [16–18]. Hereafter we concentrate on the $B^{(*)}$ mesons, but the same equations hold for the $D^{(*)}$ mesons as well. In the

limit $m_b \rightarrow \infty$, the pseudoscalar, B , and the vector, B^* , mesons are degenerate. All results in this paper are in the leading order in the heavy quark expansion. Thus in the following we neglect the mass splitting $\Delta = m_{B^*} - m_B$. To implement the heavy quark symmetries it is convenient to assemble them into a single field

$$H_a(v) = \frac{1 + \not{v}}{2} [B_{a\mu}^*(v)\gamma^\mu - B_a(v)\gamma_5], \quad (\text{IV.4})$$

where v is the fixed four-velocity of the heavy meson, a is a flavour index corresponding to the light quark in the heavy meson. Therefore $B_1 = B^+$, $B_2 = B^0$, $B_3 = B_s$, while $D_1 = \bar{D}^0$, $D_2 = D^-$, $D_3 = \bar{D}_s$ and similarly for the vector mesons B_μ^* and D_μ^* . In (IV.4) the operator $(1 + \not{v})/2$ projects out the particle component of the heavy meson only. The conjugate field is defined as $\bar{H}_a(v) \equiv \gamma_0 H_a^\dagger(v) \gamma_0$. We assume the field $H_a(v)$ to transform under the chiral transformation $g_L \times g_R \in SU(n)_L \times SU(n)_R$ as

$$H_a(v) \longrightarrow h_{ab} H_b(v), \quad (\text{IV.5})$$

so we introduce the covariant derivative

$$D_{ab}^\mu H_b(v) = \delta_{ab} \partial^\mu H_b(v) + \Gamma_{ab}^\mu H_b(v), \quad (\text{IV.6})$$

where $\Gamma_{ab}^\mu = \frac{1}{2} [u^\dagger (\partial_\mu - i r_\mu) u + u (\partial_\mu - i l_\mu) u^\dagger]_{ab}$, and the indices a, b run over the light quark flavours. Finally, the Lagrangian for the heavy-light mesons in the static heavy quark limit reads

$$\mathcal{L}_{\text{heavy}} = -i \text{Tr} \bar{H}_a v \cdot D_{ab} H_b + g \text{Tr} \bar{H}_a u_{ab}^\mu H_b \gamma_\mu \gamma_5, \quad (\text{IV.7})$$

where g is the coupling of the heavy meson doublet to the Goldstone boson and the traces, Tr , are over spin indices, the γ -matrix indices. The Lagrangian (IV.7) satisfies chiral symmetry and heavy quark spin flavour symmetry. We neglect in the following the mass differences for the heavy mesons containing the same heavy quark.

IV.2.3 Relativistic theory

When the momentum transfer to the light degrees of freedom is not small as in HPChPT, very off-shell heavy mesons may appear in the loops. Different treatments of the off-shell behaviour modify the loop-functions. Thus in principle it might change the non-analyticities in the light meson masses. If this were the case, the arguments summarized in Sect. IV.2.4 would be wrong. In fact, provided that the two formalisms are both sufficiently complete, the soft singularities must be the same, since they are arising in the same way. This is

the reason why both here and in [11] we are calculating not only using HM-ChPT but also in a relativistic formulation as a check on the arguments.

We use a relativistic Lagrangian that respects the spin-flavour symmetries of HMChPT. It is essentially the same Lagrangian introduced in [11], but now in the three-flavour case. The B_a and $B_{a\mu}^*$ fields are in the relativistic form and we treat them as column-vectors in the light-flavour index a .

$$\mathcal{L}_{\text{kin}} = \nabla^\mu B^\dagger \nabla_\mu B - m_B^2 B^\dagger B - \frac{1}{2} B_{\mu\nu}^{*\dagger} B^{*\mu\nu} + m_B^2 B_\mu^{*\dagger} B^{*\mu}, \quad (\text{IV.8})$$

$$\begin{aligned} \mathcal{L}_{\text{int}} &= gM_0 \left(B^\dagger u^\mu B_\mu^* + B_\mu^{*\dagger} u^\mu B \right) \\ &+ \frac{g}{2} \epsilon^{\mu\nu\alpha\beta} \left(-B_\mu^{*\dagger} u_\alpha \nabla_\nu B_\beta^* + \nabla_\mu B_\nu^{*\dagger} u_\alpha B_\beta^* \right), \end{aligned} \quad (\text{IV.9})$$

with $B_{\mu\nu}^* = \nabla_\mu B_\nu^* - \nabla_\nu B_\mu^*$, and $\nabla_\mu = \partial_\mu + \Gamma_\mu$. The constant g of (IV.9) is the same in (IV.7), M_0 is the mass of the B meson in the chiral limit. The fields B and B^* transform under chiral transformations as $B \rightarrow hB$. The two terms of \mathcal{L}_{int} in (IV.9) contain the vertices BB^*M and B^*B^*M for $M = \pi, K, \eta$.

From \mathcal{L}_{kin} in (IV.8) we find the propagators of the B and B^* meson respectively:

$$\frac{i}{p^2 - m_B^2}, \quad \frac{-i \left(g_{\mu\nu} - \frac{p_\mu p_\nu}{m_B^2} \right)}{p^2 - m_B^2}. \quad (\text{IV.10})$$

This is to be contrasted with the propagator $1/v \cdot p$ in the HMChPT showing the different off-shell behavior.

IV.2.4 Hard pion Chiral Perturbation Theory

In general, the use of ChPT and HMChPT is valid as long as the interacting light mesons are soft, i.e. if they have momenta much smaller than the scale of spontaneous chiral symmetry breaking ($\Lambda_{\text{ChSB}} \simeq 1 \text{ GeV}$). Only in this regime is the power counting of ChPT well defined.

On the other hand the arguments presented in great detail in Sect. 5 of [11] show that the predictions of the soft singularities in the light meson masses appearing in the final amplitudes are reliable even outside the range of applicability of HMChPT. Hereafter we present a short summary of these arguments, but for a comprehensive discussion we refer the reader to Sect. 5 of [11].

The underlying idea is that in a loop diagram, the internal soft light mesons are the source of the infrared non-analyticities arising, even if hard, i.e. large momentum, light mesons are present. Since the soft lines do not see the hard or short-distance structure of the diagram, we can separate them from the rest of the process. We should thus be able to describe the hard part of any diagram by an effective Lagrangian which must include the most general terms

consistent with all the symmetries. The coefficients of this Lagrangian depend on the hard kinematical quantities and can even be complex. This Lagrangian must be sufficiently complete to describe the neighbourhood of the underlying hard process.

Extra caution must be taken to build up the Lagrangian describing the hard part. As a matter of fact we can not neglect operators with an arbitrary numbers of derivatives since the momenta into play can be large. However it turns out that matrix elements of operators with higher number of derivatives are all proportional to the lowest order ones up to terms of higher order, i.e. the coefficients of the leading non-analyticities are calculable in terms of the lowest order Lagrangians.

We expect that a full power counting can be formulated along the lines of SCET [21] but the leading prediction can be obtained in the simpler fashion done here.

IV.3 Pion and kaon formfactors

IV.3.1 Electromagnetic formfactors in three-flavour HPChPT

The vector (electromagnetic) formfactors of the charged pion and kaon are defined as

$$\langle \pi(K)^+(p_2) | j_\mu^{\text{elm}} | \pi(K)^+(p_1) \rangle = (p_2 + p_1)_\mu F_V^{\pi(K)}(s), \quad (\text{IV.11})$$

with $s = (p_1 - p_2)^2$ and $j_\mu^{\text{elm}} = \frac{2}{3}\bar{u}\gamma_\mu u - \frac{1}{3}\bar{d}\gamma_\mu d - \frac{1}{3}\bar{s}\gamma_\mu s$ is the electromagnetic current. The arguments of HPChPT can be used here as well and we get from the relevant one-loop diagrams and wave function renormalization that

$$\begin{aligned} F_V^\pi(s) &= F_V^{\pi\chi}(s) \left(1 + \frac{1}{F^2} \bar{A}(m_\pi^2) + \frac{1}{2F^2} \bar{A}(m_K^2) + \mathcal{O}(m_L^2) \right), \\ F_V^K(s) &= F_V^{K\chi}(s) \left(1 + \frac{1}{2F^2} \bar{A}(m_\pi^2) + \frac{1}{F^2} \bar{A}(m_K^2) + \mathcal{O}(m_L^2) \right). \end{aligned} \quad (\text{IV.12})$$

The superscript χ here means in the limit $m_u = m_d = m_s = 0$. In the remainder we will usually drop the $\mathcal{O}(m_L^2)$ part but all results should be interpreted as up to analytic terms in the light meson masses squared. The loop integral $\bar{A}(m^2)$ is defined in the appendix. The result (IV.12) can be calculated directly or by expanding the known ChPT result [22, 23] for $s \gg m_L^2$.

IV.3.2 Vector and scalar pion formfactors in two-flavour HPChPT

It is important to test the arguments behind HPChPT as much as possible. We can do a nontrivial test by looking at the two-flavour case for the pion vector and scalar formfactors. The vector form factor is defined in (IV.11) and the scalar formfactor is defined by

$$\langle \pi^0(p_2) | \bar{u}u + \bar{d}d | \pi^0(p_1) \rangle = f_S^\pi(0) F_S^\pi(s). \quad (\text{IV.13})$$

We have factored out here as is customary [2, 12, 22] the value at $s = 0$. From the general discussion we again expect that the leading non-analytic correction should be in both cases of the form

$$f(s) = C(s) \times \left(1 + \alpha \frac{m^2}{F^2} \log \frac{m^2}{\mu^2} + \mathcal{O}(m^2) \right). \quad (\text{IV.14})$$

In principle α could depend on s but it is calculable. $C(s)$ is a free parameter in HPChPT and can even be complex.

Calculating the formfactors from wave-function renormalization and the needed one-loop diagrams we obtain

$$\begin{aligned} F_V^\pi(s) &= F_V^{\pi\chi}(s) \left(1 + \frac{1}{F^2} \bar{A}(m_\pi^2) \right), \\ F_S^\pi(s) &= F_S^{\pi\chi}(s) \left(1 + \frac{5}{2F^2} \bar{A}(m_\pi^2) \right). \end{aligned} \quad (\text{IV.15})$$

Here χ means in the limit $m_u = m_d = 0$. This agrees with the large s expansion of the one-loop result of [2].

In normal ChPT these formfactors are known fully analytically up till two-loop order [12]. We can now choose a value of m_π^2 and s such that $s \gg m_\pi^2$ but with both s and m_π^2 in the regime of validity of standard HPChPT. The expansion for $s \gg m_\pi^2$ can be done and the result should be of the form (IV.15) where the form of $F_V^{\pi\chi}(s)$, $F_S^{\pi\chi}(s)$ follows from the one-loop calculation in the limit $m_\pi^2 = 0$. This gives

$$\begin{aligned} F_V^{\pi\chi}(s) &= 1 + \frac{s}{16\pi^2 F^2} \left(\frac{5}{18} - 16\pi^2 l_6^r + \frac{i\pi}{6} - \frac{1}{6} \ln \frac{s}{\mu^2} \right), \\ F_S^{\pi\chi}(s) &= 1 + \frac{s}{16\pi^2 F^2} \left(1 + 16\pi^2 l_4^r + i\pi - \ln \frac{s}{\mu^2} \right). \end{aligned} \quad (\text{IV.16})$$

Let us see what happens when the full two-loop results are taken into account. Our arguments still hold as long as we are working at the desired

order i.e. $\mathcal{O}(m_\pi^2)$. On the other hand now different kind of terms arise. Some of them are suppressed by m_π^4 with or without logarithms and so can be neglected. The ones like s^2 or $s^2 \log s^2 / \mu^2$ and without $\log(m_\pi^2 / \mu^2)$ cannot be predicted by HPChPT and are absorbed in the unknown part of the coefficient $C(s)$ of (IV.14). Terms like $s^2 \log^2 m_\pi^2 / \mu^2$ or $s^2 \log m_\pi^2 / \mu^2$ can also arise. Those not only would be large in our limit, but even divergent when $m_\pi \rightarrow 0$, therefore they must cancel. Terms like $sm_\pi^2 \log^2 m_\pi^2 / \mu^2$ are predicted by HPChPT not to occur. Finally there are terms as $sm_\pi^2 \log(m_\pi^2 / \mu^2)$ and $sm_\pi^2 \log(m_\pi^2 / \mu^2) \log(s / \mu^2)$ which are of special interest. The coefficients of these are predicted by HPChPT. They are given by (IV.16) and (IV.15). Performing the expansion of the full two-loop result for $s \gg m_\pi^2$ we indeed find that the result is of the required form with the chiral limit value given exactly by (IV.16). This is a rather nontrivial check on HPChPT.

IV.4 $B \rightarrow M$ and $D \rightarrow M$ transitions

IV.4.1 Definition of formfactors

In this section we review the formalism for the transitions of a B or a D meson into a light pseudoscalar meson (π, K, η). We restrict ourselves to the case of a B meson, but the same definitions hold also for the D -decay. All the following discussion can be found also in [11] for the two-flavour case. We report it here for the sake of completeness. The hadronic current for pseudoscalar to pseudoscalar vector transitions ($P_i(\bar{q}_i, q) \rightarrow P_f(\bar{q}_f, q)$) has the structure

$$\begin{aligned} \langle P_f(p_f) | \bar{q}_i \gamma_\mu q_f | P_i(p_i) \rangle &= (p_i + p_f)_\mu f_+(q^2) + (p_i - p_f)_\mu f_-(q^2) \\ &= \left[(p_i + p_f)_\mu - q_\mu \frac{(m_i^2 - m_f^2)}{q^2} \right] f_+(q^2) + q_\mu \frac{(m_i^2 - m_f^2)}{q^2} f_0(q^2), \end{aligned} \quad (\text{IV.17})$$

where q^μ is the momentum transfer $q^\mu = p_i^\mu - p_f^\mu$. In our case P_f is a light pseudoscalar meson, P_i is a B meson and $q_i = b$. For example, to find the $B^0 \rightarrow \pi^+$ formfactors we need then to evaluate the hadron matrix elements of the quark bilinear $\bar{b} \gamma_\mu q$, where $q = u$.

Parity invariance, heavy quark and chiral symmetry dictate that the matching of QCD bilinears onto operators of HMChPT take the form [19, 24],

$$\bar{b} \gamma^\mu q_a \propto c \left\{ \text{Tr} \gamma^\mu \left(u_{ab}^\dagger + u_{ab} \right) H_b(v) + \text{Tr} \gamma_5 \gamma^\mu \left(u_{ab}^\dagger - u_{ab} \right) H_b(v) \right\}. \quad (\text{IV.18})$$

If no hard pions appear in the final state we can use the definition of the decay

constant

$$\langle 0 | \bar{b} \gamma_\mu \gamma_5 q | B(p_B) \rangle = i F_B p_B^\mu \quad (\text{IV.19})$$

and obtain $c = \frac{1}{2} F_B \sqrt{m_B}$. This latter result does not hold for momenta away from q_{\max}^2 in which case c is just an effective coupling depending on q^2 .

In HMChPT the definitions of the formfactors are chosen such that those are independent of the heavy meson mass. So for example for the $B \rightarrow M$ transition

$$\begin{aligned} \langle M(p_M) | \bar{b} \gamma_\mu q | B(v) \rangle_{\text{HMChPT}} &= [p_{M\mu} - (v \cdot p_M) v_\mu] f_p(v \cdot p_M) \\ &+ v_\mu f_v(v \cdot p_M). \end{aligned} \quad (\text{IV.20})$$

In (IV.20) $v \cdot p_M$ is the energy of the light meson in the heavy meson rest frame

$$v \cdot p_M = \frac{m_B^2 + m_M^2 - q^2}{2m_B}. \quad (\text{IV.21})$$

The formfactors defined in (IV.17) and in (IV.20) are related by matching the relativistic and the HMChPT hadronic current:

$$\begin{aligned} \sqrt{m_B} f_p(v \cdot p_M) &= f_+(q^2) + \frac{m_B^2 - m_M^2}{q^2} f_+(q^2) - \frac{m_B^2 - m_M^2}{q^2} f_0(q^2) \\ &= f_+(q^2) - f_-(q^2), \end{aligned} \quad (\text{IV.22})$$

$$\begin{aligned} \sqrt{m_B} (f_v(v \cdot p_M) - f_p(v \cdot p_M) v \cdot p_M) &= m_B \left(\frac{q^2 - m_B^2 + m_M^2}{q^2} f_+(q^2) \right. \\ &\quad \left. + \frac{m_B^2 - m_M^2}{q^2} f_0(q^2) \right) \\ &= m_B (f_+(q^2) + f_-(q^2)). \end{aligned} \quad (\text{IV.23})$$

The $\sqrt{m_B}$ factors in (IV.22) and (IV.23) are due to the different normalizations of states used in the two formalisms. At $q^2 \approx q_{\max}^2$, neglecting terms suppressed by powers of m_M and of $1/m_B$, (IV.22) and (IV.23) become

$$f_0(q^2) = \frac{1}{\sqrt{m_B}} f_v(v \cdot p_M), \quad f_+(q^2) = \frac{\sqrt{m_B}}{2} f_p(v \cdot p_M). \quad (\text{IV.24})$$

We remark that the relations in (IV.24) are valid only when $q^2 \approx q_{\max}^2$ contrary to what was said in the original version¹ of [11]. At general q^2 away from q_{\max}^2 we must use (IV.22) and (IV.23).

¹Notice that this does not invalidate the results of [11]. Indeed all the formfactors involved have the same chiral logarithms, thus the tree-level part can still be factorized out, as shown in Sect. IV.4.2

A matching similar to (IV.18) has to be done also for the relativistic theory described in Sect. IV.2.3. We identify four possible operators²

$$J_\mu^L = \frac{1}{2}E_1 t u^\dagger \nabla_\mu B + \frac{i}{2}E_2 t u^\dagger u_\mu B + \frac{i}{2}E_3 t u^\dagger B_\mu^* + \frac{1}{2}E_4 t u^\dagger (\nabla_\nu u_\mu) B^{*\nu}, \quad (\text{IV.25})$$

where E_1, \dots, E_4 , are effective couplings. t is a constant spurion vector transforming as $t \rightarrow t g_L^\dagger$, so that J_μ^L is invariant under $SU(3)_L$ transformations. The heavy quark symmetry implies $m_B E_1 = E_3$. Analogously we can introduce a right-handed J_μ^R current and thus an axial-vector $J_\mu^5 = J_\mu^R - J_\mu^L$ and a vector $J_\mu^V = J_\mu^R + J_\mu^L$ current. They are used respectively to evaluate the amplitudes of $B \rightarrow \ell \nu_\ell$ and the $B \rightarrow M$ formfactors as defined in (IV.17). We leave the discussion for the latter in Sects. IV.4.2 and IV.4.4, while we quote here the expression of the $B(B_s)$ decay constants that can be found evaluating the $B(B_s) \rightarrow$ vacuum matrix element at one loop:

$$F_B = E_1 \left\{ 1 + \frac{1}{F^2} \left[\left(\frac{3}{8} + \frac{9}{8}g^2 \right) \bar{A}(m_\pi^2) + \left(\frac{1}{4} + \frac{3}{4}g^2 \right) \bar{A}(m_K^2) + \left(\frac{1}{24} + \frac{1}{8}g^2 \right) \bar{A}(m_\eta^2) \right] \right\}, \quad (\text{IV.26})$$

$$F_{B_s} = E_1 \left\{ 1 + \frac{1}{F^2} \left[\left(\frac{1}{2} + \frac{3}{2}g^2 \right) \bar{A}(m_K^2) + \left(\frac{1}{6} + \frac{1}{2}g^2 \right) \bar{A}(m_\eta^2) \right] \right\}. \quad (\text{IV.27})$$

$\bar{A}(m^2)$ is defined in (IV.58) in the appendix. Here we only quote the non-analytic dependence on the light quark masses for the one-loop part. The results (IV.26) and (IV.27) agree with those obtained with HMChPT [18]. We see that E_1 plays the role of F_H in [18] and that the relativistic theory predicts the same coefficient of the chiral logarithm in $\bar{A}(m^2)$ as expected.

IV.4.2 The chiral logarithms away from the endpoint

In this section we present results for the formfactors of the vector transitions $B \rightarrow \pi$, $B \rightarrow K$, $B \rightarrow \eta$, $B_s \rightarrow K$ and $B_s \rightarrow \eta$ calculated using three-flavour HPChPT. The results for the $B \rightarrow \pi$ transition in two-flavour ChPT can be found in [11]. We quote only the relevant terms, i.e. the leading ones which contain free parameters and the predicted chiral logarithms up to $\mathcal{O}(m_M^2)$. The tree-level diagrams contributing to the amplitude are shown in Fig. IV.1. The

²The last one is higher order but we included it since it has a different type of contraction of the Lorentz indices and as an explicit check on the arguments of HPChPT [11].

(1)



(2)



Figure IV.1: The tree-level diagrams contributing to the amplitude. A double line corresponds to a B , a zigzag line to a B^* , a single line to a light meson, i.e. π , K or η . A black circle represents the insertion of a vector current.

formfactors at tree level read for HMChPT

$$f_p^{\text{Tree}}(v \cdot p_M) = C_{B \rightarrow M} \frac{\alpha}{F} \frac{g}{v \cdot p_M + \Delta}, \quad f_v^{\text{Tree}}(v \cdot p_M) = C_{B \rightarrow M} \frac{\alpha}{F}, \quad (\text{IV.28})$$

where $C_{B \rightarrow M}$ is a constant that changes depending on the meson transition and takes the values

$$C_{B \rightarrow M} = \begin{cases} 1 & B^- \rightarrow \pi^0 \\ \sqrt{2} & \bar{B}^0 \rightarrow \pi^+ \\ \sqrt{2} & B \rightarrow K \\ \frac{1}{\sqrt{3}} & B \rightarrow \eta \\ \sqrt{2} & B_s \rightarrow K \\ -\frac{2}{\sqrt{3}} & B_s \rightarrow \eta. \end{cases}$$

In (IV.28) α is a constant that takes the value $\sqrt{m_B/2}F_B$ at q_{max}^2 . We also obtain $c = \alpha/\sqrt{2}$. Near $q_{\text{max}}^2 = (m_B - m_M)^2$ the results remain obviously the same, but the propagator in the first equation of (IV.28) becomes $1/m_M$. In the case of the relativistic theory of Sect. IV.2.3, we distinguish the formfactors for the two q^2 ranges. At q^2 away from q_{max}^2

$$\begin{aligned} f_+^{\text{Tree}}(q^2) &= C_{B \rightarrow M} \left\{ -\frac{1}{4} \frac{E_3}{F} \frac{m_B}{q^2 - m_B^2} g + \frac{1}{8} \frac{E_1}{F} - \frac{1}{4} \frac{E_2}{F} \right\}, \\ f_0^{\text{Tree}}(q^2) &= C_{B \rightarrow M} \left\{ \frac{1}{8} \frac{E_1}{F} \left(1 + \frac{q^2}{m_B^2 - m_M^2} \right) \right. \\ &\quad \left. - \frac{1}{4} \left(\frac{E_2}{F} + \frac{E_3}{F} \frac{m_B}{q^2 - m_B^2} g \right) \left(1 - \frac{q^2}{m_B^2 - m_M^2} \right) \right\}. \end{aligned} \quad (\text{IV.29})$$

At $q^2 \approx q_{\max}^2$ (IV.29) simplifies to

$$f_+^{\text{Tree}}(q^2)_{q^2 \approx q_{\max}^2} = C_{B \rightarrow M} \frac{1}{4} \frac{E_3}{F} \frac{1}{2m_M} g, \quad f_0^{\text{Tree}}(q^2)_{q^2 \approx q_{\max}^2} = C_{B \rightarrow M} \frac{1}{4} \frac{E_1}{F}. \quad (\text{IV.30})$$

We stress once more that the relation of E_1 and E_3 to F_B holds only when $q^2 \approx q_{\max}^2$. As the momentum transfer is out of this range the coupling constants are different at the different values of q^2 and can even be complex.

At one-loop we need to include the contributions of the wavefunction renormalization Z_π, Z_K, Z_η, Z_B and Z_{B_s} . They are the same for HMChPT and the relativistic theory and read:

$$\begin{aligned} Z_\pi &= 1 - \frac{2}{3} \frac{\bar{A}(m_\pi^2)}{F^2} - \frac{1}{3} \frac{\bar{A}(m_K^2)}{F^2}, \\ Z_K &= 1 - \frac{1}{4} \frac{\bar{A}(m_\pi^2)}{F^2} - \frac{1}{2} \frac{\bar{A}(m_K^2)}{F^2} - \frac{1}{4} \frac{\bar{A}(m_\eta^2)}{F^2}, \\ Z_\eta &= 1 - \frac{\bar{A}(m_K^2)}{F^2}, \\ Z_B &= 1 + \frac{9}{4} g^2 \frac{\bar{A}(m_\pi^2)}{F^2} + \frac{3}{2} g^2 \frac{\bar{A}(m_K^2)}{F^2} + \frac{3}{12} g^2 \frac{\bar{A}(m_\eta^2)}{F^2}, \\ Z_{B_s} &= 1 + 3g^2 \frac{\bar{A}(m_K^2)}{F^2} + g^2 \frac{\bar{A}(m_\eta^2)}{F^2}. \end{aligned} \quad (\text{IV.31})$$

The one-loop corrections to the vector current J_μ^V are shown in Fig. IV.2.

To find the results in HMChPT we expanded the one-loop calculation of [25] at $v \cdot p_M \rightarrow m_B, m_M^2 \rightarrow 0$. Note however that their results are only valid near the endpoint. The arguments of HPCChPT allow us to use their results also away from the endpoint.

In the relativistic theory we first calculated the formfactors and then we expanded the loop integrals for $m_M^2 \ll m_B^2, (m_B^2 - q^2)$. These latter expansions are given in App. IV.1. Notice that we keep terms of the kind m/M in the expansion of the \bar{C} and \bar{B} functions (IV.65), (IV.66) that had not been included explicitly in [11]. Those terms could cause corrections like mM/F^2 in the final results, that would violate the heavy quark limit $M \rightarrow \infty$. We verified that all these corrections do cancel. To achieve the final results, we sum up all the contributions coming from the several diagrams and include the wavefunction renormalization pieces. This corresponds to sum $(1/2)Z_M$ for $M = \pi, K, \eta$ and $(1/2)Z_B$ or $(1/2)Z_{B_s}$, according to the external legs of the process under study, multiplied by the tree-level part of the formfactors. We find for the different transitions that the two formfactors always have the same chiral logarithms. We can write the results in the form

$$f_{v/p}(v \cdot p_M) = f_{v/p}^{\text{Tree}}(v \cdot p_M) F_{B \rightarrow M} \quad (\text{IV.32})$$

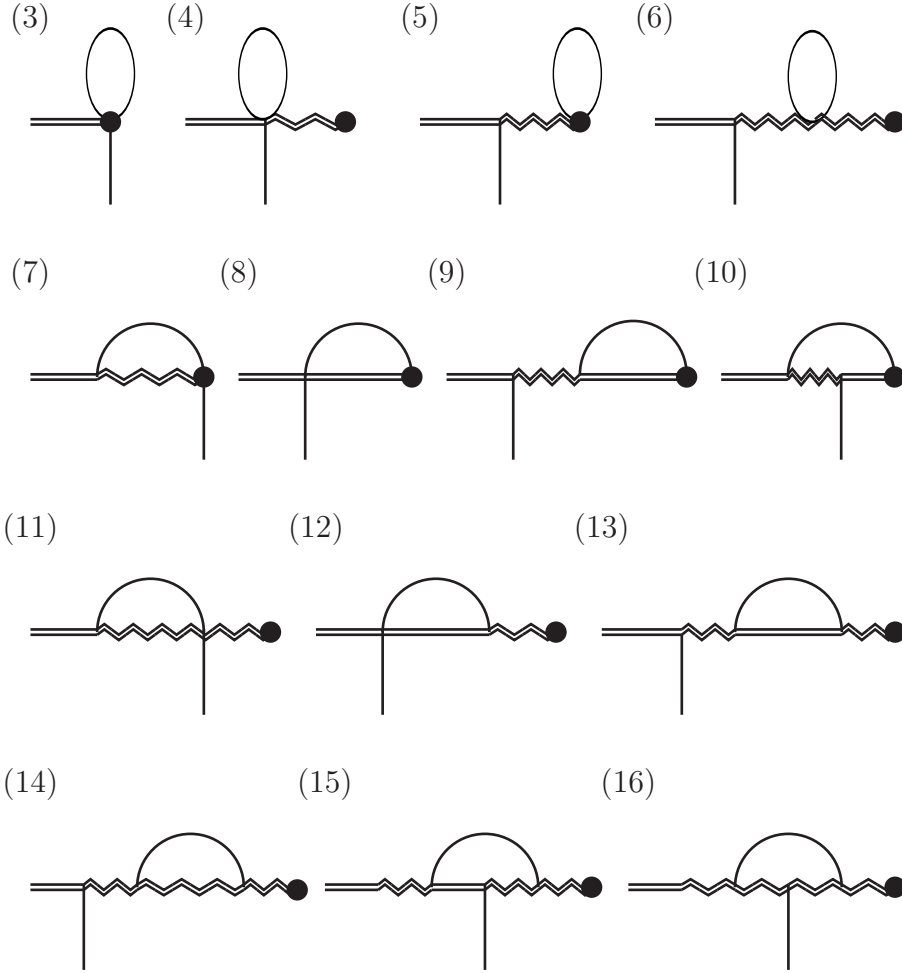


Figure IV.2: The one-loop diagrams contributing to the amplitude. Vertices and lines as in Fig. IV.1

The chiral logarithms are in $F_{B \rightarrow M}$ and read for the different transitions

$$F_{B \rightarrow \pi} = 1 + \left(\frac{3}{8} + \frac{9}{8}g^2 \right) \frac{\bar{A}(m_\pi^2)}{F^2} + \left(\frac{1}{4} + \frac{3}{4}g^2 \right) \frac{\bar{A}(m_K^2)}{F^2} + \left(\frac{1}{24} + \frac{1}{8}g^2 \right) \frac{\bar{A}(m_\eta^2)}{F^2}, \quad (\text{IV.33})$$

$$F_{B \rightarrow K} = 1 + \frac{9}{8}g^2 \frac{\bar{A}(m_\pi^2)}{F^2} + \left(\frac{1}{2} + \frac{3}{4}g^2\right) \frac{\bar{A}(m_K^2)}{F^2} + \left(\frac{1}{6} + \frac{1}{8}g^2\right) \frac{\bar{A}(m_\eta^2)}{F^2}, \quad (\text{IV.34})$$

$$F_{B \rightarrow \eta} = 1 + \left(\frac{3}{8} + \frac{9}{8}g^2\right) \frac{\bar{A}(m_\pi^2)}{F^2} + \left(\frac{1}{4} + \frac{3}{4}g^2\right) \frac{\bar{A}(m_K^2)}{F^2} + \left(\frac{1}{24} + \frac{1}{8}g^2\right) \frac{\bar{A}(m_\eta^2)}{F^2}, \quad (\text{IV.35})$$

$$F_{B_s \rightarrow K} = 1 + \frac{3}{8} \frac{\bar{A}(m_\pi^2)}{F^2} + \left(\frac{1}{4} + \frac{3}{2}g^2\right) \frac{\bar{A}(m_K^2)}{F^2} + \left(\frac{1}{24} + \frac{1}{2}g^2\right) \frac{\bar{A}(m_\eta^2)}{F^2}, \quad (\text{IV.36})$$

$$F_{B_s \rightarrow \eta} = 1 + \left(\frac{1}{2} + \frac{3}{2}g^2\right) \frac{\bar{A}(m_K^2)}{F^2} + \left(\frac{1}{6} + \frac{1}{2}g^2\right) \frac{\bar{A}(m_\eta^2)}{F^2}. \quad (\text{IV.37})$$

$F_{B_s \rightarrow \pi}$ vanishes due to the possible flavour quantum numbers.

In all the transitions we obtain, as predicted by our arguments, the same coefficients for the relativistic theory. I.e.

$$f_{+/0}(q^2) = f_{+/0}^{\text{Tree}}(q^2) F_{B \rightarrow M}. \quad (\text{IV.38})$$

The correction is also the same for the formfactors f_0 and f_+ or for f_v and f_p in all the cases. Notice that (IV.33) is also in agreement with the results in two-flavour HPChPT of [11]

The chiral logarithms for both form factors are always the same in these decays as can be seen in (IV.38) and (IV.32). This was also already the case for the $K_{\ell 3}$ formfactors in HPChPT [9] and we noticed it as well in [11]. It cannot simply be something like heavy quark symmetry since it is not valid at the endpoint, see below and [24,25]. This would also not be a valid reason for the $K_{\ell 3}$ case. An alternative explanation would be if something similar to Low's theorem for electromagnetic soft corrections holds. Low's theorem states that the amplitude for the process with Bremsstrahlung is proportional to the amplitude without Bremsstrahlung by a factor depending only on the external legs. A corresponding result holds for the infrared logarithms in virtual photon diagrams. But, if here there was only dependence on the external legs, we obtain the relation

$$F_{B \rightarrow K} - F_{B \rightarrow \eta} - F_{B_s \rightarrow K} + F_{B_s \rightarrow \eta} = 0. \quad (\text{IV.39})$$

Inspection of the results in (IV.37) show that this is not satisfied. The same argument would have predicted that the chiral logarithms in $F_V^\pi(s)$ and $F_S^\pi(s)$ of (IV.15) are the same which is again clearly not the case.

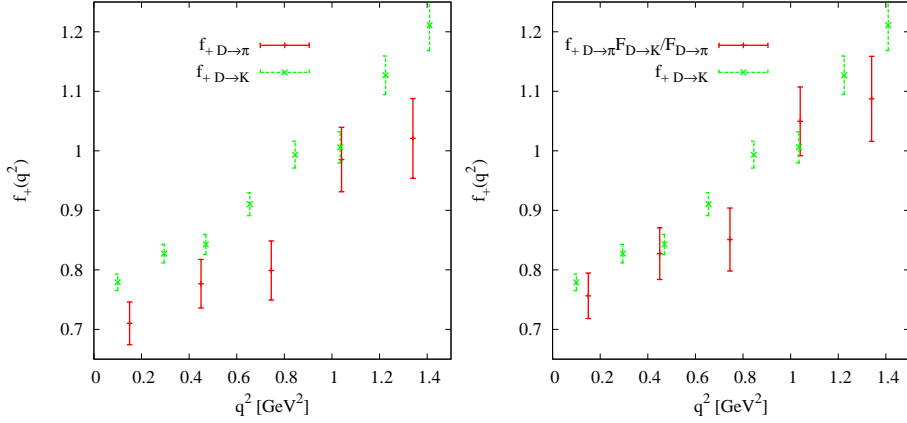


Figure IV.3: The measurements of CLEO [4] for the formfactor $f_+(q^2)$ for the $D \rightarrow \pi$ and the $D \rightarrow K$ semileptonic decays. In the two plots we have divided by the values of the CKM matrix elements $|V_{cd}| = 0.2253$ and $|V_{cs}| = 0.9743$ respectively. On the left we plot only the formfactors without corrections, while on the right we plot each of the two members of (IV.40).

IV.4.3 Comparison with experiment

We did not find any lattice data published in a form that allows us to test the chiral logarithms in (IV.37). However, there are published data on the formfactors in $D \rightarrow \pi$ and $D \rightarrow K$ semileptonic decays. The most precise data come from CLEO. In [4] are reported the data points of $f_+(q^2)|V_{cd}|$ for $D^{+(0)} \rightarrow \pi^{0(+)}$ decays and of $f_+(q^2)|V_{cs}|$ for $D^{0(+)} \rightarrow K^{+(0)}$ decays. We can then use the known value for the Cabibbo angle to get at the form factors. We used the PDG value for $\sin \theta_C = 0.2253$ [26] to obtain $|V_{cd}| = \sin \theta_C = 0.2253$ and $|V_{cs}| = \cos \theta_C = 0.9743$. In Fig. IV.3 on the left-hand-side we plot the CLEO data for both $D \rightarrow \pi$ and $D \rightarrow K$ decays. We included only the $D^0 \rightarrow \pi^+(K^+)$ data. A similar study can be done using the $D^+ \rightarrow \pi^0(K^0)$ since they give basically the same data points as isospin symmetry dictates.

The following relation should approximately hold using (IV.38) and the fact that the lowest order result is the same.

$$f_{+D \rightarrow K}(q^2) = f_{+D \rightarrow \pi}(q^2) \frac{F_{D \rightarrow K}}{F_{D \rightarrow \pi}}, \quad (\text{IV.40})$$

where $F_{D \rightarrow \pi(K)}$ are the logarithmic corrections due to loop diagrams quoted in (IV.37). The corrections to relation (IV.40) are mainly due to higher order terms i.e. $\mathcal{O}(m_M^2)$ without logarithms. We expect these corrections to be about 10%. The value of g^2 , which enters through the $F_{D \rightarrow \pi(K)}$ of (IV.40) is set to

0.44 [27]. However it does not affect the plots since the coefficients of the chiral logarithms proportional to g^2 are the same for the two decays. The scale of renormalization μ is set to $\Lambda_{\text{ChPT}} \approx 1$ GeV. In the right plot of Fig. IV.3 the $f_{D \rightarrow K}^+$ formfactor almost overlaps the $f_{D \rightarrow \pi}^+$ one once the logarithmic corrections are taken into account as (IV.40) indicates. By comparing the left with the right plots in Fig. IV.3 it is clear that our chiral logarithms compensate for the differences. Notice also that the $F_{D \rightarrow \pi(K)}$ contributes to a good 30% of the total formfactor but the total correction in the ratio is much smaller. The terms which depend on g^2 also cancel out in the ratio. (IV.40) holds in principle both for $q^2 \ll q_{\text{max}}^2$ and at the endpoint $q^2 \approx q_{\text{max}}^2$. It should be kept in mind that the endpoint has quite different logarithms which are given below. The q_{max}^2 are rather different in the two decays, being $q_{\text{max}}^2 \approx (1.86 - 0.49)^2 = 1.88$ GeV² for the K channel while $q_{\text{max}}^2 \approx (1.86 - 0.14)^2 = 2.9$ GeV² for the π channel. Therefore making a similar comparison at large q^2 is in practice not possible. This is the reason why in Fig. IV.3 we stopped at $q^2 \approx 1.5$ GeV², the rightmost point is already rather close to the endpoint for $D \rightarrow K$.

IV.4.4 Chiral logarithms at the endpoint

At the endpoint HPChPT is not valid but standard HMChPT is. The $B \rightarrow K$ formfactors were calculated in [24] and the $B \rightarrow \pi, K$ in [25]. The latter paper also discussed them in the partially quenched case. We do not show diagram by diagram results, these can be partly found in [24, 25]. Here we only quote the final results but we also calculate the results for the $B \rightarrow \eta$ transitions.

Again the results in this limit must give the same outcome for the two theories, since one is the relativistic limit of the other. So this is another check of the validity of our relativistic theory. Notice that we are performing a three-flavour calculation and thus there are three light masses entering into the loop-functions, i.e. m_π, m_K and m_η . This complicates the structures of the functions involved and therefore of the non-analyticities arising. For this reason a few more loop functions are also needed in the relativistic formalism compared to the two-flavour case [11]. They have been reported in the appendix. We present the results at $q^2 = q_{\text{max}}^2$ for each transition using

$$f_p(q_{\text{max}}^2) = f_p^{\text{Tree}}(q_{\text{max}}^2) F_{B \rightarrow M}^p, \quad f_v(q_{\text{max}}^2) = f_v^{\text{Tree}}(q_{\text{max}}^2) F_{B \rightarrow M}^v. \quad (\text{IV.41})$$

The relativistic theory correctly reproduces all these results provided that the substitutions $f_v^{\text{Tree}}(v \cdot p) \rightarrow f_0^{\text{Tree}}(q^2)$ and $f_p^{\text{Tree}}(v \cdot p) \rightarrow f_+^{\text{Tree}}(q^2)$ are performed.

$$F_{B \rightarrow \pi}^p = 1 + \left(\frac{3}{8} + \frac{43}{24} g^2 \right) \frac{\bar{A}(m_\pi^2)}{F^2} + \left(\frac{1}{4} + \frac{9}{4} g^2 - \frac{m_\pi^2}{m_K^2} g^2 \right) \frac{\bar{A}(m_K^2)}{F^2}$$

$$\begin{aligned}
& + \left(\frac{1}{24} + \frac{11}{24}g^2 - \frac{2}{9} \frac{m_\pi^2}{m_\eta^2} g^2 \right) \frac{\bar{A}(m_\eta^2)}{F^2} \\
& + 2g^2 \frac{(m_\pi^2 - m_K^2)}{F^2} \mathcal{F} \left(\frac{m_\pi}{m_K} \right) + \frac{4}{9} g^2 \frac{(m_\pi^2 - m_\eta^2)}{F^2} \mathcal{F} \left(\frac{m_\pi}{m_\eta} \right) \\
F_{B \rightarrow \pi}^v & = 1 + \left(\frac{11}{8} + \frac{9}{8}g^2 \right) \frac{\bar{A}(m_\pi^2)}{F^2} + \left(-\frac{1}{4} + \frac{3}{4}g^2 + \frac{m_\pi^2}{m_K^2} \right) \frac{\bar{A}(m_K^2)}{F^2} \\
& + \left(\frac{1}{24} + \frac{1}{8}g^2 \right) \frac{\bar{A}(m_\eta^2)}{F^2} - 2 \frac{m_\pi^2}{F^2} \mathcal{F} \left(\frac{m_\pi}{m_K} \right), \tag{IV.42}
\end{aligned}$$

$$\begin{aligned}
F_{B \rightarrow K}^p & = 1 + \frac{9}{8} g^2 \frac{\bar{A}(m_\pi^2)}{F^2} + \left(\frac{1}{2} + \frac{7}{4}g^2 \right) \frac{\bar{A}(m_K^2)}{F^2} \\
& + \left(\frac{1}{6} + \frac{23}{24}g^2 - \frac{5}{9} \frac{m_K^2}{m_\eta^2} g^2 \right) \frac{\bar{A}(m_\eta^2)}{F^2} + \frac{10}{9} g^2 \frac{(m_K^2 - m_\eta^2)}{F^2} \mathcal{F} \left(\frac{m_K}{m_\eta} \right), \\
F_{B \rightarrow K}^v & = 1 + \frac{9}{8} g^2 \frac{\bar{A}(m_\pi^2)}{F^2} + \left(\frac{3}{2} + \frac{3}{4}g^2 \right) \frac{\bar{A}(m_K^2)}{F^2} \\
& + \left(-\frac{1}{3} + \frac{1}{8}g^2 + \frac{m_K^2}{m_\eta^2} \right) \frac{\bar{A}(m_\eta^2)}{F^2} - 2 \frac{m_K^2}{F^2} \mathcal{F} \left(\frac{m_K}{m_\eta} \right), \tag{IV.43}
\end{aligned}$$

$$\begin{aligned}
F_{B \rightarrow \eta}^p & = 1 + \left(\frac{3}{8} + \frac{33}{8}g^2 - 2 \frac{m_\pi^2}{m_\eta^2} g^2 \right) \frac{\bar{A}(m_\pi^2)}{F^2} \\
& + \left(\frac{1}{4} + \frac{5}{4}g^2 - \frac{1}{3} \frac{m_\eta^2}{m_K^2} g^2 \right) \frac{\bar{A}(m_K^2)}{F^2} + \left(\frac{1}{24} + \frac{17}{72}g^2 \right) \frac{\bar{A}(m_\eta^2)}{F^2} \\
& + 4g^2 \frac{(m_\eta^2 - m_\pi^2)}{F^2} \mathcal{F} \left(\frac{m_\eta}{m_\pi} \right) + \frac{2}{3} g^2 \frac{(m_\eta^2 - m_K^2)}{F^2} \mathcal{F} \left(\frac{m_\eta}{m_K} \right), \\
F_{B \rightarrow \eta}^v & = 1 + \left(\frac{3}{8} + \frac{9}{8}g^2 \right) \frac{\bar{A}(m_\pi^2)}{F^2} + \left(-\frac{5}{4} + \frac{3}{4}g^2 + 3 \frac{m_\eta^2}{m_K^2} \right) \frac{\bar{A}(m_K^2)}{F^2} \\
& + \left(\frac{1}{24} + \frac{1}{8}g^2 \right) \frac{\bar{A}(m_\eta^2)}{F^2} - 6 \frac{m_\eta^2}{F^2} \mathcal{F} \left(\frac{m_\eta}{m_K} \right), \tag{IV.44}
\end{aligned}$$

$$\begin{aligned}
F_{B_s \rightarrow K}^p & = 1 + \left(\frac{3}{8} + \frac{9}{4}g^2 - \frac{3}{2} \frac{m_K^2}{m_\pi^2} g^2 \right) \frac{\bar{A}(m_\pi^2)}{F^2} \\
& + \left(\frac{1}{4} + 2g^2 \right) \frac{\bar{A}(m_K^2)}{F^2} + \left(\frac{1}{24} + \frac{7}{12}g^2 - \frac{1}{18} \frac{m_K^2}{m_\eta^2} g^2 \right) \frac{\bar{A}(m_\eta^2)}{F^2}
\end{aligned}$$

$$\begin{aligned}
& +3g^2 \frac{(m_K^2 - m_\pi^2)}{F^2} \mathcal{F}\left(\frac{m_K}{m_\pi}\right) + \frac{1}{9} \frac{(m_K^2 - m_\eta^2)}{F^2} \mathcal{F}\left(\frac{m_K}{m_\eta}\right), \\
F_{B_s \rightarrow K}^v &= 1 + \left(-\frac{3}{8} + \frac{3}{2} \frac{m_K^2}{m_\pi^2}\right) \frac{\bar{A}(m_\pi^2)}{F^2} + \left(\frac{3}{4} + \frac{3}{2} g^2\right) \frac{\bar{A}(m_K^2)}{F^2} \\
& + \left(-\frac{5}{24} + \frac{1}{2} g^2 + \frac{1}{2} \frac{m_K^2}{m_\eta^2}\right) \frac{\bar{A}(m_\eta^2)}{F^2} \\
& - 3 \frac{m_K^2}{F^2} \mathcal{F}\left(\frac{m_K}{m_\pi}\right) - \frac{m_K^2}{F^2} \mathcal{F}\left(\frac{m_K}{m_\eta}\right), \tag{IV.45}
\end{aligned}$$

$$\begin{aligned}
F_{B_s \rightarrow \eta}^p &= 1 + \left(\frac{1}{2} + 4g^2 - \frac{5}{3} \frac{m_\eta^2}{m_K^2} g^2\right) \frac{\bar{A}(m_K^2)}{F^2} + \left(\frac{1}{6} + \frac{17}{18} g^2\right) \frac{\bar{A}(m_\eta^2)}{F^2} \\
& + \frac{10}{3} \frac{(m_\eta^2 - m_K^2)}{F^2} \mathcal{F}\left(\frac{m_\eta}{m_K}\right), \\
F_{B_s \rightarrow \eta}^v &= 1 + \left(-1 + \frac{3}{2} g^2 + 3 \frac{m_K^2}{m_\pi^2}\right) \frac{\bar{A}(m_K^2)}{F^2} + \left(\frac{1}{6} + \frac{1}{2} g^2\right) \frac{\bar{A}(m_\eta^2)}{F^2} \\
& - 6 \frac{m_\eta^2}{F^2} \mathcal{F}\left(\frac{m_\eta}{m_K}\right), \tag{IV.46}
\end{aligned}$$

with

$$\mathcal{F}\left(\frac{m_1}{m_2}\right) = \begin{cases} -\frac{1}{(4\pi)^2} \frac{\sqrt{m_2^2 - m_1^2}}{m_1} \left[\frac{\pi}{2} - \arctan\left(\frac{m_1}{\sqrt{m_2^2 - m_1^2}}\right) \right] & m_1 \leq m_2 \\ \frac{1}{(4\pi)^2} \frac{\sqrt{m_1^2 - m_2^2}}{m_1} \tanh^{-1}\left(\frac{\sqrt{m_1^2 - m_2^2}}{m_1}\right) & m_1 \geq m_2 \end{cases} \tag{IV.47}$$

Our results agree with the earlier published ones in [24, 25].

IV.5 $B \rightarrow D$ transition

IV

IV.5.1 Definition of formfactors

In this section we present the formalism involved in the calculation of the $B \rightarrow D$ formfactor. The matrix element for this decay is

$$\langle D(p') | \bar{b} \gamma_\mu c | B(p) \rangle = (p + p')_\mu \tilde{f}_+(q^2) + (p - p')_\mu \tilde{f}_-(q^2) \tag{IV.48}$$

where q^μ is the momentum transfer $q^\mu = p - p'$.

To perform the calculation in HMChPT we need the hadronic current corresponding to the one of QCD:

$$\bar{b} \gamma_\mu c \rightarrow \text{Tr} X(v, v') \tilde{H}(v') \gamma_\mu H(v) \tag{IV.49}$$

where v, v' are the fixed four-velocities of the B and D hadron respectively, while $X(v, v')$ is the most general bispinor constructed starting from the invariants v and v' . As explained in [20], spin symmetry for heavy quarks constrains X to be a scalar function $-\xi(v \cdot v')$, called the Isgur-Wise function [28]. The variable $v \cdot v'$ is of special importance. It can be related to q^2 through the relation

$$w \equiv v \cdot v' = \frac{m_B^2 + m_D^2 - q^2}{2m_B m_D}. \quad (\text{IV.50})$$

The allowed kinematic range is thus $0 \leq w - 1 \leq \frac{(m_B - m_D)^2}{2m_B m_D}$. w is a measure of what is the momentum transfer to the light degrees of freedom i.e. it gives us an indication of the range of applicability of HMChPT. The light degrees of freedom have momentum of order $\Lambda_{\text{QCD}} v^{(\prime)}$, thus the momentum transfer to the light system is $q_{\text{light}}^2 \approx (\Lambda_{\text{QCD}} v - \Lambda_{\text{QCD}} v')^2 = 2\Lambda_{\text{QCD}}^2(1 - w)$. HMChPT can be applied as far as $q_{\text{light}}^2 \ll m_{b,c}^2$ which means on the scale $w \approx 1$ (region of zero recoil or near the endpoint) [29]. The matrix element in HMChPT is

$$\langle D(v') | \bar{b} \gamma_\mu c | B(v) \rangle_{\text{HMChPT}} = (v + v')_\mu h_+(w). \quad (\text{IV.51})$$

Evaluating explicitly the trace in (IV.49) it is easy to obtain $h_+(w) = \xi(w)$ at leading order. It can be also shown that heavy flavour symmetry implies $\xi(1) = 1$ [20, 28]. The result that one single formfactor is enough to describe the matrix element of (IV.51) can also be achieved using the helicity formalism for counting the number of independent amplitudes [20, 30]. To compare with the results of HMChPT it is convenient to reparametrize the matrix element of QCD defined in (IV.48) as

$$\frac{\langle D(p') | \bar{b} \gamma_\mu c | B(p) \rangle}{\sqrt{m_B m_D}} = (v + v')_\mu h_+(w) + (v - v')_\mu h_-(w). \quad (\text{IV.52})$$

where the formfactors $h_\pm(w)$ are linear combinations of $\tilde{f}_\pm(q^2)$. Comparing (IV.51) and (IV.52) it is straightforward to see that, at leading order in $1/m_{\text{heavy}}$, $h_+(w)$ must be the same formfactor in the two formalisms and that $h_-(w) = 0$.

To perform the calculation in the relativistic framework we need the J_μ^L current responsible for the $B \rightarrow D$ transition, analogous to the one in (IV.25). Therefore we write down all the possible independent and chiral-invariant operators that respect also heavy quark symmetries. They must contain interactions of the kind BD or B^*D^* . The first one is needed for the tree-level diagram (1) in Fig. IV.4, while the second for the one-loop (2) in Fig. IV.4. Thus

the current is

$$\begin{aligned}
J_\mu^L = & X_1 \left(-tD^\dagger \nabla_\mu B + t\nabla_\mu D^\dagger B \right) + X_2 \left(tD_\alpha^{*\dagger} \nabla_\mu B^{*\alpha} - t\nabla_\mu D_\alpha^{*\dagger} B^{*\mu} \right) \\
& + X_3 \left(-t\nabla^\alpha D_\alpha^{*\dagger} B_\mu^* + tD_\mu^{*\dagger} \nabla^\alpha B_\alpha^* + t\nabla^\alpha D_\mu^{*\dagger} B_\alpha^* - tD_\alpha^{*\dagger} \nabla^\alpha B_\mu^* \right)
\end{aligned} \tag{IV.53}$$

where X_1, X_2, X_3 are effective couplings and the spurion t is now a singlet under the chiral $SU(n)_L \times SU(n)_R$ symmetry since $\bar{b}\gamma_\mu c$ is a singlet. Heavy quark symmetry implies furthermore that $X_1 = X_2 = X_3$. From (IV.53) it is easy to construct the vector current J_μ^V causing the decay.

Before concluding this section we stress once more that the zero recoil region is the only one where HMChPT is in principle applicable, as shown by [29]. This does not mean that it is not possible to extend the effective theory outside that range to calculate the infrared singularities. Indeed exactly the same arguments applied to $B \rightarrow \pi$ semileptonic decays go through for the $B \rightarrow D$ case as well, thus HPChPT can be used. As a matter of fact there have been already confirmations of how well the effective theory can do when $w - 1 \gg 0$ (see for example Fig 2.5 in [20]). The use of HPChPT justify those results.

IV.5.2 Chiral logarithms

We now present the results for the $B_{(s)} \rightarrow D_{(s)}$ semileptonic decay. The results in two-flavour HMChPT at zero recoil ($w = 1$) can be found in [29]. The three-flavour extension has been calculated in [31] and [32]. The result at one loop and leading order in $1/m_B$ and $1/m_D$ is

$$h_+(w) = \xi(w) \left[1 + \frac{g^2}{F^2} \left(\frac{3}{2} \bar{A}(m_\pi^2) + \bar{A}(m_K^2) + \frac{1}{6} \bar{A}(m_\eta^2) \right) (r(w) - 1) \right], \tag{IV.54}$$

and for the $B_s \rightarrow D_s$ transition it is

$$h_+(w) = \xi(w) \left[1 + \frac{g^2}{F^2} \left(2\bar{A}(m_K^2) + \frac{2}{3} \bar{A}(m_\eta^2) \right) (r(w) - 1) \right], \tag{IV.55}$$

where

$$r(w) = \frac{1}{\sqrt{w^2 - 1}} \log(w + \sqrt{w^2 - 1}), \tag{IV.56}$$

and $r(1) = 1$ so that the chiral logarithms cancel at zero recoil. While in [29] it has been clearly stated that the calculation is valid only at the zero recoil point, the authors of [31] and [32] present the result for the Isgur-Wise function in the whole energy range, but no explicit arguments why it should



Figure IV.4: The diagrams contributing to the $B \rightarrow D$ transition up to one-loop. Notation is the same as in Fig. IV.1. The double lines at the left of the insertion of the current are always B mesons, while the ones in the right are D mesons.

be valid are given there. The arguments of HPChPT given before imply that the formula given there are indeed valid in the whole energy regime $0 \leq w - 1 \leq \frac{(m_B - m_D)^2}{2m_B m_D} \approx 1.6$. Note that here the correction is not a simple chiral logarithm as in the previous cases but there is a strong dependence on w and the result connects smoothly to the endpoint region.

We checked that our relativistic formulation gives the same result as [32]. The result up to one-loop reads

$$\begin{aligned}
 h_+(w) &= \frac{X_1}{\sqrt{2}} \left[1 + \frac{g^2}{F^2} \left(\frac{3}{2} \bar{A}(m_\pi^2) + \bar{A}(m_K^2) + \frac{1}{6} \bar{A}(m_\eta^2) \right) \right. \\
 &\quad \left. \times \left(1 - 2m_B m_D \tilde{C}(m_D^2, m_B^2, q^2) \right) \right], \\
 h_-(w) &= 0,
 \end{aligned} \tag{IV.57}$$

where $\tilde{C}(m_D^2, m_B^2, q^2)$ comes from the three-point function $C(m^2, m_B^2, m_D^2, m_B^2, q^2, m_D^2)$ which is needed to evaluate the loop diagram in Fig. IV.4. In (IV.73) in the appendix we define the function $\tilde{C}(m_D^2, m_B^2, q^2)$ and show that $\tilde{C}(m_D^2, m_B^2, q^2) = r(w)/(2m_B m_D)$. We also agree with the $B_s \rightarrow D_s$ result of [32].

Comparing (IV.57) with (IV.54) it is straightforward to see that the two formalisms give the same results as foreseen. Notice that now we do not need to distinguish the two limits $w - 1 \approx 0$ and $w - 1 \gg 0$: the function $r(w)$ describes the whole energy range.

Note that the results here assume that there are no other nearby states, see e.g. the discussion in [33].

IV.6 Conclusions

In the paper we have extended HPChPT to several processes. First we calculated the three-flavour results for the charged pion and kaon electromagnetic

formfactor and the two-flavour result for the pion vector and scalar formfactor. The latter have then been used to check the underlying arguments of HPChPT in a two-loop setting.

Using the three-flavour spontaneous symmetry breaking pattern we could explicitly evaluate the dependence on the light meson masses for the $B \rightarrow \pi$ formfactors in addition to our earlier two-flavour results [11]. We could also extend the theory to other transitions as the $B \rightarrow K$ and $B \rightarrow \eta$ transitions and the corresponding B_s transitions. The corrections are of the expected size of about 30%. An unexplained feature of our results is that the two possible formfactors have always the same chiral logarithm and we ruled out two possible explanations. A comparison with the experimental data for the $D \rightarrow \pi, K$ transition formfactors has also been performed. It shows that the corrections obtained go in the right direction and are sizable. We have reproduced the known results at the endpoints and added these for the transitions to η .

Finally, we justified and reproduced already known results for the formfactors of the $B \rightarrow D$ transition at one loop.

Further investigations in this framework are desirable, since they could significantly improve the chiral extrapolations of the lattice data. In particular it could be very useful to develop the same approach also for Partially Quenched ChPT. As stated above we expect that a formalism with an explicit power counting can be formulated along the lines of SCET.

Acknowledgments

This work is supported in part by the European Community-Research Infrastructure Integrating Activity ‘‘Study of Strongly Interacting Matter’’ (Hadron-Physics2, Grant Agreement n. 227431) and the Swedish Research Council grants 621-2008-4074 and 621-2008-4252. This work heavily used FORM [34].

IV.A Expansion of the needed loop integrals

We collect here the one-loop functions and their expansions, used to evaluate the diagrams in Fig. IV.2 and in Fig. IV.4 in the framework of the relativistic theory of Sect. IV.2.3. Much of what is written here is also present in the appendix of [11]. We need the one-, two- and three-point functions defined as ($d = 4 - 2\epsilon$)

$$A(m_1^2) = \frac{1}{i} \int \frac{d^d k}{(2\pi)^d} \frac{1}{k^2 - m_1^2}, \quad (\text{IV.58})$$

$$B(m_1^2, m_2^2, p^2) = \frac{1}{i} \int \frac{d^d k}{(2\pi)^d} \frac{1}{(k^2 - m_1^2)((p-k)^2 - m_2^2)}, \quad (\text{IV.59})$$

$$C(m_1^2, m_2^2, m_3^2, p_1^2, p_2^2, q^2) = \frac{1}{i} \int \frac{d^d k}{(2\pi)^d} \frac{1}{(k^2 - m_1^2)((k - p_1)^2 - m_2^2)((k - p_1 - p_2)^2 - m_3^2)}, \quad (\text{IV.60})$$

with $q^2 = (p_1 + p_2)^2$. Two- and three-point functions with extra powers of momenta in the numerator contribute too. They are defined similarly and the explicit definitions can be found in [35]. All these functions can be rewritten in terms of (IV.58), (IV.59) and (IV.60) [36]. The finite parts of $A(m_1^2)$ and $B(m_1^2, m_2^2, q^2)$ are using the standard ChPT subtractions [2,3,37]

$$\bar{A}(m_1^2) = -\frac{m_1^2}{16\pi^2} \log\left(\frac{m_1^2}{\mu^2}\right), \quad (\text{IV.61})$$

$$\bar{B}(m_1^2, m_2^2, q^2) = \frac{1}{16\pi^2} \left[-1 - \int_0^1 dx \log\left(\frac{m_1 x + m_2(1-x) - x(1-x)q^2}{\mu^2}\right) \right]. \quad (\text{IV.62})$$

As far as regards the B transitions to a light pseudoscalar meson, the three-point function $C(m_1^2, m_2^2, m_3^2, p_1^2, p_2^2, q^2)$ always depends on the masses as $(m_1^2, M^2, M^2, M^2, m_2^2, q^2)$ where m_1 is the mass of the light meson in the loop, m_2 is the mass of the light external meson and $M = m_B$. It can be rewritten using Feynman parameters x, y

$$C(m_1^2, M^2, M^2, M^2, m_2^2, q^2) = -\frac{1}{16\pi^2} \int_0^1 dx \int_0^{1-x} dy \left[m_1^2(1-x-y) + m_2^2(-y+y^2) + M^2(x+y)^2 + (q^2 - M^2 - m_2^2)(-y+y(x+y)) \right]^{-1}. \quad (\text{IV.63})$$

In order to find the appropriate chiral logarithms we expanded (IV.62) and (IV.63) for small ratios m^2/M^2 . We quote only the terms of the expansions containing non-analyticities in the light masses m_i . First those only valid for $q^2 \ll q_{\text{max}}^2$, i.e. away from the endpoint:

$$\bar{B}(m^2, M^2, q^2) = -\frac{1}{M^2 - q^2} \bar{A}(m^2), \quad (\text{IV.64})$$

$$C(m_1^2, M^2, M^2, M^2, m_2^2, q^2) = \frac{1}{(M^2 - q^2)} \frac{1}{16\pi} \frac{m_1}{M} - \frac{1}{(M^2 - q^2)^2} \bar{A}(m_1^2). \quad (\text{IV.65})$$

The next ones are those relevant at the endpoint or for wavefunction renormalization

$$\bar{B}(m^2, M^2, M^2) = -\frac{1}{16\pi} \frac{m}{M} + \frac{1}{16\pi} \frac{m^2}{M^2} + \frac{1}{2M^2} \bar{A}(m^2), \quad (\text{IV.66})$$

$$\bar{B}(m^2, M^2, m^2) = 0, \quad (\text{IV.67})$$

$$\begin{aligned} \bar{B}(m_1^2, M^2, (M - m_2)^2) &= \frac{1}{M} \left[2m_2 \mathcal{F} \left(\frac{m_1}{m_2} \right) - \frac{m_2}{m_1^2} \bar{A}(m_1^2) \right] \\ &+ \frac{1}{M^2} \left[3m_2^2 \mathcal{F} \left(\frac{m_1}{m_2} \right) + \bar{A}(m_1^2) \left(\frac{1}{2} - \frac{3}{2} \frac{m_2^2}{m_1^2} \right) \right]. \end{aligned} \quad (\text{IV.68})$$

The function $\mathcal{F}(m_1/m_2)$ was defined in (IV.47). The expansion in (IV.68) holds in both the cases $m_2 \leq m_1$ and also for $m_1 = m_2$ where it correctly reduces to the expansion reported in the appendix of [11].

The expansions of the three-point functions at q_{max}^2 are a bit more involved. The reason is that the reduction formulas present a singularity at $q_{\text{max}}^2 = (M - m_2)^2$ for $m_2^2 = 0$. Furthermore we need to distinguish different cases depending on the m_1 and m_2 appearing in the arguments of the three-loop functions. We use again the same technique used in [11]. We expand each of the functions directly from the Feynman parameter integral, without first rewriting them in terms of (IV.58), (IV.59) and (IV.60). To do this one rewrites the integral in (IV.63) using $z = x + y$ as

$$\begin{aligned} C(m_1^2, M^2, M^2, M^2, m_2^2, (M - m_2)^2) &= -\frac{1}{16\pi^2} \int_0^1 dz \int_0^z dy \times \\ &\frac{1}{[M^2 z^2 + m_1^2 + 2m_2 M y + (-m_1^2 z + m_2^2(-y + y^2) - 2m_2 M y z)]}. \end{aligned} \quad (\text{IV.69})$$

The part in the denominator in brackets is always suppressed by at least m/M compared to the first three terms for all values of z and y and we can thus expand in it. The remaining integrals can be done with elementary means. The expansions obtained are many and long, therefore we quote only those needed and restricted to those terms where an infrared singularity appears. We do not quote terms like $1/(4\pi)^2 m/M^3$, also non-analytic for small m , because they always cancel in the final results (IV.42)-(IV.46). The expansions read

$$C(m_1^2, M^2, M^2, M^2, m_2^2, (M - m_2)^2) = \frac{1}{M^2} \left[-\frac{1}{2} \frac{1}{m_1^2} \bar{A}(m_1^2) + \mathcal{F} \left(\frac{m_1}{m_2} \right) \right]$$

$$\begin{aligned}
& + \frac{1}{M^3} \left[\mathcal{F} \left(\frac{m_1}{m_2} \right) m_2 - \frac{1}{2} \frac{m_2}{m_1^2} \bar{A}(m_1^2) \right] \\
& + \frac{1}{M^4} \left[-\frac{1}{2} \frac{m_2^2}{m_1^2} \bar{A}(m_1^2) + \mathcal{F} \left(\frac{m_1}{m_2} \right) \left(m_2^2 + \frac{3}{8} m_1^2 \right) \right], \quad (\text{IV.70})
\end{aligned}$$

$$\begin{aligned}
C_{11}(m_1^2, M^2, M^2, M^2, m_2^2, (M - m_2)^2) &= \frac{1}{M^3} \left(-\mathcal{F} \left(\frac{m_1}{m_2} \right) m_2 + \frac{1}{2} \frac{m_2}{m_1^2} \bar{A}(m_1^2) \right) \\
&+ \frac{1}{M^4} \left[\left(-\frac{1}{2} + \frac{13}{12} \frac{m_2^2}{m_1^2} \right) \bar{A}(m_1^2) - \mathcal{F} \left(\frac{m_1}{m_2} \right) \left(\frac{13}{6} m_2^2 - \frac{1}{6} m_1^2 \right) \right], \\
C_{12}(m_1^2, M^2, M^2, M^2, m_2^2, (M - m_2)^2) &= \frac{1}{M^3} \left(-\mathcal{F} \left(\frac{m_1}{m_2} \right) \left(\frac{2}{3} m_2 + \frac{1}{3} \frac{m_1^2}{m_2} \right) \right. \\
&+ \left. \frac{1}{3} \frac{m_2}{m_1^2} \bar{A}(m_1^2) \right) + \frac{1}{M^4} \left[\left(-\frac{1}{4} + \frac{5}{6} \frac{m_2^2}{m_1^2} \right) \bar{A}(m_1^2) - \mathcal{F} \left(\frac{m_1}{m_2} \right) \left(\frac{5}{3} m_2^2 + \frac{1}{3} m_1^2 \right) \right], \\
C_{21}(m_1^2, M^2, M^2, M^2, m_2^2, (M - m_2)^2) &= \frac{1}{M^4} \left[-\mathcal{F} \left(\frac{m_1}{m_2} \right) \left(-\frac{4}{3} m_2^2 + \frac{1}{3} m_1^2 \right) \right. \\
&+ \left. \bar{A}(m_1^2) \left(\frac{1}{2} - \frac{2}{3} \frac{m_2^2}{m_1^2} \right) \right], \\
C_{22}(m_1^2, M^2, M^2, M^2, m_2^2, (M - m_2)^2) &= \frac{1}{M^4} \left[\mathcal{F} \left(\frac{m_1}{m_2} \right) \left(\frac{4}{5} m_2^2 + \frac{1}{15} m_1^2 + \frac{2}{15} \frac{m_1^4}{m_2^2} \right) \right. \\
&+ \left. \bar{A}(m_1^2) \left(\frac{1}{6} - \frac{2}{5} \frac{m_2^2}{m_1^2} \right) \right], \\
C_{23}(m_1^2, M^2, M^2, M^2, m_2^2, (M - m_2)^2) &= \frac{1}{M^4} \left[\mathcal{F} \left(\frac{m_1}{m_2} \right) m_2^2 \right. \\
&+ \left. \bar{A}(m_1^2) \left(\frac{1}{4} - \frac{1}{2} \frac{m_2^2}{m_1^2} \right) \right], \\
C_{24}(m_1^2, M^2, M^2, M^2, m_2^2, (M - m_2)^2) &= \frac{1}{M^2} \left[-\mathcal{F} \left(\frac{m_1}{m_2} \right) \frac{1}{3} (m_2^2 - m_1^2) \right. \\
&+ \left. \bar{A}(m_1^2) \left(-\frac{1}{4} + \frac{1}{6} \frac{m_2^2}{m_1^2} \right) \right]. \quad (\text{IV.71})
\end{aligned}$$

Setting the masses $m_1 = m_2$ all the expansions in (IV.71) coincide correctly with the ones reported in the appendix of [11]. The function $\mathcal{F}(m_1/m_2)$ is the one defined in (IV.47). Notice that it takes different forms depending if $m_1 \leq m_2$. Furthermore for $m_1 = m_2$ $\mathcal{F}(m_1/m_2) = 0$. The other three-point

functions do not give any leading contribution.

We focus now on the semileptonic decay $B \rightarrow D$. The three-point function entering in the loop diagram of Fig. IV.4 is $C(m^2, M_1^2, M_2^2, M_1^2, q^2, M_2^2)$, where m is the mass of the light meson in the loop, $M_1 = m_B$ and $M_2 = m_D$. To expand it, similarly to what has been done above, we first rewrite it in terms of the Feynman parameters x, y

$$C(m^2, M_1^2, M_2^2, M_1^2, q^2, M_2^2) = -\frac{1}{16\pi^2} \int_0^1 dx \int_0^{1-x} dy \left[m^2(1-x-y) + x^2 M_1^2 + y^2 M_2^2 + xy(M_1^2 + M_2^2 - q^2) \right]^{-1}. \quad (\text{IV.72})$$

The $m^2(x+y)$ term in (IV.72) is suppressed by at least one power of m so we can neglect it. Setting $x = X/M_1$, $y = Y/M_2$ and $w = (M_1^2 + M_2^2 - q^2)/(2M_1M_2)$ the integral becomes

$$C(m^2, M_1^2, M_2^2, M_1^2, q^2, M_2^2) = -\frac{1}{16\pi^2} \frac{1}{M_1M_2} \int_0^{M_1} dX \int_0^{M_2 - \frac{M_2}{M_1}X} dY \left[m^2 + X^2 + Y^2 + 2wXY \right]^{-1}.$$

Then we can perform another change of variable and set polar coordinates $X = R \cos \phi$, $Y = R \sin \phi$:

$$C(m^2, M_1^2, M_2^2, M_1^2, q^2, M_2^2) = -\frac{1}{16\pi^2} \frac{1}{M_1M_2} \int_0^{\pi/2} d\phi \int_0^{R_{\max}} dR \left[m^2 + R^2 + 2wR^2 \sin(2\phi) \right]^{-1},$$

where the upper boundary is $R_{\max} = M_2/(\sin \phi + M_2/M_1 \cos \phi)$. We are interested in isolating the infrared singularities. Those only arise from the lower bound of the integral. Therefore, performing the integral in dR , we keep only the term coming from the small R region. However we checked explicitly that the large R region does not produce any soft singularity at the desired order. The result for the integral in R reads

$$C(m^2, M_1^2, M_2^2, M_1^2, q^2, M_2^2) = \frac{1}{16\pi^2} \frac{1}{2M_1M_2} \int_0^{\pi/2} d\phi \log \left(\frac{m^2}{\mu^2} \right) \left[1 + 2w \sin(2\phi) \right]^{-1} + \dots,$$

where the ellipsis are the terms coming from the upper bound and μ is a parameter with the dimension of a mass. The integral in $d\phi$ can be done analytically

cally and after tedious calculations we arrive to the final result

$$\begin{aligned}
C(m^2, M_1^2, M_2^2, M_1^2, q^2, M_2^2) &= \frac{1}{16\pi^2} \frac{1}{2M_1 M_2} \frac{1}{\sqrt{w^2 - 1}} \log(w + \sqrt{w^2 - 1}) \\
&\quad \times \log\left(\frac{m^2}{\mu}\right) + \dots \\
&= \frac{1}{16\pi^2} \tilde{C}(M_2^2, M_1^2, q^2) \log\left(\frac{m^2}{\mu^2}\right) + \dots \quad .(IV.73)
\end{aligned}$$

IV References

- [1] S. Weinberg, "Phenomenological Lagrangians," *Physica* **A96** (1979) 327.
- [2] J. Gasser and H. Leutwyler, "Chiral Perturbation Theory to One Loop," *Ann. Phys.* **158** (1984) 142.
- [3] J. Gasser and H. Leutwyler, "Chiral Perturbation Theory: Expansions in the Mass of the Strange Quark," *Nucl. Phys.* **B250** (1985) 465.
- [4] CLEO Collaboration, J. Y. Ge *et al.*, "Study of $D^0 \rightarrow \pi^- e^+ \nu_e$, $D^+ \rightarrow \pi^0 e^+ \nu_e$, $D^0 \rightarrow K^- e^+ \nu_e$, and $D^+ \rightarrow \bar{K}^0 e^+ \nu_e$ in Tagged Decays of the $\psi(3770)$ Resonance," *Phys. Rev.* **D79** (2009) 052010, arXiv:0810.3878 [hep-ex].
- [5] CLEO Collaboration, N. E. Adam *et al.*, "A Study of Exclusive Charmless Semileptonic B Decay and $|V_{ub}|$," *Phys. Rev. Lett.* **99** (2007) 041802, arXiv:hep-ex/0703041.
- [6] Belle Collaboration, T. Hokuue *et al.*, "Measurements of branching fractions and q^2 distributions for $B \rightarrow \pi \ell \nu$ and $B \rightarrow \rho \ell \nu$ Decays with $B \rightarrow D^{(*)} \ell \nu$ Decay Tagging," *Phys. Lett.* **B648** (2007) 139–148, arXiv:hep-ex/0604024.
- [7] BABAR Collaboration, B. Aubert *et al.*, "Measurement of the $B^0 \rightarrow \pi^- \ell^+ \nu$ form-factor shape and branching fraction, and determination of $|V_{ub}|$ with a loose neutrino reconstruction technique," *Phys. Rev. Lett.* **98** (2007) 091801, arXiv:hep-ex/0612020.
- [8] E. Gamiz, "Heavy flavour phenomenology from lattice QCD," *PoS LATTICE2008* (2008) 014, arXiv:0811.4146 [hep-lat].
- [9] RBC Collaboration, J. M. Flynn and C. T. Sachrajda, " $SU(2)$ chiral perturbation theory for $K_{\ell 3}$ decay amplitudes," *Nucl. Phys.* **B812** (2009) 64–80, arXiv:0809.1229 [hep-ph].
- [10] J. Bijnens and A. Celis, " $K \rightarrow \pi\pi$ Decays in $SU(2)$ Chiral Perturbation Theory," *Phys. Lett.* **B680** (2009) 466–470, arXiv:0906.0302 [hep-ph].
- [11] J. Bijnens and I. Jemos, "Hard Pion Chiral Perturbation Theory for $B \rightarrow \pi$ and $D \rightarrow \pi$ Formfactors," *Nucl. Phys.* **B840** (2010) 54–66, [Erratum–*ibid.* **B844** (2011) 182], arXiv:1006.1197 [hep-ph].
- [12] J. Bijnens, G. Colangelo, and P. Talavera, "The Vector and scalar form-factors of the pion to two loops," *JHEP* **9805** (1998) 014, arXiv:hep-ph/9805389 [hep-ph].



- [13] J. Bijnens, G. Colangelo, and G. Ecker, "The mesonic chiral Lagrangian of order p^6 ," *JHEP* **02** (1999) 020, arXiv:hep-ph/9902437.
- [14] A. Pich, "Effective field theory: Course," arXiv:hep-ph/9806303 [hep-ph].
- [15] S. Scherer, "Introduction to chiral perturbation theory," *Adv.Nucl.Phys.* **27** (2003) 277, arXiv:hep-ph/0210398 [hep-ph].
- [16] M. B. Wise, "Chiral perturbation theory for hadrons containing a heavy quark," *Phys. Rev.* **D45** (1992) 2188–2191.
- [17] G. Burdman and J. F. Donoghue, "Union of chiral and heavy quark symmetries," *Phys. Lett.* **B280** (1992) 287–291.
- [18] J. L. Goity, "Chiral perturbation theory for $SU(3)$ breaking in heavy meson systems," *Phys. Rev.* **D46** (1992) 3929–3936, arXiv:hep-ph/9206230.
- [19] M. B. Wise, "Combining chiral and heavy quark symmetry," arXiv:hep-ph/9306277.
- [20] A. V. Manohar and M. B. Wise, "Heavy quark physics," *Camb. Monogr. Part. Phys. Nucl. Phys. Cosmol.* **10** (2000) 1–191.
- [21] S. Fleming, "Soft Collinear Effective Theory: An Overview," *PoS EFT09* (2009) 002, arXiv:0907.3897 [hep-ph].
- [22] J. Gasser and H. Leutwyler, "Low-Energy Expansion of Meson Form-Factors," *Nucl. Phys.* **B250** (1985) 517–538.
- [23] J. Bijnens and F. Cornet, "Two Pion Production in Photon-Photon Collisions," *Nucl.Phys.* **B296** (1988) 557.
- [24] A. F. Falk and B. Grinstein, " $\bar{B} \rightarrow \bar{K}e^+e^-$ in chiral perturbation theory," *Nucl. Phys.* **B416** (1994) 771–785, arXiv:hep-ph/9306310.
- [25] D. Becirevic, S. Prelovsek, and J. Zupan, " $B \rightarrow \pi$ and $B \rightarrow K$ transitions in partially quenched chiral perturbation theory," *Phys. Rev.* **D68** (2003) 074003, arXiv:hep-lat/0305001.
- [26] **Particle Data Group** Collaboration, K. Nakamura *et al.*, "Review of particle physics," *J.Phys.G* **G37** (2010) 075021.
- [27] **UKQCD** Collaboration, G. M. de Divitiis *et al.*, "Towards a lattice determination of the $B^*B\pi$ coupling," *JHEP* **10** (1998) 010, arXiv:hep-lat/9807032.

- [28] N. Isgur and M. B. Wise, “Weak transition form-factors between heavy mesons,” *Phys. Lett.* **B237** (1990) 527.
- [29] L. Randall and M. B. Wise, “Chiral perturbation theory for $B \rightarrow D^*$ and $B \rightarrow D$ semileptonic transition matrix elements at zero recoil,” *Phys. Lett.* **B303** (1993) 135–139, arXiv:hep-ph/9212315.
- [30] H. D. Politzer, “Counting form-factors using the Wisgur symmetry,” *Phys. Lett.* **B250** (1990) 128–129.
- [31] E. E. Jenkins and M. J. Savage, “Light quark dependence of the Isgur-Wise function,” *Phys. Lett.* **B281** (1992) 331–335.
- [32] C. G. Boyd and B. Grinstein, “ $SU(3)$ corrections to $B \rightarrow D\ell\bar{\nu}_\ell$ form-factors at $\mathcal{O}(1/M)$,” *Nucl. Phys.* **B451** (1995) 177–193, arXiv:hep-ph/9502311.
- [33] J. O. Eeg, S. Fajfer, and J. F. Kamenik, “Chiral loop corrections to weak decays of B mesons to positive and negative parity charmed mesons,” *JHEP* **07** (2007) 078, arXiv:0705.4567 [hep-ph].
- [34] J. A. M. Vermaseren, “New features of FORM,” arXiv:math-ph/0010025.
- [35] J. Bijnens and P. Talavera, “Pion and kaon electromagnetic form factors,” *JHEP* **03** (2002) 046, arXiv:hep-ph/0203049.
- [36] G. Passarino and M. J. G. Veltman, “One Loop Corrections for e^+e^- Annihilation Into $\mu^+\mu^-$ in the Weinberg Model,” *Nucl. Phys.* **B160** (1979) 151.
- [37] G. 't Hooft and M. J. G. Veltman, “Scalar One Loop Integrals,” *Nucl. Phys.* **B153** (1979) 365–401.